RELIABILITY ENHANCEMENT IN AUTOMATED GUIDEWAY TRANSIT (AGT) VEHICLES: A GENERALIZED LIKELIHOOD RATIO APPROACH

by

ERIC DAVID HELFENBEIN

B.S. UNIVERSITY OF CALIFORNIA, LOS ANGELES
(1977)

SUBMITTED IN PARTIAL FULFILLMENT
OF THE REQUIREMENTS FOR THE
DEGREE OF

MASTER OF SCIENCE

at the

MASSACHUSETTS INSTITUTE OF TECHNOLOGY

September, 1980

Signature of Author.....
Department of Electrical Engineering
and Computer Science, June 5, 1980.

Certified by.....
Thesis Supervisor

Certified by.....
Thesis Supervisor

Accepted by.....
Chairman, Departmental Committee on Graduate Students

RELIABILITY ENHANCEMENT IN
AUTOMATED GUIDEWAY TRANSIT (AGT) VEHICLES:
A GENERALIZED LIKELIHOOD RATIO APPROACH

by

ERIC DAVID HELFENBEIN

Submitted to the Department of Electrical Engineering and Computer Science on June 5, 1980 in partial fulfillment of the requirements for the Degree of Master of Science.

ABSTRACT

A systematic method for the improvement of the safety and reliability of automated guideway transit (AGT) vehicles via a failure detection algorithm is developed. This algorithm is based on the generalized likelihood ratio (GLR) method which detects failures by observing a departure of the vehicle system from an idealized linear vehicle model.

The research explores the effect of model choice and complexity and the use of dual-redundant sensors on key detection performance issues.

Detection ability of vehicle failures is demonstrated by vehicle simulations and experiments, and sensitivity to wind, grade, and maneuvers is examined.

Detection methodology is developed for single AGT vehicles, and is extended to AGT systems employing vehicle-follower longitudinal control.

THESIS SUPERVISOR: Paul Houpt

TITLE: Assistant Professor of Mechanical Engineering

THESIS SUPERVISOR: Alan S. Willsky

TITLE: Associate Professor of Electrical Engineering

ACKNOWLEDGEMENTS

I would like to thank my thesis supervisors Paul Houpt and Alan S. Willsky for their guidance, assistance, and ever constant encouragement during the course of this research. Paul's help in editing the final document was superb, and most appreciated. I have learned a great deal from both of them, and have enjoyed our working together.

I greatfully thank Michael Athans for his support and patience during my first year as a graduate student, and for motivating my interest in detection and estimation theory.

Jeff Lewis deserves sincere thanks for his help and camaraderie during this project. I also thank Ed Chow and Jim Lewis for their technical advice.

I am truly in awe of the abilities of Fifa Monserrate and Arthur Giordani; Fifa's typing can only be described as beautiful - Art's technical drawings as excellent. They are both superb artists. I will never understand how they managed to decode my handwriting.

I give special thanks to Diane Miller for her constant encouragement, support, and help with the figures, and her tolerance of many weeks of compulsive behavior.

Finally, thanks to my relatives, house-mates and friends; their never ending support has been greatfully appreciated.

This work was conducted at the Laboratory for Information and Decision Systems and was supported by the Department of Transportation Transportation Systems Center under grant DOT/TSC-1685.

I also acknowledge the support received from the NASA Ames Research Center Grant NASA/NGL-22-009-124.

TABLE OF CONTENTS

TABLE OF CONTENTS (Continuation) PAGE

TABLE OF CONTENTS (Continuation) PAGE

TABLE OF CONTENTS (Continuation) PAGE

LIST OF FIGURES

PAGE

Dual Velocity Sensors

Detection of Non-Bias Failures

CHAPTER V:

LIST OF TABLES

CHAPTER I

INTRODUCTION

Public use of future automated guideway transit (AGT) systems [1] will depend in part on the development of safe and reliable control systems. The design of reliable failure detection and identification technology will play a key role in reaching this goal.

Systems must be designed to accurately and rapidly detect and identify failures which occur in AGT vehicles and their sub-systems. Such detection systems are essential for high capacity systems since headways between vehicles may be on the order of one-half second.

In this research study, a systematic methodology for AGT vehicle failure detection employing a generalized likelihood ratio (GLR) approach will be developed. This work will be centered on the design of a software algorithm for digital processing of vehicle measurements.

A failure detection system which employs a generalized likelihood ratio approach has many advantages over conventional methods (i.e., those relying on comparisons of dual or triple redundant physical sensors). A GLR system makes use of 'analytic redundancy', the known relationships between outputs of unlike sensors. This use of analytic vs. physical redundancy can significantly reduce hardware costs since fewer sensors are required with this approach. In addition, a system based on analytic redundancy is less likely to miss the detection of generic sensor failures (for example, a temperature change similarly affecting all like sensors in a physically redundant set).

An added bonus of the use of the GLR approach is that during unfailed operation, optimal estimates of vehicle states (i.e., optimally filtered measurements) are readily available to the control system for use in control law calculations. Finally, a GLR based detection system can permit a 'fail-operational' response (continued vehicle operation) to certain types of vehicle failures, since estimates of failure location, type, and magnitude can be determined by the algorithm and made available to the control system for compensation.

1.1 Background

Much work has appeared on the design of real-time AGT control systems [2-27]. Most notably, the design of vehicle-follower type longitudinal control systems appears to permit stable control of closely packed strings of vehicles. The successful implementation of a vehicle-follower control strategy depends on accurate knowledge of vehicle and neighboring vehicle states and the availability of a responsive propulsion system. Undetected faults in propulsion or in the sensors providing measurements of vehicle states to the control system will certainly cause problems, and may lead to collisions.

In this light, relatively little has appeared on the systematic development of methodologies for the detection of and response to vehicle failures. One report which has recently appeared, however, is the work of Vander Velde at M.I.T. [28]. Vander Velde employs a failure detection filter approach, developed by Beard [29] and Jones [30]. The detection filter incorporates a

linear system model specifying nominal system behavior (Figure 1.1). Any deviation from nominal behavior of the system, due to an actuator failure, a sensor failure, or a significant change in some parameter describing the system, will result in a discrepancy between the observations of the actual system and the outputs, or predictions, of the model. This difference is often called the error, e(t), or the residual signal vector. The detection filter uses the system model with a feedback gain matrix D which not only makes the filter stable, but in the presence of a failure, holds the error signal vector e(t) to be uni-directional. The direction of e(t) indicates an element which has failed. Thus elements of e(t) are compared to fixed thresholds to declare the occurrance of various failures.

The detection filter approach has many advantages over other failure detection strategies, most notably its simplicity in terms of required on-line computations. In addition, the filter design does not require a-priori specification of vehicle component failure modes, i.e., the way in which components will fail. However, the detection filter technique has a number of limitations:

(1) It is sometimes not possible to design detection filters in such a way that sensor failures can be unambiguously identified.

(2) More than one detection filter is usually required to detect failures in all the components for which failure detection is desired. Choosing the failures to be associated with each filter still remains an ad hoc procedure.

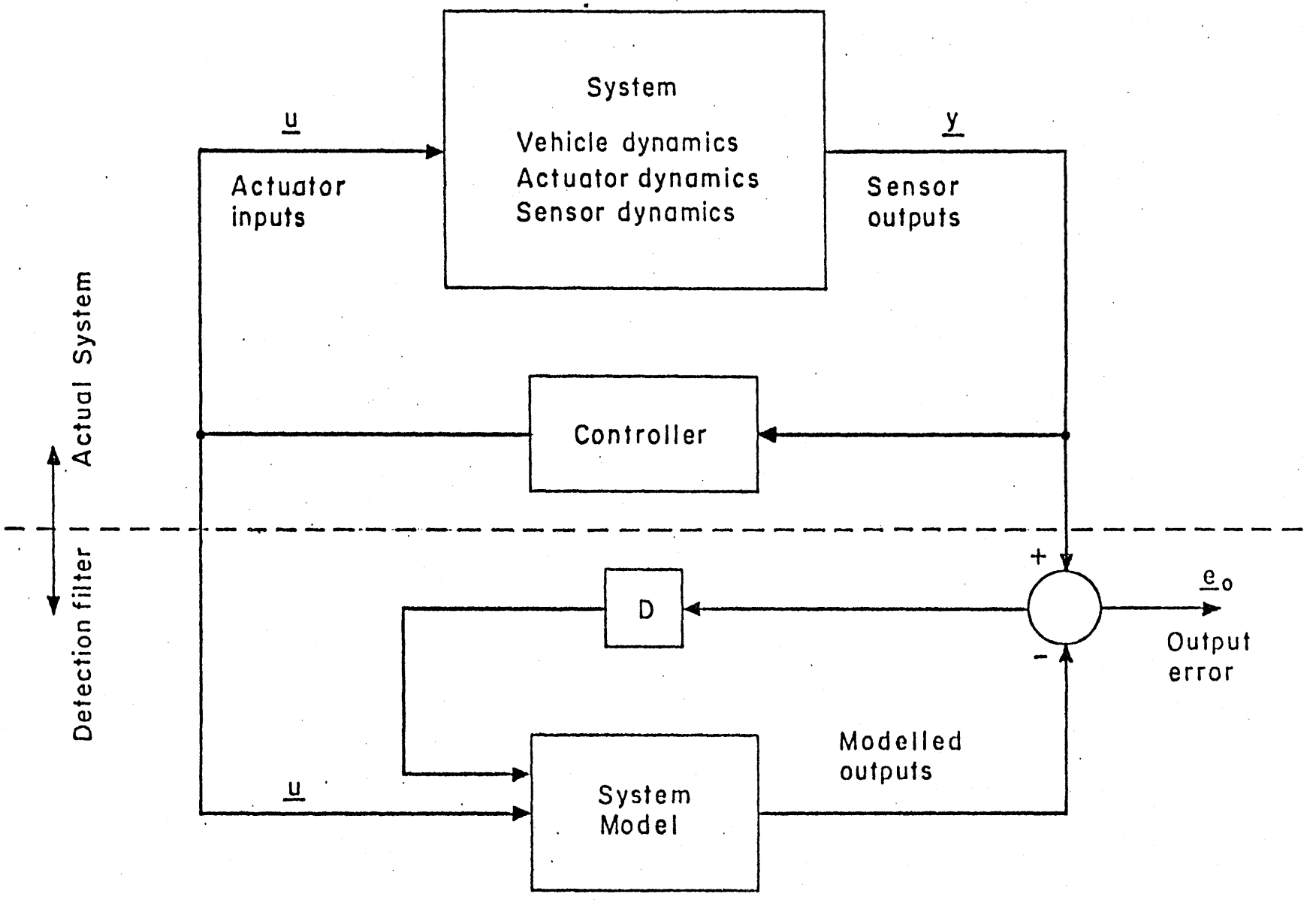

Figure 1.1 - Detection Filter Block Diagram [28]

(3) The detection filter can only declare that a failure has occurred in a given component. It is unable to determine or estimate the type of failure or the extent (magnitude) of the failure. Thus failure compensation by the control system cannot be done unless all components appear in dual-redundant pairs, in which case the faulty component is completely removed from operation.

The generalized likelihood ratio method for failure detection is not as simple to implement as the detection filter. Whereas the detection filter algorithm simply compares the residual at a single instant of time to a threshold, the GLR algorithm examines the entire trajectory over a period of time of the residual. However, the added complexity of the GLR algorithm results in a highly sophisticated failure detection and identification system.

CHAPTER II

AN IDEALIZED AGT VEHICLE MODEL

2.1 Introduction

A key component of a failure detection system based on the generalized likelihood ratio method is a simplified, linear model of the AGT vehicle. Failures of vehicle components will be detected in real-time by observing and analyzing sudden discrepancies between the idealized model and the actual AGT vehicle.

In order to illustrate the GLR methodology, we will present a simple model of an AGT vehicle, and will show how the GLR algorithm would be developed for the vehicle based on the model.

2.2 Vehicle Description

A block diagram of a typical AGT vehicle which was used in this study is shown in Figure 2.1. A wayside computer transmits control commands to the vehicle via a communication link. The control commands are processed by an on-board control computer which translates these commands into an appropriate motor voltage command, E_c. The voltage command is amplified by a power conditioning unit (PCU), which applies a voltage E to a DC traction motor. The PCU will be referred to as the voltage actuator. The PCU, DC motor and the vehicle drive train will be referred to as the propulsion system.

On board the vehicle also exists a set of sensors. These sensors measure the vehicle's position and velocity. We will assume that these two sensors

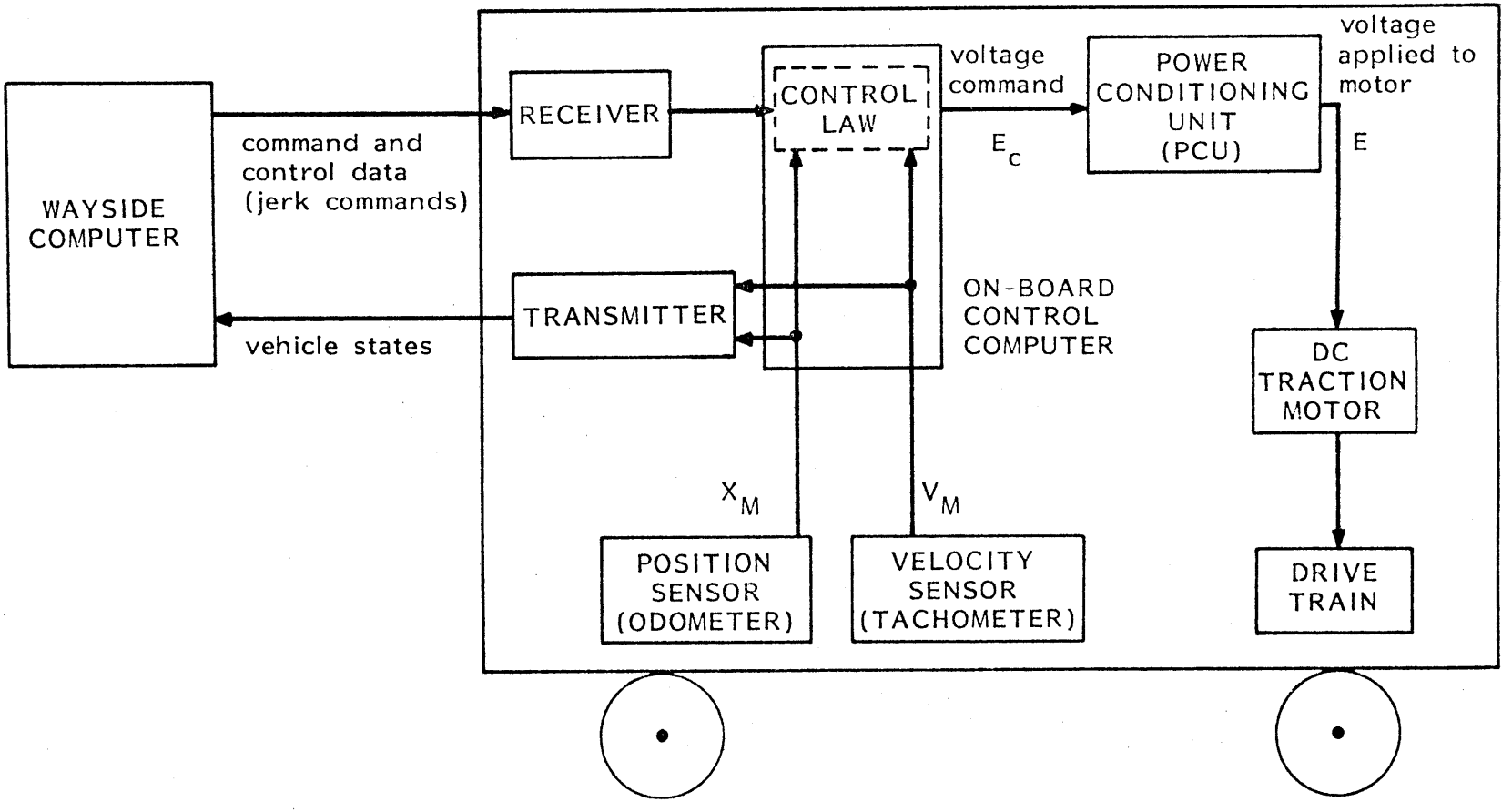

Figure 2.1 - AGT Vehicle Block Diagram

are independent devices. The outputs of the sensors are used as feedback signals by the on-board control computer. The sensor outputs are also transmitted back to the wayside computer.

2.3 Control System

The on-board control computer consists of two components: a velocity command generator and a velocity regulator. The velocity command generator doubly integrates jerk commands sent to the vehicle from the wayside computer. Jerk is used as the control input so that vehicle jerk and acceleration can be constrained within service limits for passenger ride comfort. The wayside computer can thus control the vehicle's line speed by transmitting a jerk profile to the vehicle. A jerk profile which would command the vehicle to increase its line speed by 3 m/s is shown in Figure 2.2. The velocity command computed by the velocity command generator is fed to the velocity regulator. The velocity regulator's function is to compute a motor voltage command which will keep the vehicle at the commanded velocity. The velocity regulator chosen for this study was developed in [26]. This regulator is shown in Figure 2.3.

2.4 Vehicle Dynamics

The dynamics of the AGT vehicle and its DC motor are modelled by Pitts [19]. A block diagram for this model is shown in Figure 2.4. Parameter values for a typical personal rapid transit AGT vehicle are given in Table 2.1. Pitts' model includes the effects of guideway grade and non-linear aerodynamic drag forces. Drag force can be linearized around a nominal

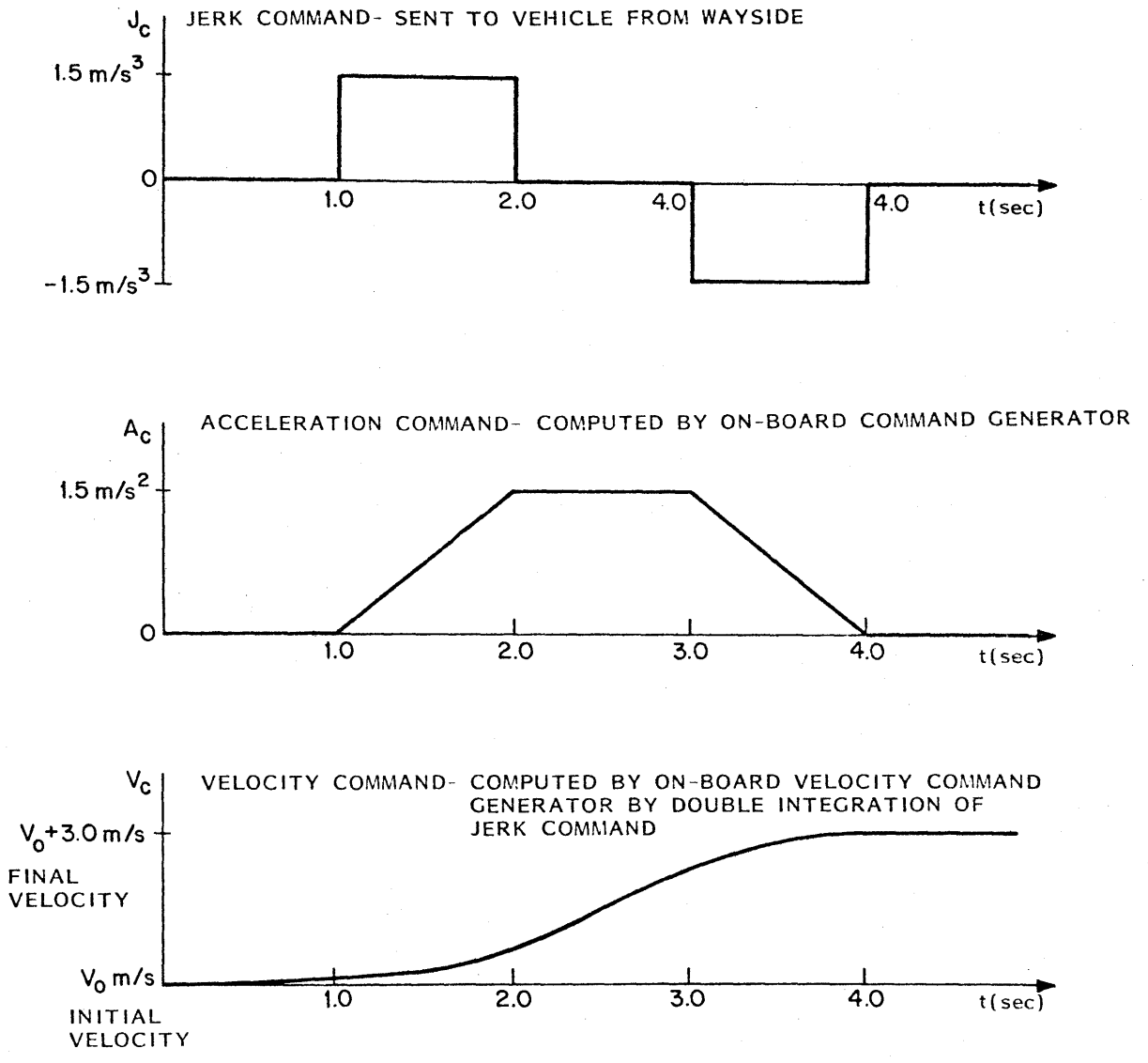

Figure 2.2

Jerk Command Profile

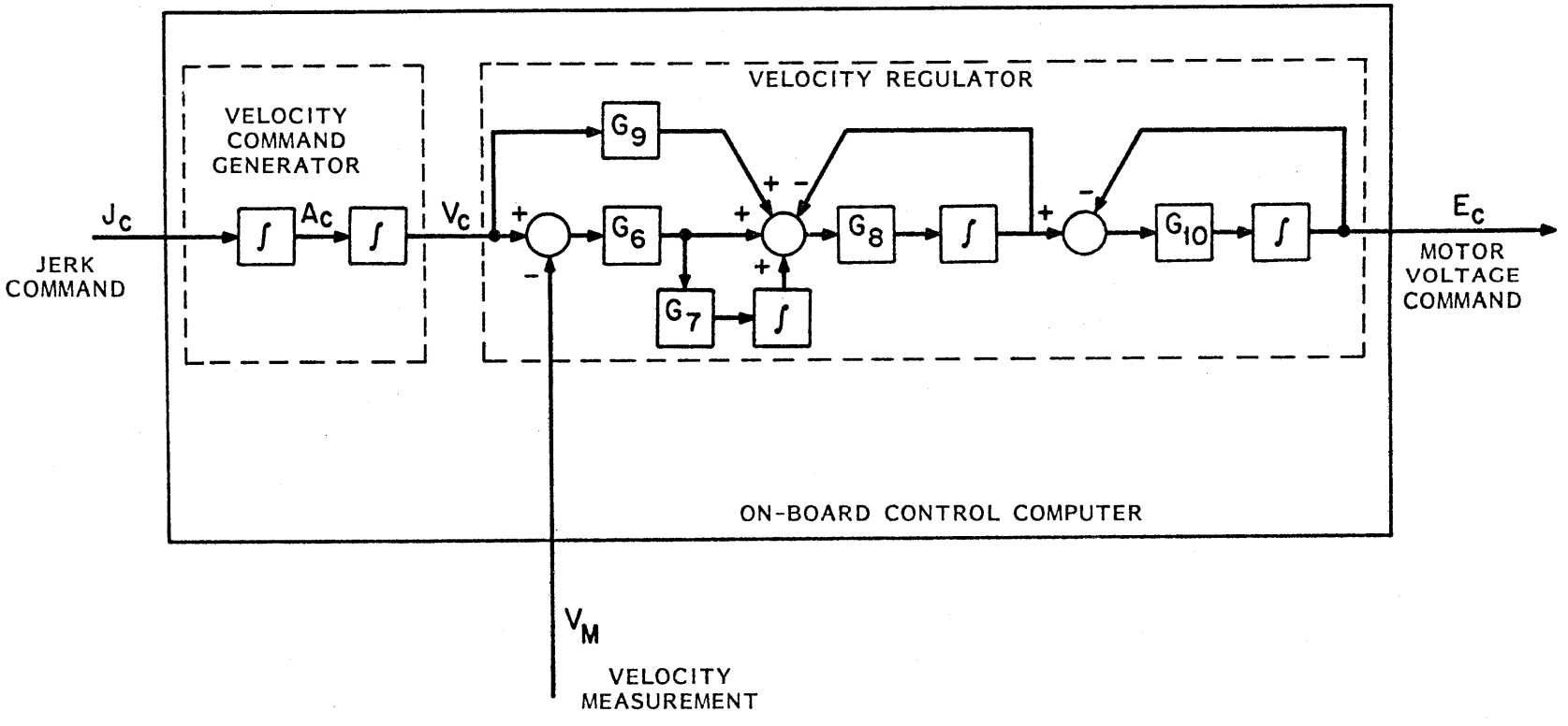

Figure 2.3 - Velocity Command Generator and Velocity Regulator

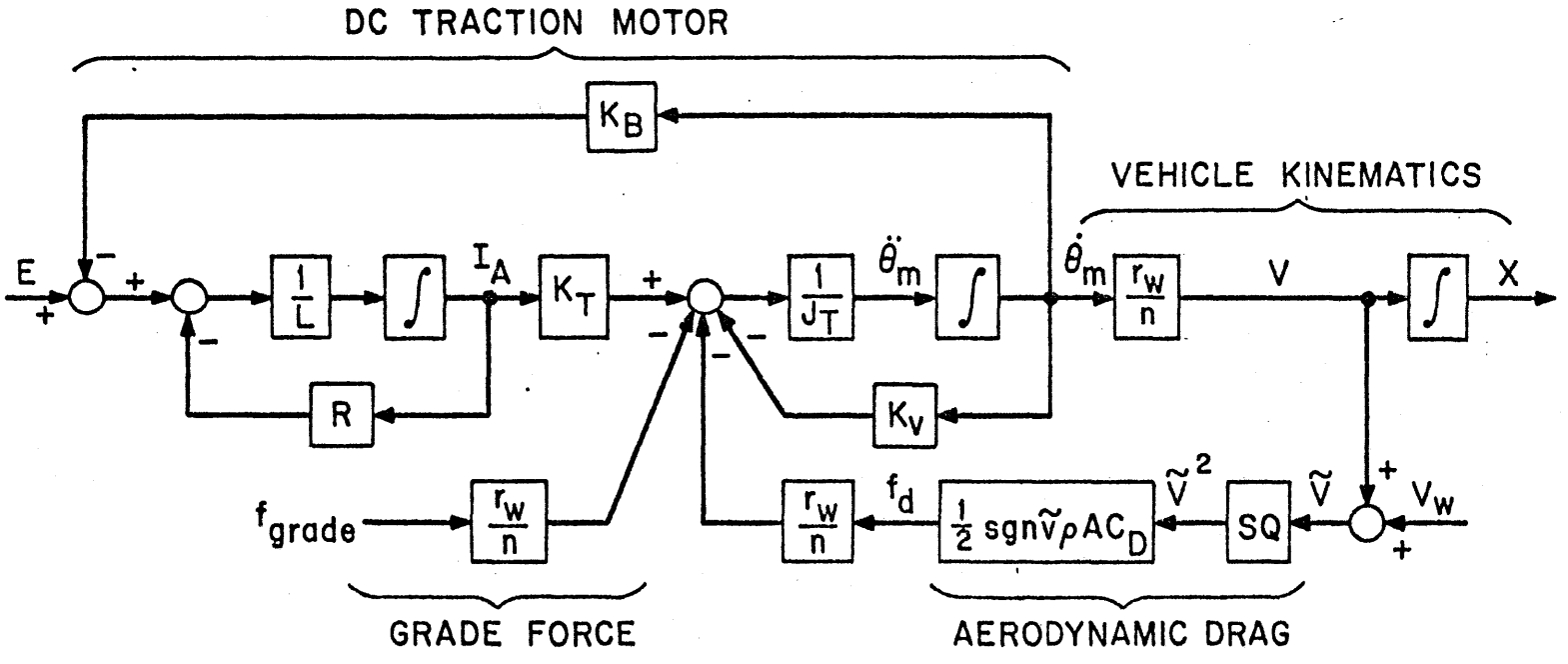

Figure 2.4

Non-Linear AGT Vehicle and DC Motor Block Diagram; Pitts [19]

TABLE 2.1

AGT VEHICLE AND MOTOR PARAMETERS

Represented is a 4-6 passenger personal rapid transit (PRT) vehicle propelled by a 60 hp. DC traction motor.

Parameter	Symbol	Nominal Value
Motor Torque Constant	K_T	.827 N-M/A
Motor Back emf Constant	K_B	.88 V/RAD-S
Armature Inductance	L	.00052 H
Armature Resistance	R	.0203 ohms
Motor Shaft Inertia	J_m	.461 Kg-M^2
Vehicle Wheel Radius	r_w	.35 M
Gear Ratio	n	3.82
Vehicle Mass	M	979 Kg.
Motor Viscous Friction	K_v	~ 0
Vehicle Wheel Inertia	J_L	~ 0
Total Rotational Inertia	J_T	8.679 Kg-M^2
Drag Coefficient	C_D	.7
Vehicle Frontal Area	A	3.4 M^2
Air Density	ρ	1.22
Linearized Drag	W_D	9.67×10^{-4} no wind, 15m/s veh. velocity

wind and vehicle velocity, with the resulting linear model shown in Figure 2.5. This model can be transformed via a change of variables into phase-variable cannonical form (so that the integrator states are position, velocity, and acceleration) and is shown in Figure 2.6. The details of the model transformation are given in [19]. The transfer function from motor voltage to velocity can be shown to be [19]:

$$\frac{V(s)}{E(s)} = \frac{K_M}{s^2+C_1 s+C_0}$$

The constants K_M, C_0, and C_1 depend on the characteristics of the vehicle and the DC motor, the load, and the nominal wind and vehicle velocities. Typical values of these parameters are given in Table 2.2.

The transformed, linear vehicle model can be written in state-space form as:

$$\begin{bmatrix} \dot{x}(t) \\ \dot{v}(t) \\ \dot{a}(t) \end{bmatrix} = \begin{bmatrix} 0 & 1 & 0 \\ 0 & 0 & 1 \\ 0 & -C_0 & -C_0 \end{bmatrix} \begin{bmatrix} x(t) \\ v(t) \\ a(t) \end{bmatrix} + \begin{bmatrix} 0 \\ 0 \\ K_M \end{bmatrix} E(t) + \begin{bmatrix} 0 \\ 0 \\ \omega(t) \end{bmatrix} \qquad (2.1)$$

where $x(t)$, $v(t)$, and $a(t)$ are the position, velocity, and acceleration state variables, and $E(t)$ is the voltage applied to the motor.

Position and velocity measurements, $x_m(t)$ and $v_m(t)$, are represented via:

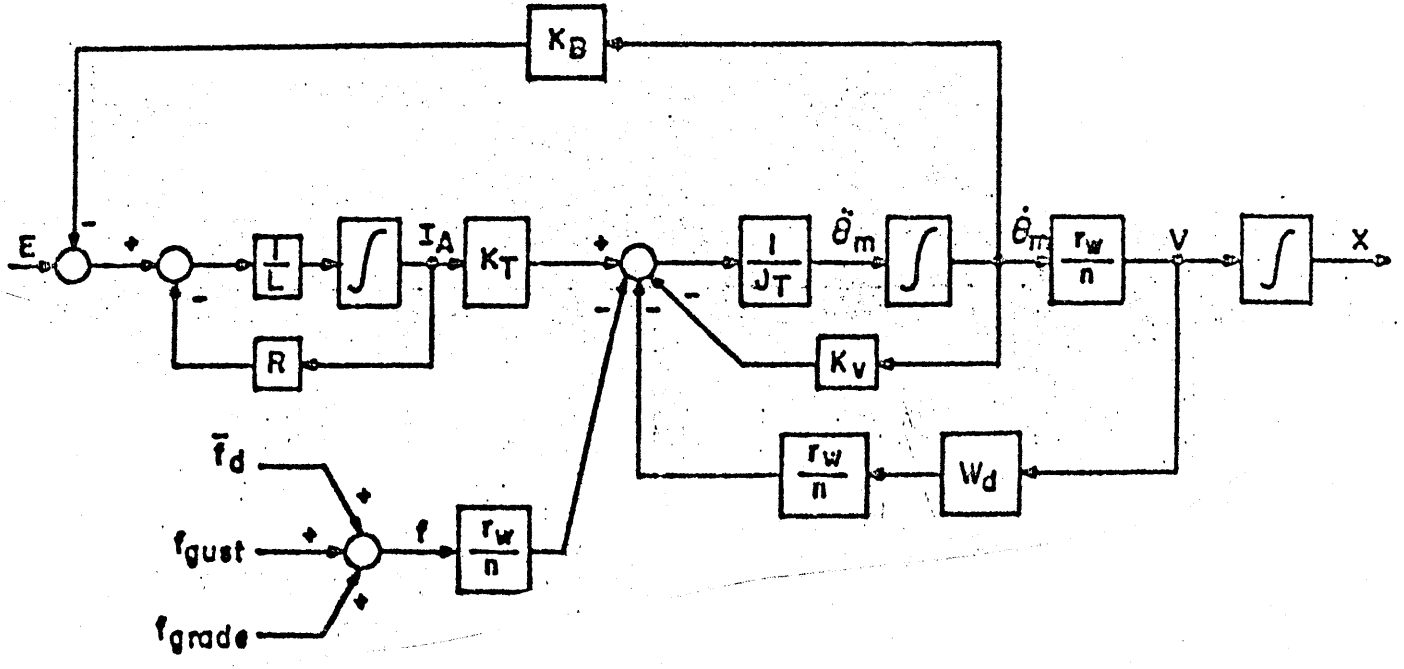

Figure 2.5
Linear Vehicle and DC Motor Block Diagram; Pitts [19]

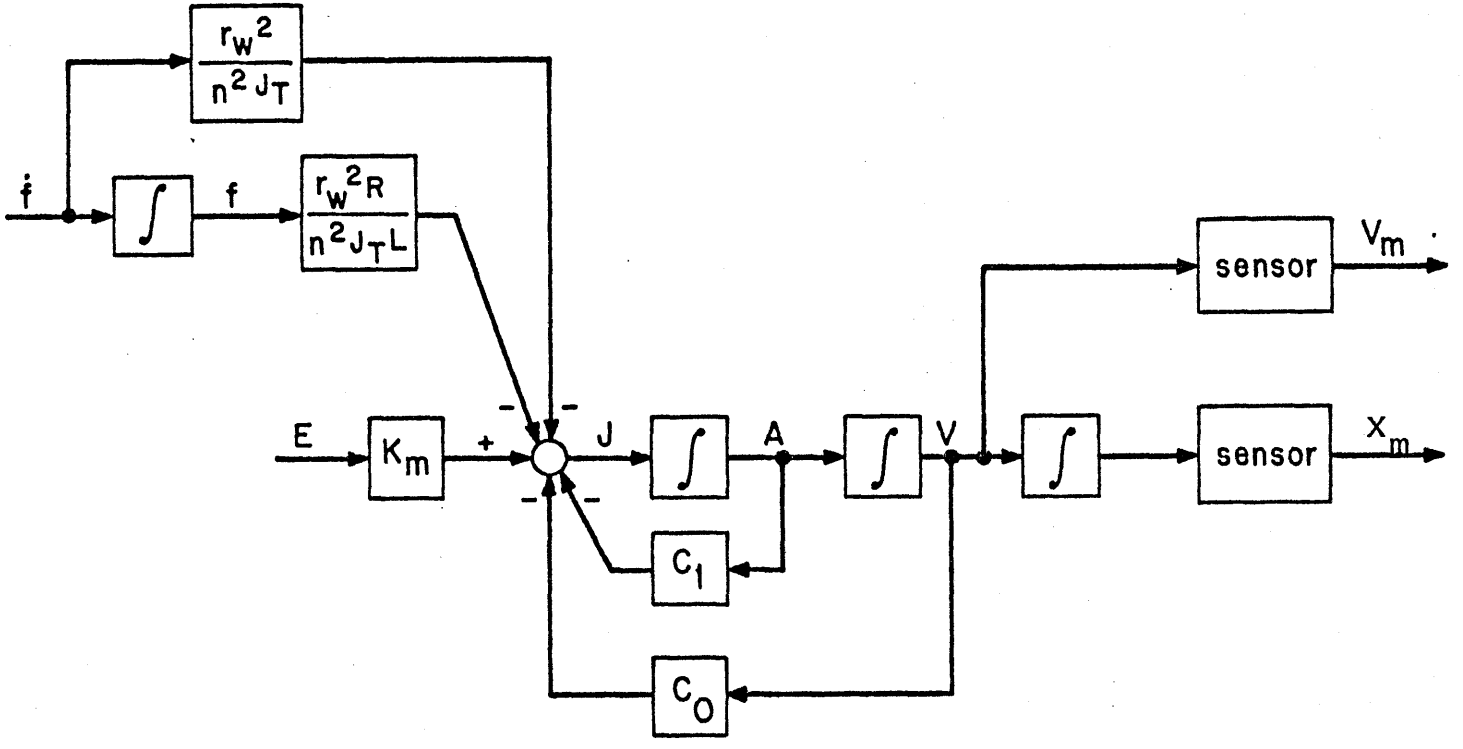

Figure 2.6

Transformed, Linear Vehicle and DC Motor Block Diagram; Pitts [19]

	EMPTY VEHICLE	NOMINAL VEHICLE	FULL VEHICLE
MASS(Kg)	663	979	1295
Km (m/S^3 Volt)	24.18	16.79	12.86
C_o (S^{-2})	234.84	162.98	124.78
C_1 (S^{-1})	39.10	39.08	39.07

Table 2.2

Transformed Vehicle Model Parameters [26]

$$\begin{bmatrix} x_m(t) \\ v_m(t) \end{bmatrix} = \begin{bmatrix} 1 & 0 & 0 \\ 0 & 1 & 0 \end{bmatrix} \begin{bmatrix} x(t) \\ v(t) \\ a(t) \end{bmatrix} + \begin{bmatrix} n_1(t) \\ n_2(t) \end{bmatrix} \qquad (2\text{-}2)$$

We will refer to (2-1) as the vehicle state equation and (2-2) as the measurement equation.

The effects of external disturbances (i.e., wind, grade) and modelling errors are included in the vehicle state equation via the plant noise process $\omega(t)$. These modelling errors are the errors made by representing the complex dynamics of the actual AGT vehicle with a simplified linear model. The errors are due in part to the linearization of the drag force, the assumptions made about the vehicle's propulsion system and load in the choice of K_M, C_0, and C_1, and the effects of unmodelled dynamics such as rolling friction, bearing loss, and slippage.

The measurement noise vector $\underline{n}(t)$ represents the difference between the vehicle's actual position and velocity and the measured values.

A block diagram of the vehicle model given by equations (2-1) and (2-2) is shown in Figure 2.7.

2.5 Discrete Equivalent of the Continuous-Time Model

The continuous-time vehicle model equations (2-1) and (2-2) represent the behavior of the vehicle at all time instants t. An equivalent discrete-time representation can be developed [31] which characterizes the vehicle behavior by quantities defined at equally spaced, discrete instants of time

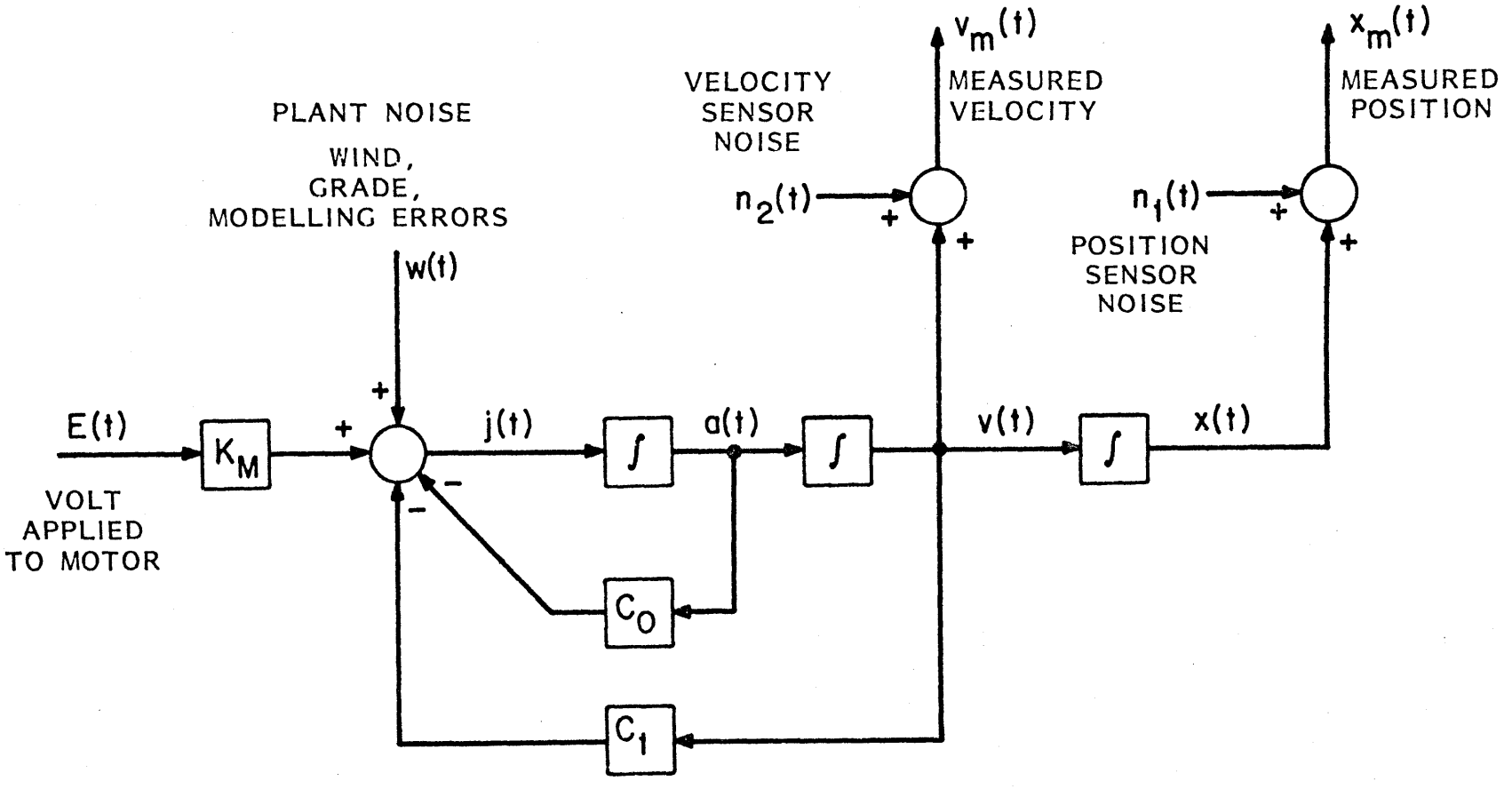

Figure 2.7
Vehicle Block Diagram (Sensor and Plant Noise Incl.)

$k\Delta t$, $k=0,1,\ldots$, where the time period Δt is called the sampling interval and $1/\Delta t$ is the sampling rate. The discrete-time vehicle model, required for the implementation of the GLR algorithm in a digital computer, will be of the following form:

$$\underline{x}(k+1) = \Phi\underline{x}(k) + B\underline{u}(k) + \underline{\omega}(k) \tag{2-3}$$

$$\underline{z}(k) = C\underline{x}(k) + \underline{n}(k) \tag{2-4}$$

with state vector $\underline{x}(k) = [x(k), v(k), a(k)]^T$, measurement vector $\underline{z}(k) = [x_m(k), v_m(k)]^T$ and control input $\underline{u}(k) = E(k)$. The discrete-time plant noise and sensor noise processes $\underline{\omega}(k)$ and $\underline{n}(k)$ are modelled to be statistically equivalent to the continuous-time processes $\underline{\omega}(t)$ and $\underline{n}(t)$. The details of the transformation from continuous-time to discrete-time are presented in Appendix B.

One significant difference between the continuous-time and discrete-time state equations is that the discrete-time model assumes that the control input $\underline{u}(k)$ is piece-wise constant over the sampling interval (eg., using a zero-order hold). The actual control, $\underline{u}(t)$, applied to the vehicle plant, however, may be a continuous signal. The effects of this assumption on the detection system is discussed in section 4.3.5.

2.6 Vehicle Failure Detection

It is essential that accurate knowledge of vehicle states is available to the control system. It is also essential that the vehicle's propulsion system be able to respond effectively to the control system's commands.

Both the sensor and propulsion systems are critical to the safety of the vehicle. Sudden failures of these systems have the potential to create disasterous results. It is desirable to provide a system to detect and respond to such vehicle component failures.

A failure detection system must have the ability to detect safety threatening failures with high probability. However, in order to minimize unnecessary delays, the systems must have a small probability of signalling alarms when no failure has occurred. Un-modelled external forces such as wind and guideway grades are likely to cause such false alarms.

The failure detection method to be presented in this report operates by comparing observations from sensors with what those observations are expected to be based on predictions from the discrete-time vehicle model. Failures will cause the predicted and actual observations to behave significantly different. Simplistically, the strategy is similar to failure detection via a dual redundant set of sensors; failures are detected when the sensor outputs differ. Analogously, the vehicle model will serve as half of the redundant pair.

To determine how the modelled observations will differ from the actual observations in the event of a failure, simple failure models will be developed for components of the vehicle. The components which will be examined are sensors, which measure vehicle states (eg., position and velocity), and actuators which implement control commands (eg., the propulsion system).

2.7 Sensor/Actuator Failure Models

Sensors and actuators can both be modelled by the simple block diagram below:

The input to a sensor is a state to be measured (e.g., the vehicle's actual velocity), and the output is a measurement of that state. The input to an actuator is a control signal, and its output is an appropriate action necessary to implement the control (eg., the application of a force or voltage). Noise is assumed to be always present in the sensor or actuator, and represents the difference between the actual state and its quantified measurement, or the difference between the desired control and the control action actually implemented by the actuator.

Failures in sensors and actuators can both be modelled in similar fashions. We have compiled a list of possible failure types or modes which are likely to occur in these devices:

1) Additive Bias - the output of the device is continually offset by a constant level.

2) Jump - the output of the device is momentarily offset by a constant level, eg., the occurrence of a brief disturbance such as a sudden noise spike or "glitch".

3) Scale Factor Change - the gain of the device has changed such that the output is in error by a constant percentage.

4) Zero Output - the output remains at the lowest or "zero" level.

5) Hard-Over - the output remains at the highest or maximum level.

6) Stuck - the output remains at an intermediate level.

A block diagram of the device which can be used to model these failures is shown in Figure 2.8.

The input/output relationships for these sensor or actuator failures are shown in Figure 2.9. A hypothetical output trajectory is shown in Figure 2.10a for an unfailed device. The output which would be obtained if a failure had occurred at time θ is shown in Figure 2.10b-g.

The effect of these failures on the failed device outputs shown in Figure 2.10b-g is similar in that there occurs a sudden departure of the output from its expected behavior. The similarity between the failed output trajectories is especially apparent when the state, $\underline{x}(t)$, or the control, $\underline{u}(t)$, remain constant over a time interval, as is the case immediately following the failure in the hypothetical examples of Figure 2.10. This will always be the case when the dynamics of the system are relatively slow compared to the sampling rate of the control and detection systems, as in an AGT vehicle.

The similarity of the various failure modes to additive bias failures will be employed in the development of the detection algorithm, as failures modelled as biases have special properties which can be utilized.

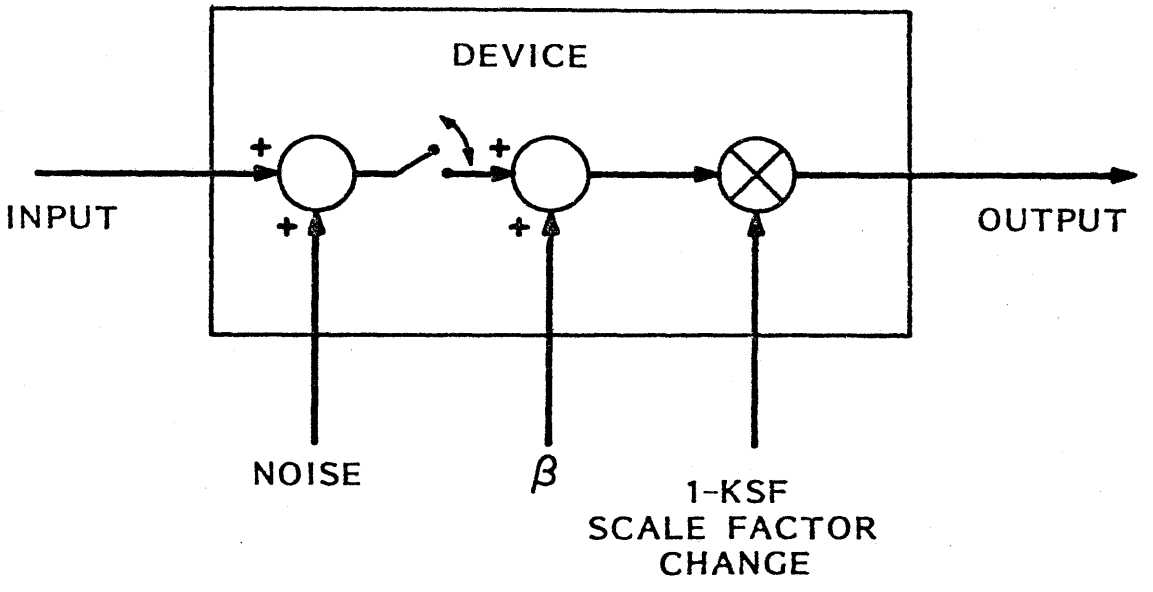

Figure 2.8
Failed Sensor/Actuator Model

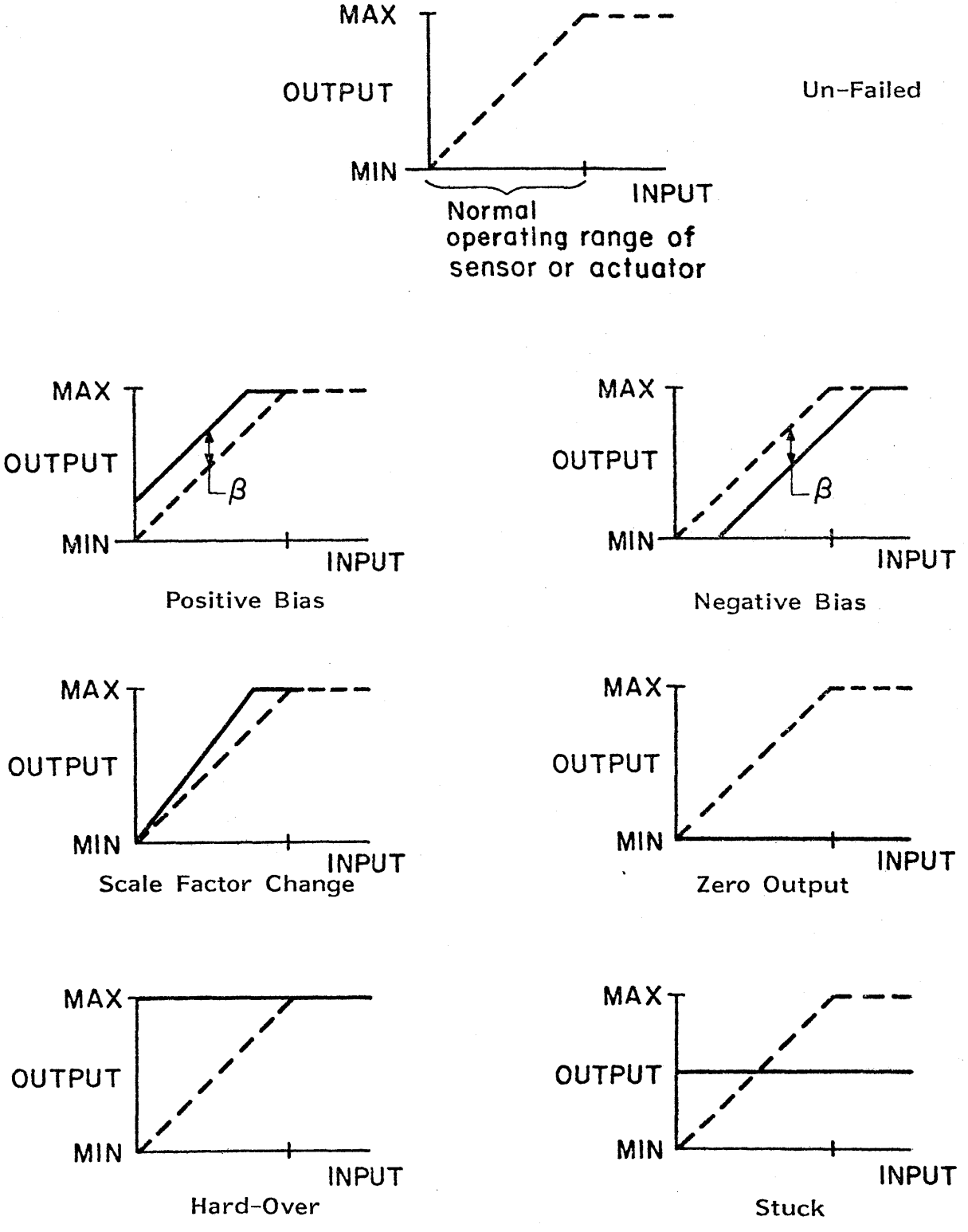

Figure 2.9

Failed Sensor/Actuator Input-Output Relationships

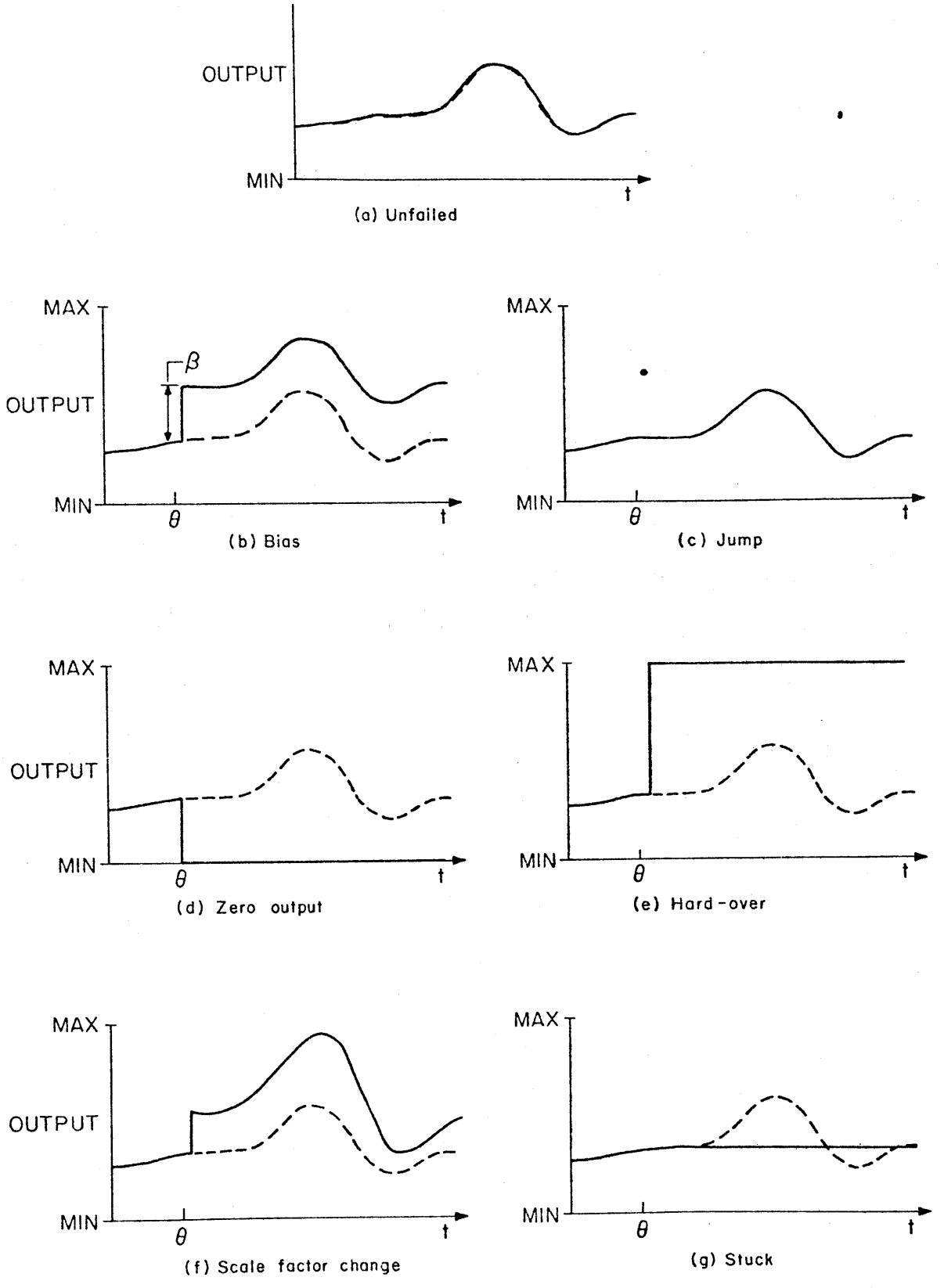

Figure 2.10 - Failed Sensor/Actuator Output Trajectories

2.8 Summary

In this chapter, a mathematical model of an AGT vehicle has been presented which will be used in developing a methodology for failure detection based on the generalized likelihood ratio method. Models of various failure modes have been developed. An important feature of these failure modes is that under certain conditions they can be modelled in a similar fashion, i.e., as additive biases. In the following chapter, we show how this approach to modelling failure modes can be exploited to develop a computer-based algorithmic procedure for detecting when a failure has occurred.

CHAPTER III

THE GLR APPROACH FOR FAILURE DETECTION

3.1 Introduction

The generalized likelihood ratio method for event detection in linear dynamic systems was developed by Willsky and Jones [32,33]. The generalized likelihood ratio is an easily implemented software algorithm. It processes data in real-time to detect the occurrance of sudden departures of a real system from a simple idealized linear model. The technique has successfully been applied to a wide variety of complex systems, such as for failure detection in aircraft systems [34], detection of incidents on freeways [35], and detection of cardiac arrythmias [36]. The GLR method has been shown to be a flexible and systematic approach, capable of detecting and identifying numerous types of failures and events.

As shown in Figure 3.1, the entire GLR algorithm consists of three main components: I) a Kalman-Bucy Filter, II) a correlator, and III) a decision rule. A linear model of the vehicle is embedded in a Kalman-Bucy filter [37]. Predictions of vehicle states generated by the model are compared to actual measurements from the vehicle's sensors; the difference between the two is called the residual. When a vehicle failure occurs, the residuals will have a unique behavior, or signature, depending on the type of failure. In the GLR calculations, the residuals are compared, or correlated, to each member of a precomputed set of signatures. The resulting likelihood ratios are measures of the correlation to each of the failure signatures. These likelihood ratios are then used in a decision rule to determine whether a failure has occurred, and if so, to decide among the possible failure types.

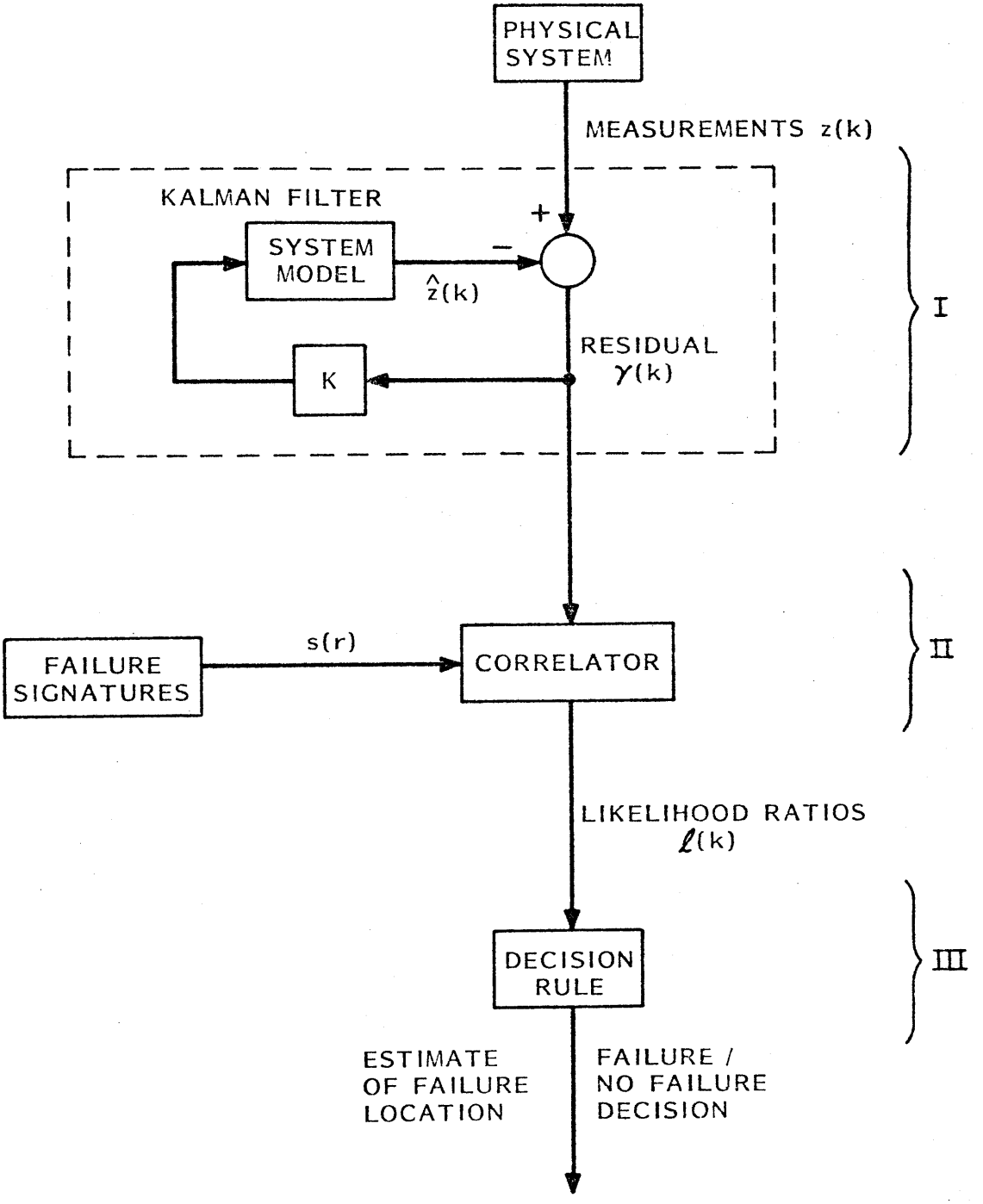

Figure 3.1

GLR Algorithm Block Diagram

The details of the GLR algorithm will now be presented.

3.2 System Model

The GLR method assumes a discrete-time state space description of a linear dynamical systems(*) described by:

State equation:

$$\underline{x}(k+1) = \Phi\underline{x}(k) + B\underline{u}(k) + \underline{\omega}(k) \tag{3-1}$$

Measurement equation:

$$\underline{z}(k) = C\underline{x}(k) + \underline{n}(k) \tag{3-2}$$

Here $\underline{x}$ is the state vector and $\underline{u}$ is a known control input; $\underline{\omega}$ and $\underline{n}$ are modelled as independent, zero mean, uncorrelated Gaussian random sequences with covariances:

$$E[\underline{\omega}(j)\ \underline{\omega}^T(k)] = \begin{cases} Q & j=k \\ 0 & j\neq k \end{cases}$$

$$E[\underline{n}(j)\ \underline{n}^T(k)] = \begin{cases} R & j=k \\ 0 & j\neq k \end{cases}$$

In section 4.2.1 more will be said about the modelling of these noise processes.

3.3 Kalman-Bucy Filter

A Kalman-Bucy filter [37] is designed for the system model (3-1) and (3-2). The filter is given by:

---

*We will restrict our attention to time-invariant systems, although extension to the time-varying case is easily done.

Predicted State Estimate:

$$\hat{\underline{x}}(k|k-1) = \Phi\hat{\underline{x}}(k-1|k-1) + B\underline{u}(k-1) \tag{3-3}$$

Residual:

$$\underline{\gamma}(k) = \underline{z}(k) - C\hat{\underline{x}}(k|k-1) \tag{3-4}$$

Updated State Estimate:

$$\hat{\underline{x}}(k|k) = \hat{\underline{x}}(k|k-1) + K\underline{\gamma}(k) \tag{3-5}$$

where $\underline{x}(k|j)$ is the estimate of the state $\underline{x}(k)$ given the measurements $\underline{z}(0)$, $\underline{z}(1),\ldots,\underline{z}(j)$. With Gaussian disturbances $\underline{\omega}$ and $\underline{n}$, $\hat{\underline{x}}(k|k)$ is the optimal minimum mean squared error state estimate. The process $\underline{\gamma}(k)$ is called the residual or innovations sequence, and will be a zero mean, uncorrelated, Gaussian process when no failure has occurred. For time-invariant systems, the optimal steady-state gain K is computed by solving the discrete algebraic matrix Riccati equation for the steady-state error covariance of $\hat{\underline{x}}(k|k-1)$, $\sum_p$:

$$-\sum_p + \Phi\sum_p\Phi^T + Q - \Phi^T\sum_p C^T[C\sum_p C^T + R]^{-1} C\sum_p\Phi = 0 \tag{3-6}$$

Then the error covariance of $\hat{\underline{x}}(k|k)$ is given by:

$$\sum = \sum_p - \sum_p C^T[C\sum_p C^T + R]^{-1} C\sum_p \tag{3-7}$$

and the Kalman gain K can then be found:

$$K = \sum C^T R^{-1} \tag{3-8}$$

The steady-state covariance V of the residual is given by:

$$V = C\sum_{p} C^{T} + R \tag{3-9}$$

3.4 Failure Signatures

3.4.1 Modelling of Failures

Failures in the system's actuators or sensors can be modelled by the addition of two failure vectors, $\underline{f}_D$ and $\underline{f}_S$, to the system model (3-1), (3-2) as follows:

$$\underline{x}(k+1) = \Phi\underline{x}(k) + B\underline{u}(k) + \underline{\omega}(k) + \underline{f}_D(k+1,\theta) \tag{3-10}$$

$$\underline{z}(k) = C\underline{x}(k) + \underline{n}(k) + \underline{f}_S(k,\theta) \tag{3-11}$$

The vector $\underline{f}_D(k,\theta)$ represents the effect (on the system dynamics) at time k of an actuator failure which occurred at time θ. The vector $\underline{f}_S(k,\theta)$ similarly represents sensor failures. The failures discussed in section 2.7 can be modelled by appropriate specification of $\underline{f}_D$ and $\underline{f}_S$. These specifications are shown in Table 3.1. Biases are modelled by the addition of a constant vector, $\underline{\nu}$, to the state or measurement equation. For example, assume that the measurement equation (3-11) represents two independent sensor measurements. A bias of size β to the first sensor is represented by the choice.

$$\underline{f}_S = \underline{\nu} = \begin{bmatrix} 1 \\ 0 \end{bmatrix} \beta \tag{3-12}$$

TABLE 3.1

FAILURE VECTOR SPECIFICATION; MODELLING OF FAILURES MODES

FAILURE MODE	SPECIFICATION
Actuator Bias	$\underline{f}_D(k+1,\theta) = \begin{cases} \underline{\nu} & k+1 \geq \theta \\ 0 & k+1 < \theta \end{cases}$
Sensor Bias	$\underline{f}_S(k,\theta) = \begin{cases} \underline{\nu} & k \geq \theta \\ 0 & k < \theta \end{cases}$
Actuator Jump (State Jump)	$\underline{f}_D(k+1,\theta) = \begin{cases} \underline{\nu} & k+1 = \theta \\ 0 & k+1 \neq \theta \end{cases}$
Sensor Jump	$\underline{f}_S(k,\theta) = \begin{cases} \underline{\nu} & k = \theta \\ 0 & k \neq \theta \end{cases}$
Actuator Scale factor change, zero output	$\underline{f}_D(k+1,\theta) = \begin{cases} \Delta B\underline{u}(k) & k+1 \geq \theta \\ 0 & k+1 < \theta \end{cases}$
Sensor Scale Factor change, zero output	$\underline{f}_S(k,\theta) = \begin{cases} \Delta C\underline{x}(k) & k \geq \theta \\ 0 & K < \theta \end{cases}$
Hard-over Actuator Stuck Actuator	$\underline{f}_D(k+1,\theta) = \begin{cases} \Delta B\underline{u}(k) \pm \nu & k+1 \geq \theta \\ 0 & k+1 < \theta \end{cases}$
Hard-over Sensor, Stuck Sensor	$\underline{f}_S(k,\theta) = \begin{cases} \Delta C\underline{x}(k) + \underline{\nu} & k \geq \theta \\ 0 & k < \theta \end{cases}$

and a bias in the second sensor by

$$\underline{f}_s = \underline{\nu} = \begin{bmatrix} 0 \\ 1 \end{bmatrix} \beta \qquad (3\text{-}13)$$

We say that the vector $\begin{bmatrix} 1 \\ 0 \end{bmatrix}$ or $\begin{bmatrix} 0 \\ 1 \end{bmatrix}$ represent the locations (i.e., the first or second sensor) or direction (i.e. direction in state-space) of the failure, and that the size of the scalar β (i.e., the size of the bias) is the magnitude of the failure.

Jump failures are modelled in a similar fashion as biases, except for the fact that the additive constant vector $\underline{\nu}$ appears only for a single time step.

Scale factor change failures are modelled by a change in one or more of the elements of the B or C matrices. Zero output failures are actually a subset of scale factor change failures. They are modelled by a change (to zero) in elements of the B or C matrices. Hard-over and stuck device failures are modelled by a scale factor change to zero in the gain matrices B or C, and the addition of a constant value representing the maximum or stuck value of the failed device's output.

3.4.2 Effects of Failures

Failures in the physical system will have a noticeable effect on the Kalman-Bucy filter; the predicted observations generated by the system model will begin to differ from the actual observations from the sensor. The difference between the two will appear in the residual sequence $\underline{\gamma}(k)$. When no failure has occurred, the mean of the residual will be zero; if a failure has occurred, the residual will no longer be zero mean but will behave in a manner

characteristic of the failure. This behavior will be exploited to detect the failures.

The effect that one of the above failure types will have on the Kalman-Bucy filter (3-3)-(3-5) can be computed. Since the system model and the filter are linear, the state estimates and the residuals can each be decomposed into two sequences:

$$\hat{\underline{x}}(k|k) = \hat{\underline{x}}_1(k|k) + \hat{\underline{x}}_2(k) \tag{3-14}$$

$$\underline{\gamma}(k) = \underline{\gamma}_1(k) + \underline{\gamma}_2(k) \tag{3-15}$$

where $\hat{\underline{x}}_1(k|k)$ and $\underline{\gamma}_1(k)$ are the state estimates and residuals, respectively, which would have appeared if the failure had not occurred. The effect of the failure is given by $\hat{\underline{x}}_2(k)$ and $\underline{\gamma}_2(k)$. The sequence $\hat{\underline{x}}_2(k)$ can be computed from one of the following recursive relations:

ACTUATOR FAILURES:

$$\hat{\underline{x}}_2(k) = (I-KC)\Phi\hat{\underline{x}}_2(k-1) + KC\underline{f}_D(k,\theta) \tag{3-16}$$

or,

SENSOR FAILURES:

$$\hat{\underline{x}}_2(k) = (I-KC)\Phi\hat{\underline{x}}_2(k-1) + K\underline{f}_s(k,\theta)$$

with

$$\hat{\underline{x}}_2(k) \equiv 0 \qquad \text{for } k<\theta \tag{3-17}$$

The sequence $\underline{\gamma}_2(k)$, the effect of the failure on the residuals, is then given by:

ACTUATOR FAILURES:

$$\underline{\gamma}_2(k) = C\underline{f}_D(k,\theta) - C\Phi\underline{\hat{x}}_2(k-1) \tag{3-18}$$

or

SENSOR FAILURES:

$$\underline{\gamma}_2(k) = \underline{f}_s(k,\theta) - C\Phi\underline{\hat{x}}_2(k-1) \tag{3-19}$$

After the occurrence of a failure at some unknown time θ, the residual process $\underline{\gamma}(k)$ will no longer be a zero mean sequence; its mean will now be $\underline{\gamma}_2(k)$.

The sequence $\underline{\gamma}_2(k)$ is called the failure signature; it is the "unique" effect of a failure on the residuals. Can we somehow use (3-16)-(3-19) to determine a-priori the behavior of the signature for various failures, so that by looking for the signature in the residuals the failure can be detected? By a re-examination of the failure vector specifications in Table 3.1 we can conclude that the answer in some cases is "yes".

Notice that the failure specifications for bias and jump failures are not state-dependent or control-dependent; the specifications do not depend on the knowledge of $\underline{x}(k)$ or $\underline{u}(k)$. We can thus use (3-16)-(3-19) and the linearity of the filter to write:

$$\underline{\gamma}_2(k) = G(k,\theta)\underline{\nu} \tag{3-20}$$

where $G(k,\theta)$ is a set of precomputable matrices called the failure signature matrices [38,39]. The matrices $G(k,\theta)$ will depend on the type of failure

(i.e., sensor/actuator, bias/jump) but are independent of the unknown a-priori direction or magnitude of the failure vector $\underline{\nu}$.

Unfortunately, the failure specifications (Table 3.1) for the failure types other than biases and jumps are state or control-dependent; their failure signatures will behave differently for different state or control trajectories, which are unknown a-priori. Thus their failure signatures can not be precomputed. However, as we have discussed in section 2.7, these failure types appear similar to bias failures, especially when the state or control remains relatively constant over a detection interval. We will thus develop a detection methodology which is designed to detect solely additive bias failures; we will show via experiments that the detection system can detect the other failure types as well.

The detection of jump failures can be performed in a manner parallel to the methodology to be presented for the detection of bias failures. We have chosen to limit ourselves to bias failures, however, since failures which persist over time are likely to have the worst effects on AGT vehicle safety. Development of failure signatures for jump failures can be found in [38] and [39].

3.5 Detection of Failures

3.5.1 Hypothesis Testing

The problem of detecting a failure can now be reduced to the problem of deciding between different hypotheses:

H_0: the residuals are zero mean (no failure)

H_i: the residuals are not zero mean (a failure has occurred in location i)

Since failures in different locations in the system have characteristic effects on the residuals, the above hypotheses can be re-written as follows:

$$H_0: \quad \underline{\gamma}(k) = \underline{\gamma}_1(k) \qquad \text{(no failures)}$$

$$H_i: \quad \underline{\gamma}(k) = \underline{\gamma}_1(k) + G(k,\theta)\underline{f}_i\beta \qquad \text{(failure of magnitude } \beta \text{ in direction } \underline{f}_i\text{)}$$

Here we have constrained the failure vector $\underline{\nu}=\underline{f}_i\beta$ to lie in a finite set of directions $\{\underline{f}_i\}$ in either state-space (actuator failures) or output-space (sensor failures) [38,39]. Each of these directions correspond to an individual sensor or actuator in the system. $G(k,\theta)$ is either the state bias or sensor bias signature matrix, depending whether the failure direction vector $\underline{f}_i$ represents an actuator or a sensor.

3.5.2 Likelihood Ratio Tests

The hypothesis testing problem can be reduced to the construction of a likelihood ratio test [31]. A likelihood ratio for each hypothesis is given by:

$$L_i(k) = \frac{p(\underline{\gamma}(1),\ldots,\underline{\gamma}(k)\,|\,H_i,\theta,\beta)}{p(\underline{\gamma}(1),\ldots,\underline{\gamma}(k)\,|\,H_0)} \qquad (3\text{-}22)$$

$L_i(k)$ is a random variable having a different mean under each hypothesis. It can thus be used in a decision rule, such as comparing it to a threshold, to decide among the hypothesis.

For each hypothesis i, the maximum likelihood estimates [31] of the failure time θ and the failure magnitude β can be computed. They are the values which maximize the probability density function for the residuals conditioned on the occurrence of a failure in direction i, i.e.,

$$\hat{\theta}_i(k),\ \hat{\beta}_i(k) = \arg \max_{\tilde{\theta},\tilde{\beta}} p(\underline{\gamma}(1),\ldots,\underline{\gamma}(k)\,|H_i,\ \theta=\tilde{\theta},\ B=\tilde{B}) \tag{3-23}$$

The maximum likelihood ratio (MLR) for each hypothesis to be used in the decision rule is then given by:

$$L_i(k) = \frac{p(\underline{\gamma}(1),\ldots,\underline{\gamma}(k)\,|H_i\ \ \theta=\hat{\theta}_i(k),\ \beta=\hat{\beta}_i(k))}{p(\underline{\gamma}(1),\ldots,\underline{\gamma}(k)\,|H_0)} \tag{3-24}$$

3.6 Maximum Likelihood Ratio Computation

Since the residuals have the multivariate Gaussian density, we can take the logarithm of the likelihood ratios, obtaining:

$$\ell_i(k) = 2\ell n\ L_i(k) = \sum_{j=1}^{k} \underline{\gamma}^T(j)V^{-1}\underline{\gamma}(j) \tag{3-25}$$

$$- \sum_{j=1}^{k} \underline{\gamma}(j)-G(j,\hat{\theta}_i(k))\underline{f}_i\hat{\beta}_i(k)]^T\ V^{-1}[\underline{\gamma}(j)-G(j,\hat{\theta}_i(k))\underline{f}_i\hat{\beta}_i(k)]^T$$

By differentiating with respect to $\hat{\beta}_i(k)$, setting the result to zero, and solving for $\hat{\beta}_i(k)$, we can express $\hat{\beta}_i(k)$ as an explicit function of $\hat{\theta}_i(k)$:

$$\hat{\beta}_i(k) = \frac{b_i(k;\hat{\theta}_i(k))}{a_i(k;\hat{\theta}_i(k))} \tag{3-26}$$

with

$$b_i(k;\theta) \equiv \underline{f}_i^T \underline{d}(k,\theta) \tag{3-27}$$

$$= \sum_{j=1}^{k} \underline{f}_i^T G^T(j,\theta) V^{-1} \underline{\gamma}(j)$$

$$= \sum_{j=1}^{k} \underline{s}_i^T(j,\theta) \underline{\gamma}(j)$$

and

$$a_i(k,\theta) = \underline{f}_i^T C(k,\theta) \underline{f}_i \tag{3-28}$$

$$= \sum_{j=1}^{k} \underline{f}_i^T G^T(j,\theta) V^{-1} G(j,\theta) \underline{f}_i$$

The scalars $a_i(k;\theta)$ are a <u>precomputable</u>, deterministic sequence. The scalar $b_i(k,\theta)$ are linear combinations of the residuals, which represent a correlation or matched filter [31] operation between the failure signatures and the residuals. The sequence $\underline{s}_i(j,\theta)$, used in the computation of $b_i(k,\theta)$, is the failure signature $G(j,\theta)\underline{f}_i$ which would appear in the residuals weighted by V^{-1}, the inverse of the residual covariance matrix. We will thus refer to $\underline{s}_i(j,\theta)$ as the <u>weighted failure signature</u>. The weighting process has the effect of giving more attention to elements of the residual which are expected to contain the least amount of background noise.

The likelihood ratio can now be written as:

$$\ell_i(k;\theta) = \frac{b_i^2(k,\theta)}{a_i(k,\theta)} \tag{3-29}$$

The maximum likelihood estimate $\hat{\theta}_i(k)$ is the value of $\theta \leq k$ which maximizes (3-29). Then the maximum likelihood ratio (MLR) for a failure in direction $\underline{f}_i$ is given by

$$\ell_i^*(k) = \ell_i(k; \hat{\theta}_i(k)) \tag{3-30}$$

3.7 Decision Rule

The maximum likelihood ratios ℓ_i^*, each representing the likelihood of a failure in the sensor or actuator represented by $\underline{f}_i$, can be used in a decision rule to decide 1) if a failure has occurred, and 2) if so, in which sensor or actuator.

A possible decision rule is to compare the largest maximum likelihood ratio to a threshold as follows:

$$\max_i \ell_i^* \underset{\text{FAILURE}}{\overset{\text{NO FAILURE}}{\lessgtr}} \varepsilon \tag{3-31}$$

The estimated location of the failure is found by choosing the i which maximized ℓ_i^*, i.e.,

$$\hat{i} = \arg \max_i \ell_i^* \tag{3-32}$$

The location of the failure is then given by $\underline{f}_{\hat{i}}$.

The threshold ε can be chosen to maximize the tradeoff between the false alarm and missed detection probabilities.

3.8 Information Measures

The scalars $b_i(k;\theta)$, equation (3-27), have been given intuitive meaning; they represent the amount of "match" between the signatures and the residuals. However, we have yet to comment on the set $a_i(k;\theta)$, equation (3-28). These scalars are derived from the matrices $C(k;\theta)$, which are called the "information matrices". (An insightful analysis of the information matrices can be found in [39].) Intuitively, $a_i(k;\theta)$ measures the information available in the residuals at time k from a failure of direction $\underline{f}_i$ which occurred at time θ. For this reason we shall coin the name "information measure" to refer to $a_i(k;\theta)$. In essence, the information measures can be thought of as a signal to noise ratio, measuring the ratio of energy in the biased part of the residual sequence (assuming a bias is present) to the energy in the background noise.

The information measures $a_i(k;\theta)$ can provide insight into the behavior of the likelihood ratios following the occurrence of a failure. When no failure has occurred, the likelihood ratios are chi-squared random variables with mean one. After occurrence of a bias failure at time θ of magnitude β in direction $\underline{f}_i$, the likelihood ratios $\ell_i(k;\theta)$ are non-central chi-squared random variables with mean given by:

$$E[\ell_i(k;\theta)] = 1 + \beta^2 a_i(k;\theta) \tag{3-33a}$$

and variance:

$$\text{Var}[\ell_i(k;\theta)] = 2 + 4\beta^2 a_i(k;\theta) \tag{3-33b}$$

A failure, therefore, has the effect of moving the mean of the likelihood ratios away from one, as shown in Figure 3.2.

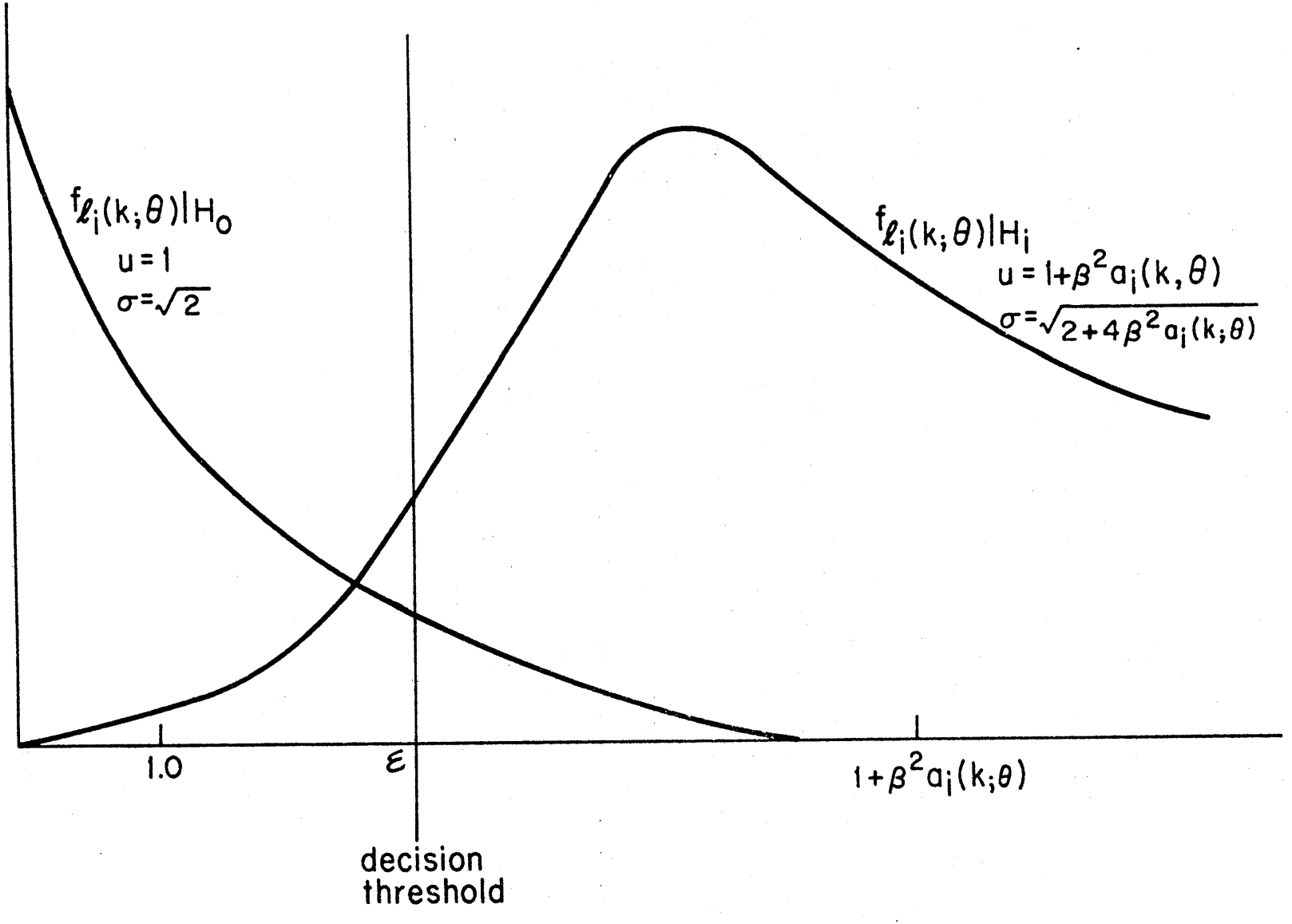

Figure 3.2 - Likelihood Ratio Densities Under No-Failure/Failure Hypotheses

The relative ease with which a bias failure can be detected thus depends on the magnitude of the bias, β, and the behavior of the information measures; the farther apart the means of the distributions are, the higher the probability the failure will be detected.

3.9 Simplifications

3.9.1 Time Invariance

Since the system (3-1), (3-2) is assumed time invariant, the failure signatures are functions of

$$r = k - \theta \tag{3.34}$$

i.e., the time since the occurrence of the failure. Thus, at each time step k, the following set of k correlations are computed

$$b_i(k,r) = \sum_{j=0}^{r} \underline{s}_i^T(j)\underline{\gamma}(k-r+j) \qquad \text{for } r=0 \text{ to } k-1 \tag{3-35}$$

with

$$\underline{s}_i^T(j) = \underline{f}_i^T G^T(j) V^{-1} \tag{3-36}$$

the weighted failure signature. At each time step k we are thus hypothesizing the possible occurrence of a failure for every time θ between 1 and k inclusive. We are in essence "sliding" the failure signatures across the residuals $\underline{\gamma}(1),\ldots,\underline{\gamma}(k)$, correlating it with the residuals at each step along the way (Figure 3.3).

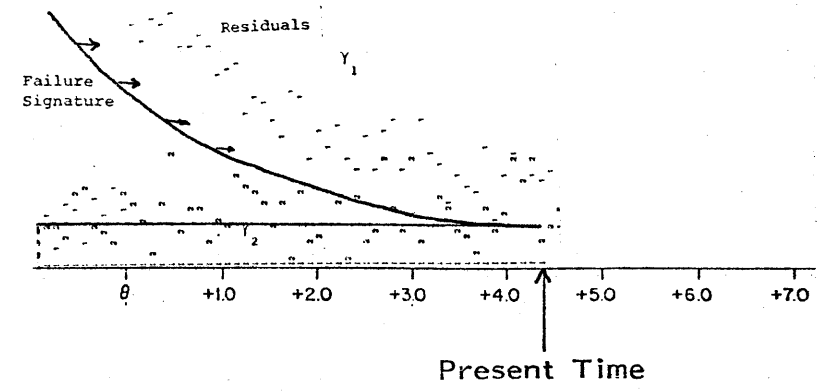

Poor Correlation

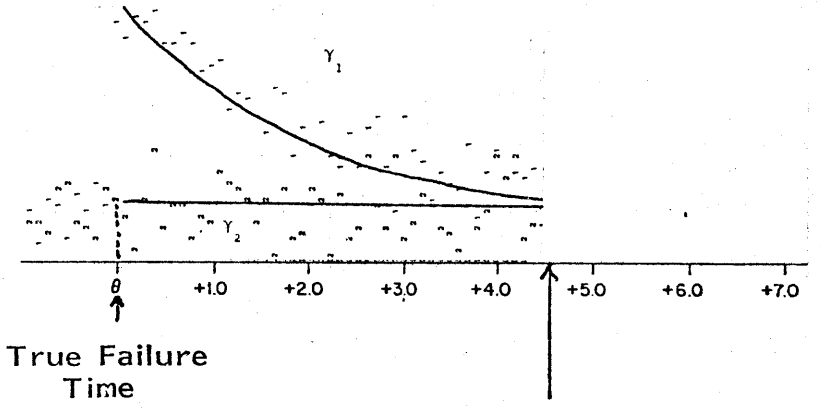

Optimal Correlation

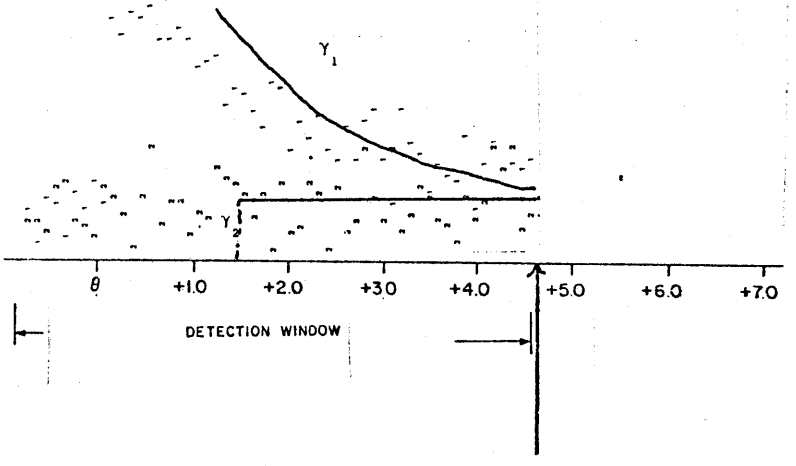

Poor Correlation

Figure 3.3
Correlation of Failure Signature with Residuals

3.9.2 Detection Window

As k increases, however, so does the number of possible values of θ. Thus implementation of the above scheme involves a growing number of correlation or matched filter computations at each step, and we need the entire precomputed signature $\underline{s}(r)$, r=0,...,k-1. Willsky and Jones [32,33] suggest, as a solution to this problem, limiting the maximization over θ to a finite window $k-M \leq \theta \leq k-N$. The assumptions made in the use of this simplification are that no decision can be made with less than N+1 observations, and that failures which occurred before time k-M should have already been detected. With the use of this detection "window", the signature, $\underline{s}(r)$, need be precomputed for $N \leq r \leq M$.

The set $a_i(k;\theta)$ is also a function of $r = k - \theta$ only. The shape of the curve $a_i(r)$, r=0,..., can provide information useful to the determination of an appropriate detection window. For example, the number of steps until convergence of $a_i(r)$ to a steady-state value is a useful indicator for the length of the window to be chosen, for additional observations will provide no additional information about a failure in direction $\underline{f}_i$. Failures for which $a_i(r)$ do not reach steady-state values imply that these failures, no matter how small the magnitude may be, will eventually be detected given a long enough detection window, since more information about the failure is obtained at each succeeding step.

3.10 GLR Algorithm Summary

A summary of the steps required for the implementation of the GLR algorithm is provided below. The steps are divided into those done a-priori and those performed during on-line operation of the algorithm (Figure 3.4).

I. Pre-Computable Calculations

1) System Model [Sec. 3.2, equations (3-1)-(3-2)]

Determine a linear, discrete-time state-space system model:

$$\underline{x}(k+1) = \Phi\underline{x}(k) + B\underline{u}(k) + \underline{\omega}(k)$$

with measurements

$$\underline{z}(k) = C\underline{x}(k) + \underline{n}(k)$$

Choose plant and sensor noise covariance matrices Q and R.

2) Kalman-Bucy Filter [Sec. 3.3, equations (3-6)-(3-9)]

Solve the discrete algebraic matrix Riccati equation for the predicted error covariance matrix Σ_p.

Compute the updated error covariance matrix Σ.

Compute the Kalman gain matrix K.

Compute the residual covariance matrix V and its inverse V^{-1}.

3) Detection Window [Sec. 3.9.2]

Choose the detection window parameters $0 \leq N \leq M$ such that the search for failures will be done in the interval

$$k - M \leq \theta \leq k-N$$

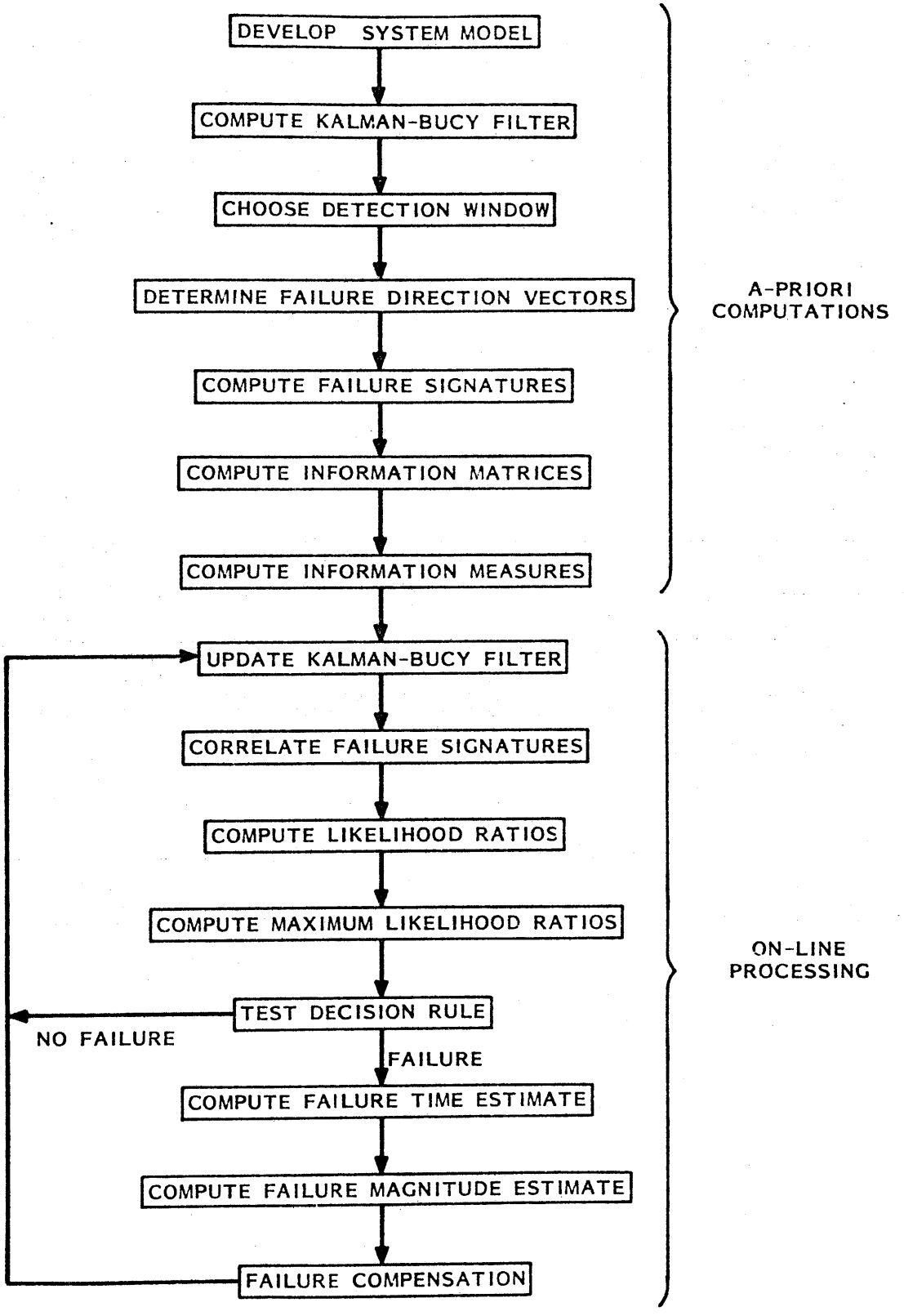

Figure 3.4 - GLR Algorithm Steps

4) Failure Direction Vectors [Sec. 3.5.1]

Determine the set $\{\underline{f}_i\}$ of failure direction vectors. Each vector will correspond to a sensor or actuator for which failure detection is to be performed.

5) Failure Signature Matrices [Sec. 3.4.2, references 38,39]

Compute the set of actuator and/or sensor failure signature matrices G(r) r=0,...,M.

6) Weighted Failure Signatures [Sec. 3.6, equations (3-27),(3-36)]

Compute the weighted set of failure signatures $\underline{s}_i(r)$ r=N,...,M for each failure direction $\underline{f}_i$.

7) Information Matrices [equations (3-28), references 38,39]

Compute the set of actuator and/or sensor failure information matrices C(r) r=N,...,M.

8) Information Measures [Sec. 3.6, 3.8, equation (3-28)]

Compute the set of information measures $a_i(r)$ r=N,...,M for each failure direction $\underline{f}_i$.

II. On-line Processing

The following steps are performed at each step k during the on-line operation of the failure detection system.

9) Kalman-Bucy Filter Update [Sec. 3.3, equations (3-3)-(3-5)]

Compute the predicted state estimate $\hat{\underline{x}}(k|k-1)$.

Compute the residual $\underline{\gamma}(k)$. The residuals

$\gamma(k)$,...,$\gamma(k-M)$ are kept in storage.

Compute the updated state estimate $\hat{\underline{x}}(k|k)$.

10) Failure Signature Correlations [Sec. 3.6, 3.9.1, equations (3-27),(3-35)]

"Slide" the failure signatures $s_i(r)$ through the detection window, computing the correlations $b_i(r)$ at each step r=N,...,M.

11) Likelihood Ratio Functions [Sec. 3.6, equation (3-29)]

Compute the likelihood ratios $\ell_i(r)$ r=N,...,M for each possible failure time in the detection window and for each failure direction $\underline{f}_i$.

12) Maximum Likelihood Ratios [Sec. 3.6, equation (3-30]

Choose the maximum (over the detection window) likelihood ratio ℓ_i^* for each failure direction.

13) Decision Rule [Sec. 3.7, equations (3-31),(3-32)]

Use the maximum likelihood ratios ℓ_i^* in a decision rule to decide if a failure has occurred, and if so, its location. If no failure, return to step 9.

Example decision rule: Choose the maximum $\ell_{\hat{i}}^*$ of the set ℓ_i^*. Compare $\ell_{\hat{i}}^*$ to a threshold ε to decide if a failure has occurred.

14) Failure Time Estimate [Sec. 3.6]

Choose $\hat{r}$ which maximized $\ell_{\hat{i}}(r)$. The maximum likelihood estimate of the failure time is $\hat{\theta} = k - \hat{r}$.

15) Failure Magnitude Estimate [Sec. 3.6, equation (3-26)]

Compute the maximum likelihood estimate of the failure magnitude $\hat{\beta} = b_{\hat{i}}(\hat{r}) / a_{\hat{i}}(\hat{r})$.

CHAPTER IV

APPLICATION OF THE GLR METHOD TO THE AGT VEHICLE

4.1 Introduction

The GLR algorithm will be illustrated by applying the method to the AGT vehicle failure detection problem described in chapter two. We will present the results of computer experiments testing the algorithms' performance in detecting sensor and propulsion system failures which can be modelled as biases. The effects of non-failure external disturbances such as noise, maneuvers, wind and grade on the algorithm will also be evaluated.

A number of important performance issues are to be examined via the examples presented in this chapter. Tradeoffs exist among the following performance indices:

1) Detection probability
2) False alarm probability
3) Time to detect
4) Probability of correct failure location identification

With the GLR algorithm as a foundation, systematic performance tradeoffs are possible; the principal design variables include:

1) System model- Increasing model complexity can result in improved detection algorithm performance, often at the cost of increased sensitivity to disturbances and un-modelled effects, leading to higher false alarm rates. Simplified models, on the other hand, may be unable to detect certain failures altogether.

2) Sensor configurations- Physically redundant sensors will improve the distinguishability of different failure locations, at the cost of additional hardware.

3) Detection Window Length- For certain failures, correct detection and identification can be assured at the expense of delayed decisions.

4) Detection sensitivity- Algorithm detection sensitivity can be optimized subject to false alarm probability constraints through the choice of decision rule thresholds and assumed plant and sensor noise intensities.

Our methodology for illustrating these design variables is organized as follows.

In section 4.2 the GLR algorithm will be applied to a typical AGT vehicle, using the vehicle model by Pitts. Experimental simulation results in detection of bias failures will be presented in section 4.3. Problems in distinguishing wind and grade forces from propulsion system failures when a detailed model is used will be demonstrated. Then section 4.4 illustrates how simplified vehicle models can decrease the algorithm's sensitivity to wind and grade. Section 4.5 provides an alternative to model choice by means of physically redundant sensors to address the problem of identification delay. Finally, detection of failure types other than biases will be addressed in section 4.6.

4.2 Design of the Algorithm - Pitts' Vehicle Model

This section shows how the steps outlined in section 3.10 can be followed to apply the GLR algorithm to the AGT vehicle.

System Model (Step 1)

4.2.1 Dynamics and Measurements

The transformed, linear, continuous-time vehicle model by Pitts [19] is chosen to represent the vehicle dynamics. The state equation is repeated here:

$$\begin{bmatrix} \dot{x}(t) \\ \dot{v}(t) \\ \dot{a}(t) \end{bmatrix} = \begin{bmatrix} 0 & 1 & 0 \\ 0 & 0 & 1 \\ 0 & -c_0 & -c_1 \end{bmatrix} \begin{bmatrix} x(t) \\ v(t) \\ a(t) \end{bmatrix} + \begin{bmatrix} 0 \\ 0 \\ K_M \end{bmatrix} E_c(t) + \begin{bmatrix} 0 \\ 0 \\ \omega(t) \end{bmatrix} \tag{2-1}$$

The position and velocity sensor measurements are represented in the measurement equation:

$$\begin{bmatrix} x_m(t) \\ v_m(t) \end{bmatrix} = \begin{bmatrix} 1 & 0 & 0 \\ 0 & 1 & 0 \end{bmatrix} \begin{bmatrix} x(t) \\ v(t) \\ a(t) \end{bmatrix} + \begin{bmatrix} n_1(t) \\ n_2(t) \end{bmatrix} \tag{2-2}$$

For illustration purposes, the constants C_0, C_1, and K_M were chosen to represent the nominal personal rapid transit vehicle of Table 2.2. A 0.10 second sampling interval (10 HZ sampling rate) was chosen as representative for AGT vehicles [26]. The discrete-time equivalent of the vehicle model (2-1), (2-2) was computed (Appendix B) and is given below:

$$\underline{x}(k+1) = \Phi\underline{x}(k) + BE_c(k) + \underline{\omega}(k) \tag{4-1}$$

$$\underline{z}(k) = C\underline{x}(k) + \underline{n}(k) \tag{4-2}$$

with $\underline{x}(k) = [x(k)v(k)a(k)]^T$, $\underline{z}(k) = [x_m(k)v_m(k)]^T$

$\underline{\omega}(k) = [\omega_1(k)\omega_2(k)\omega_3(k)]^T$, $\underline{n}(k) = [n_1(k)n_2(k)]^T$

and

$$\Phi = \begin{bmatrix} 1.0 & 8.79E\text{-}2 & 1.74E\text{-}3 \\ 0 & 0.717 & 1.99E\text{-}2 \\ 0 & -3.25 & -6.25E\text{-}2 \end{bmatrix}$$

$$B = \begin{bmatrix} 1.25E\text{-}3 \\ 2.92E\text{-}2 \\ 3.35E\text{-}1 \end{bmatrix} \qquad C = \begin{bmatrix} 1 & 0 & 0 \\ 0 & 1 & 0 \end{bmatrix}$$

4.2.2 Characterization of Plant and Sensor Noise

In section 3.1 we stated that the plant noise process $\underline{\omega}(k)$ and the sensor noise process $\underline{n}(k)$ are modelled as independent, zero mean, uncorrelated Gaussian sequences with covariances

$$E[\underline{\omega}(j)\underline{\omega}^T(k)] = \begin{cases} Q & j=k \\ 0 & j\neq k \end{cases}$$

$$E[\underline{n}(j)\underline{n}^T(k)] = \begin{cases} R & j=k \\ 0 & j\neq k \end{cases}$$

The numerical values chosen for Q and R in essence determine the sensitivity of the Kalman filter, and hence of the detection algorithm. This choice, in

conjunction with the decision rule, will determine the algorithm's sensitivity to both actual failures, and external disturbances which may cause false alarms.

Finding appropriate numerical values for Q and R can often be a difficult task. If it is known that $\underline{\omega}(k)$ and $\underline{n}(k)$ are indeed Gaussian with statistics which can be determined, these values should be used; the filter will then be optimal. In reality, however, the processes which $\underline{\omega}(k)$ and $\underline{n}(k)$ model are not necessarily, or even likely, Gaussian processes. This nevertheless does not constrain systematic tradeoffs in algorithm performance as measured by false alarms and missed detections. The matrices Q and R can be used <u>parametrically</u> to facilitate the algorithm's performance tradeoffs.

In this study, in order to illustrate the GLR methodology, the characterization of the plant and sensor noise was done in a relatively ad-hoc procedure. Lacking accurate information, it was estimated that the standard deviation (1σ level) of the noise in the voltage applied to the motor, E(k), compared to the voltage command, $E_c(k)$, might be on the order of 1.0 volt (1% at 10 m/s line speed).

Noise in the voltage applied to the motor propagates into the position, velocity, and acceleration states during each sampling interval. The noise can be modelled in the discrete-time state equation (4-1) by the correlated random variables $\omega_1(k)$, $\omega_2(k)$ and $\omega_3(k)$ which comprise the plant noise covariance matrix Q was computed (Appendix B) to be a statistically equivalent

representation of the noise in the motor voltage, and is given in Table 4.1.

Position measurements were modelled to contain noise having a 1σ level of 0.1 meter. The 1σ level of the velocity sensor noise was chosen to be 0.1 m/s and is assumed to be uncorrelated with the position sensor noise. These values were chosen to be consistent with the simulations done in [26]. The resulting covariance matrix R of the sensor noise vector $\underline{n}(k)$ appears in Table 4.1.

If the statistics of the plant and sensor noise processes were known with more accuracy, the same methodology which will be presented would be applied.

4.2.3 Kalman-Bucy Filter Gain (Step 2)

With the above choices of Φ, C, Q, and R, the Kalman-Bucy filter was computed, via a computer solution to the discrete algebraic matrix Riccati equation (Appendix C). The resulting values of the predicted error covariance matrix Σ_p, updated error covariance Σ, Kalman gain matrix K, residual covariance matrix V and its inverse, V^{-1}, are given in Table 4.2.

TABLE 4.1

PLANT AND SENSOR NOISE COVARIANCE MATRICES; PITTS' VEHICLE MODEL

PLANT NOISE

$$Q = E[\underline{\omega}^T(k)\underline{\omega}(k)] = \begin{bmatrix} 8.50E\text{-}7 & & \\ 1.51E\text{-}5 & 3.31E\text{-}4 & \\ 1.56E\text{-}5 & 1.99E\text{-}3 & 1.19E\text{-}1 \end{bmatrix}$$

States: 1) Position 2) Velocity 3) Acceleration

SENSOR NOISE

$$R = E[\underline{n}(k)^T\underline{n}(k)] = \begin{bmatrix} .01 & \\ 0 & .01 \end{bmatrix}$$

Measurements: 1) Position 2) Velocity

STANDARD DEVIATIONS

PLANT NOISE			SENSOR NOISE	
Position	Velocity	Acceleration	Position	Velocity
9.2E-4m	0.018m/s	$0.34m/s^2$	.1m	.1m/s

Table 4.2

Kalman-Bucy Filter Matrices

Pitts' Vehicle Model

K A L M A N F I L T E R -

CLOSED LOOP EIGENVALUES

REAL PART	IMAGINARY PART
0.3268136302121680-01	0.0
0.573314240622441D+00	0.0
0.948811848384158D+00	0.0

CLOSED LOOP MATRIX

9.51128D-01	7.44609D-02	1.39982D-03
-1.27122D-02	6.66327D-01	1.85410D-02
5.49864D-02	-3.25820D+00	-6.26477D-02

KBF FILTER GAIN MATRIX H

4.88718D-02	1.27122D-02
1.27122D-02	6.87491D-02
-5.49864D-02	1.99493D-02

PREDICTED ERROR COVARIANCE MATRIX

5.15748D-04	1.43547D-04	-5.75359D-04
1.43547D-04	7.40205D-04	2.06366D-04
-5.75359D-04	2.06366D-04	1.26981D-01

UPDATED ERROR COVARIANCE MATRIX

4.88718D-04	1.27122D-04	-5.49864D-04
1.27122D-04	6.87491D-04	1.99493D-04
-5.49864D-04	1.99493D-04	1.26945D-01

RESIDUAL COV MATRIX (V) -

1.05157D-02	1.43547D-04
1.43547D-04	1.07402D-02

RESIDUAL COV MATRIX INVERSE (V-INVERSE) -

9.51128D+01	-1.27122D+00
-1.27122D+00	9.31251D+01

4.2.4 Detection Window (Step 3)

For purposes of fully illustrating the GLR methodology, a sliding window containing the previous three seconds of data was chosen as the detection window. The choice of a detection window with no delay was done so that the behavior of the likelihood ratios would not be obscured. The size window is represented by the parameter values N=0 and M=30, since the sampling rate is 10HZ. The detection window is represented in Figure 4.1.

4.2.5 Failure Direction Vectors (Step 4)

Sensor Failures

The measurement equation (4-2) represents the position and velocity sensor measurements. As was illustrated in Chapter 3, (3-12), (3-13) the choice of failure direction vectors:

$$\underline{f}_1 = \begin{bmatrix} 1 \\ 0 \end{bmatrix} \qquad \text{Position sensor bias failure direction vector} \qquad (4\text{-}3)$$

and

$$\underline{f}_2 = \begin{bmatrix} 0 \\ 1 \end{bmatrix} \qquad \text{Velocity sensor bias failure direction vector} \qquad (4\text{-}4)$$

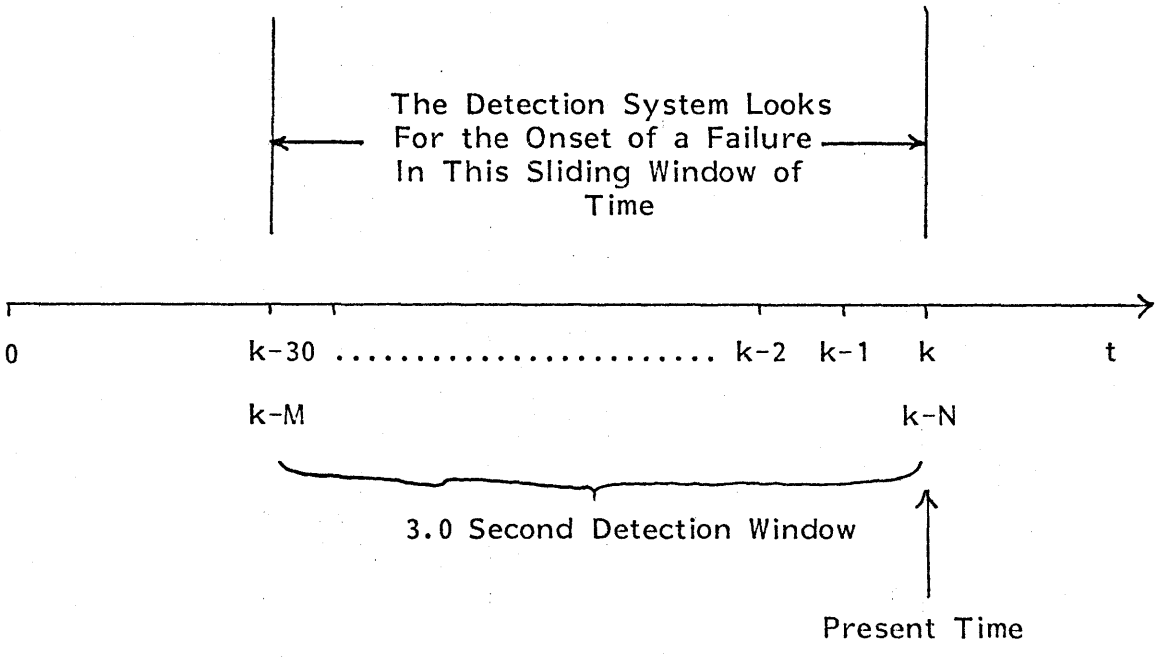

$\Delta t = 0.1$ Sec.

$N = 0$ (Delay)

$M = 30$

$M - N + 1 = 31$
Observations in Window

Figure 4.1
Visualization of Detection Window

can be used to represent position and velocity sensors failures. These vectors lie in the two-dimensional output space of the measurement equation.

Propulsion System Failures

The failure direction vector for actuator failures can be found by modelling the failure as a bias in the continuous-time state equation. The equivalent discrete-time failure direction vector can then be found.

A failure in any component (e.g., PCU, DC motor, drive train) of the vehicle's propulsion system which changes its overall effectiveness can be modelled by the addition of a bias, β, to the voltage actuator, as shown in Figure 4.2. The continuous-time state equation (2-1) with the inclusion of the bias can then be written as:

$$\dot{\underline{x}}(t) = A\underline{x}(t) + B_c(E_c(t)+\beta) + \underline{\omega}(t) \tag{4-5a}$$

$$= A\underline{x}(t) + B_c u(t) + \underline{\omega}(t) + B_c\beta \tag{4.5b}$$

where B_c is the continuous-time control matrix $[0\ 0\ K_M]^T$. By comparison of (4-5b) to equation (3-10) we see the failure vector is given by:

$$\underline{f}_D = \begin{bmatrix} 0 \\ 0 \\ K_M \end{bmatrix} \beta \tag{4-6}$$

Thus the direction in state-space of the bias failure is $[0\ 0\ K_M]^T$ and the magnitude is β volts.

The equivalent discrete-time failure direction vector can be found in the same manner as the discrete-time control matrix B is found from the continuous-time control matrix B_c (Appendix B), and is thus given by:

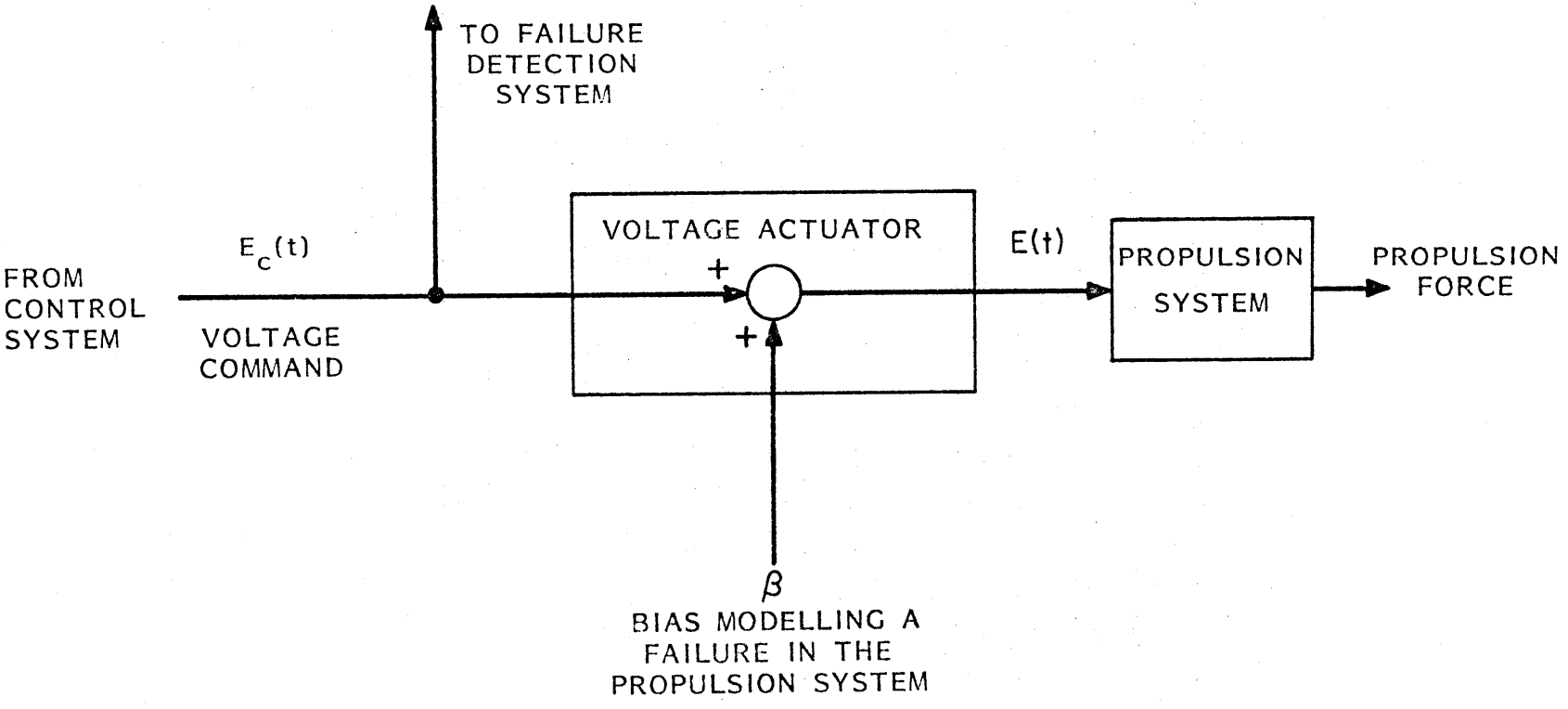

Figure 4.2 - Model of a Propulsion System Failure

$$\underline{f}_3 = \begin{bmatrix} 1.25E\text{-}3 \\ 2.92E\text{-}2 \\ 3.35E\text{-}1 \end{bmatrix} \qquad \begin{matrix} \text{Propulsion system} \\ \text{bias failure} \\ \text{direction vector} \end{matrix} \qquad (4\text{-}7)$$

The above vector can be scaled to be of unit magnitude; however, this was not done, so that the magnitude of a propulsion system bias would remain in units of volts.

We have thus defined the set of failure direction vectors $\{\underline{f}_i\}$ for a position sensor failure (i=1), velocity sensor failure (i=2), and propulsion system failure (i=3).

4.2.6. Failure Signatures

Failure Signature Matrices (Step 5)

The set of sensor bias and actuator bias failure signature matrices are given in Table 4.3. They were computed from the equations given in [39, Appendix A].

Weighted Failure Signatures (Step 6)

The failure signatures $\underline{s}_i(r) = [s_{i,1}(r)\ s_{i,2}(r)]$ i=1,2,3, for a position sensor, velocity sensor, and propulsion system bias failure are shown in Figures 4.3, 4.4, and 4.5.

Information Matrices (Step 7)

The sensor bias and actuator bias information matrices are given in Table 4.4.

Table 4.3a

Failure Signature Matrices

a.) Sensor Failures

G(0) -
 1.00000D+00 0.0
 0.0 1.00000D+00

G(1) -
 9.50107D-01 -1.87876D-02
-8.01500D-03 9.50329D-01

G(2) -
 9.02215D-01 -3.96787D-02
-1.22066D-02 9.21823D-01

G(3) -
 8.56458D-01 -6.12611D-02
-1.42203D-02 9.05677D-01

G(4) -
 8.12862D-01 -8.27483D-02
-1.50051D-02 8.96614D-01

G(5) -
 7.71393D-01 -1.03714D-01
-1.51043D-02 8.91602D-01

G(6) -
 7.31987D-01 -1.23939D-01
-1.48283D-02 8.88903D-01

G(7) -
 6.94564D-01 -1.43319D-01
-1.43544D-02 8.87522D-01

G(8) -
 6.59037D-01 -1.61815D-01
-1.37830D-02 8.86887D-01

G(9) -
 6.25317D-01 -1.79428D-01
-1.31712D-02 8.86672D-01

G(10) -
 5.93317D-01 -1.96174D-01
-1.25507D-02 8.86691D-01

G(11) -
 5.62951D-01 -2.12084D-01
-1.19390D-02 8.86836D-01

G(12) -
 5.34137D-01 -2.27192D-01
-1.13456D-02 8.87046D-01

G(13) -
 5.06798D-01 -2.41533D-01
-1.07749D-02 8.87288D-01

G(14) -
 4.80856D-01 -2.55143D-01
-1.02292D-02 8.87541D-01

G(15) -
 4.56243D-01 -2.68059D-01
-9.70889D-03 8.87795D-01

G(16) -
 4.32889D-01 -2.80316D-01
-9.21382D-03 8.88044D-01

G(17) -
 4.10730D-01 -2.91945D-01
-8.74328D-03 8.88285D-01

G(18) -
 3.89706D-01 -3.02980D-01
-8.29635D-03 8.88516D-01

G(19) -
 3.69758D-01 -3.13450D-01
-7.87204D-03 8.88737D-01

G(20) -
 3.50830D-01 -3.23384D-01
-7.46929D-03 8.88947D-01

G(21) -
 3.32872D-01 -3.32810D-01
-7.08707D-03 8.89147D-01

G(22) -
 3.15833D-01 -3.41754D-01
-6.72436D-03 8.89337D-01

G(23) -
 2.99666D-01 -3.50239D-01
-6.38019D-03 8.89517D-01

G(24) -
 2.84327D-01 -3.58291D-01
-6.05362D-03 8.89688D-01

G(25) -
 2.69773D-01 -3.65930D-01
-5.74376D-03 8.89851D-01

G(26) -
 2.55963D-01 -3.73178D-01
-5.44976D-03 8.90005D-01

G(27) -
 2.42861D-01 -3.80055D-01
-5.17080D-03 8.90152D-01

G(28) -
 2.30430D-01 -3.86580D-01
-4.90612D-03 8.90291D-01

G(29) -
 2.18634D-01 -3.92771D-01
-4.65498D-03 8.90422D-01

G(30) -
 2.07443D-01 -3.98646D-01
-4.41670D-03 8.90547D-01

Table 4.3b

Failure Signature Matrices

b.) Actuator Failures

G(0) -

1.00000D+00	0.0	0.0
0.0	1.00000D+00	0.0

G(1) -

1.95011D+00	6.90786D-02	1.73816D-03
-8.01500D-03	1.66705D+00	1.99336D-02

G(2) -

2.85232D+00	1.75533D-01	4.65822D-03
-2.02216D-02	2.05116D+00	3.19735D-02

G(3) -

3.70878D+00	3.00036D-01	8.16637D-03
-3.44419D-02	2.27013D+00	3.88584D-02

G(4) -

4.52164D+00	4.31639D-01	1.19181D-02
-4.94470D-02	2.39439D+00	4.27693D-02

G(5) -

5.29303D+00	5.64229D-01	1.57204D-02
-6.45513D-02	2.46441D+00	4.49763D-02

G(6) -

6.02502D+00	6.94462D-01	1.94672D-02
-7.93796D-02	2.50340D+00	4.62082D-02

G(7) -

6.71959D+00	8.20566D-01	2.31019D-02
-9.37340D-02	2.52466D+00	4.68829D-02

G(8) -

7.37862D+00	9.41672D-01	2.65962D-02
-1.07517D-01	2.53581D+00	4.72396D-02

G(9) -

8.00394D+00	1.05741D+00	2.99380D-02
-1.20688D-01	2.54122D+00	4.74157D-02

G(10) -

8.59726D+00	1.16771D+00	3.31236D-02
-1.33239D-01	2.54338D+00	4.74896D-02

G(11) -

9.16021D+00	1.27263D+00	3.61549D-02
-1.45178D-01	2.54373D+00	4.75063D-02

G(12) -

9.69434D+00	1.37234D+00	3.90359D-02
-1.56523D-01	2.54309D+00	4.74915D-02

G(13) -

1.02011D+01	1.46704D+00	4.17722D-02
-1.67298D-01	2.54193D+00	4.74599D-02

G(14) -

1.06820D+01	1.55694D+00	4.43702D-02
-1.77528D-01	2.54050D+00	4.74199D-02

G(15) -

1.11382D+01	1.64226D+00	4.68360D-02
-1.87236D-01	2.53896D+00	4.73762D-02

G(16) -

1.15711D+01	1.72324D+00	4.91762D-02
-1.96450D-01	2.53740D+00	4.73314D-02

G(17) -

1.19819D+01	1.80008D+00	5.13969D-02
-2.05194D-01	2.53586D+00	4.72870D-02

G(18) -

1.23716D+01	1.87300D+00	5.35041D-02
-2.13490D-01	2.53436D+00	4.72438D-02

G(19) -

1.27413D+01	1.94218D+00	5.55035D-02
-2.21362D-01	2.53291D+00	4.72022D-02

G(20) -

1.30922D+01	2.00783D+00	5.74007D-02
-2.28831D-01	2.53153D+00	4.71623D-02

G(21) -

1.34250D+01	2.07011D+00	5.92008D-02
-2.35918D-01	2.53022D+00	4.71243D-02

G(22) -

1.37409D+01	2.12921D+00	6.09087D-02
-2.42643D-01	2.52896D+00	4.70882D-02

G(23) -

1.40405D+01	2.18528D+00	6.25292D-02
-2.49023D-01	2.52777D+00	4.70537D-02

G(24) -

1.43249D+01	2.23849D+00	6.40668D-02
-2.55076D-01	2.52664D+00	4.70211D-02

G(25) -

1.45946D+01	2.28897D+00	6.55257D-02
-2.60820D-01	2.52557D+00	4.69900D-02

G(26) -

1.48506D+01	2.33686D+00	6.69099D-02
-2.66270D-01	2.52455D+00	4.69606D-02

G(27) -

1.50934D+01	2.38231D+00	6.82232D-02
-2.71441D-01	2.52358D+00	4.69326D-02

G(28) -

1.53239D+01	2.42543D+00	6.94694D-02
-2.76347D-01	2.52266D+00	4.69061D-02

G(29) -

1.55425D+01	2.46634D+00	7.06517D-02
-2.81002D-01	2.52179D+00	4.68809D-02

G(30) -

1.57500D+01	2.50516D+00	7.17735D-02
-2.85419D-01	2.52097D+00	4.68571D-02

Failure Signatures;

Pitts' Vehicle Model

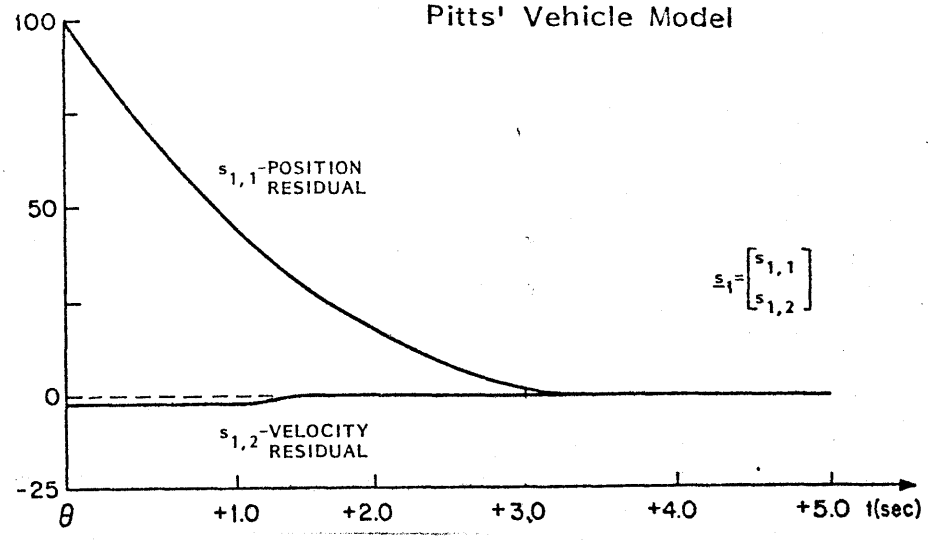

Figure 4.3
Position Sensor Bias

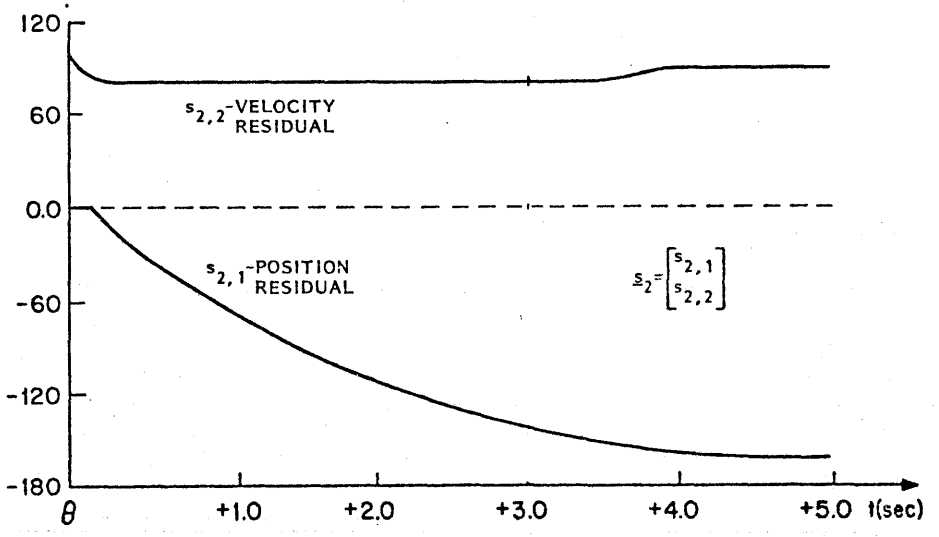

Figure 4.4
Velocity Sensor Bias

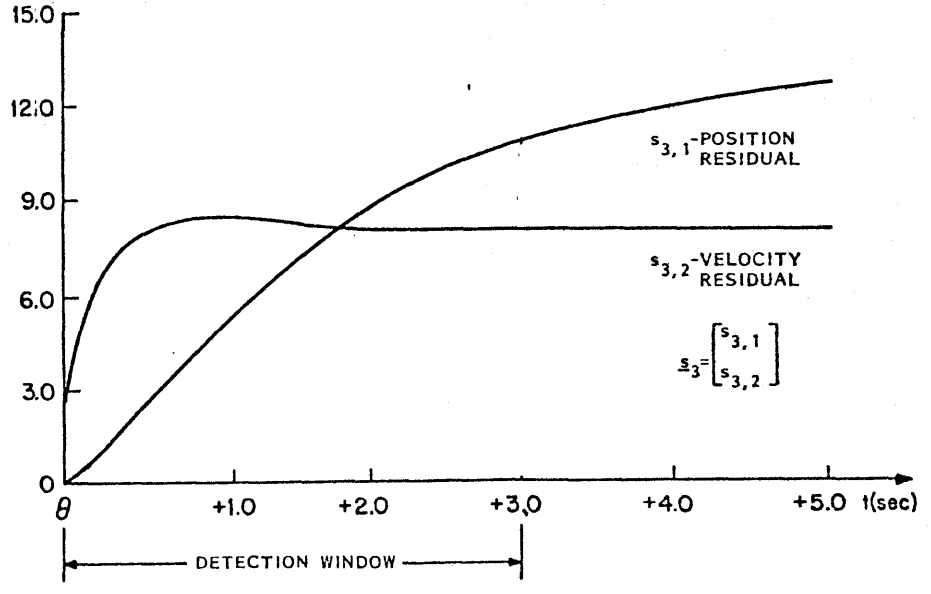

Figure 4.5
Propulsion System Bias

Table 4.4a

Information Matrices

a.) Sensor Failures

C(0) -
 9.51128D+01 -1.27122D+00
-1.27122D+00 9.31251D+01

C(1) -
 1.80997D+02 -4.82633D+00
-4.82633D+00 1.77308D+02

C(2) -
 2.58460D+02 -1.03370D+01
-1.03370D+01 2.56684D+02

C(3) -
 3.28277D+02 -1.75139D+01
-1.75139D+01 3.33568D+02

C(4) -
 3.91174D+02 -2.60924D+01
-2.60924D+01 4.09273D+02

C(5) -
 4.47821D+02 -3.58322D+01
-3.58322D+01 4.84561D+02

C(6) -
 4.98831D+02 -4.65180D+01
-4.65180D+01 5.59885D+02

C(7) -
 5.44760D+02 -5.79585D+01
-5.79585D+01 6.35516D+02

C(8) -
 5.86111D+02 -6.99858D+01
-6.99858D+01 7.11621D+02

C(9) -
 6.23339D+02 -8.24528D+01
-8.24528D+01 7.88301D+02

C(10) -
 6.56855D+02 -9.52315D+01
-9.52315D+01 8.65621D+02

C(11) -
 6.87028D+02 -1.08211D+02
-1.08211D+02 9.43618D+02

C(12) -
 7.14191D+02 -1.21296D+02
-1.21296D+02 1.02231D+03

C(13) -
 7.38645D+02 -1.34404D+02
-1.34404D+02 1.10172D+03

C(14) -
 7.60660D+02 -1.47464D+02
-1.47464D+02 1.18185D+03

C(15) -
 7.80478D+02 -1.60418D+02
-1.60418D+02 1.26269D+03

C(16) -
 7.98320D+02 -1.73213D+02
-1.73213D+02 1.34423D+03

C(17) -
 8.14381D+02 -1.85808D+02
-1.85808D+02 1.42648D+03

C(18) -
 8.28841D+02 -1.98169D+02
-1.98169D+02 1.50942D+03

C(19) -
 8.41858D+02 -2.10265D+02
-2.10265D+02 1.59302D+03

C(20) -
 8.53577D+02 -2.22073D+02
-2.22073D+02 1.67729D+03

C(21) -
 8.64126D+02 -2.33576D+02
-2.33576D+02 1.76220D+03

C(22) -
 8.73623D+02 -2.44759D+02
-2.44759D+02 1.84774D+03

C(23) -
 8.82173D+02 -2.55612D+02
-2.55612D+02 1.93388D+03

C(24) -
 8.89870D+02 -2.66127D+02
-2.66127D+02 2.02061D+03

C(25) -
 8.96799D+02 -2.76300D+02
-2.76300D+02 2.10792D+03

C(26) -
 9.03037D+02 -2.86129D+02
-2.86129D+02 2.19577D+03

C(27) -
 9.08652D+02 -2.95614D+02
-2.95614D+02 2.28416D+03

C(28) -
 9.13708D+02 -3.04757D+02
-3.04757D+02 2.37306D+03

C(29) -
 9.18259D+02 -3.13560D+02
-3.13560D+02 2.46246D+03

C(30) -
 9.22356D+02 -3.22029D+02
-3.22029D+02 2.55233D+03

Table 4.4b

Information Matrices

b.) Actuator Failures

C(0) -

9.51128D+01	-1.27122D+00	0.0
-1.27122D+00	9.31251D+01	0.0
0.0	0.0	0.0

C(1) -

4.56865D+02	6.16527D+00	2.58119D-01
6.16527D+00	3.52085D+02	3.10055D+00
2.58119D-01	3.10055D+00	3.72022D-02

C(2) -

1.23086D+03	4.24905D+01	1.34583D+00
4.24905D+01	7.45902D+02	9.26643D+00
1.34583D+00	9.26643D+00	1.34089D-01

C(3) -

2.53958D+03	1.30358D+02	3.91906D+00
1.30358D+02	1.23265D+03	1.76760D+01
3.91906D+00	1.76760D+01	2.80242D-01

C(4) -

4.48498D+03	2.91230D+02	8.60260D+00
2.91230D+02	1.78164D+03	2.76421D+01
8.60260D+00	2.76421D+01	4.62801D-01

C(5) -

7.15094D+03	5.43932D+02	1.59451D+01
5.43932D+02	2.37396D+03	3.87263D+01
1.59451D+01	3.87263D+01	6.72889D-01

C(6) -

1.06054D+04	9.04289D+02	2.64074D+01
9.04289D+02	2.99903D+03	5.06819D+01
2.64074D+01	5.06819D+01	9.05487D-01

C(7) -

1.49025D+04	1.38522D+03	4.03652D+01
1.38522D+03	3.65138D+03	6.33844D+01
4.03652D+01	6.33844D+01	1.15818D+00

C(8) -

2.00839D+04	1.99704D+03	5.81181D+01
1.99704D+03	4.32847D+03	7.67798D+01
5.81181D+01	7.67798D+01	1.43009D+00

C(9) -

2.61809D+04	2.74777D+03	7.98984D+01
2.74777D+03	5.02937D+03	9.08513D+01
7.98984D+01	9.08513D+01	1.72109D+00

C(10) -

3.32155D+04	3.64346D+03	1.05881D+02
3.64346D+03	5.75392D+03	1.05601D+02
1.05881D+02	1.05601D+02	2.03147D+00

C(11) -

4.12017D+04	4.68847D+03	1.36193D+02
4.68847D+03	6.50230D+03	1.21037D+02
1.36193D+02	1.21037D+02	2.36160D+00

C(12) -

5.01466D+04	5.88570D+03	1.70916D+02
5.88570D+03	7.27483D+03	1.37170D+02
1.70916D+02	1.37170D+02	2.71186D+00

C(13) -

6.00513D+04	7.23686D+03	2.10100D+02
7.23686D+03	8.07177D+03	1.54010D+02
2.10100D+02	1.54010D+02	3.08254D+00

C(14) -

7.09119D+04	8.74255D+03	2.53762D+02
8.74255D+03	8.89331D+03	1.71562D+02
2.53762D+02	1.71562D+02	3.47385D+00

C(15) -

8.27202D+04	1.04025D+04	3.01894D+02
1.04025D+04	9.73955D+03	1.89829D+02
3.01894D+02	1.89829D+02	3.88587D+00

C(16) -

9.54643D+04	1.22157D+04	3.54466D+02
1.22157D+04	1.06104D+04	2.08811D+02
3.54466D+02	2.08811D+02	4.31859D+00

C(17) -

1.09129D+05	1.41805D+04	4.11428D+02
1.41805D+04	1.15059D+04	2.28504D+02
4.11428D+02	2.28504D+02	4.77189D+00

C(18) -

1.23698D+05	1.62948D+04	4.72719D+02
1.62948D+04	1.24256D+04	2.48901D+02
4.72719D+02	2.48901D+02	5.24560D+00

C(19) -

1.38150D+05	1.85557D+04	5.38259D+02
1.85557D+04	1.33693D+04	2.69993D+02
5.38259D+02	2.69993D+02	5.73943D+00

C(20) -

1.55456D+05	2.09604D+04	6.07963D+02
2.09604D+04	1.43367D+04	2.91768D+02
6.07963D+02	2.91768D+02	6.25307D+00

C(21) -

1.72621D+05	2.35056D+04	6.81735D+02
2.35056D+04	1.53271D+04	3.14213D+02
6.81735D+02	3.14213D+02	6.78612D+00

C(22) -

1.90593D+05	2.61877D+04	7.59470D+02
2.61877D+04	1.63402D+04	3.37315D+02
7.59470D+02	3.37315D+02	7.33817D+00

C(23) -

2.09358D+05	2.90029D+04	8.41063D+02
2.90029D+04	1.73754D+04	3.61056D+02
8.41063D+02	3.61056D+02	7.90876D+00

C(24) -

2.23891D+05	3.19475D+04	9.26400D+02
3.19475D+04	1.84321D+04	3.85421D+02
9.26400D+02	3.85421D+02	8.49739D+00

C(25) -

2.49166D+05	3.50175D+04	1.01537D+03
3.50175D+04	1.95098D+04	4.10391D+02
1.01537D+03	4.10391D+02	9.10357D+00

Information Measures (Step 8)

The information measures $a_i(r)$ i=1,2,3 for a position sensor, velocity sensor, and propulsion system bias failure are shown in Figure 4.6.

4.3 Testing of the GLR Algorithm on a Simulated Vehicle-Detection of Bias Failures

To test the performance of the GLR algorithm, a computer program was developed to simulate the dynamics of an AGT vehicle. With this program, the effects of maneuvers, grade transitions, and wind forces can be simulated. Simulated sensor outputs, with or without additive Gaussian noise, can be produced and stored for processing by a GLR detection algorithm under test, implemented in another computer program. The vehicle simulator allows for the emulation of a variety of vehicle failures, both in the sensors and in the propulsion system. The details of the vehicle simulator and GLR programs are provided in Appendix C. A block diagram representation of the system which was simulated appears in Figure 4.7. In this simulated vehicle, the motor voltage command and the velocity sensor and position sensor outputs are digitized and sent to the failure detection computer which performs the Kalman-Bucy filter and GLR algorithm calculations. The algorithm produces three maximum likelihood ratios, ℓ_i^* for the three possible failure locations: position sensor (i=1), velocity sensor (i=2), and propulsion system (i=3).

In practice, these likelihood ratios would be used in a decision rule to decide whether a failure has occurred; here, we will merely examine the qualitative behavior of the maximum likelihood ratios, without choosing a

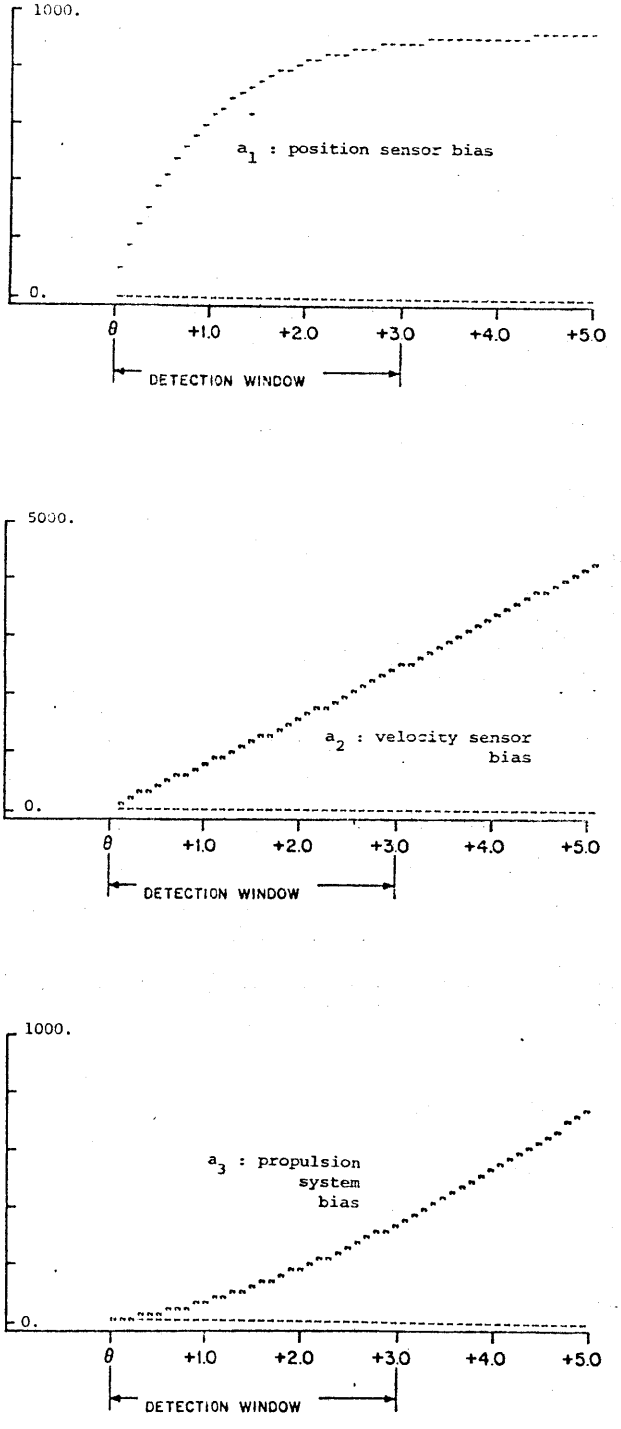

Figure 4.6

Information Measures; Pitts' Vehicle Model

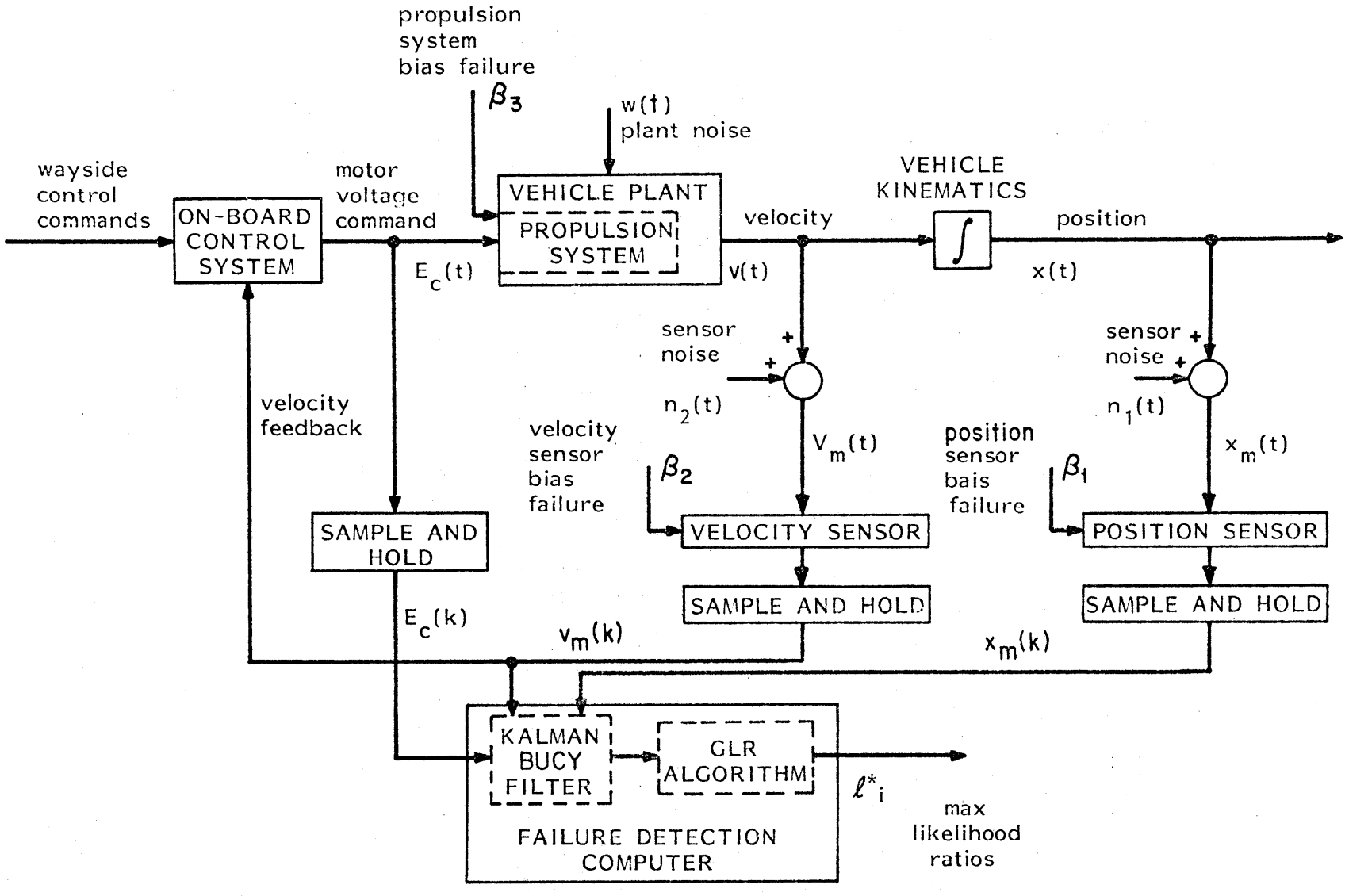

Figure 4.7 - Simulated Vehicle Block Diagram

specific decision rule. However, we will say that a failure can be detected if one of the MLR's becomes "large" (i.e., relative to their nominal values). If the largest of the three likelihood ratio ℓ_i^*, i=1,2,3 corresponds to the true location of the failure, then we will say that the location of failure has been correctly identified.

The following sections will present the performance results of the GLR algorithm in detecting bias failures in the simulated vehicle's sensors and propulsion system. Detection of failure types other than biases will be discussed in section 4.6.

Vehicle simulations were done both with and without additive Gaussian noise in the sensors and vehicle plant. The simulations performed without the noise were done to determine the mean trajectories of the likelihood ratios, so that the expected performance could be seen without being obscured by random effects. Noise will cause the likelihood ratios to have mean trajectories which follow those to be shown in the figures plus a constant value of 1. Likelihood ratios following a failure will have random fluctuations with standard deviation $\sqrt{2+4\beta^2 a_i(k;\theta)}$ as a result of the noise.

4.3.1 Position Sensor Bias Failure

Scenario

The AGT vehicle was initialized to a constant velocity of 15 m/s at position zero. At time θ=1.0 sec. a bias of magnitude 1.0 meter was added to the vehicle's position sensor measurement, as shown in Figure 4.8. No background noise was present in the plant or sensors.

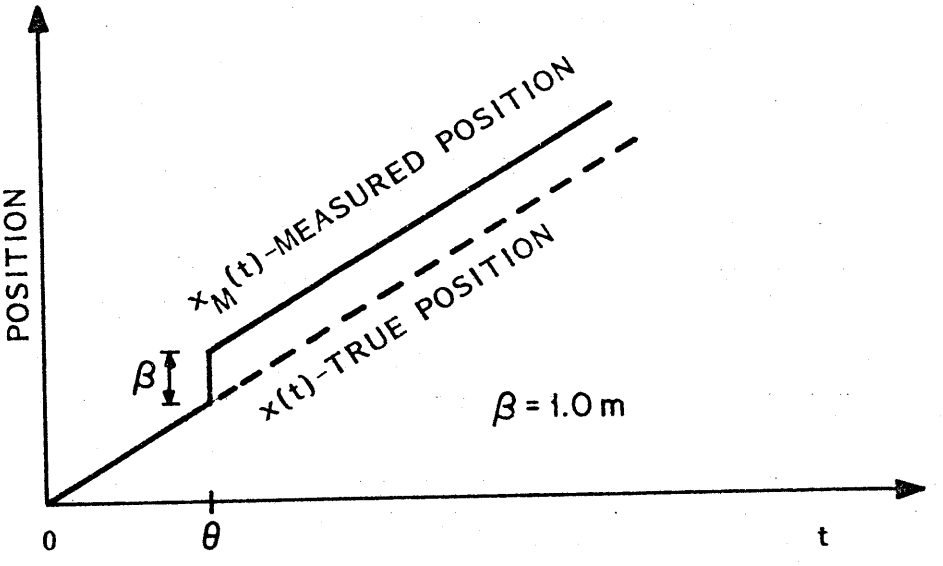

Figure 4.8

Position Sensor Output Trajectory, Bias Failure

Results

The simulated measurements and motor voltage command were processed by the Kalman-Bucy filter and GLR algorithm. The likelihood ratios $\ell_i(r)$ i=1,2,3 for the hypothesized position sensor, velocity sensor, and propulsion system failures, respectively, were computed. For each set, the maximum over the detection window, ℓ_i^* i=1,2,3, was chosen. This process was repeated at each step in the simulation, producing the filter residuals, Figure 4.9, and the trajectories of the three maximum likelihood ratios ℓ_i^*, Figure 4.10.

The maximum likelihood ratio (MLR) for the position sensor failure, ℓ_1^*, jumps to a value of 95.1 at the failure time θ. At each succeeding time step, ℓ_1 increases, tending toward an asymptotic value of about 900. The asymptotic behavior is expected from the shape of $a_1(r)$, Figure 4.6. The MLR suddenly begins decreasing, however, three seconds following the failure. This is because the onset of the bias begins to pass out of the three second detection window and thus less of the signature is observed. It continues to decay as time progresses, as less and less of the signature is present in the residuals.

The maximum likelihood ratios for the other failure types, ℓ_2^* and ℓ_3^*, also increase after the failure, reaching a peak value approximately two seconds after the failure, but then decay. At every step following the failure, however, they remain well below ℓ_1^*, the maximum likelihood ratio for the actual failure type; this implies the failure is both detected and identified correctly.

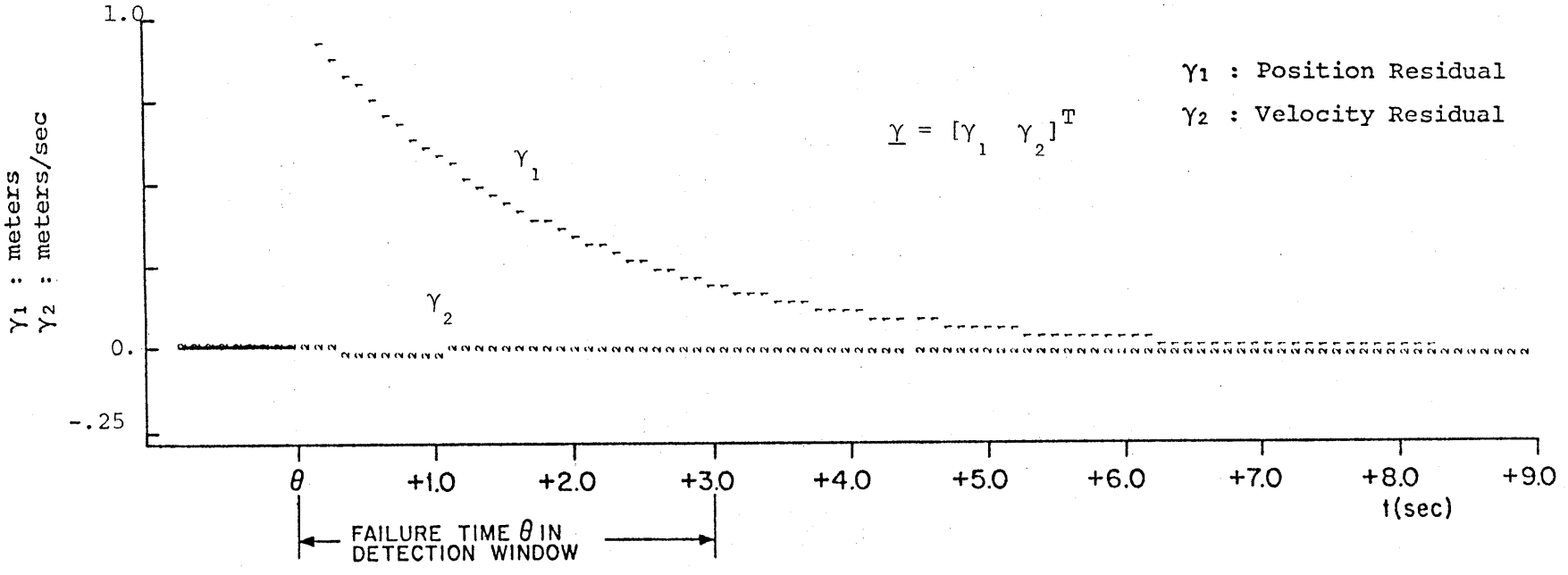

Figure 4.9

Kalman-Bucy Filter Residuals, Position Sensor Bias

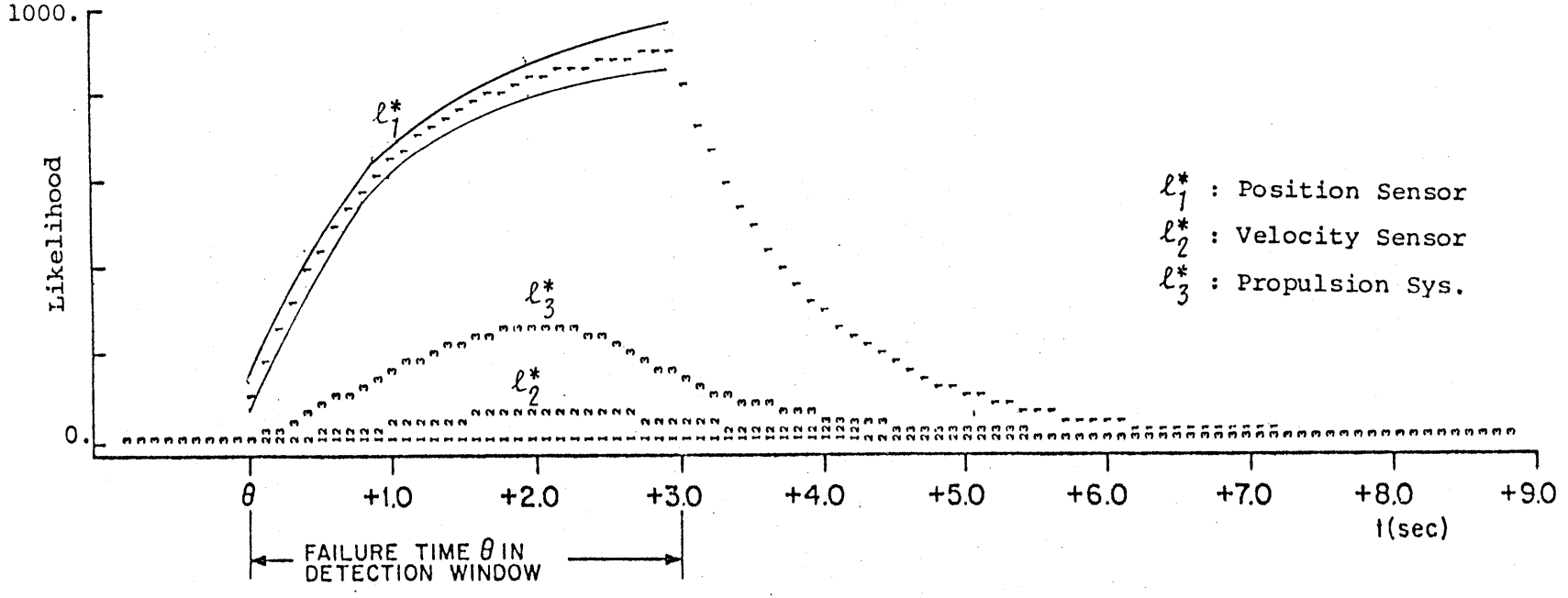

Figure 4.10

Maximum Likelihood Ratios, Position Sensor Bias

The likelihood ratios in Figure 4.10 correspond to a position sensor bias with a magnitude of 1.0 meter. The values of the likelihood ratios for a bias of arbitrary magnitude β can be determined by scaling the curves in Figure 4.10 by the constant β^2.

The standard deviation of the fluctuations expected in the behavior of ℓ_1^* following the failure as a result of the background plant and sensor noise is shown in Figure 4.10. Nevertheless, the position sensor bias failure was repeated, with Gaussian plant and sensor noise included in the simulation. The variances of these disturbances were equal to the statistics assumed in the system model and Kalman-Bucy filter, Table 4.1. The filter residuals are plotted in Figure 4.11. Note the correspondence between the observed residuals here and the position sensor bias signature, Figure 4.3. The maximum likelihood ratio trajectories for the noisy run are shown in Figure 4.12. The magnitude of ℓ_1^* is only slightly less than it is in the case without the noise, Figure 4.10.

It is common practice to relate the magnitude of a sensor failure bias to the standard deviation, σ, of the additive Gaussian noise for that sensor. The 1.0 meter bias magnitude used for the above simulated failure represents a 10σ failure. To examine the detection sensitivity, a 1σ failure was also simulated with a bias to the position sensor of 10cm. The signature in the residuals is barely discernable by a visual examination (Figure 4.13). The maximum likelihood ratios are shown in Figure 4.14. The MLR for the position sensor failure, ℓ_1^*, remains greater than the others from 0.5 second after the failure until the true failure time passes out of the detection window. Thus,

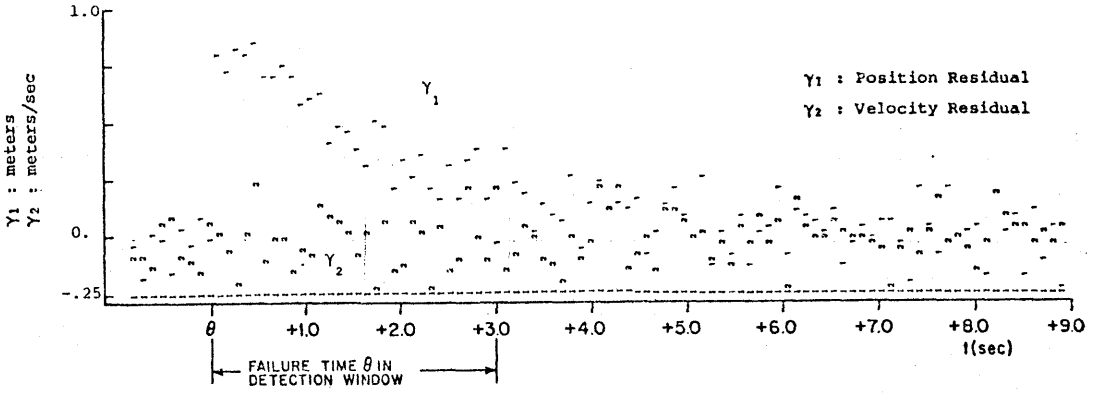

Figure 4.11
Residuals, Position Sensor Bias, 1.0 m Bias
Gaussian Sensor Noise

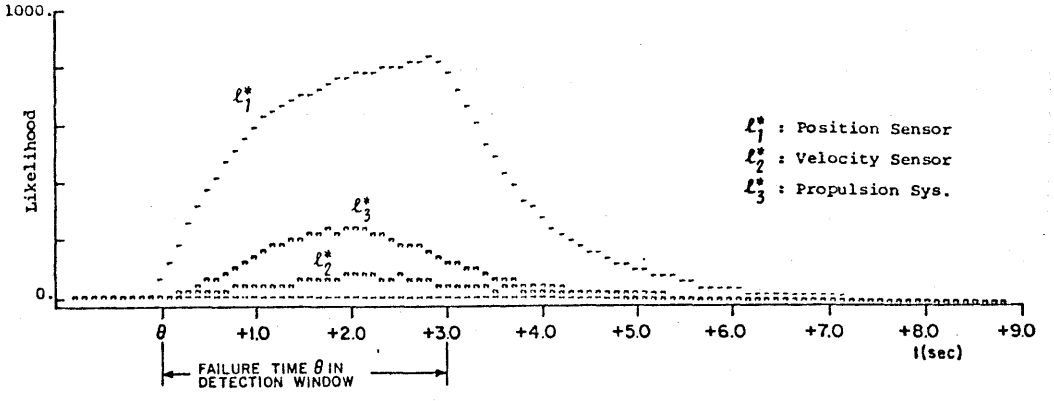

Figure 4.12
Maximum Likelihood Ratios

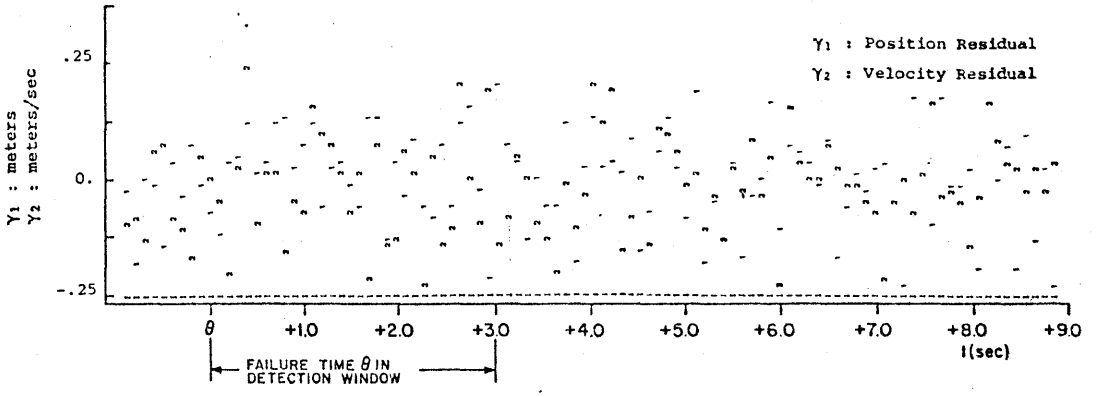

Figure 4.13

Residuals, 1.0 cm Position Sensor Bias with Noise

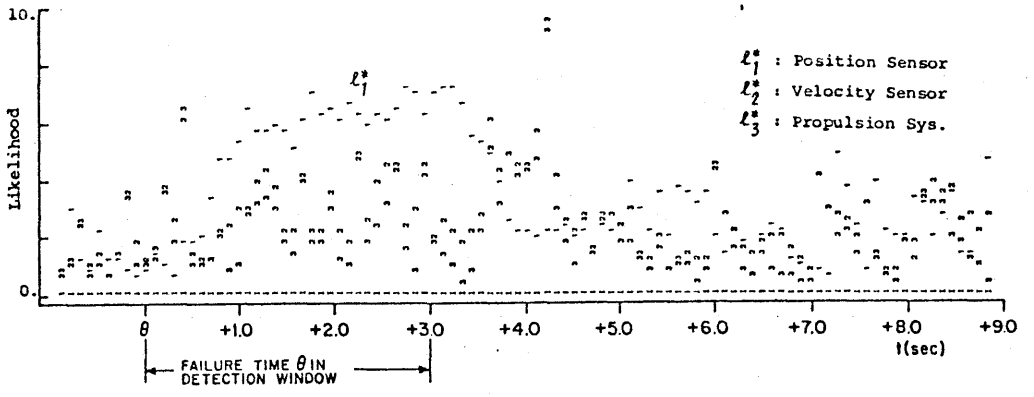

Figure 4.14

Maximum Likelihood Ratios

if a failure of this size is to be detected, it would have to be done during this interval, as the failure signature rapidly disappears.

Summary of Results

The preceeding results can be summarized as follows:

1) The position sensor bias caused ℓ_1^* to approach an asymptotic value proportional to β^2.

2) ℓ_1^* decayed rapidly once the failure time θ left the detection window.

3) The algorithm could unambiguously identify the true location of the failure.

4) Background noise did not affect detection of a 10σ failure. A 1σ failure is barely detectable.

5) Lengthening the detection window will not improve detection of small failures.

4.3.2 Velocity Sensor Bias Failure

Scenario

A velocity sensor failure was simulated with the addition of a 1.0m/s bias to the velocity measurement. Since the velocity sensor is part of the control feedback loop, the bias caused the vehicle behavior shown in Figure 4.15. The velocity regulator, believing the vehicle to suddenly be travelling 1.0m/s faster than the commanded velocity, ordered the vehicle to decrease its speed, as shown in the figure. Before the failure, the vehicle was travelling at a velocity of 15m/s. No background noise was present.

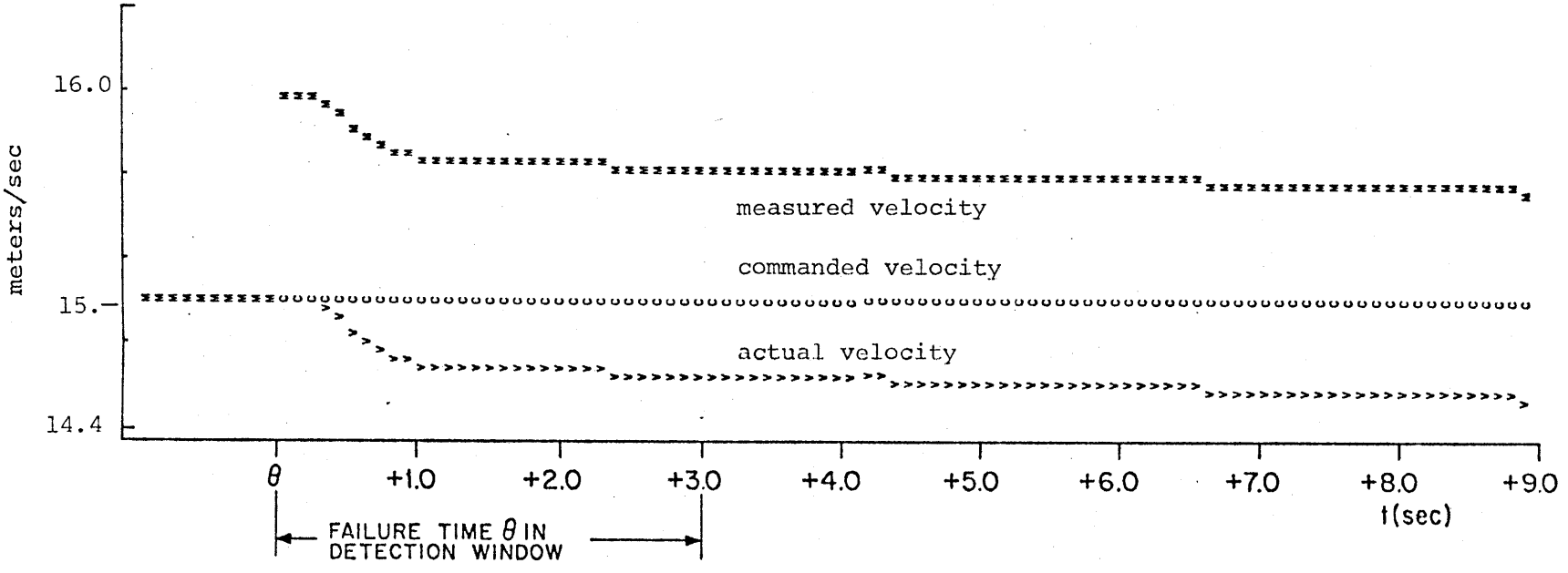

Figure 4.15

Vehicle Behavior, Velocity Sensor Bias

Results

The maximum likelihood ratios ℓ_i^* following the sensor bias are shown in Figure 4.16. At time θ, the MLR's ℓ_2^* and ℓ_3^* both jump to a value of 93. With the one observation at time θ, the algorithm can detect the failure, but cannot uniquely identify the failure's location since ℓ_2^* and ℓ_3^* are the same. This behavior is expected, since by looking at only the first point, the velocity sensor and propulsion system failure signatures (Figure 4.4 and 4.5) are indistinguishable. As more observations are made, the algorithm identifies the true failure location, and ℓ_2^* grows larger than ℓ_3^*.

The standard deviation of the expected random fluctuations of ℓ_2^* following the failure is shown in Figure 4.16. The time until ℓ_3^* leaves this "band" around ℓ_2^* provides an estimate of the time required for unambiguous identification of the failure location.

The velocity sensor MLR, ℓ_2^*, continues to increase, even after the failure time has left the detection window, in contrast to the behavior of ℓ_1^* following the position sensor failure (section 4.3.1). The value of ℓ_2^* continues to grow in this case as the residuals contain a non-zero mean as long as the bias persists, as shown in Figure 4.17.

The velocity sensor bias failure simulation was repeated with the addition of Gaussian plant and sensor noise. Noisy residuals for the 1.0m/s bias are shown in Figure 4.18, and the resulting MLR's in Figure 4.19. Addition of the noise produced only a slight degradation of performance. As the 1.0m/s bias represents a 10σ bias magnitude, a 1σ failure was also

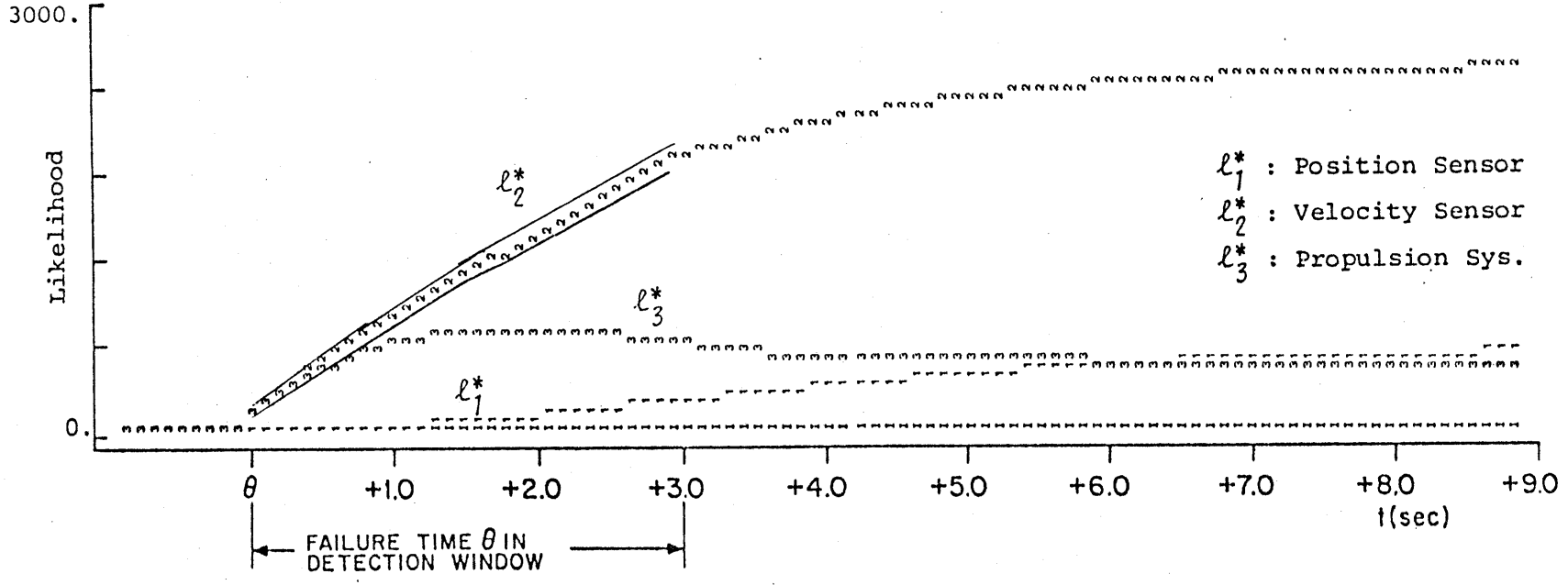

Figure 4.16

Maximum Likelihood Ratios, Velocity Sensor Bias

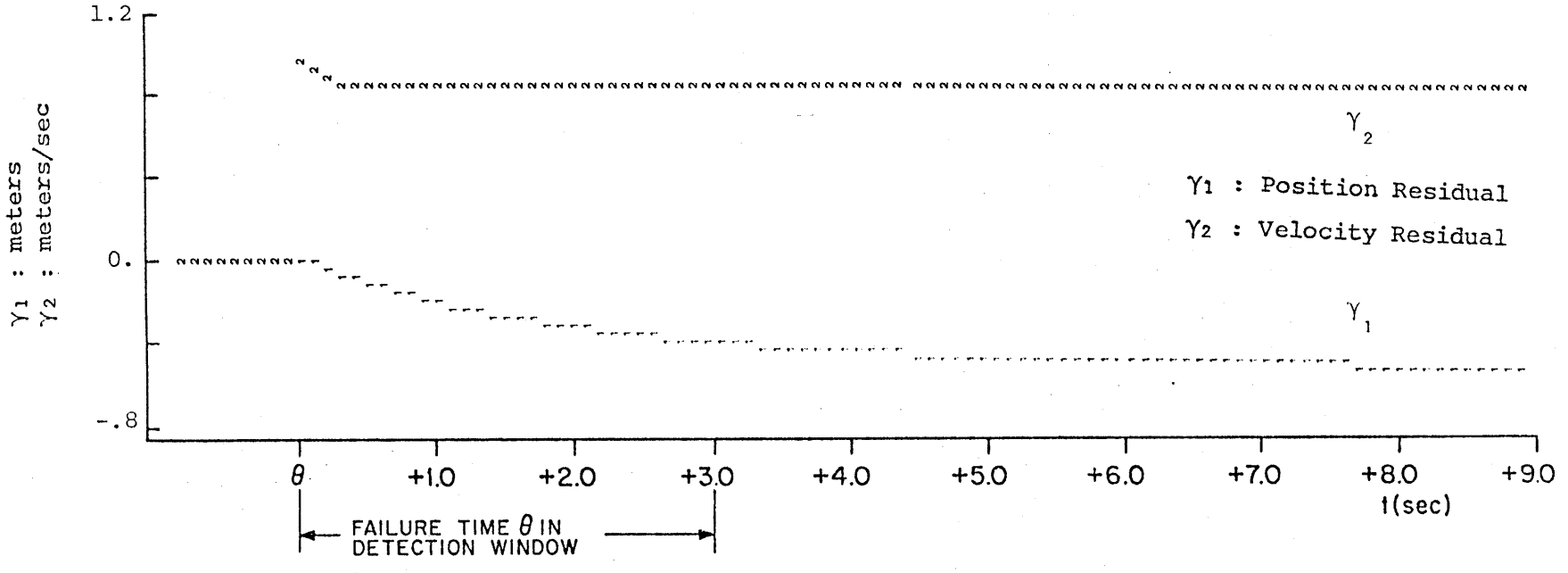

Figure 4.17
Residuals, Velocity Sensor Bias

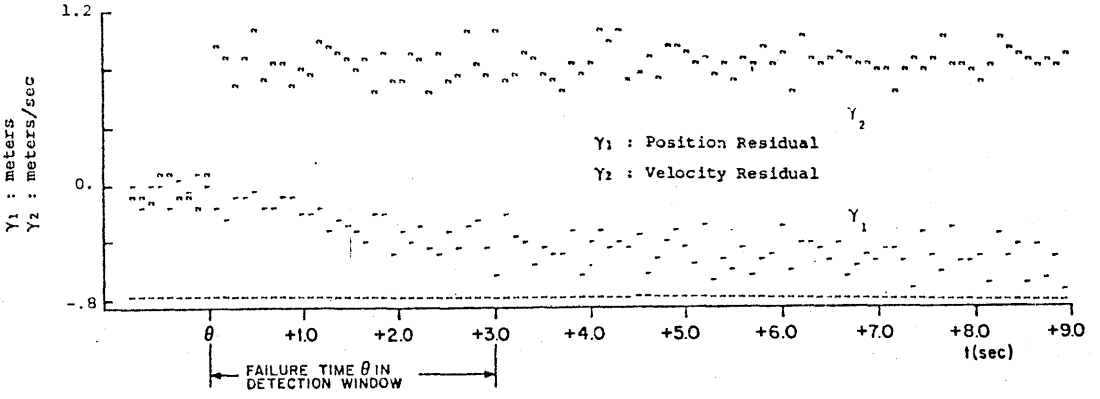

Figure 4.18

Residuals, 1.0 m/s Velocity Sensor Bias with Noise

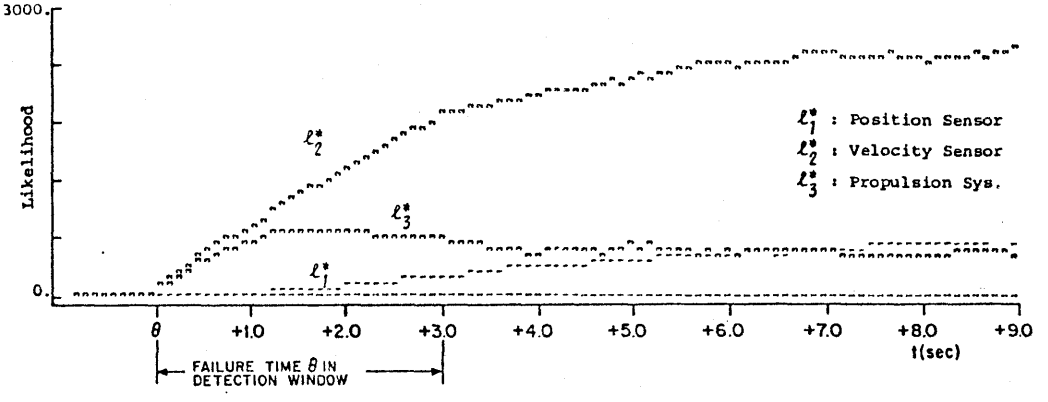

Figure 4.19

Maximum Likelihood Ratios

simulated, via a bias magnitude of 0.1m/s. The resulting residuals and MLR's are shown in Figures 4.20 and 4.21. Since ℓ_2^* continues to grow, independent of the length of the detection window, the failure would eventually be detected.

Summary of Results

1) The velocity sensor bias caused ℓ_2^* to grow linearly with time.
2) ℓ_2^* continued to grow, although at a slower rate, even when the failure time θ left the detection window.
3) There was a delay until the true location of the failure could be unambiguously identified to be a velocity sensor and not a propulsion system failure.
4) Background noise did not affect detection of either a 10σ or 1σ failure.
5) Small failures will be detected independent of the length of the detection window, although they can be detected sooner with a longer window.

4.3.3 Propulsion System Bias Failure

Scenario

A bias failure in the propulsion system was simulated by the addition of a 10 volt bias to the PCU (voltage actuator), as shown in Figure 4.2. The bias caused the vehicle to rapidly accelerate from its initial velocity of 15m/s to a velocity of 15.8m/s. The control system, sensing the overspeed

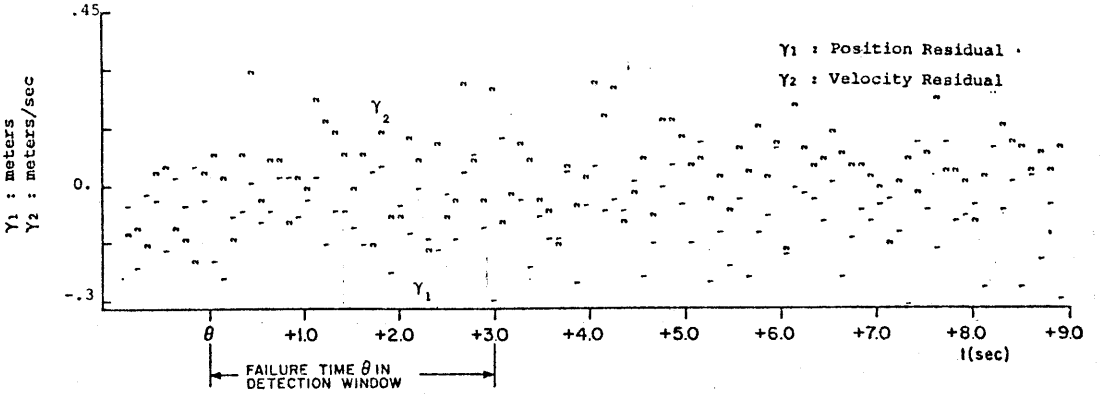

Figure 4.20

Residuals, 0.1 m/s Velocity Sensor Bias with Noise

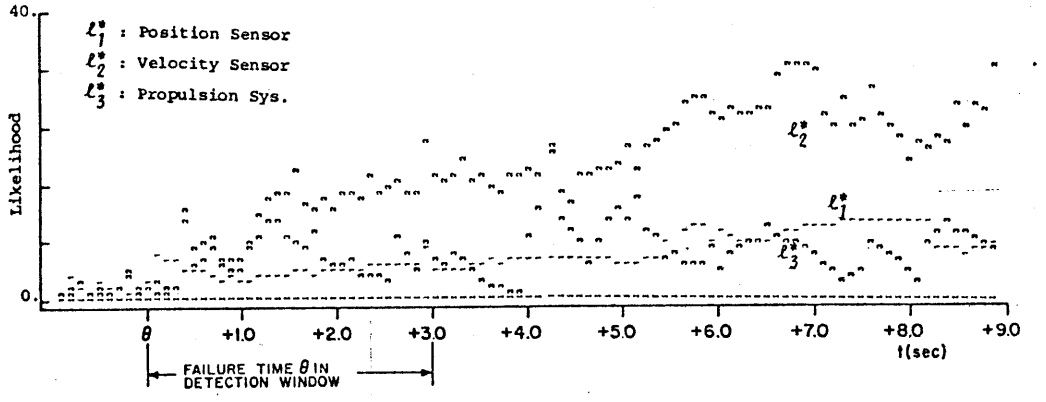

Figure 4.21

Maximum Likelihood Ratios

condition via the velocity sensor feedback, began to slowly decrease the motor voltage command (Figure 4.22). The vehicle's behavior is shown in Figure 4.23.

Results

The signature of the propulsion system failure is clearly seen in the filter residuals, Figure 4.24. Increasing in an exponential fashion, ℓ_3^* does not exhibit a large "jump" at the time of the failure. Not able to initially determine the location of the failure, ℓ_2^* and ℓ_3^* both remain close for approximately one-half second following the failure. As more observations are made, the location of the failure is identified, and ℓ_3^* grows larger than ℓ_2^*, Figure 4.25. Since the residual remain non-zero, ℓ_3^* continues to increase after the failure time θ has left the detection window.

With the addition of plant and sensor Gaussian noise in the simulation, a 10σ (10 volt) and 1σ (1 volt) bias failure was performed. Detection of the 10σ failure was not significantly affected by the noise (Figure 4.26 and 4.27). Although the effect of the noise is apparent on the residuals (Figure 4.28) and MLR's (Figure 4.29) detection of the 1σ failure is still possible.

Summary of Results

1) The propulsion system bias caused ℓ_3^* to grow in an exponential fashion, increasing slowly during the first one half second.

2) Although continuing to grow once θ left the detection window, the rate of increase was reduced.

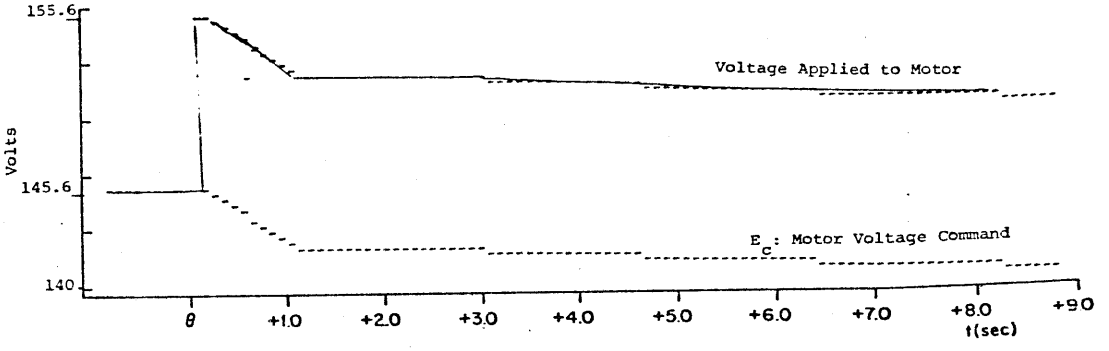

Figure 4.22
Commanded and Actual Motor Voltages
10 Volt Propulsion System Bias

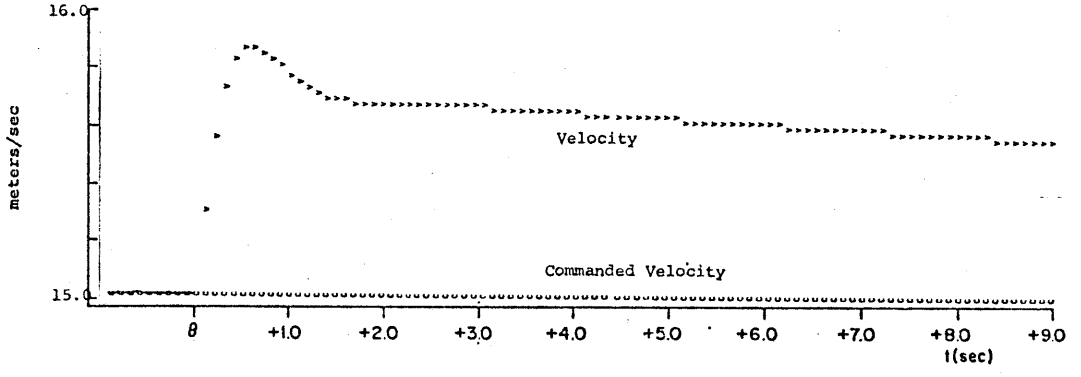

Figure 4.23
Vehicle Behavior, Propulsion System Bias

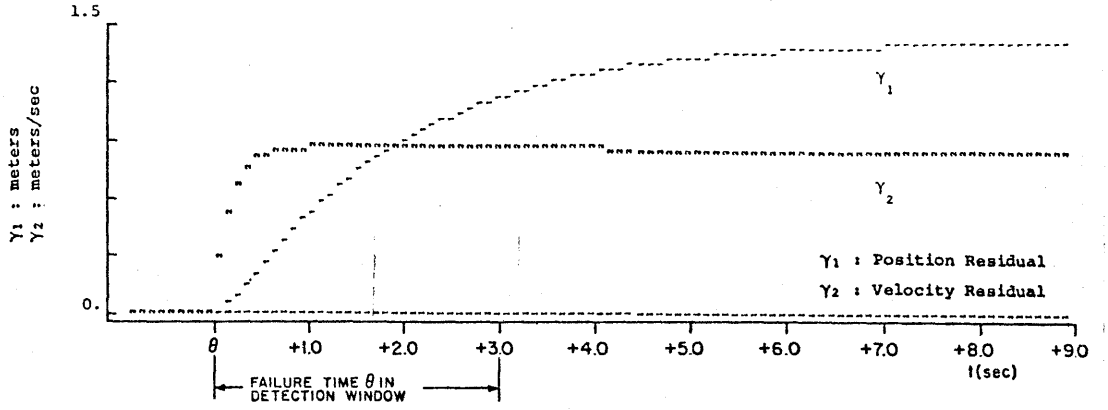

Figure 4.24
Residuals, Propulsion System Bias

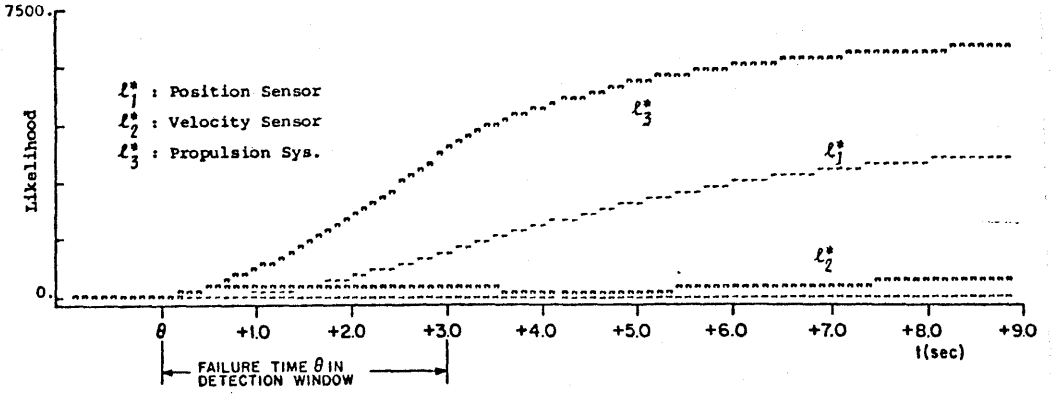

Figure 4.25
Maximum Likelihood Ratios

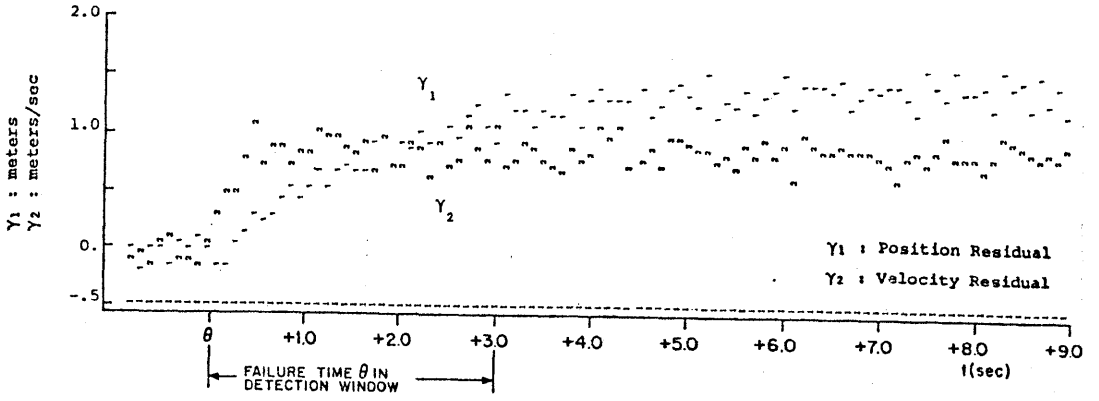

Figure 4.26
Residuals, 10 v. Propulsion Sys. Bias with Noise

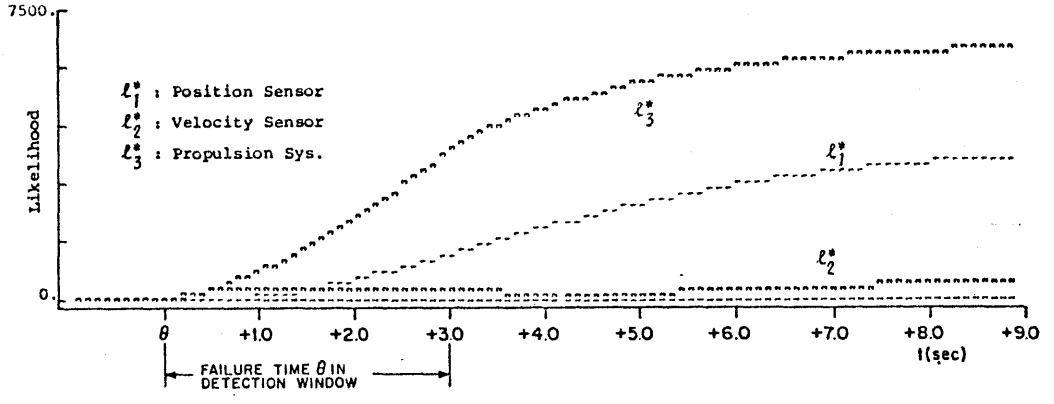

Figure 4.27
Maximum Likelihood Ratios

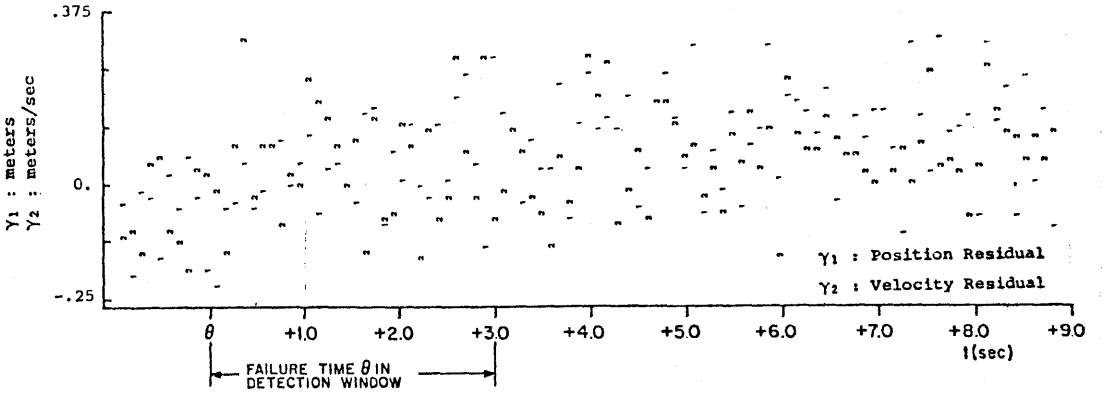

Figure 4.28

Residuals, 1 v. Propulsion Sys. Bias with Noise

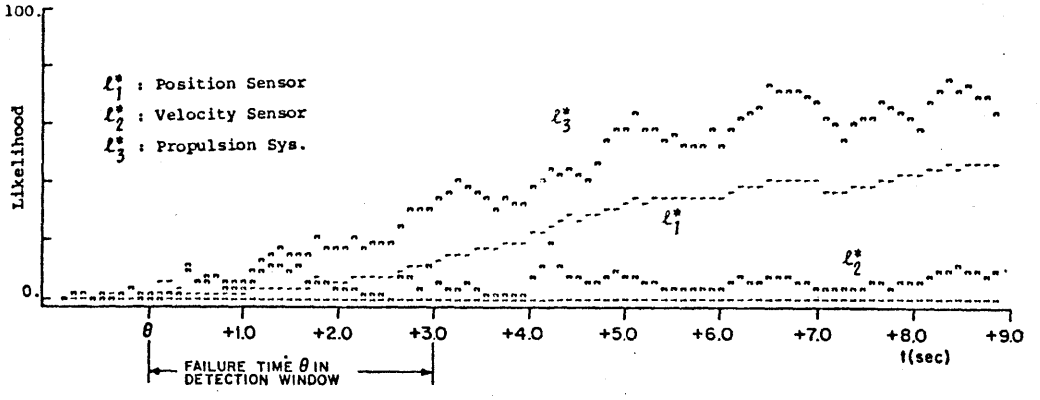

Figure 4.29

Maximum Likelihood Ratios

3) There was a delay until the true location of the failure could be unambiguously identified to be in the propulsion system and not the velocity sensor.

4) Background noise did not affect the detection of a 10σ failure.

5) Detection of a 1σ failure is still possible.

Failure-Free Performance: Noise, Maneuvers, Grade and Wind

In the previous sections we have demonstrated the GLR algorithm's ability to detect sensor and propulsion system bias failures. A key performance characteristic which remains to be examined is the response of the algorithm to failure-free noise, maneuvers, and unmodelled forces such as wind and grade acting on the vehicle. The sensitivity of the algorithm to these effects will determine the false-alarm characteristics of the algorithm. The following sections present tests of the GLR algorithm on simulated vehicle data which includes these disturbances and forces, but is free of any vehicle failures.

4.3.4 Gaussian Plant and Sensor Noise

The effects of Gaussian plant and sensor noise on the likelihood ratios in the presence of a failure have been examined. The variance, due to the noise, of $\ell_i^* = \ell_i(k;\ \hat{\theta}=\theta)$ can be computed analytically (equation 3-33b).

Under failure-free conditions, each likelihood ratio $\ell_i(k;\tilde{\theta})$ in the detection window $k-M \leq \tilde{\theta} \leq k-N$ is a central chi-squared random variable,

with mean 1 and a variance of 2. However, the density function for $\ell_i^*(k)$, the maximum of the likelihood ratios over the detection window, can not readily be determined (the LR's are mutually correlated). Since ℓ_i^* is used in the decision rule, clearly its nominal behavior and range of values must be determined. We shall do this via simulations.

Scenario

In this ten second simulation, the vehicle was commanded to maintain a constant velocity of 15m/s. Gaussian plant and sensor noise was added to the propulsion system and measurements. The intensity of the noise "matched" the intensity assumed in the design of the Kalman-Bucy filter.

Results

The response of the vehicle to the random disturbances is illustrated in Figure 4.30. Residual and maximum likelihood ratios appear in Figure 4.31 and 4.32. It is observed that the MLR's lie in a range 0-7. We could use this observation in determining thresholds in a decision rule, since the observed range of the MLR's implies that a lower bound on a failure decision threshold must be at least 7 to avoid false alarms caused solely by the background noise. However, as shall be seen, the effect of wind and grade forces will in practice play the largest role in the determination of decision thresholds.

4.3.5 Commanded Vehicle Maneuvers

It is clearly essential that the failure detection system not respond to normal maneuvers of the vehicle. During maneuvers, however, the effects

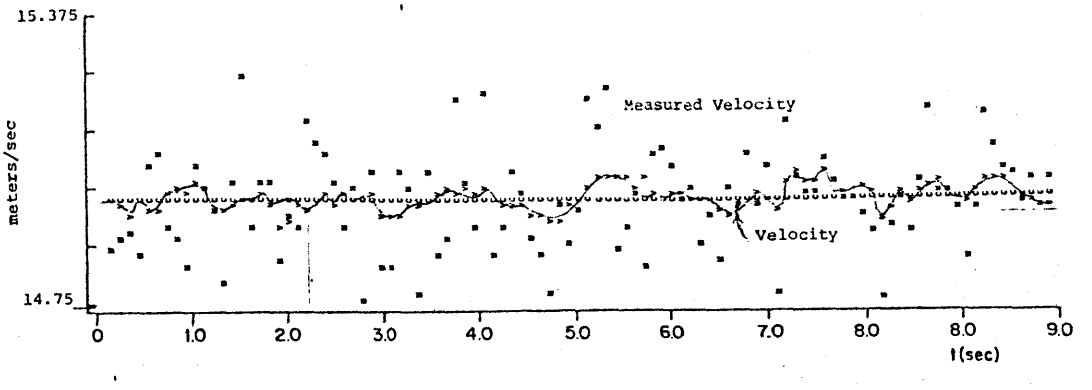

Figure 4.30 - Vehicle Behavior, Random Gaussian Noise

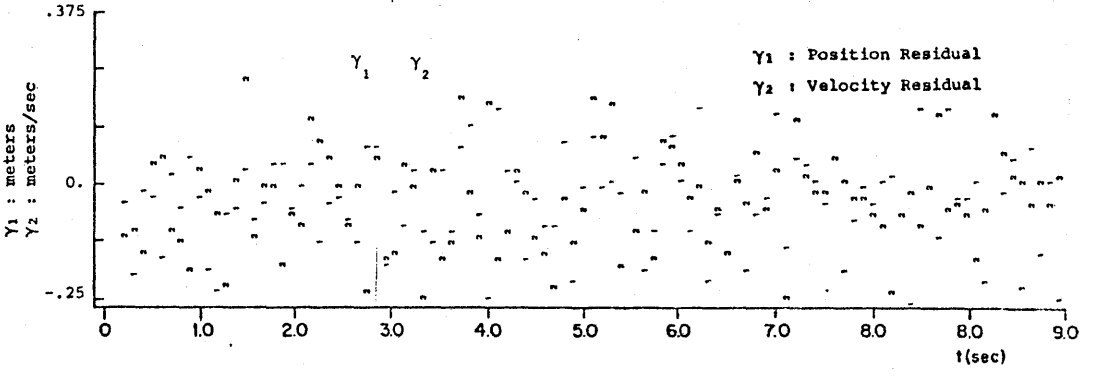

Figure 4.31 - Residuals

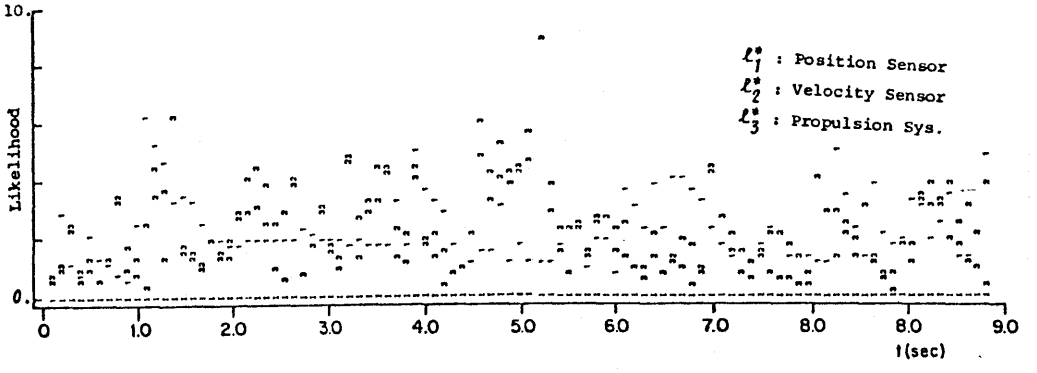

Figure 4.32 - Maximum Likelihood Ratios

of sampling may be the greatest, thus adversely affecting the failure detection system.

The discretized vehicle model embedded in the Kalman-Bucy filter assumes that the input to the model, $E_c(k)$ is the same as the input to the motor, and is held constant over the time period k to k+1 with a zero-order hold (Figure 4.7); in fact the motor voltage command $E_c(t)$ is not constant over the interval when maneuversare being performed. This will cause a slight discrepancy between the actual vehicle and the discretized model in the failure detection system. The discrepancy will be the greatest when the vehicle is at maximum acceleration, for then the rate of change of the motor voltage command will be at its maximum, and the error (shaded area, Figure 4.33) will be greatest. The amount of error in the approximation to the voltage command will depend on the sampling rate.

Scenario

The vehicle was commanded to increase its velocity from 15m/s to 18m/s at service limits, via the jerk profile, Figure 2.2. Vehicle response is shown in Figure 4.34. No Gaussian noise was present.

Results

As predicted, the peak of the velocity residual (Figure 4.35) coincides with the vehicle's period of maximum acceleration. The propulsion system MLR ℓ_3^* reaches a peak value of 12 during the maneuvers (Figure 4.36).

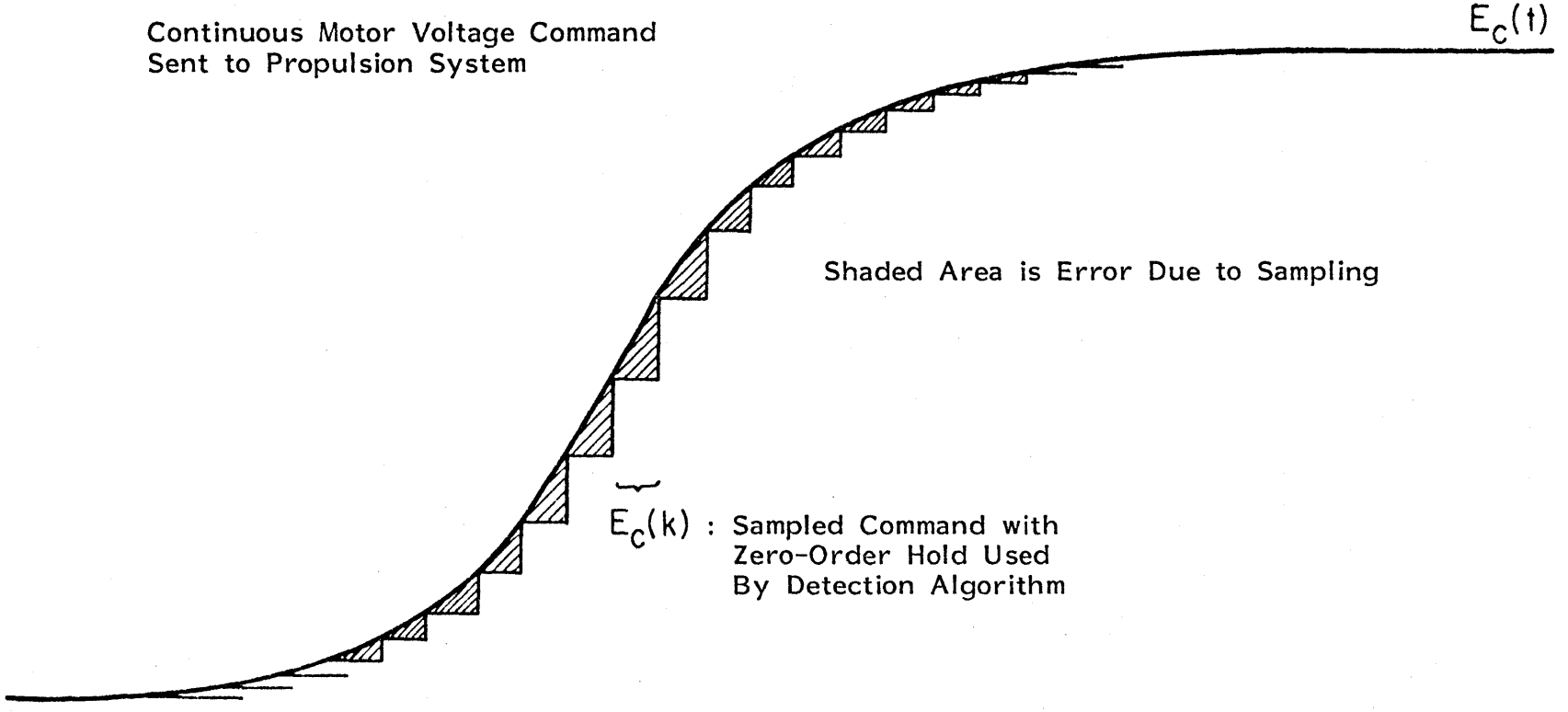

Figure 4.33

Error Due to Sampling Continuous Motor Voltage Command

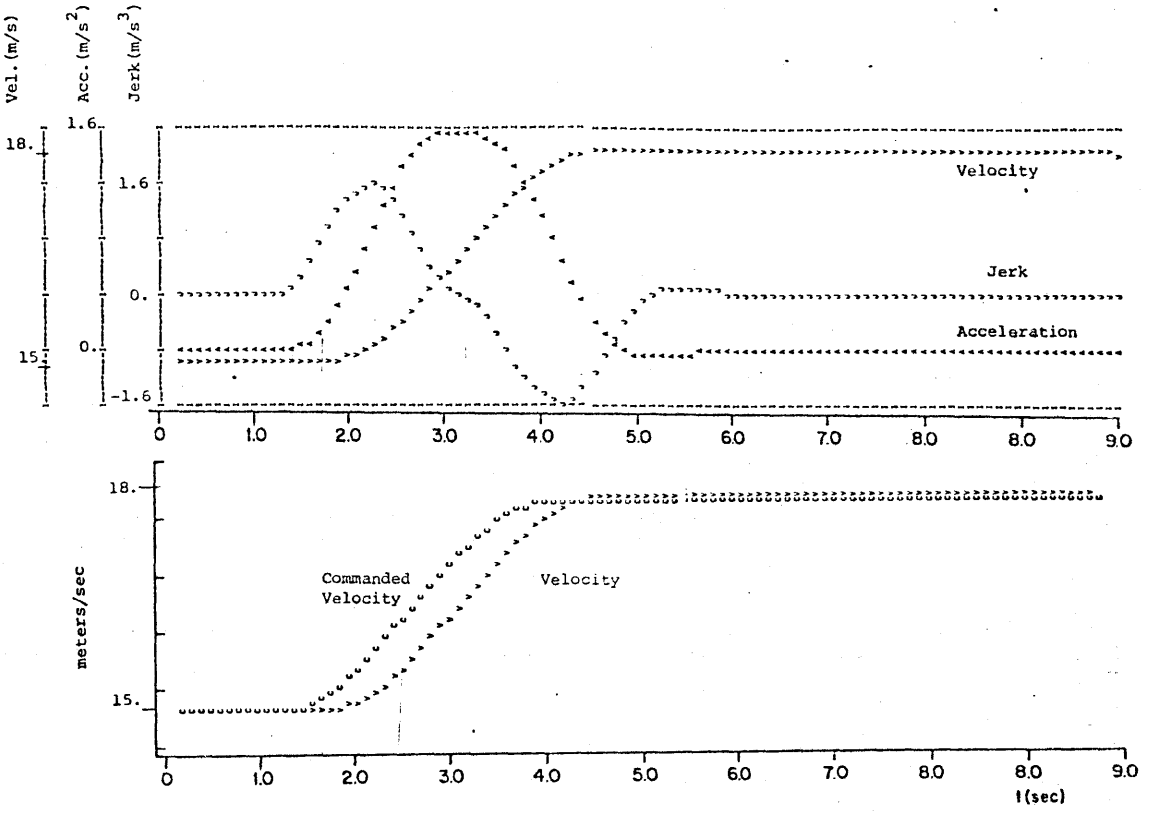

Figure 4.34 - Vehicle Behavior, Line-Speed Chg. Maneuver

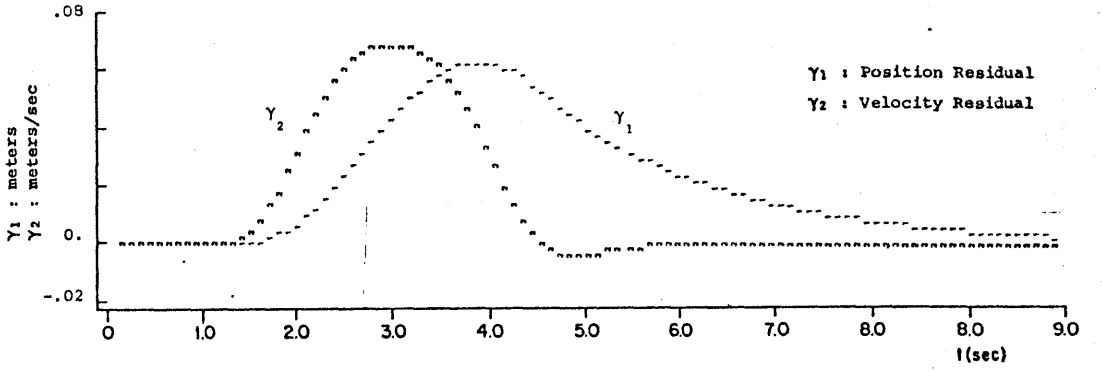

Figure 4.35 - Residuals

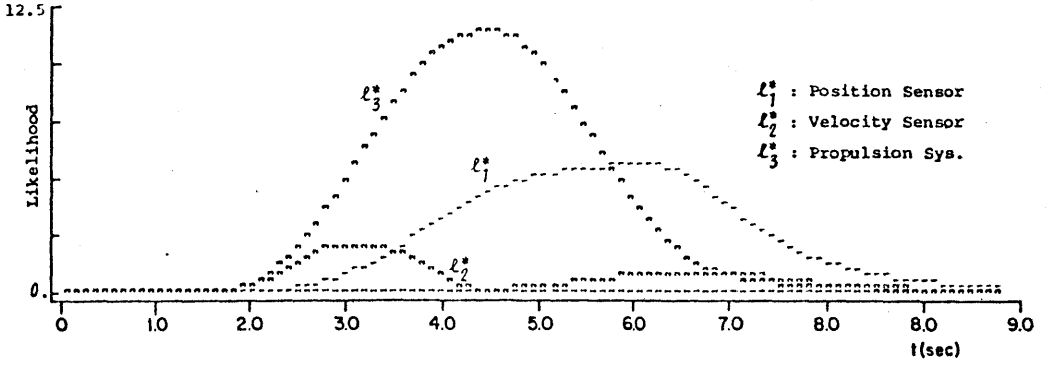

Figure 4.36 - Maximum Likelihood Ratios

Summary

The effects of errors induced by discrete-time sampling must be taken into consideration, as these errors may become large during vehicle maneuvers. If sampling rates are high enough, however, vehicle maneuvers will not cause false alarms.

4.3.6 Wind and Grade

The two forces acting on the vehicle which are most likely to cause false alarms are wind and grade forces. These unmodelled forces will appear to the GLR algorithm as bias failures in the propulsion system. To gain an appreciation for the magnitude of these forces, the propulsive force required to maintain a constant velocity in the presence of a 6% grade or a 30m/s headwind may be on the order of 5 times the propulsive force necessary to maintain that velocity on a level guideway with no wind. Simulations were performed to determine the GLR algorithm's sensitivity to these forces.

Scenario (Grade)

To determine the effects of grade, the transition from a level guideway to a 6% grade was simulated. The grade transition, beginning at time t=1.0, occurred at a constant rate of 10%/sec so that the 6% transition was completed in 0.6 sec. (Figure 4.37). This represents a transition length of 9 meters. The grade remained in effect for the remainder of the simulation. The response of the vehicle to the grade force is shown in Figure 4.38.

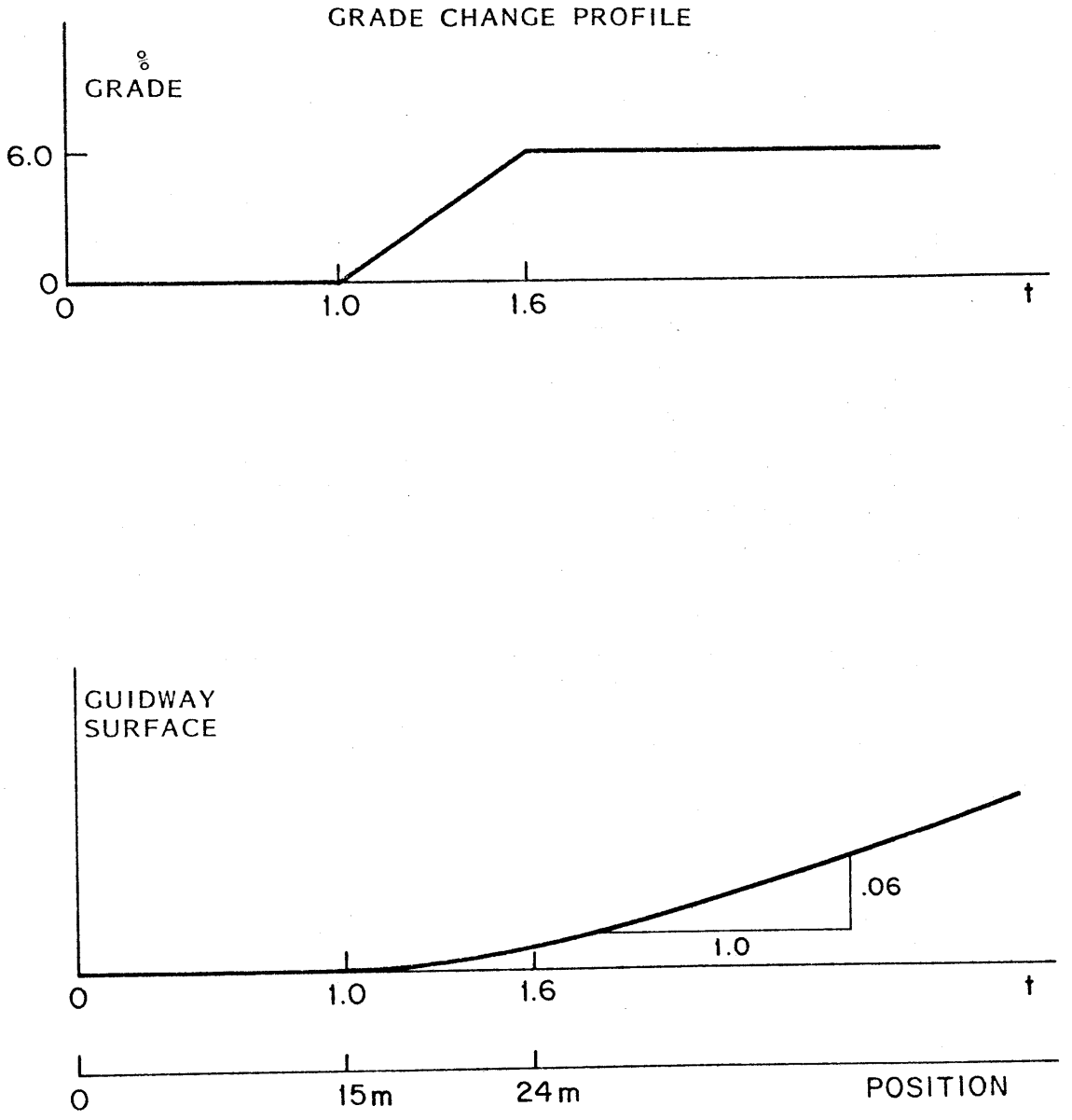

Figure 4.37
Grade Profile

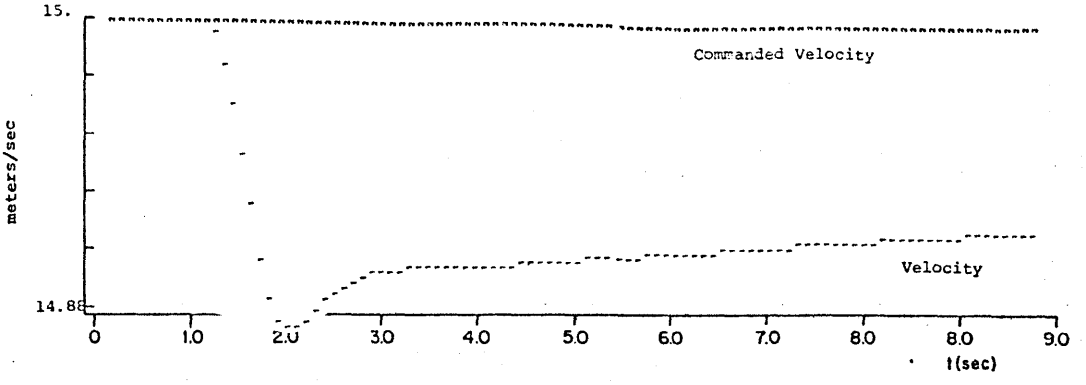

Figure 4.38 - Vehicle Behavior, 6% Grade

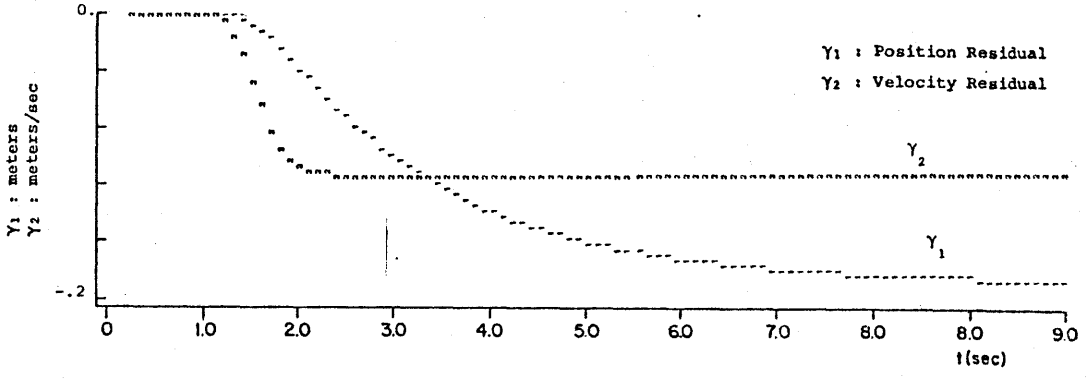

Figure 4.39 - Residuals

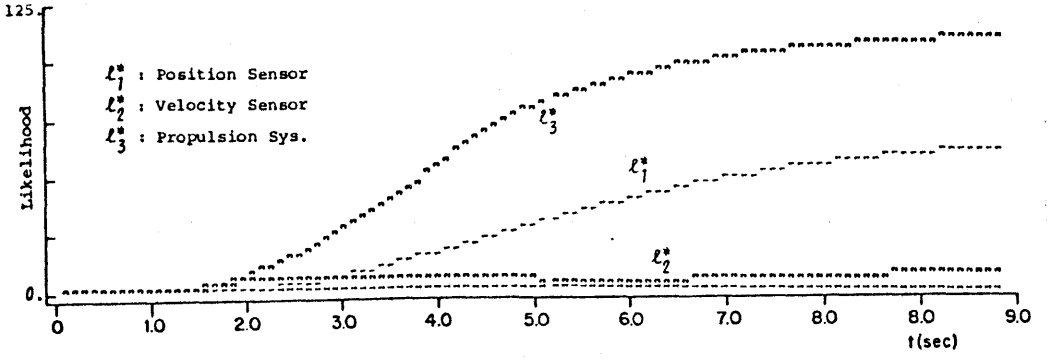

Figure 4.40 Maximum Likelihood Ratios

Results

The Kalman-Bucy filter residuals are shown in Figure 4.39. Observe that they contain a signature similar to a propulsion bias failure. The maximum likelihood ratio for the voltage actuator failure, ℓ_3^*, shows in Figure 4.40, that this is indeed the case. Nine seconds after the transition was begun, this MLR reaches a value near 125.

Scenario (Wind)

A simulation was performed in which the vehicle, at a velocity of 15m/s, encountered an 18m/s headwind gust. Relative to the vehicle, the wind transition from 0-18m/s lasted one-half second, occurring at a constant rate (Figure 4.41). Vehicle response to the headwind is shown in Figure 4.42.

Results

Filter residuals (Figure 4.43) and likelihood ratios (Figure 4.44) are similar to those caused by the grade, although of a larger magnitude. Nine seconds after the initiation of the gust, ℓ_3^* has reached a value near 1000.

Summary of Results

1) Wind and grade appear to the detection system as propulsion failures, since although the motor voltage command is increasing, observed velocity decreases.
2) The likelihood ratio ℓ_3^* continues to grow as long as the wind or grade force is present, even when the transition time has passed out of the detection window.
3) Wind and grades are thus likely to cause false alarms.

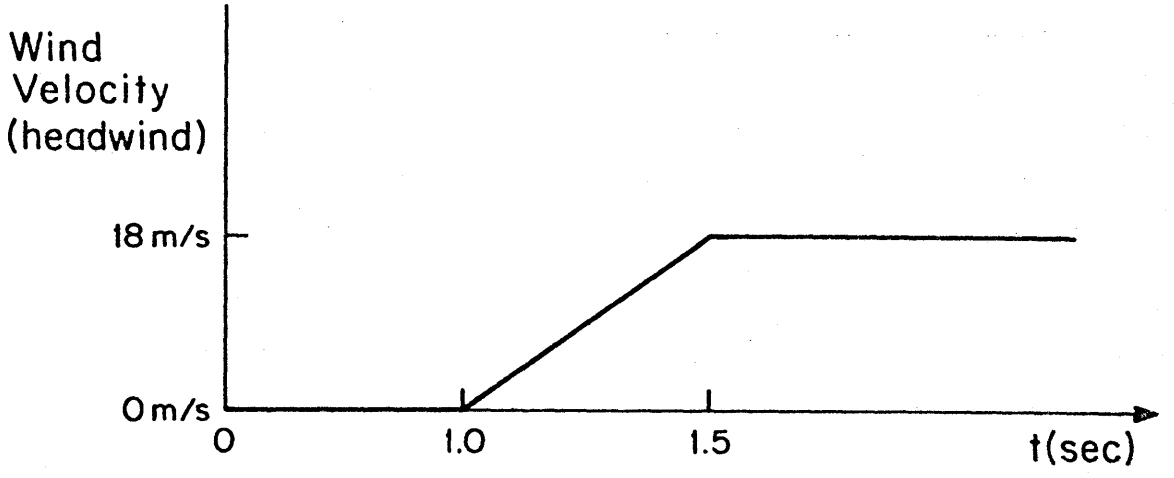

Figure 4.41

18 m/s Headwind Profile

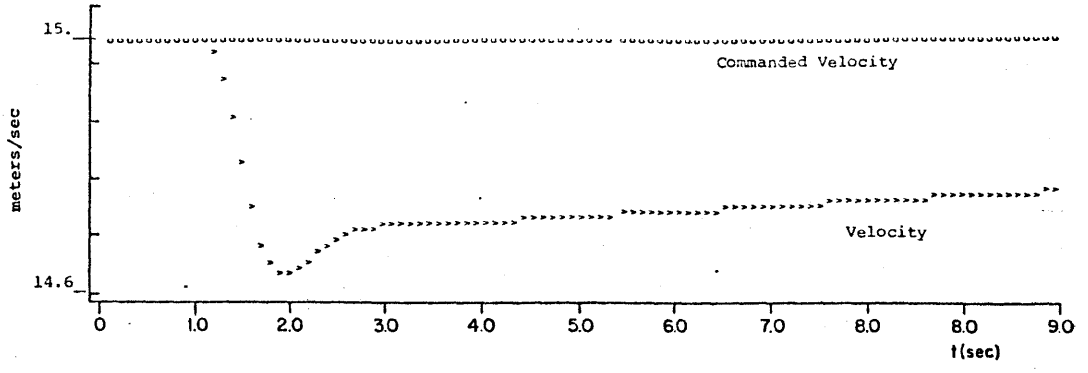

Figure 4.42 - Vehicle Behavior, 18 m/s Headwind

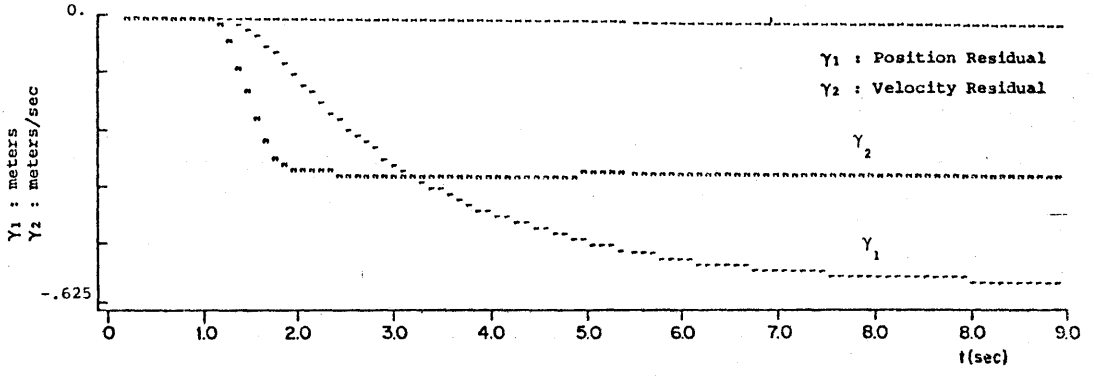

Figure 4.43 - Residuals

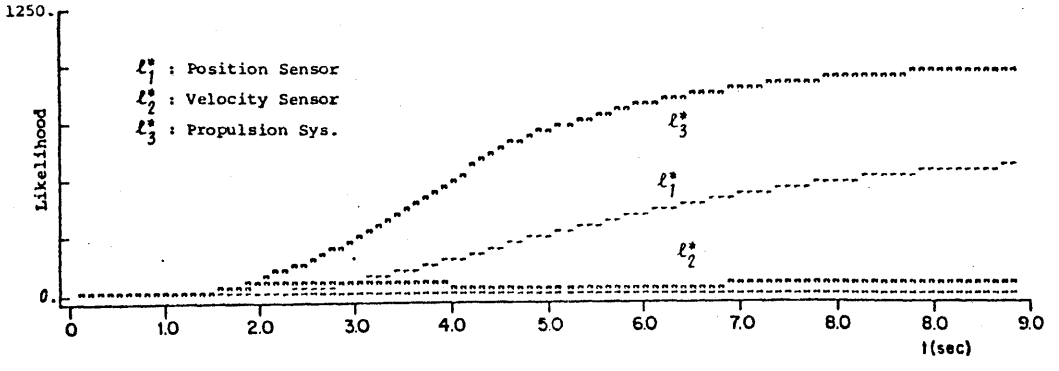

Figure 4.44 - Maximum Likelihood Ratios

Discussion

Wind and grade forces may pose formidable problems for the failure detection system, as the distinguishability between the effects of these forces and failures in the propulsion system is difficult.

Decreasing the sensitivity of the algorithm, either by raising decision thresholds or by increasing the assumed variance of the plant noise is not a viable solution since 1) the likelihood ratios keep growing, and 2) this will worsen propulsion failure detection performance.

One possible solution to the false alarm problem is to model wind and grade explicitly in the vehicle model. This would require on-line measurements of these forces. Although guideway grade information could be stored on-board the vehicle (e.g., in a processor's read-only-memory), an on-board air speed indicator is required for wind measurement; the cost of the additional hardware would be prohibitive.

Another alternative is to replace Pitts' relatively detailed vehicle model with a simplified model which will not contain modelling errors in the presence of wind and grade. This possible solution will now be examined.

4.4 Simplified Vehicle Models

4.4.1 Introduction

The system model, (3-1) and (3-2) plays a key role in the GLR algorithms ability to detect various failures, to identify the location of the failure in the system, and to avoid false alarms caused by various disturbances. The purpose of this section is to illustrate how the choice of different system

models can provide tradeoffs of the algorithms performance under both failure and failure-free conditions.

In Pitts' vehicle model (2-1), used in developing the GLR algorithm, assumptions about the vehicle's motor characteristics, load, and forces acting on the vehicle were made in the choice of the parameters C_0, C_1, and K_M. These uncertain parameters cause the modelling errors which cause false alarms. The vehicle models we will now examine contain no parameter uncertainty; they employ kinematic relationships which are known with certainty.

4.4.2 Model Descriptions

The first alternative vehicle model we will present makes only one assumption about the AGT vehicle's dynamics - namely, that the vehicle's velocity will follow, reasonably well, the velocity command generated by the velocity command generator. The extent to which this assumption is valid, even in the presence of winds and grades, will depend on the ability of the velocity regulator to maintain commanded velocity. The assumption can be modelled as follows:

$$\dot{x}(t) = [0]x(t) + v_c(t) + \omega(t) \tag{4-8}$$

where $x(t)$ is the vehicle's position, $v_c(t)$ is the velocity command, and $\omega(t)$ represents the difference between the commanded and actual velocities.

A measurement of position is represented by:

$$x_m(t) = [1]x(t) + n_1(t) \tag{4-9}$$

where $x_m(t)$ is the position sensor measurement and $n_1(t)$ is the measurement noise.

The above model's single state variable, position, prevents the representation of a velocity sensor measurement. Through the addition of a velocity state variable, and by modelling the kinematic relationship between position and velocity (i.e., that the derivative w.r.t. time of position is velocity) we are able to employ the available velocity measurement in the model:

$$\begin{bmatrix} \dot{x}(t) \\ \dot{v}(t) \end{bmatrix} = \begin{bmatrix} 0 & 1 \\ 0 & 0 \end{bmatrix} \begin{bmatrix} x(t) \\ v(t) \end{bmatrix} + \begin{bmatrix} 0 \\ 1 \end{bmatrix} a_c(t) + \begin{bmatrix} 0 \\ \omega(t) \end{bmatrix} \tag{4-10}$$

$$\begin{bmatrix} x_m(t) \\ v_m(t) \end{bmatrix} = \begin{bmatrix} 1 & 0 \\ 0 & 1 \end{bmatrix} \begin{bmatrix} x(t) \\ v(t) \end{bmatrix} + \begin{bmatrix} n_1(t) \\ n_2(t) \end{bmatrix} \tag{4-11}$$

where $x(t)$ is the vehicle's position, $v(t)$ its velocity, $a_c(t)$ the commanded acceleration (the derivative of $v_c(t)$), $\omega(t)$ the difference between actual and commanded acceleration, $x_m(t)$ and $v_m(t)$ the sensor measurements of position and velocity, and $n_1(t)$ and $n_2(t)$ the measurement noise. Due to the structure of the velocity command generator of our study vehicle (Figure 2.3), the acceleration command $a_c(t)$ could be made readily available.

Intuitively, position and velocity sensor failures will be detected by the GLR algorithm employing the above models by the apparent violation of the kinematic relationship between position and velocity which is observed during

a sensor failure. Propulsion system failures will be detected when the commanded velocity (acceleration) differs greatly from the actual velocity (acceleration).

Since the above models represent Kinematic relationships and use velocity or acceleration Commands as input, we shall refer to (4-8), (4-9) and (4-10), (4-11) as vehicle models KC1 and KC2 respectively.

The discrete-time equivalents to the above continuous-time models can be found (Appendix B) and are given below for a sampling interval of $\Delta t=0.1$ second:

KC1 - Kinematic Vehicle Model; Velocity Command Input

State Equation

$$x(k+1) = [1]x(k) + [0.1]v_c(k) + \omega(k) \tag{4-12}$$

Measurement Equation

$$x_m(k) = [1]x(k) + n_1(k) \tag{4-13}$$

KC2 - Kinematic Vehicle Model; Acceleration Command Input

State Equation

$$\begin{bmatrix} x(k+1) \\ v(k+1) \end{bmatrix} = \begin{bmatrix} 1.0 & .1 \\ 0 & 1.0 \end{bmatrix} \begin{bmatrix} x(k) \\ v(k) \end{bmatrix} + \begin{bmatrix} 5.0E\text{-}3 \\ 0.1 \end{bmatrix} a_c(k) + \begin{bmatrix} \omega_1(k) \\ \omega_2(k) \end{bmatrix} \tag{4-14}$$

Measurement Equation

$$\begin{bmatrix} x_m(k) \\ v_m(k) \end{bmatrix} = \begin{bmatrix} 1 & 0 \\ 0 & 1 \end{bmatrix} \begin{bmatrix} x(k) \\ v(k) \end{bmatrix} + \begin{bmatrix} n_1(k) \\ n_2(k) \end{bmatrix} \tag{4-15}$$

The above models can be simplified even further by a model which makes no assumptions about the vehicles control or propulsion system. The following model simply represents the kinematic relationship between position and velocity measurements:

State Equation

$$\dot{x}(t) = [0]x(t) + v_m(t) + n_2(t) \qquad (4\text{-}16)$$

Measurement Equation

$$x_m(t) = [1]x(t) + n_1(t)$$

where $x(t)$ is the vehicle's position, $x_m(t)$ and $v_m(t)$ the measured position and velocity, and $n_1(t)$ and $n_2(t)$ the measurement noise. This representation is comparable to (4-8), except the velocity sensor measurement is used to drive the state variable, instead of the velocity command. Notice the manipulated model above contains no plant noise; only measurement noise is present.

Intuitively, the GLR algorithm, when based on this vehicle model, will detect sensor failures by the invalidation of the kinematic relation which should relate the position and velocity measurements. Since the propulsion system is not modelled, propulsion system failures can not be detected; however, wind and grade will not cause false alarms, since these forces will not affect the sensors' kinematic relationship. Thus we see the tradeoff between detection ability and false alarms taken to one extreme.

Since the above model employs Kinematic relationships and uses a Sensor measurement as input, it will be referred to as KS1. The equivalent discrete-time representation is given below:

KS1 - Kinematic Vehicle Model; Velocity Sensor Input

State Equation

$$x(k+1) = [1]x(k) + [0.1]v_m(k) + n_2(k) \tag{4-18}$$

Measurement Equation

$$x_m(k) = [1]x(k) + n_1(k) \tag{4-19}$$

The three models KS1, KC1 and KC2, whose block diagrams are shown in Figure 4.45, were used in the GLR algorithm and tested under conditions identical to those used in testing the algorithm based on Pitts' model. The failure signatures are shown in Figures 4.46 - 4.48 for position sensor, velocity sensor, and propulsion system bias failures. Tha plant and sensor noise statistics chosen and the resulting Kalman-Bucy filter matrices are given in Tables 4.5 - 4.7.

4.4.3 Performance Results with Simplified Models

4.4.3.1 Position Sensor Bias Failure

The GLR algorithm using the three simplified vehicle models KS1, KC1, and KC2 was run on the position sensor bias failure data (section 4.3.1) Maximum likelihood ratios, (including those previously shown when Pitts' model was used) appear in Figure 4.49.

a) KS1 - Kinematic, Sensor Driven Model

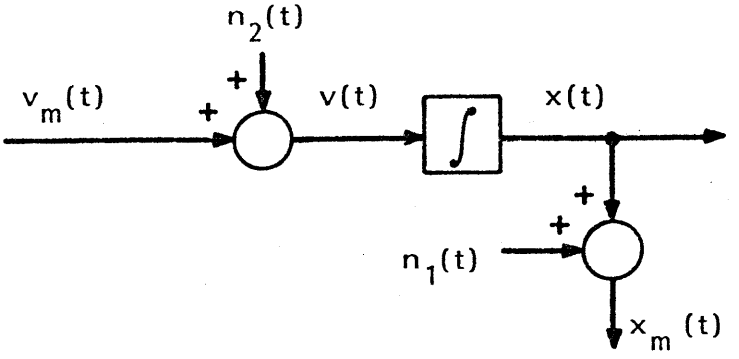

b) KC1 - Kinematic, Velocity Command Driven Model

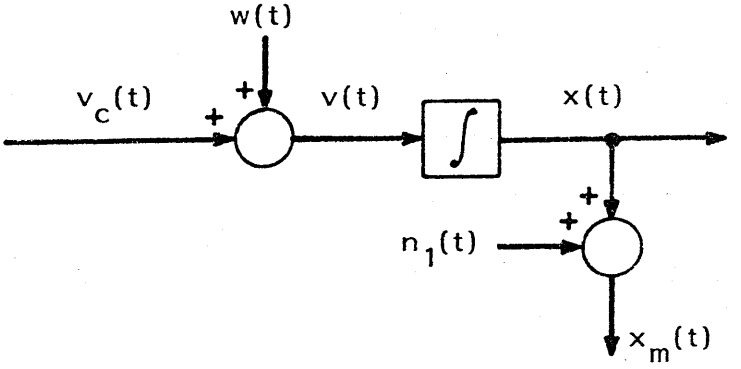

c) KC2 - Kinematic, Acceleration Command Driven Model

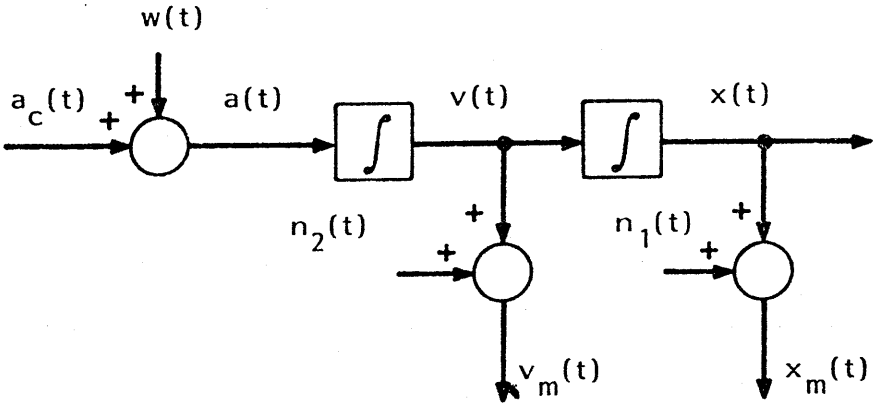

Figure 4.45
Simplified Vehicle Model Block Diagrams

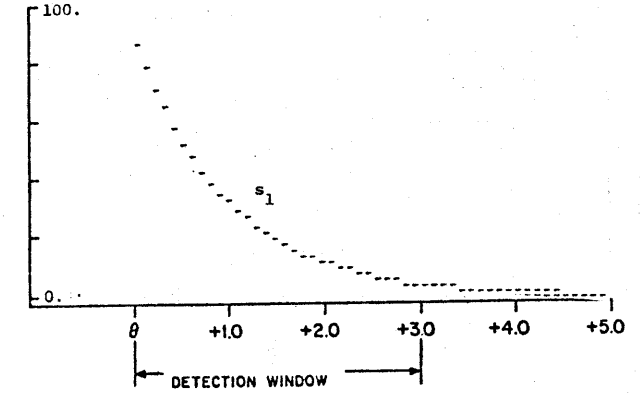

Position Sensor Bias

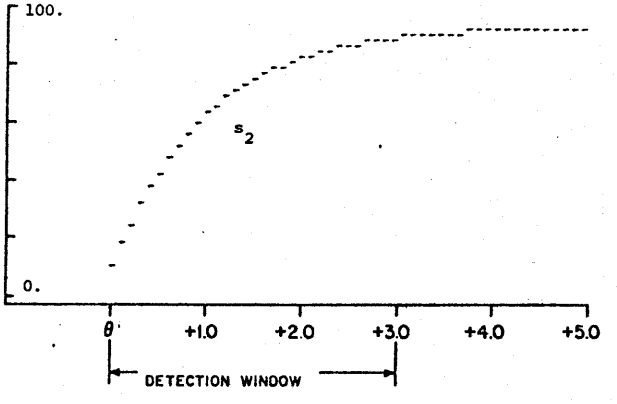

Velocity Sensor Bias

Figure 4.46
Failure Signatures; KS1

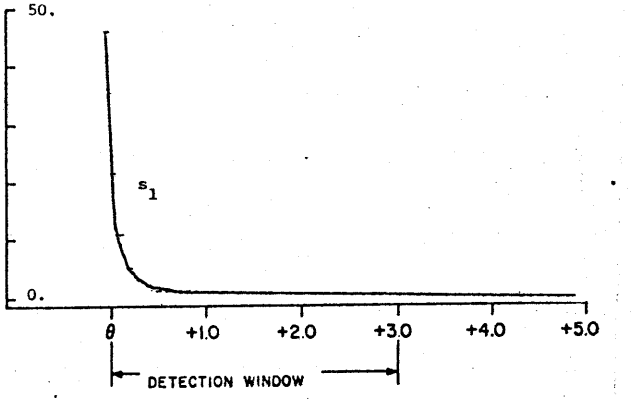

Position Sensor Bias

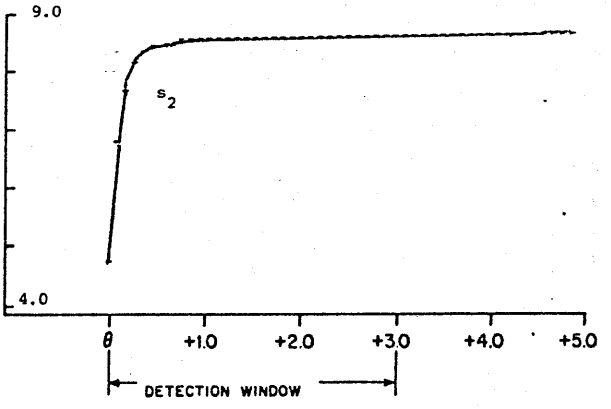

Propulsion System Bias

Figure 4.47
Failure Signatures; KC1

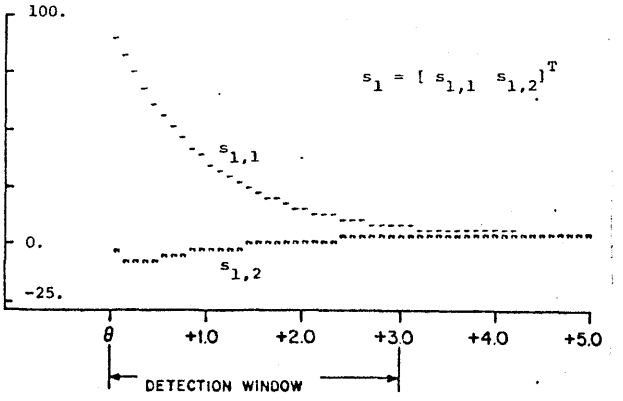

Position Sensor Bias

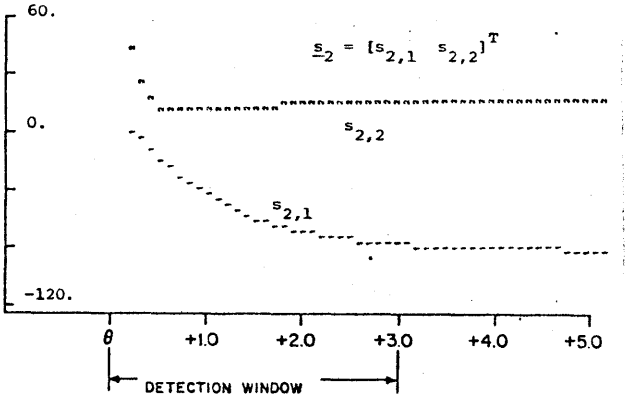

Velocity Sensor Bias

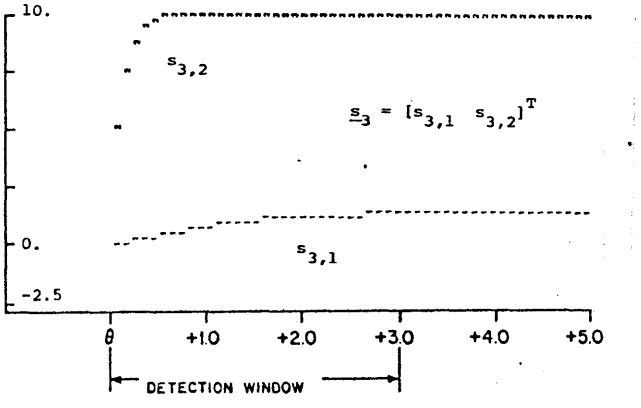

Propulsion System Bias

Figure 4.48 - Failure Signatures; KC2

Table 4.5

Noise Covariance and Kalman-Bucy Filter Matrices

Sensor Driven Kinematic Vehicle Model KS1

```
DISCRETE DRIVING NOISE COVARIANCE MATRIX (Q) -
 1.00000D-04


MEASUREMENT NOISE COVARIANCE MATRIX (R) -
 1.00000D-02


K A L M A N   F I L T E R -
- - - - - -   - - - - - -

CLOSED LOOP EIGENVALUES
      REAL PART                IMAGINARY PART
    0.904875078027496D+00        0.0

CLOSED LOOP MATRIX
 9.04875D-01

KBF FILTER GAIN MATRIX H
 9.51249D-02

PREDICTED ERROR COVARIANCE MATRIX
 1.05125D-03

UPDATED ERROR COVARIANCE MATRIX
 9.51249D-04

RESIDUAL COV MATRIX (V) -
 1.10512D-02

RESIDUAL COV MATRIX INVERSE (V-INVERSE) -
 9.04875D+01
```

Table 4.6

Noise Covariance and Kalman-Bucy Filter Matrices

Velocity Command Driven Kinematic Model KC1

DISCRETE DRIVING NOISE COVARIANCE MATRIX (Q) -
6.40000D-03

MEASUREMENT NOISE COVARIANCE MATRIX (R) -
1.00000D-02

K A L M A N F I L T E R -

CLOSED LOOP EIGENVALUES

REAL PART	IMAGINARY PART
0.4583736308584 80D+00	0.0

CLOSED LOOP MATRIX
4.58374D-01

KBF FILTER GAIN MATRIX H
3.41626D-01

PREDICTED ERROR COVARIANCE MATRIX
1.18163D-02

UPDATED ERROR COVARIANCE MATRIX
5.41626D-03

RESIDUAL COV MATRIX (V) -
2.18163D-02

RESIDUAL COV MATRIX INVERSE (V-INVERSE) -
4.58374D+01

Table 4.7

Noise Covariance and Kalman-Bucy Filter Matrices

Acceleration Command Driven Kinematic Model KC2

```
DISCRETE DRIVING NOISE COVARIANCE MATRIX (Q) -
 1.25000D-05  2.50000D-04
 2.50000D-04  5.00000D-03


MEASUREMENT NOISE COVARIANCE MATRIX (R) -
 1.00000D-02  0.0
 0.0          1.00000D-02


K A L M A N   F I L T E R -
- - - - - -   - - - - - -

CLOSED LOOP EIGENVALUES
      REAL PART                  IMAGINARY PART
    0.503867959357659D+00          0.0
    0.903819494724811D+00          0.0

CLOSED LOOP MATRIX
 9.08219D-01  2.85807D-02
-6.22412D-02  4.99469D-01

KBF FILTER GAIN MATRIX H
 9.17811D-02  6.22412D-02
 6.22412D-02  4.94307D-01

PREDICTED ERROR COVARIANCE MATRIX
 1.10422D-03  1.36672D-03
 1.36672D-03  9.94307D-03

UPDATED ERROR COVARIANCE MATRIX
 9.17811D-04  6.22412D-04
 6.22412D-04  4.94307D-03

RESIDUAL COV MATRIX (V) -
 1.11042D-02  1.36672D-03
 1.36672D-03  1.99431D-02

RESIDUAL COV MATRIX INVERSE (V-INVERSE) -
 9.08219D+01 -6.22412D+00
-6.22412D+00  5.05693D+01
```

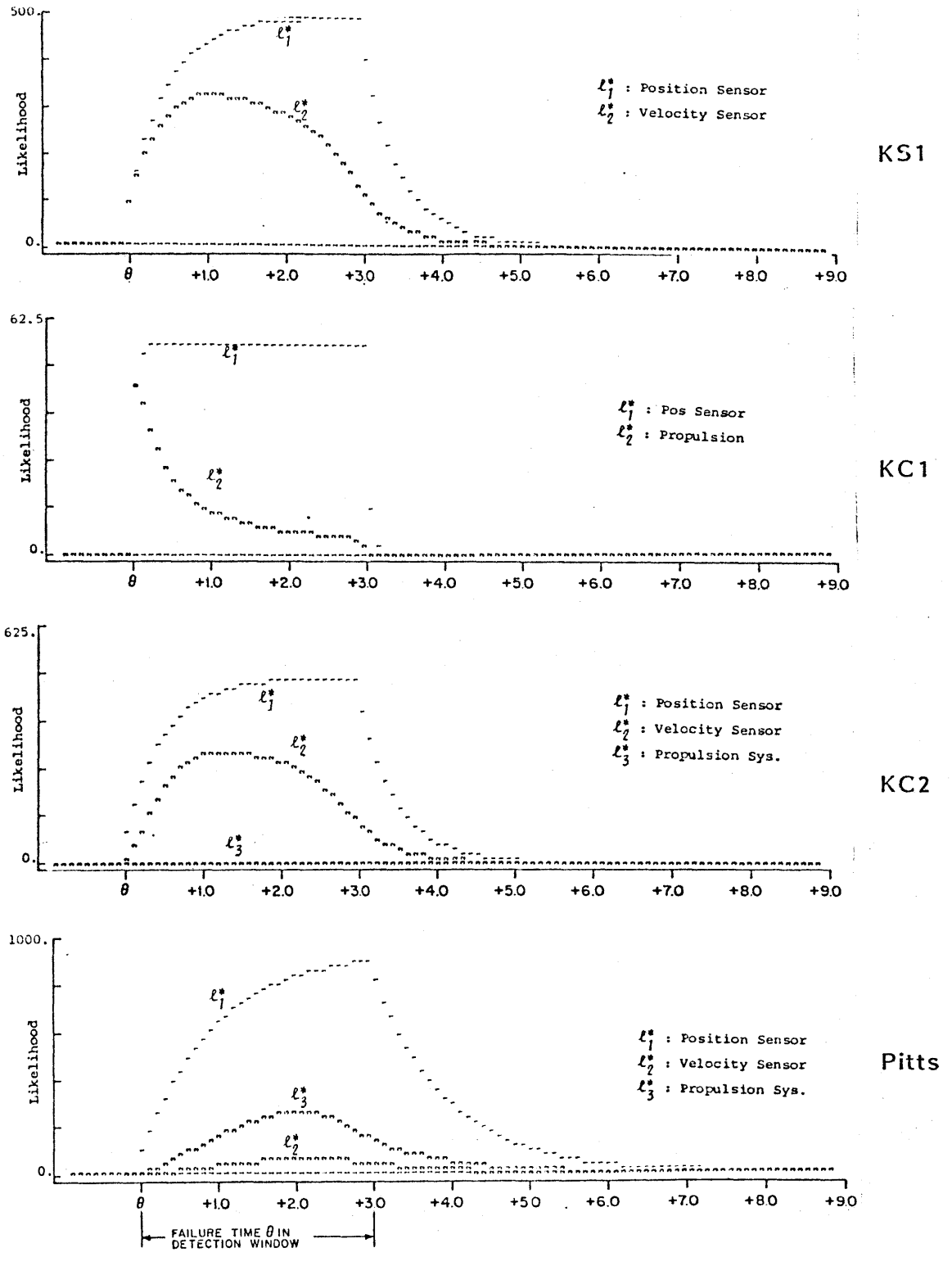

Figure 4.49

Maximum Likelihood Ratios, Position Sensor Bias

The position sensor failure was detected and eventually identified correctly with all of the models. The ability of the algorithm to initially identify the location of the failure varies, however, with the use of the different models. Only after a number of observations have been taken can KS1 and KC1 properly identify the failure location, as the two MLR's in each case jump initially to the same value. Intuitively, the situation is comparable to a dual-redundant set of sensors - when one fails, it can be deduced that there has been a failure, but not which one has failed. In the case of KS1 and KC1, the algorithm has two pieces of "analytically redundant" information - the measurement and the input to the state equation; initially, there is no way to determine which one corresponds to the failure. The physically redundant sensors require a third sensor to properly identify the location of the failure; the GLR algorithm uses the structure of the models KS1 and KC1 to act as the third piece of information required for proper identification.

The detection algorithms based on Pitts' model and KC2, are able to initially identify the true failure location. This result is useful, as it implies that with these models no delay is required to detect and identify a position sensor failure.

Summary of Results

1) Detection of the failure is comparable using all four vehicle models.
2) The single-state variable models KS1 and KC1 require a delay before the location of the failure can be identified.

3) The algorithm using Pitts' model provides the minimum identification delay.

4.4.3.2 Velocity Sensor Bias Failure

The MLR's from the simulated velocity sensor bias (section 4.3.2) are shown in Figure 4.50. The model KC1 is not included as it does not model a velocity measurement. The velocity sensor failure was detected and eventually identified correctly by the algorithm with the three models KS1, KC2, and Pitts'. Even after the true failure time has passed out of the detection window, the MLR's continue to increase, so that biases of small magnitudes will eventually be detected.

Initially, the algorithm based on KC2 and Pitts' models cannot distinguish between the velocity sensor failure and a propulsion failure. A strategy to improve this failure location identification delay will be discussed in section 4.5.

Summary of Results

1) Detection ability is comparable using the models KS1, KC2, and Pitts'.
2) A delay before the location of the failure can be identified is required with the three models.

4.4.3.3 Propulsion System Bias Failure

The GLR algorithms based on the models KS1, KC1, KC2 and Pitts were run on the simulated 10 volt PCU bias failure data (section 4.3.3). Maximum

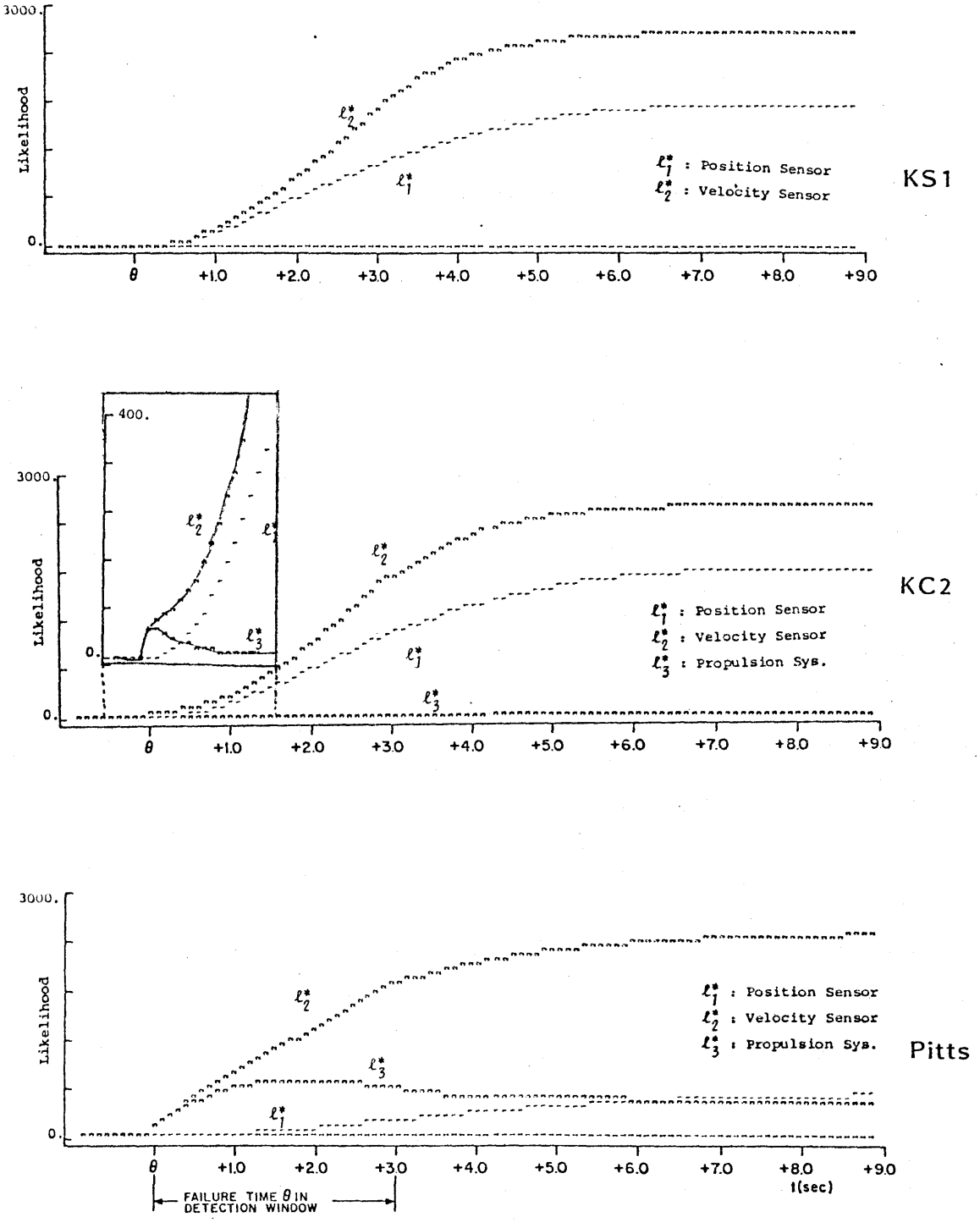

Figure 4.50

Maximum Likelihood Ratios, Velocity Sensor Bias

likelihood ratios are shown in Figure 4.51.

The algorithm based on the model KS1 could not detect the failure, as the propulsion system is not modelled in the algorithm.

With KC1 used in the algorithm, the propulsion system likelihood ratio grows due to the continued discrepancy between the commanded and actual vehicle velocities. With KC2, the transient acceleration, causing a temporary discrepancy between commanded and actual acceleration, produces a peak in the likelihood ratio.

Summary of Results

1) The kinematic sensor model KS1 could not detect the failure.
2) The velocity command driven model KC1 performed better than the acceleration command driven model KC2.
3) Initial identification of failure location was not possible with any of the models used in the algorithm.

4.4.3.4 Wind, Grade, Maneuvers, and Noise

The MLR's obtained from the wind and grade disturbance runs appear in Figures 4.52 and 4.53. The improvement in false alarm performance afforded by the models KS1, KC1, and KC2 compared to Pitts' is clearly evident.

The MLR's obtained when the model KS1 was used remain extremely small, as expected, since the wind or grade forces do not affect the sensors' kinematic relationship. The slight increase which is observed is due solely to the effects of sampling.

The wind and grade forces appear to the algorithm using the model KC1 as a small propulsion system failure, due to the difference between

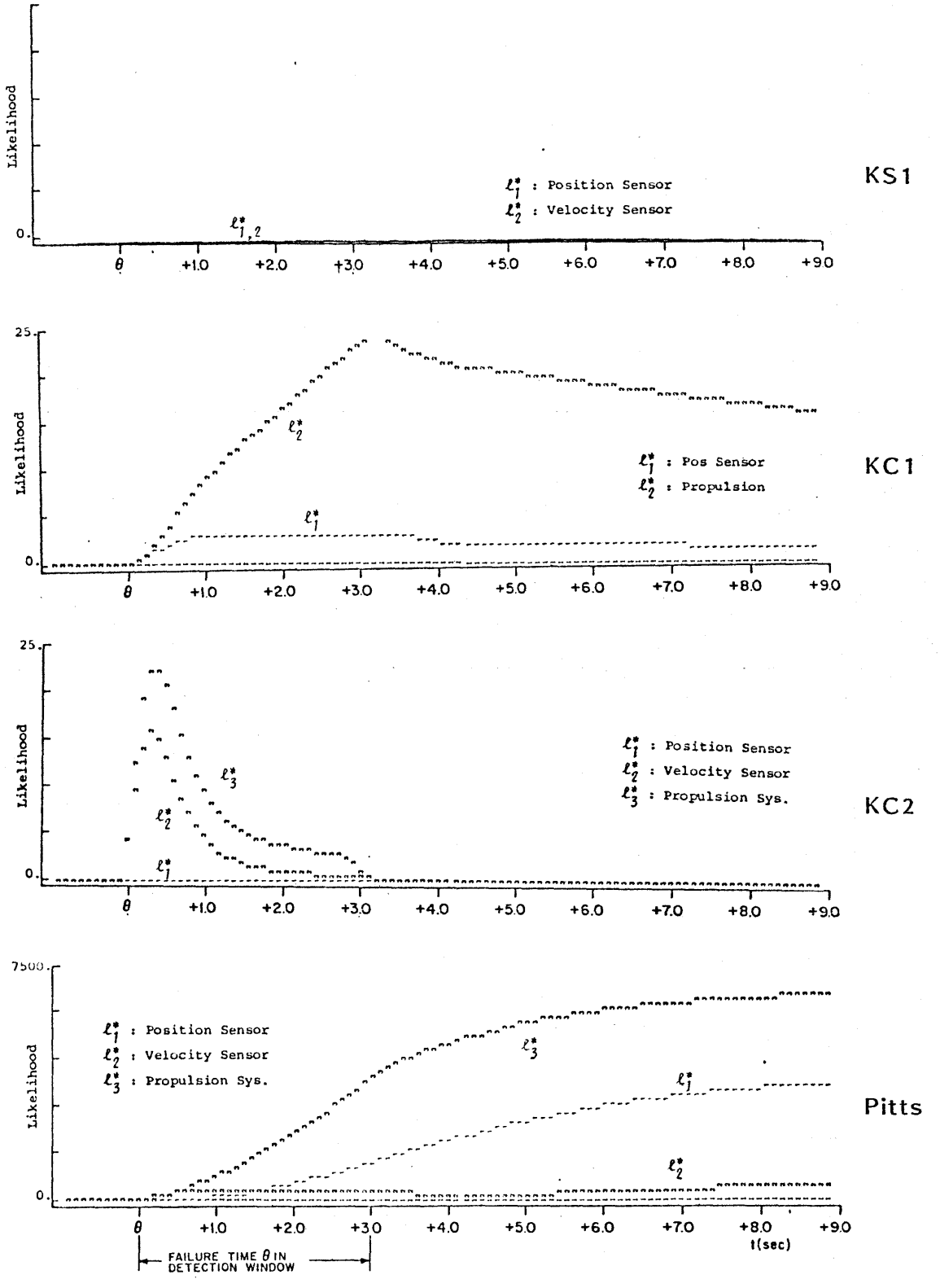

Figure 4.51

Maximum Likelihood Ratios, Propulsion System Bias

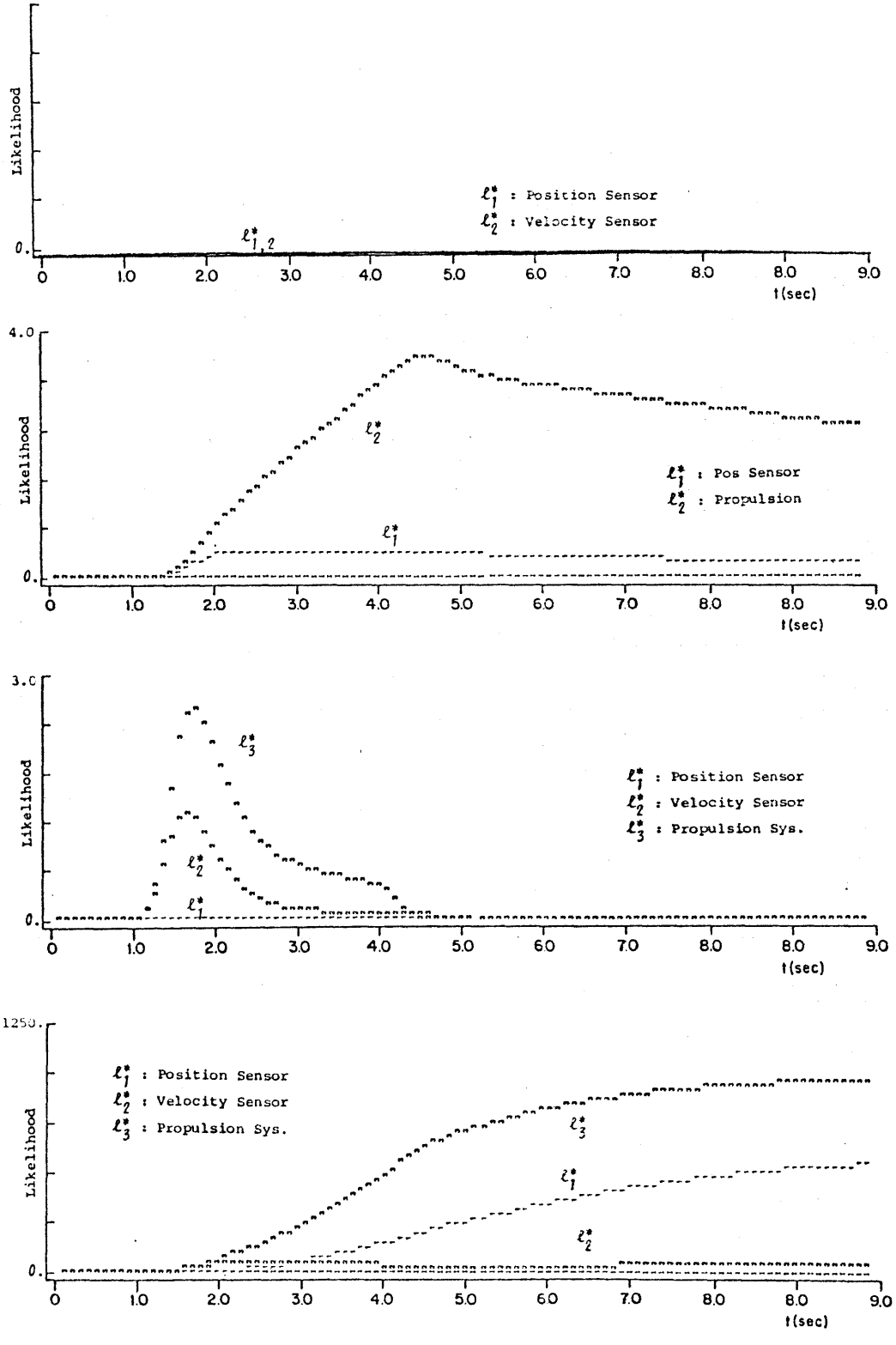

Figure 4.52

Maximum Likelihood Ratios, 18 m/s Headwind

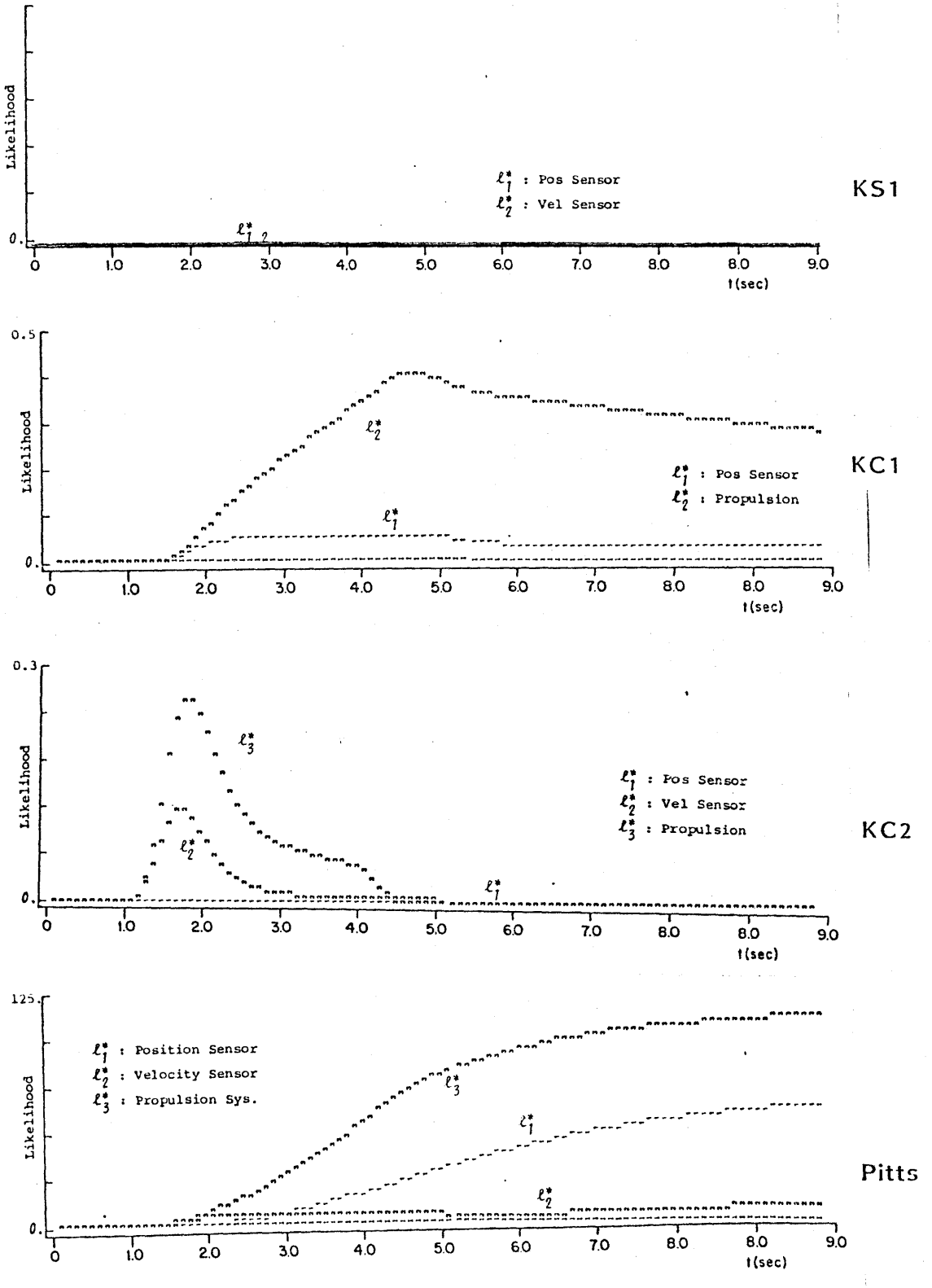

Figure 4.53

Maximum Likelihood Ratios, 6% Grade

the vehicle's commanded velocicty and its actual velocity which has decreased slightly as a result of the force. With the vehicle model and the control system we have simulated, in the presence of the wind the MLR reaches a peak of only 4.0 and then decreases. In general, the peak value of the MLR will depend on the control system's ability to keep the vehicle's velocity at the commanded velocity; if the control system has a high enough bandwidth we would not expect a false alarm with this model used in the algorithm.

The algorithm with the model KC2 detects the temporary acceleration as a result of the application of the wind and grade forces. The MLR reaches a maximum value of 3.0 and then decays rapidly.

The peak values of the MLR's for both models KC1 and KC2 are seen to be insignificant when compared to the MLR's obtained during the line speed change maneuver (Figure 4.54) and random Gaussian noise (Figure 4.55). Since the thresholds in the decision rule would have to be set to tolerate these values, it is unlikely that false alarms would be generated solely by the wind or grade forces.

Regardless of the numerical values of the MLR peaks as a result of the wind or grade, the behavior of the MLR's contrasts significantly with their behavior when Pitts' vehicle model was used in the algorithm. The fact that they do not continue to increase, as they do with Pitts, illustrates how the choice of the vehicle model can have a significant effect on false alarm performance.

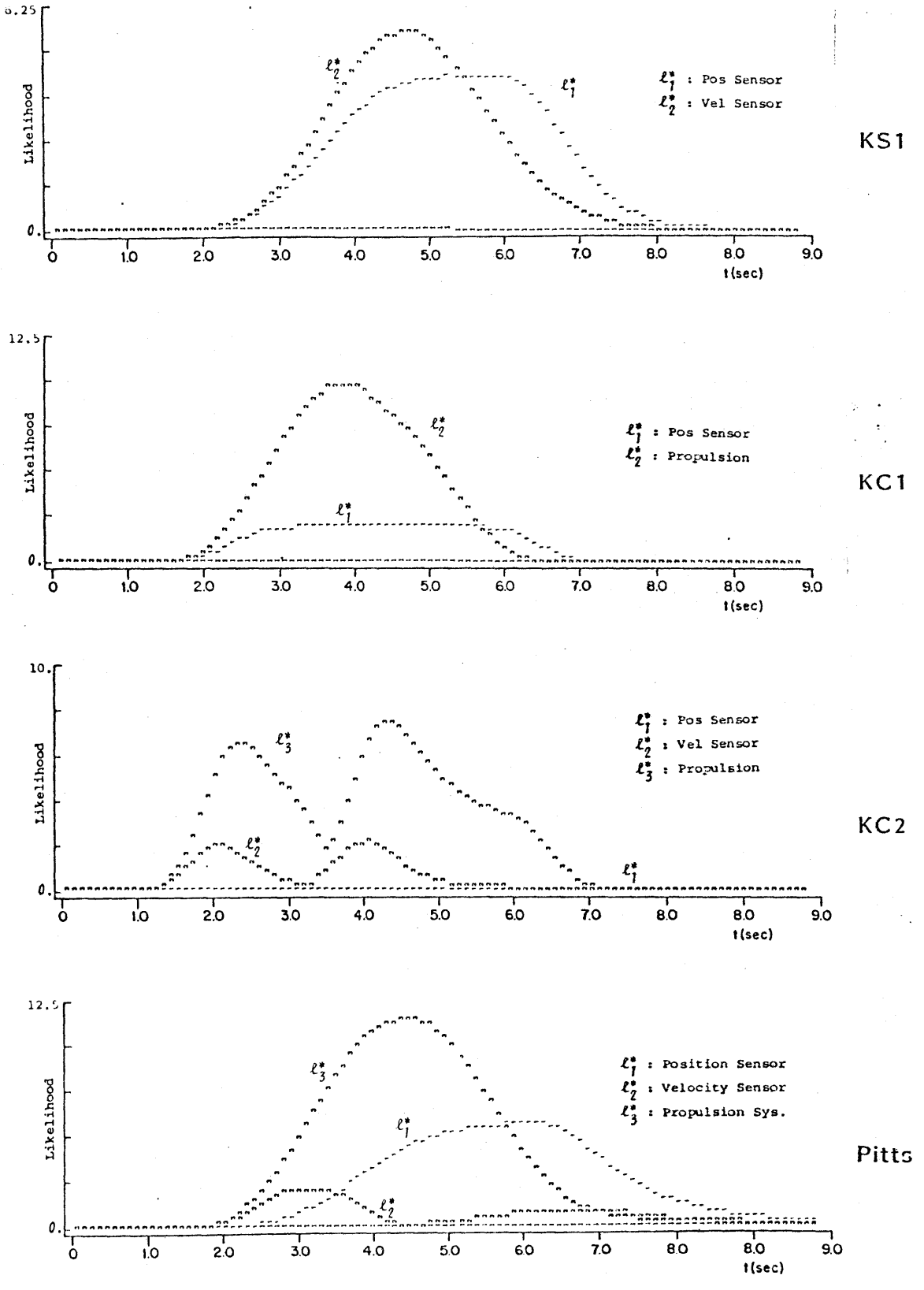

Figure 4.54 - Maximum Likelihood Ratios, Vehicle Maneuver

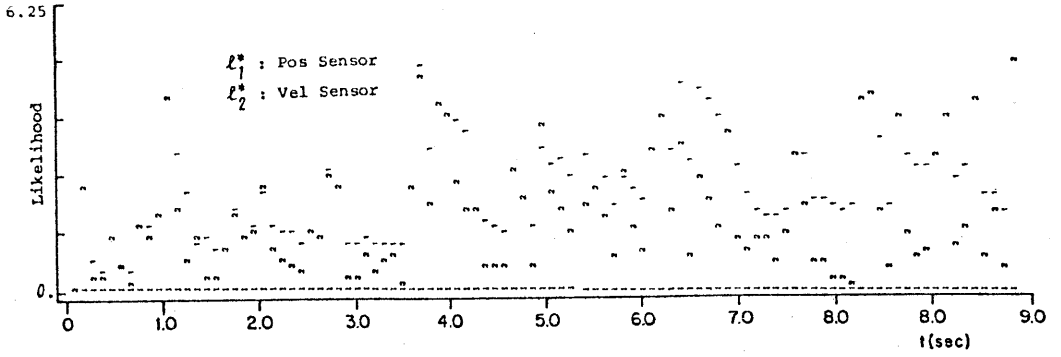

KS1

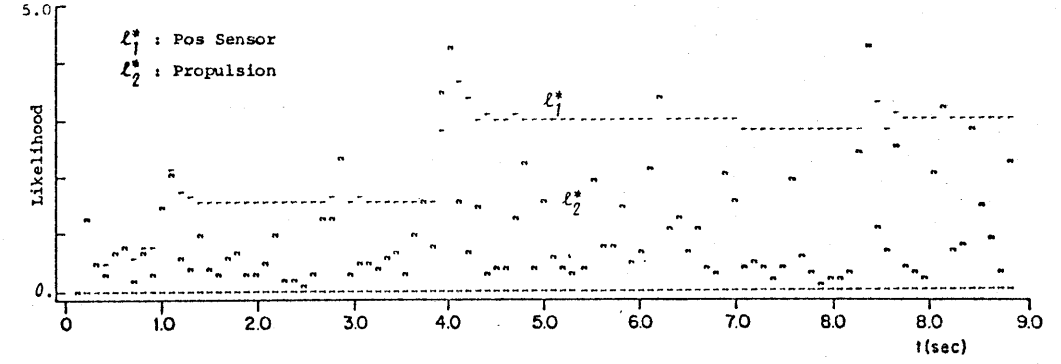

KC1

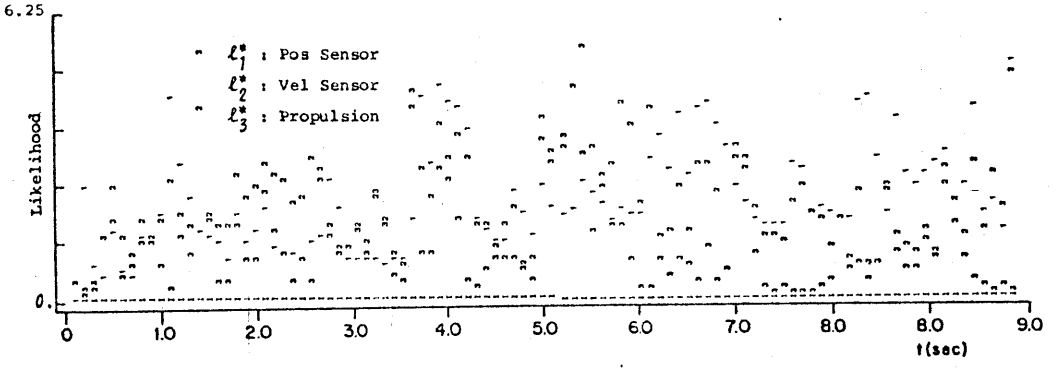

KC2

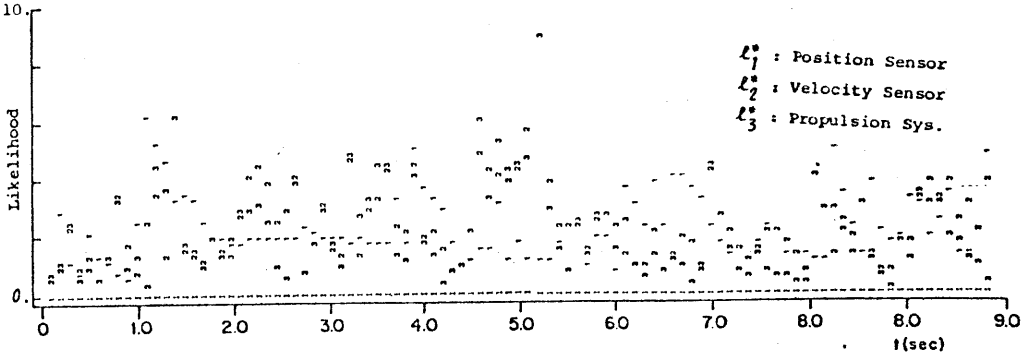

Pitts

Figure 4.55
Maximum Likelihood Ratios, Random Noise

To illustrate the improvement in performance afforded by the simplified models, we have simulated a worst case situation in which a fully loaded vehicle is commanded to increase its velocity just as a 6% grade and 18m/s headwind are encountered. The behavior of the vehicle is shown in Figure 4.56. The MLR's from the algorithm using the models KC1 and KC2 (Figure 4.57) reach peaks values sightly higher than those from the 10 volt propulsion system bias failure. By setting thresholds at these levels, propulsion system bias failures greater than 10 volts could still be detected and false alarms could be avoided.

Since the detection of sensor failures is not compromised with the use of the simplified vehicle models, the added complexity of Pitts' vehicle model may not to be required to maintain acceptable detection performance.

Summary of Results

1) The simplified vehicle models provide improved false alarm performance for wind and grade disturbances. The likelihood ratios produced by these forces are less than those produced from maneuvers and background noise.

2) Decision rule thresholds could be set so that the algorithm using a simplified model would not cause a false alarm during a worst case combination of wind, grade and load, and still retain the ability to detect propulsion system failures.

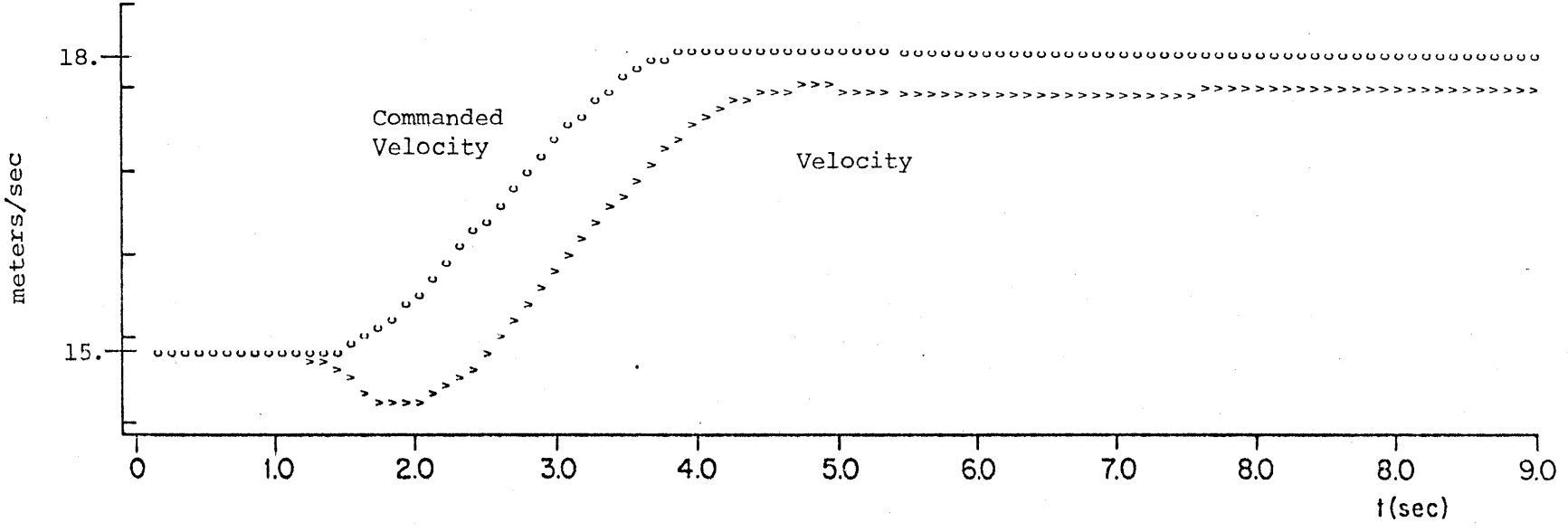

Figure 4.56

Vehicle Behavior, Worst Case Combination of Maneuver, Wind, Grade, & Load

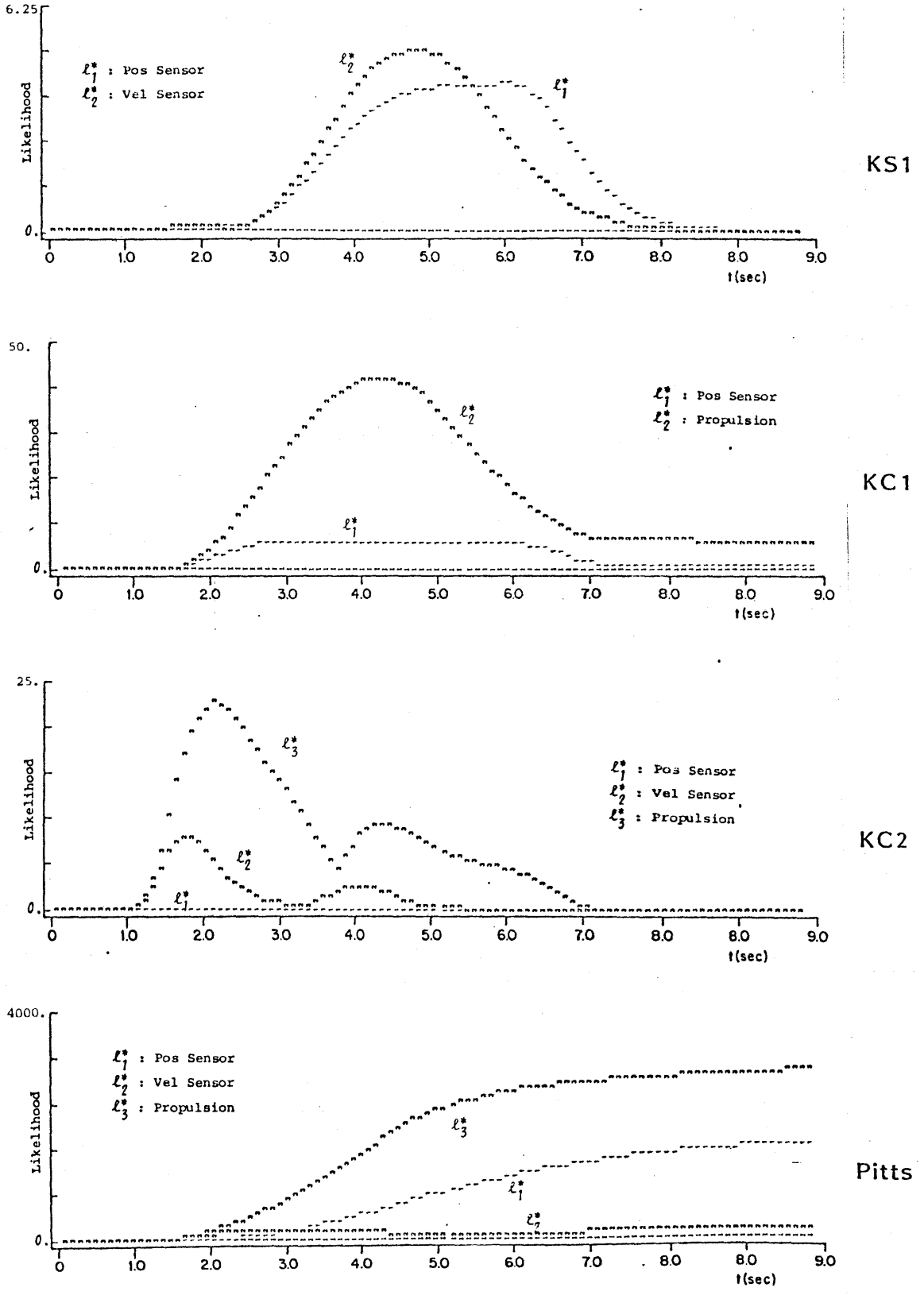

Figure 4.57
Maximum Likelihood Ratios, Worst Case Situation

4.4.4 Summary

The models discussed in this section were chosen to illustrate how varying degrees of model complexity can be used in the GLR algorithm. On one end of the spectrum lies the simple kinematic model KS1, valid for any vehicle; on the other, Pitts' model represents the dynamics of a particular DC motor driven vehicle.

The models we have examined can be divided into three model classes, and generalizations made about the algorithm's performance using each model class:

1) Kinematic, Sensor Driven Models (KS1)
   a) Can detect sensor failures
   b) Cannot detect propulsion system failures
   c) Will not false alarm from external disturbances

2) Kinematic, Control Command Driven Model (KC1 and KC2)
   a) Can detect sensor failures
   b) Can detect propulsion failures
   c) Distinguishability between sensor and propulsion system failures can be achieved with a delay
   d) Disturbances will not cause false alarms, although the extent to which this is true will depend on the vehicle control system

3) Parameterized Models (Pitts)

a) Can detect sensor failures

b) Parameter uncertainty must be dealt with

c) Failure detection may be superior than with the simplified models when the parameters are "matched" to true vehicle conditions.

d) When parameters are not matched, false alarms will occur.

It appears that very simple vehicle models are the least sensitive to external disturbances, but can still maintain failure detection capability. In the long run, they may thus prove to be the best suited for use in AGT vehicle systems.

4.5 Physically Redundant Sensors

4.5.1 Introduction

Failure detection and identification, in general, can nearly always be improved with the use of redundant sets of like sensors. Such redundancy is called "physical" redundancy. The performance of the GLR algorithm, based on the concept of "analytic" redundancy, can also be improved with the addition of physically redundant sensor measurements. The modification to the algorithm is (trivially) straightforward - the improvement in failure detection and identification can be significant.

The GLR algorithm is well suited to the management of redundant sensors; additional voting algorithms or voting hardware is not required. In the absence of failures, the algorithm produces the minimum-mean-squared-error estimate of the true state being measured (i.e., optimally filtered

measurements), employing information from not only the redundant set of sensors, but from all other analytically redundant sensors as well. If a failure occurs, the algorithm uses all available information in producing a set of maximally informative statistics (the MLR's) which can then be used to identify the failed sensor. Whereas voting algorithms require at least three redundant sensors to identify which sensor has failed, the GLR algorithm uses the analytic redundancy provided by the system model and measurements from un-like sensors to provide the "third vote."

With the vehicle models we have examined up to this point, we have seen that there is a delay before velocity sensor and propulsion system failures can be unambiguously identified - the algorithm cannot initially distinguish between these two failures. The different forms of action required in response to these failures make identification delays extremely undesirable.

We will illustrate how physically redundant sensor measurements can be used in the GLR algorithm by examining the use of a dual set of velocity sensor measurements; we will see that the use of the additional velocity sensor greatly improves the correct identification of and distinguishability between, velocity sensor and propulsion system failures.

4.5.2 Modelling of Dual Sensors

The effects of a set of dual velocity sensors will be examined via the use of the vehicle models KC2 and Pitts'.

The measurement equation (4-15) for the modek KC2 is modified to reflect an additional velocity measurement:

$$\begin{bmatrix} x_m(k) \\ v_{m,1}(k) \\ v_{m,2}(k) \end{bmatrix} = \begin{bmatrix} 1 & 0 \\ 0 & 1 \\ 0 & 1 \end{bmatrix} \begin{bmatrix} x(k) \\ v(k) \end{bmatrix} + \begin{bmatrix} n_1(k) \\ n_2(k) \\ n_3(k) \end{bmatrix} \tag{4-20}$$

where $v_{m,1}(k)$ and $v_{m,2}(k)$ are the dual velocity measurements and the velocity sensor noise processes $n_2(k)$ and $n_3(k)$ are assumed to have equal, but mutually uncorrelated, zero-mean Gaussian statistics, with:

$$R = E[\underline{n}(k)\underline{n}(k)^T] = \begin{bmatrix} 0.1 & & \\ 0 & 0.1 & \\ 0 & 0 & 0.1 \end{bmatrix} \tag{4-21}$$

The measurement equation (4-2) from Pitts' vehicle model is similarly modified:

$$\begin{bmatrix} x_m(k) \\ v_{m,1}(k) \\ v_{m,2}(k) \end{bmatrix} = \begin{bmatrix} 1 & 0 & 0 \\ 0 & 1 & 0 \\ 0 & 1 & 0 \end{bmatrix} \begin{bmatrix} x(k) \\ v(k) \\ a(k) \end{bmatrix} + \begin{bmatrix} n_1(k) \\ n_2(k) \\ n_3(k) \end{bmatrix} \tag{4-22}$$

with the same sensor noise statistics defined above.

4.5.3 Failure Signature

The GLR algorithm can now be applied to the two vehicle models, as before. However, since the additional measurement increases the dimension of the output space from two to three dimensions, the failure direction

vectors in output space are re-defined as follows:

$$\underline{f}_1 = \begin{bmatrix} 1 \\ 0 \\ 0 \end{bmatrix} \qquad \text{Position Sensor} \quad (i=1)$$

$$\underline{f}_2 = \begin{bmatrix} 0 \\ 1 \\ 0 \end{bmatrix} \qquad \text{Velocity Sensor 1} \quad (i=2)$$

$$\underline{f}_3 = \begin{bmatrix} 0 \\ 0 \\ 1 \end{bmatrix} \qquad \text{Velocity Sensor 2} \quad (i=3)$$

Propulsion system failures will have the same direction in state space as found in section 4.2.5., but the direction vector will be renumbered $\underline{f}_4$ (i=4).

The Kalman-Bucy filter matrices for the two models are given in Tables 4.8 and 4.9. Note that the error covariance of the updated state estimates (diagonal elements of the updated error covariance matrix Σ) have decreased (compared to Tables 4.2 and 4.7) as a result of the additional information provided by the second velocity sensor.

The failure signatures, now having three components are shown in Figures 4.58 and 4.59 for the two vehicle models. The effect of the redundant velocity sensor is to produce signatures which are unique to each failure location at every point following the failure. The behavior of a third component of the signature provides the "third vote" in distinguishing velocity sensor failures from propulsion system failures.

Table 4.8

Kalman-Bucy Filter Matrices

Acceleration Command Driven Kinematic Model KC2

Dual Velocity Sensors

```
K A L M A N   F I L T E R -
- - - - - -   - - - - - -

CLOSED LOOP EIGENVALUES
      REAL PART                  IMAGINARY PART
    0.383042580913285D+00          0.0
    0.931537369320263D+00          0.0

CLOSED LOOP MATRIX
 9.33305D-01   3.14386D-02
-3.09460D-02   3.81275D-01

KBF FILTER GAIN MATRIX H
 6.66946D-02   3.09460D-02   3.09460D-02
 3.09460D-02   3.07815D-01   3.07815D-01

PREDICTED ERROR COVARIANCE MATRIX
 7.72119D-04   8.67275D-04
 8.67275D-04   8.07815D-03

UPDATED ERROR COVARIANCE MATRIX
 6.66946D-04   3.09460D-04
 3.09460D-04   3.07815D-03

RESIDUAL COV MATRIX (V) -
 1.07721D-02   8.67275D-04   8.67275D-04
 8.67275D-04   1.80782D-02   8.07815D-03
 8.67275D-04   8.07815D-03   1.80782D-02

RESIDUAL COV MATRIX INVERSE (V-INVERSE) -
 9.33305D+01  -3.09460D+00  -3.09460D+00
-3.09460D+00   6.92185D+01  -3.07815D+01
-3.09460D+00  -3.07815D+01   6.92185D+01
```

Table 4.9

Kalman-Bucy Filter Matrices;

Pitts' Vehicle Model, Dual Velocity Sensors

K A L M A N F I L T E R -

CLOSED LOOP EIGENVALUES

REAL PART	IMAGINARY PART
0.331197206172607D-01	0.0
0.531961215665336D+00	0.0
0.954570125859029D+00	0.0

CLOSED LOOP MATRIX

9.56146D-01	6.90103D-02	1.24475D-03
-1.04660D-02	6.27030D-01	1.74480D-02
4.74776D-02	-3.28997D+00	-6.35246D-02

KBF FILTER GAIN MATRIX H

4.38540D-02	1.04660D-02	1.04660D-02
1.04660D-02	6.19163D-02	6.19163D-02
-4.74776D-02	3.15103D-02	3.15103D-02

PREDICTED ERROR COVARIANCE MATRIX

4.61390D-04	1.24963D-04	-4.88807D-04
1.24963D-04	7.08165D-04	3.53799D-04
-4.88807D-04	3.53799D-04	1.26313D-01

UPDATED ERROR COVARIANCE MATRIX

4.38540D-04	1.04660D-04	-4.74776D-04
1.04660D-04	6.19163D-04	3.15103D-04
-4.74776D-04	3.15103D-04	1.26268D-01

RESIDUAL COV MATRIX (V) -

1.04614D-02	1.24963D-04	1.24963D-04
1.24963D-04	1.07082D-02	7.08165D-04
1.24963D-04	7.08165D-04	1.07082D-02

RESIDUAL COV MATRIX INVERSE (V-INVERSE) -

9.56146D+01	-1.04660D+00	-1.04660D+00
-1.04660D+00	9.38084D+01	-6.19163D+00
-1.04660D+00	-6.19163D+00	9.38084D+01

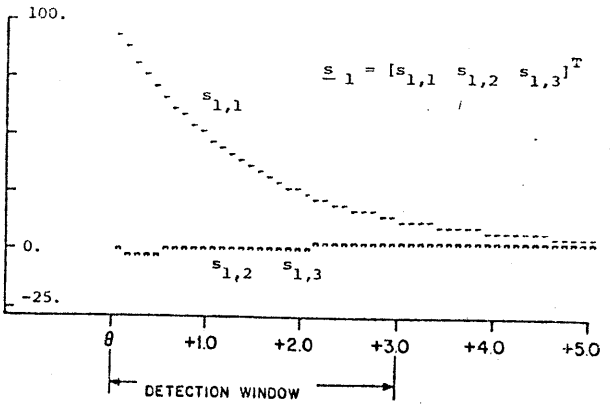

Position Sensor Bias

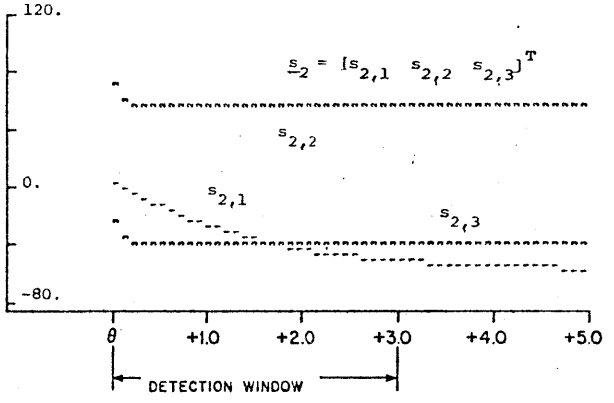

Vel Sensor(1) Bias

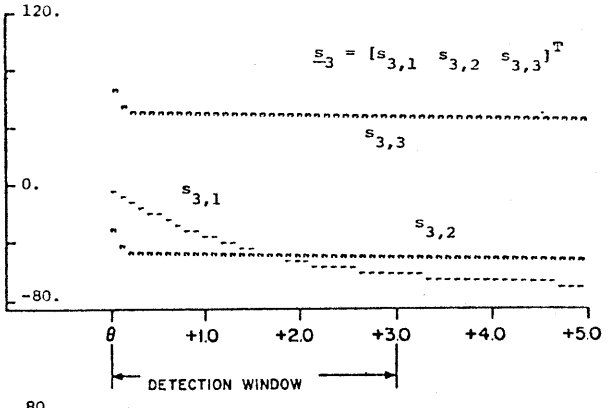

Vel Sensor(2) Bias

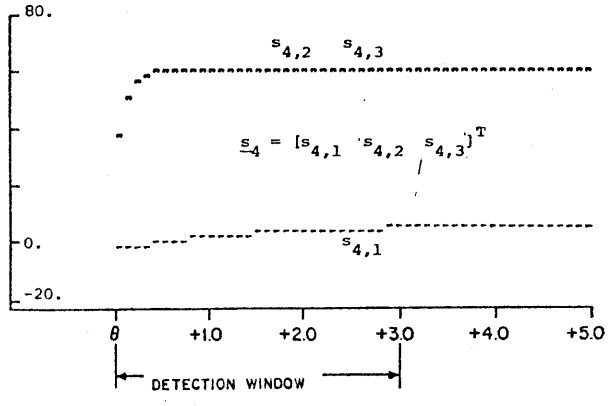

Propulsion System Bias

Figure 4.58 - Failure Signatures, Dual Vel Sensors; KC2

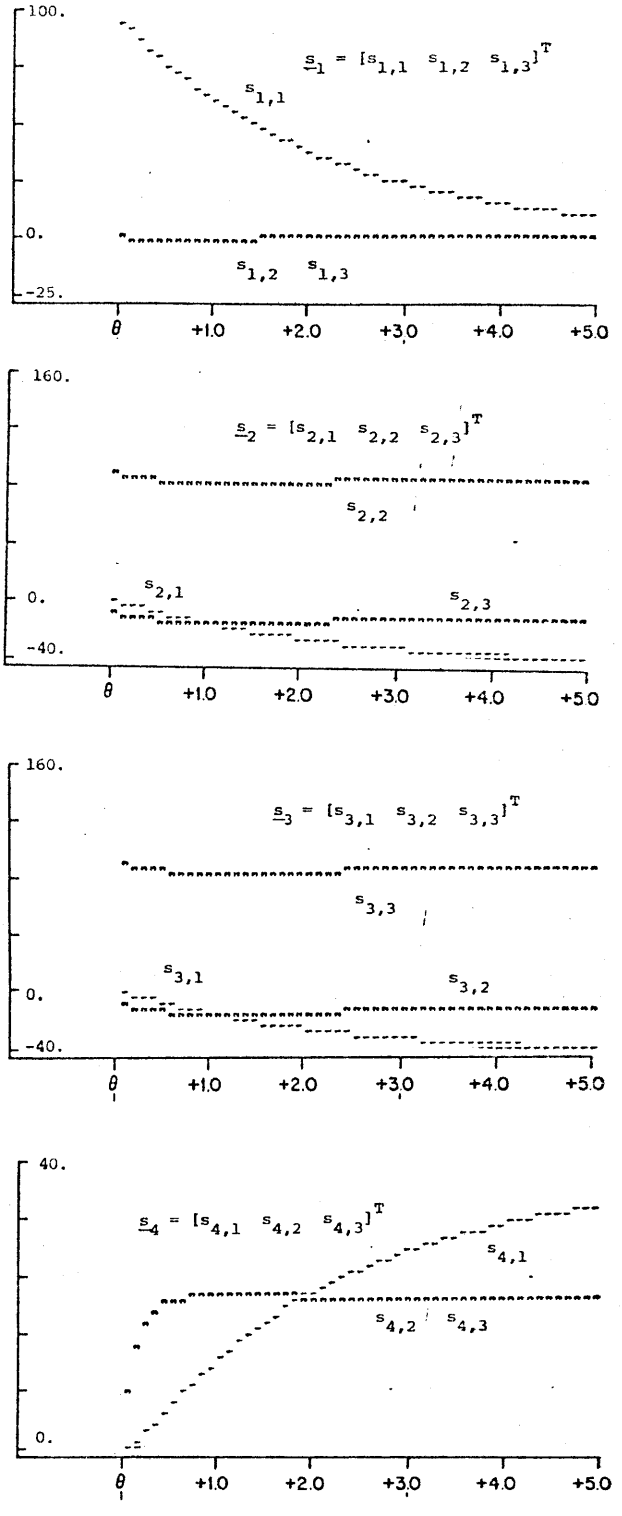

Position Sensor Bias

Vel Sensor(1) Bias

Vel Sensor(2) Bias

Propulsion System Bias

Figure 4.59

Failure Signatures, Dual Vel Sensors; Pitts

4.5.4 Performance Results

The failure scenarios described in sections 4.3.2 and 4.3.3 were repeated, with the addition of a redundant velocity measurement. No background Gaussian noise was included.

4.5.4.1 Velocity Sensor Bias

Results

Filter residuals from the two vehicle models are shown in Figures 4.60 and 4.61. The residuals produced when only one velocity measurement was available are reproduced for comparison.

Improvement in the algorithms' ability to identify the true failure location can be seen in the maximum likelihood ratios, Figures 4.62 and 4.63. Using the dual sensor set, the MLR for the failed velocity sensor, ℓ_2^*, is initially significantly larger than the propulsion system MLR. This will improve the performance of the algorithm in that:

1) the probability that the correct failure location is identified will be higher.
2) the delay until a decision is made as to the failure's location can be shortened.

Since wrong failure location decisions and/or long detection delays may have disasterous effects, the improvement will significantly affect vehicle safety.

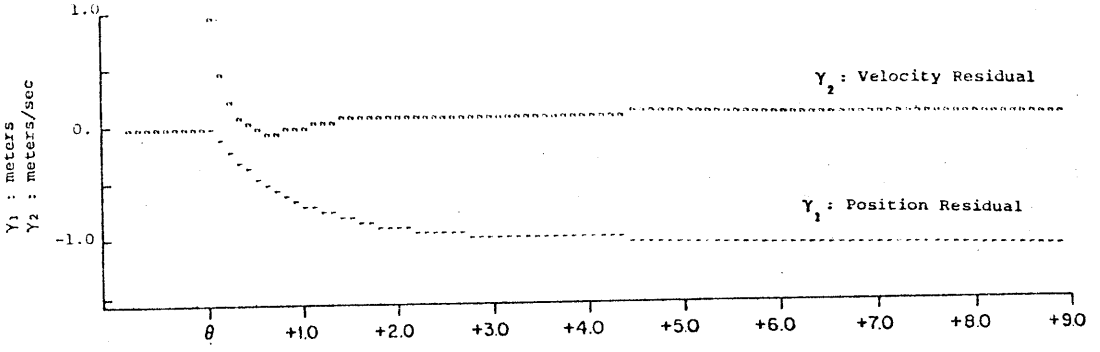

Single Velocity Sensor

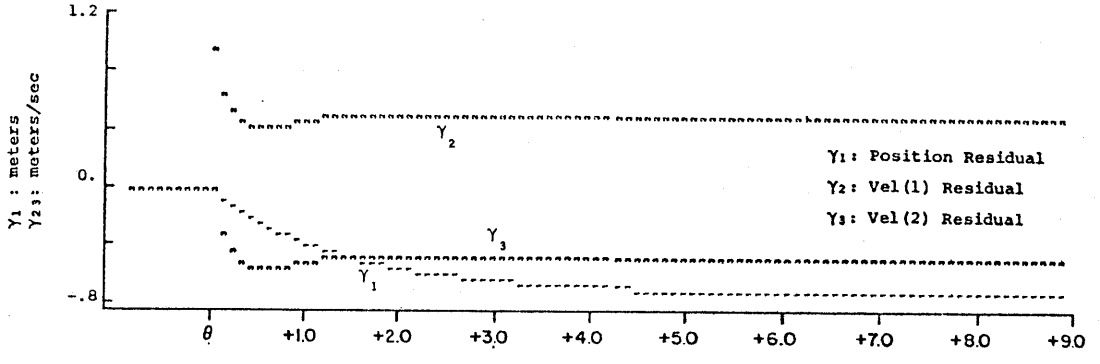

Dual Velocity Sensors

Figure 4.60

Residuals, Velocity Sensor Bias; KC2

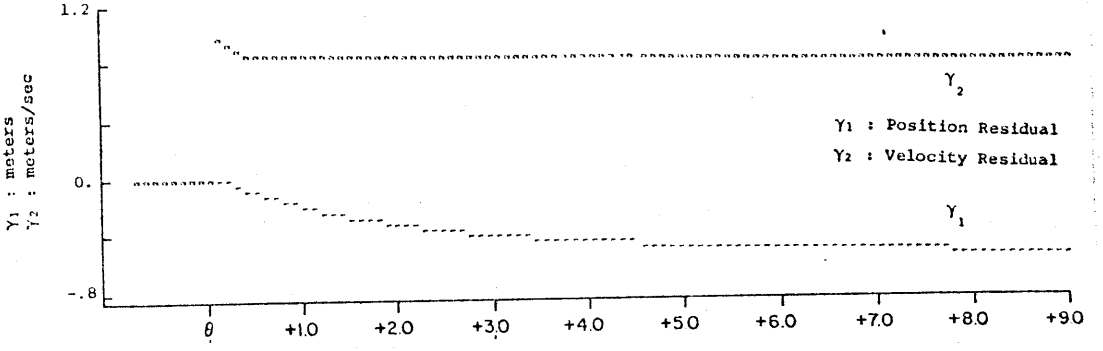

Single Velocity Sensor

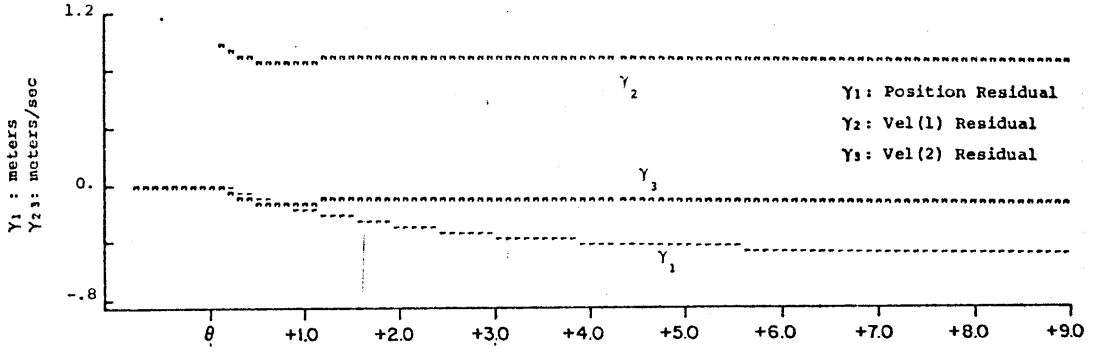

Dual Velocity Sensors

Figure 4.61
Residuals, Velocity Sensor Bias; Pitts

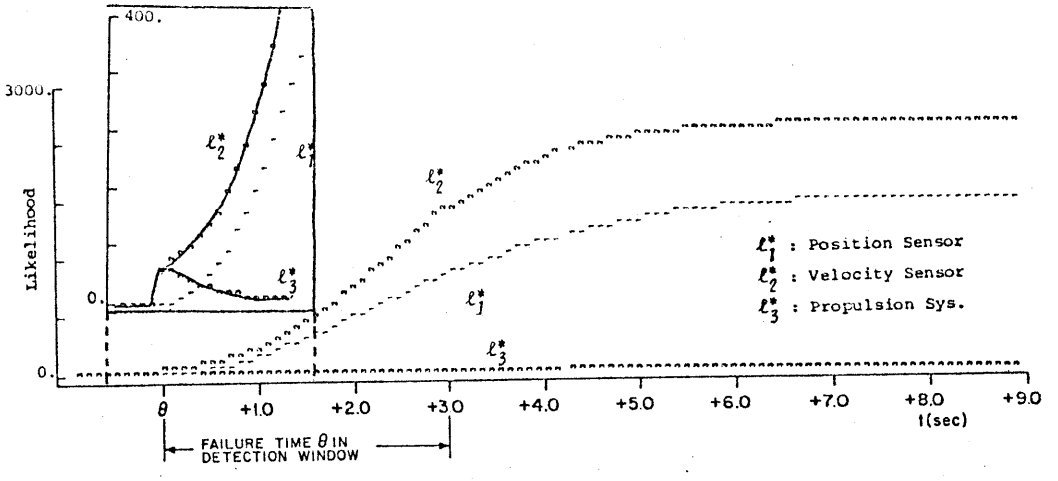

Single Velocity Sensor

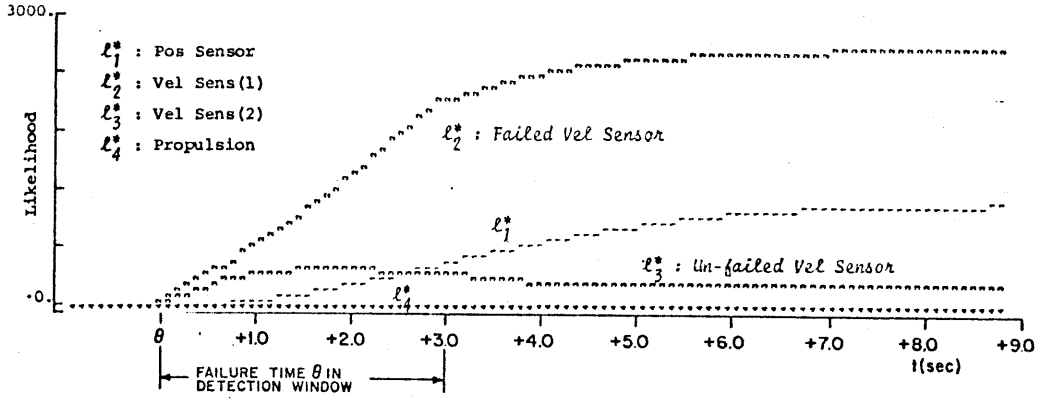

Dual Velocity Sensors

Figure 4.62

Maximum Likelihood Ratios, Velocity Sensor Bias; KC2

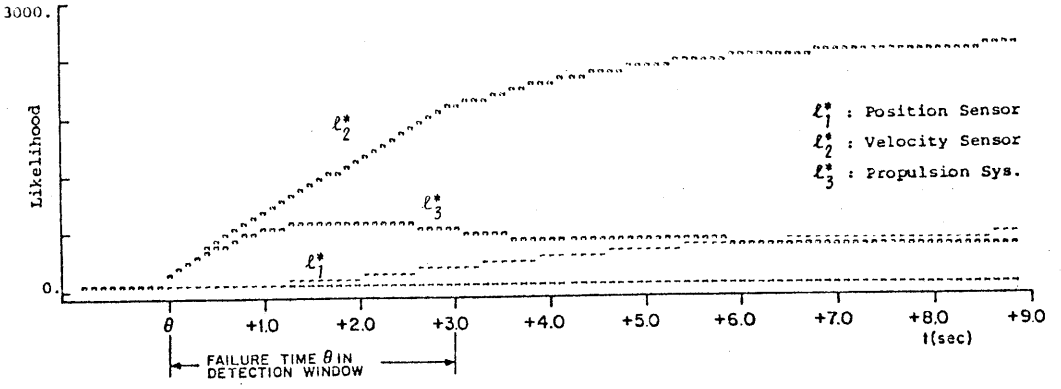

Single Velocity Sensor

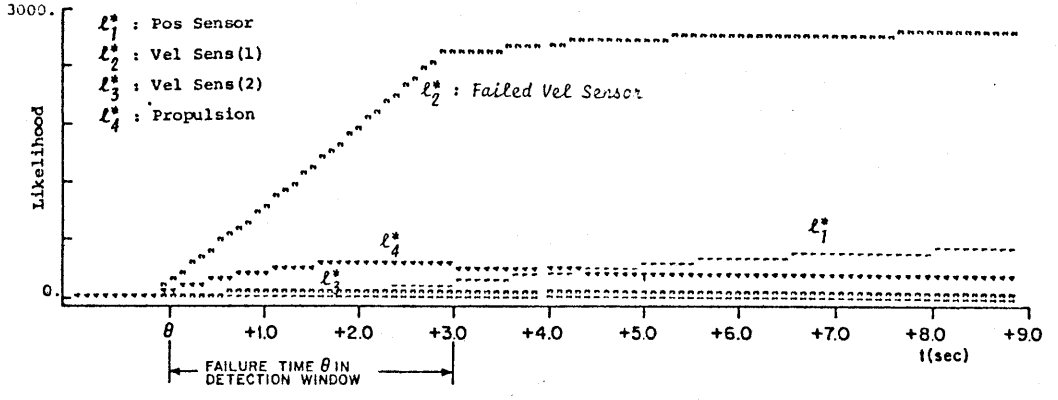

Dual Velocity Sensors

Figure 4.63

Maximum Likelihood Ratios, Velocity Sensor Bias; Pitts

4.5.4.2 Propulsion System Bias

Results

Filter residuals appear in Figures 4.64 and 4.65.

Improvements in failure location identification can be observed in the likelihood ratios, Figures 4.66 and 4.67, for the propulsion system failure.

4.5.5 Summary

Physically redundant sensor sets can significantly improve failure detection and identification. The cost of the additional hardware must be weighed agains the improvements in detection algorithm performance.

Use of the GLR algorithm with physically redundant sensors has advantages over simple voting schemes. Information from other analytically redundant sensors can improve identification of failed members of the phsyically redundant set. Failures affecting all members of a physically redundant set can also be detected with the GLR algorithm, whereas voting methods can not do so.

4.6 Detection of Stuck Outputs and Scale Factors Changes in Sensors and Actuators

4.6.1 Introduction

We claimed in chapter three that the GLR algorithm, designed for the detection of additive bias failures, could be applied to the detection of other types of failures as well. In this section the GLR algorithm's ability

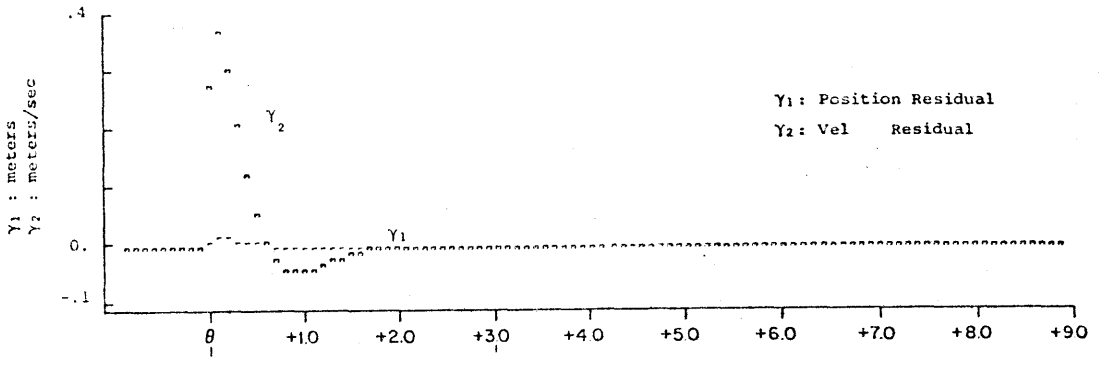

Single Velocity Sensor

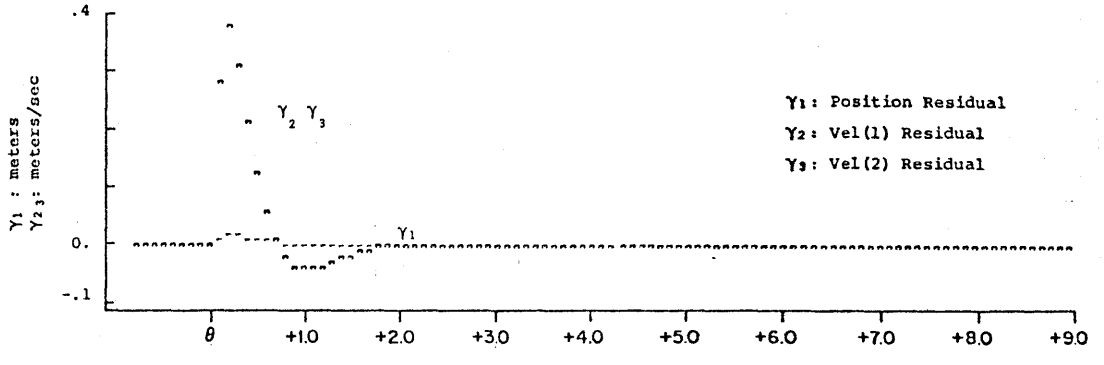

Dual Velocity Sensors

Figure 4.64

Residuals, Propulsion Sys. Bias; KC2

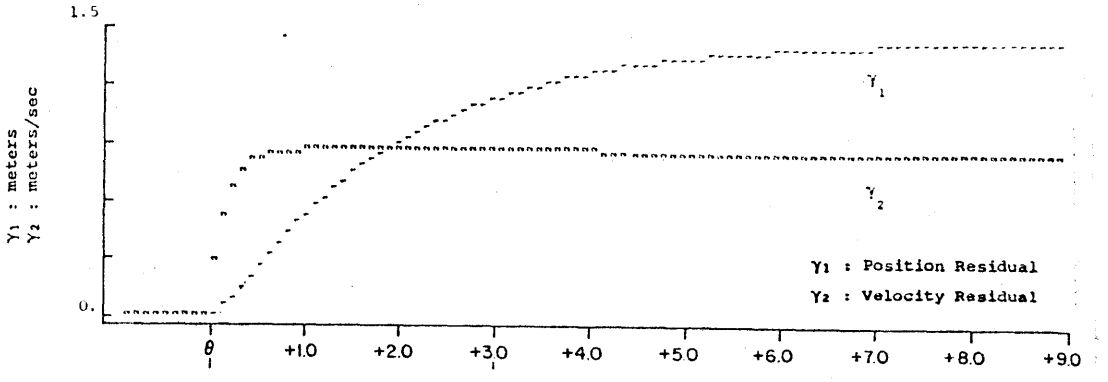

Single Velocity Sensor

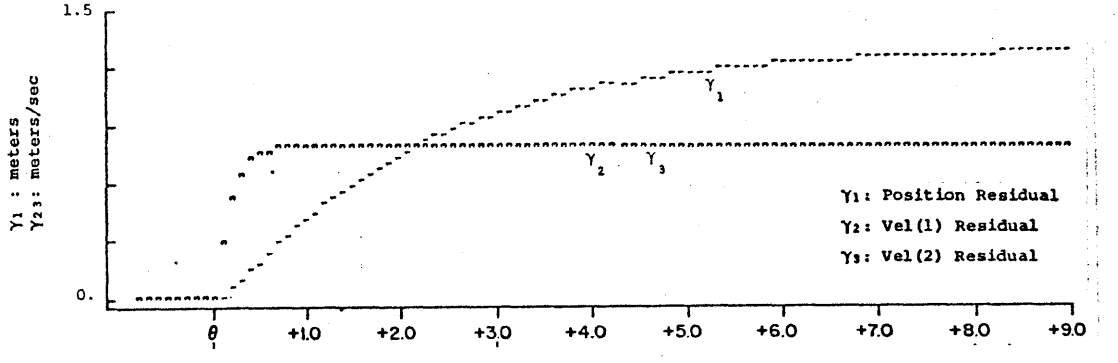

Dual Velocity Sensors

Figure 4.65

Residuals, Propulsion Sys. Bias; Pitts

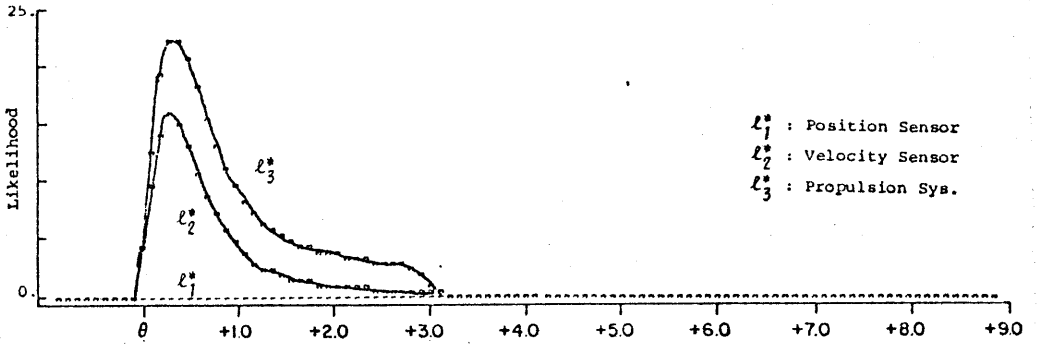

Single Velocity Sensor

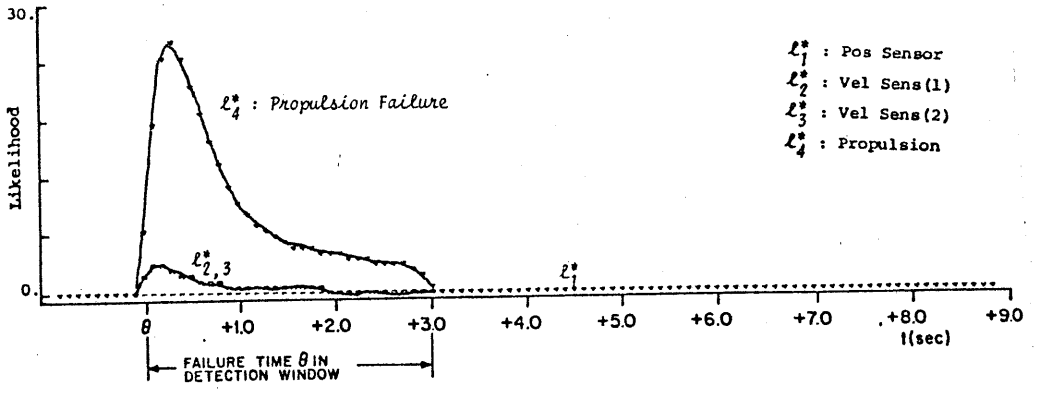

Dual Velocity Sensors

Figure 4.66

Maximum Likelihood Ratios, Propulsion Sys. Bias; KC2

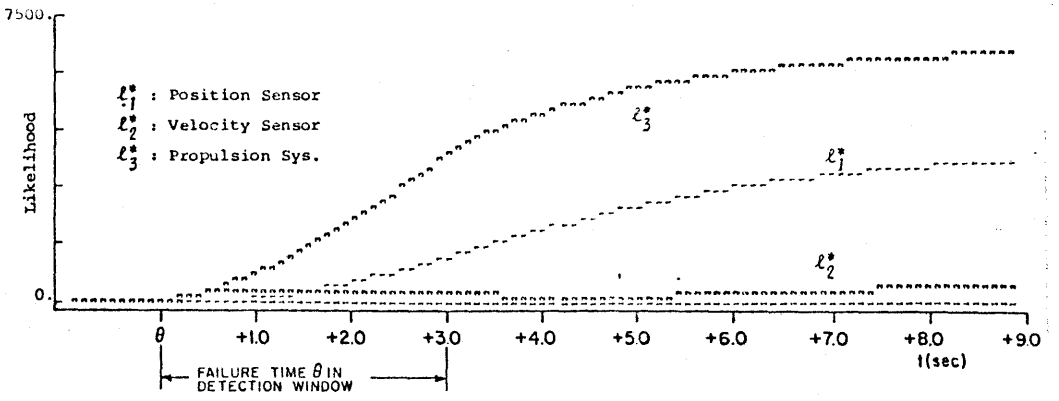

Single Velocity Sensor

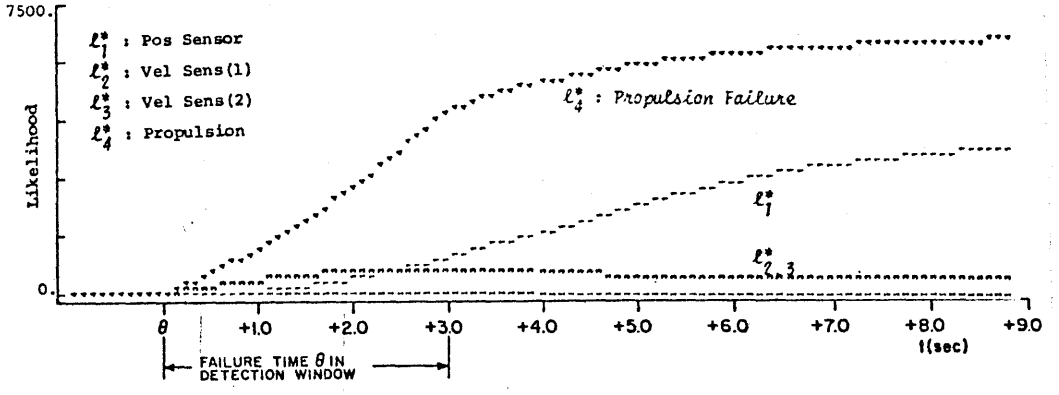

Dual Velocity Sensors

Figure 4.67

Maximum Likelihood Ratios, Propulsion Sys. Bias; Pitts

to detect some of these other failure modes will be demonstrated.

Two of the more subtle failure modes, scale factor change and stuck sensor/actuator failures, will be examined. The magnitudes of zero-output and hard-over failures are such that they can easily be detected, and thus will not be examined in detail.

4.6.2 Stuck Position Sensor Failure

Failures in which the output of a sensor or actuator becomes stuck at an intermediate level may be difficult to detect, for a sudden jump in the output is not observed (Figure 2.10). We will begin by examinig a stuck position sensor.

Scenario

A simulation was performed in which the position sensor remained stuck at a value of 15 meters on a vehicle travelling at 15m/s. The GLR algorithm using the four vehicle models, KS1, KC1, KC2, and Pitts, was evaluated on the data.

Results

The maximum likelihood ratios are shown in Figure 4.68. Using the models KS1 and KC1, the algorithm detected a failure, but incorrectly identified its location. With the model KC2, the algorithm detected the failure and initially identified the location correctly. However, one

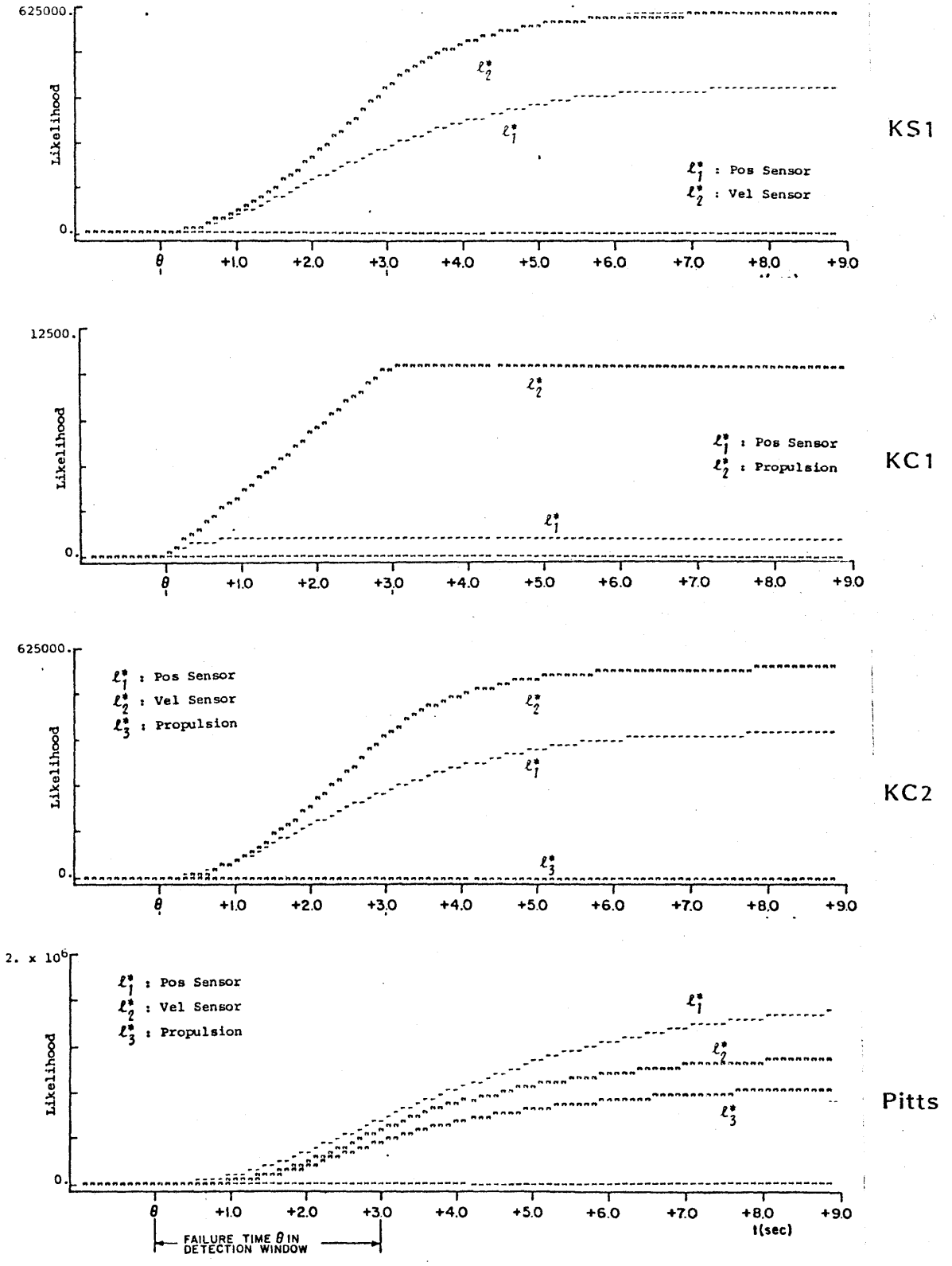

Figure 4.68

Maximum Likelihood Ratios, Stuck Position Sensor

second later the decision was changed and the wrong location identified. The algorithm with Pitts' model detected the failure and correctly identified the location.

4.6.3 Stuck Velocity Sensor Failure

Scenario

A simulation was performed in which the velocity sensor remained stuck at a reading of 15m/s just as the vehicle was commanded to decrease its velocity from 15m/s to 12m/s. Commanded, actual, and measured velocities are shown in Figure 4.69. The vehicle control system, believing the vehicle to be travelling constantly at 15m/s, continues to apply increasingly smaller voltages to the motor, which causes the vehicle to undershoot the commanded velocity.

Results

Maximum likelihood ratios using the vehicle models KS1, KC2 and Pitts, are shown in Figure 4.70. With all three models, the GLR algorithm detected and identified the failed sensor.

The algorithm's ability to determine the error in the measured velocity, even when the failure is not a true bias failure, is shown by the bias magnitude estimates (Figure 4.71) produced by the algorithm using KS1. The estimate of the bias size, $\hat{\beta}$, could be subtracted from the velocity measurement to estimate the vehicle's true velocity.

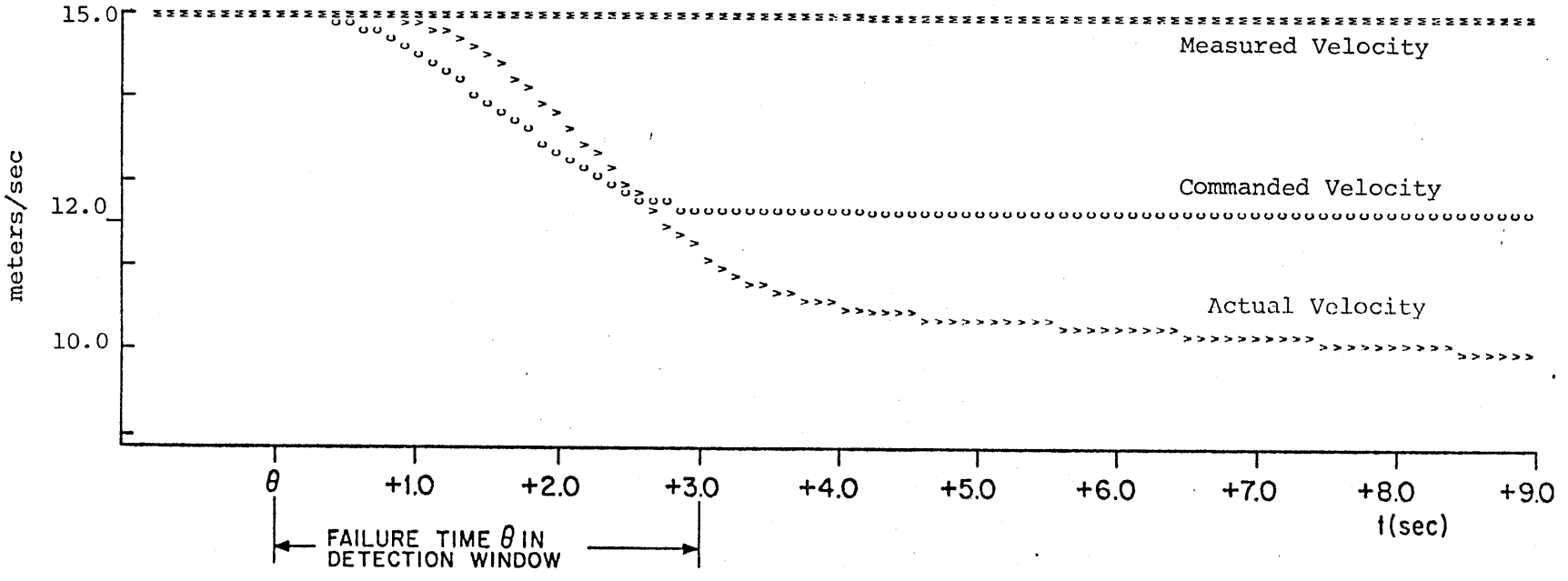

Figure 4.69

Vehicle Behavior, Stuck Velocity Sensor

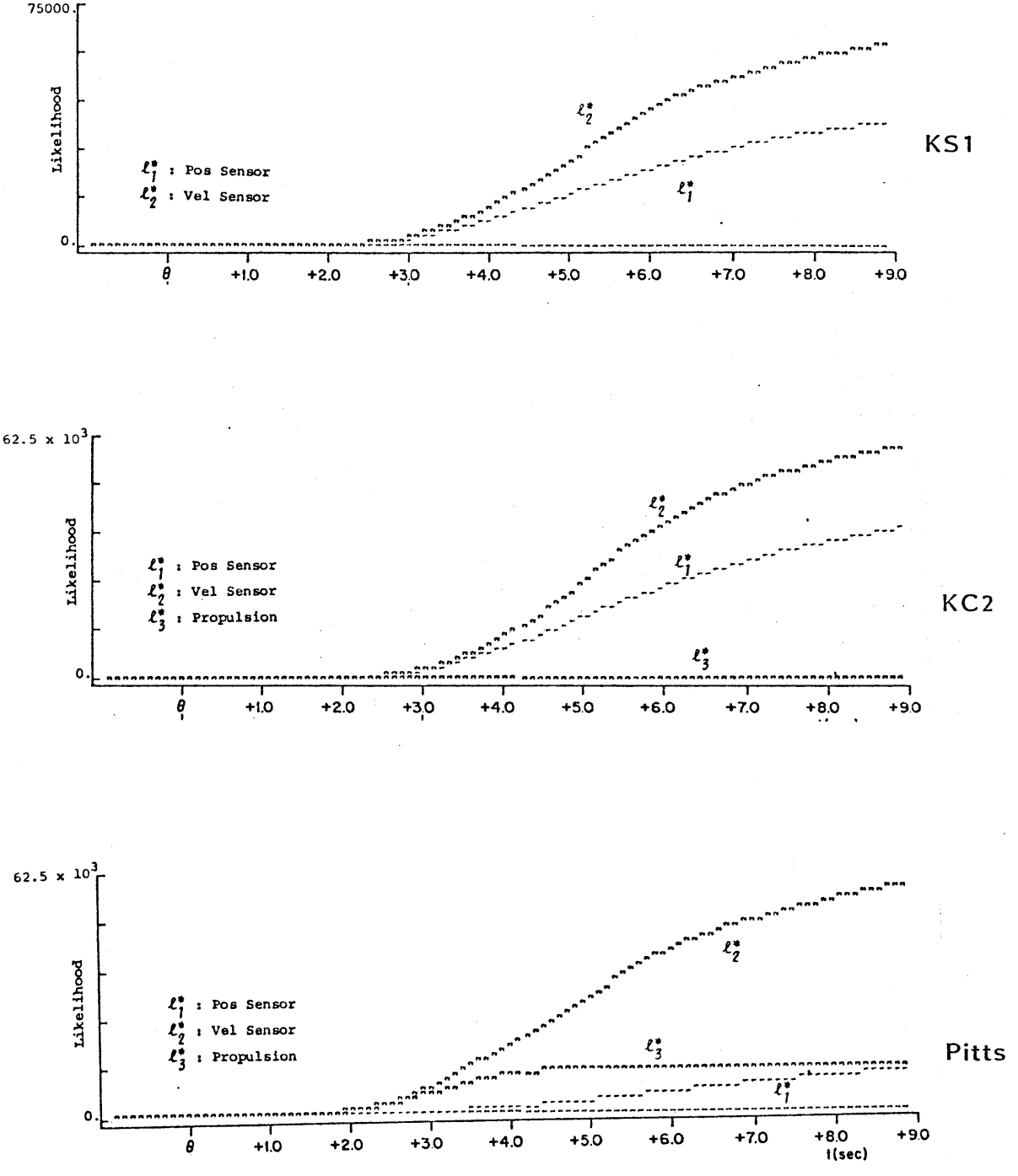

Figure 4.70

Maximum Likelihood Ratios, Stuck Velocity Sensor

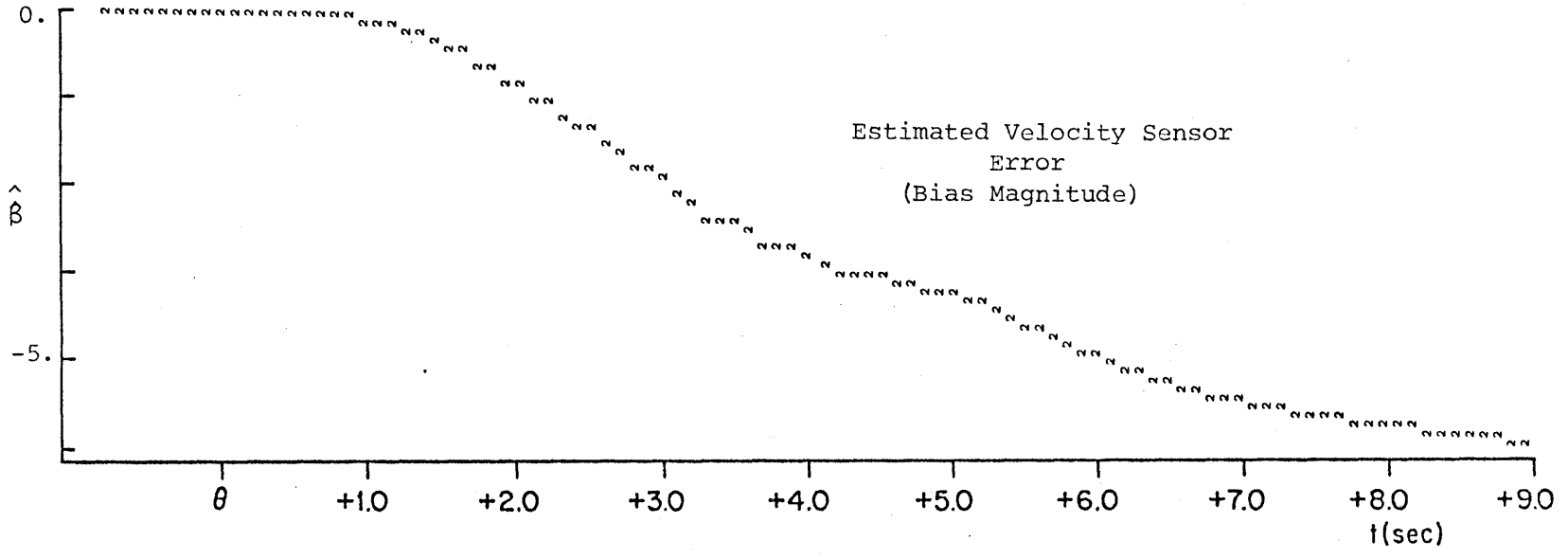

Figure 4.71
Estimated Bias Magnitude, Stuck Velocity Sensor

4.6.4 Stuck PCU (Motor Drive Voltage Actuator)

Should the power conditioning unit fail in an "ON" state, essentially operating open-loop from the control system, the results would be catastrophic if the failure not detected.

Scenario

A simulation was performed in which the voltage applied to the motor remained at a constant value of 145 volts, independent of the voltage command. The vehicle remained at a constant velocity of 15m/s, although it was commanded to decelerate to 12m/s. The commanded and actual velocities are shown in Figure 4.72.

Results

Maximum likelihood ratios are shown in Figure 4.73. The algorithm using the kinematic sensor model KS1 did not detect the failure since the propulsion system is not modelled. The algorithm using the models KC1, KC2, and Pitts was able to detect the failure and identify its location. The use of Pitts' vehicle model clearly produced the best detection performance.

4.6.5. Velocity Sensor Scale Factor Change

At a constant velocity, a sudden scale factor change in the velocity sensor would appear identical to a bias failure, which we have already examined. Much more subtle is a scale factor change which occurs before

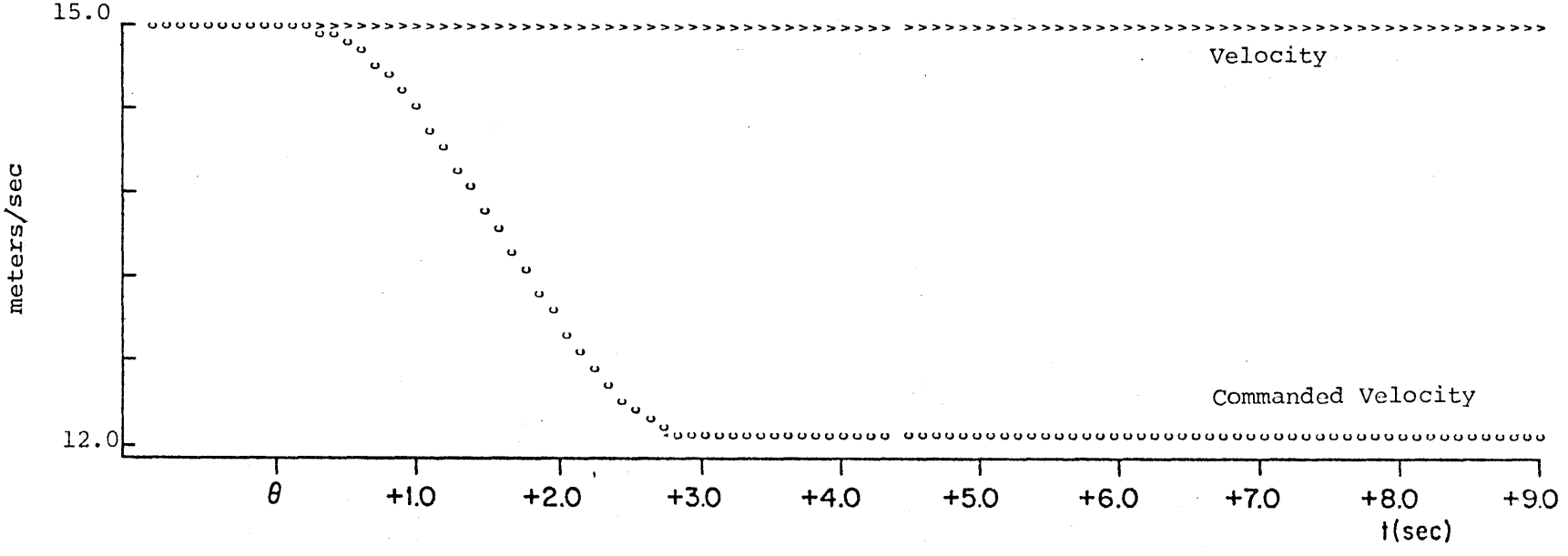

Figure 4.72
Vehicle Behavior, Stuck PCU

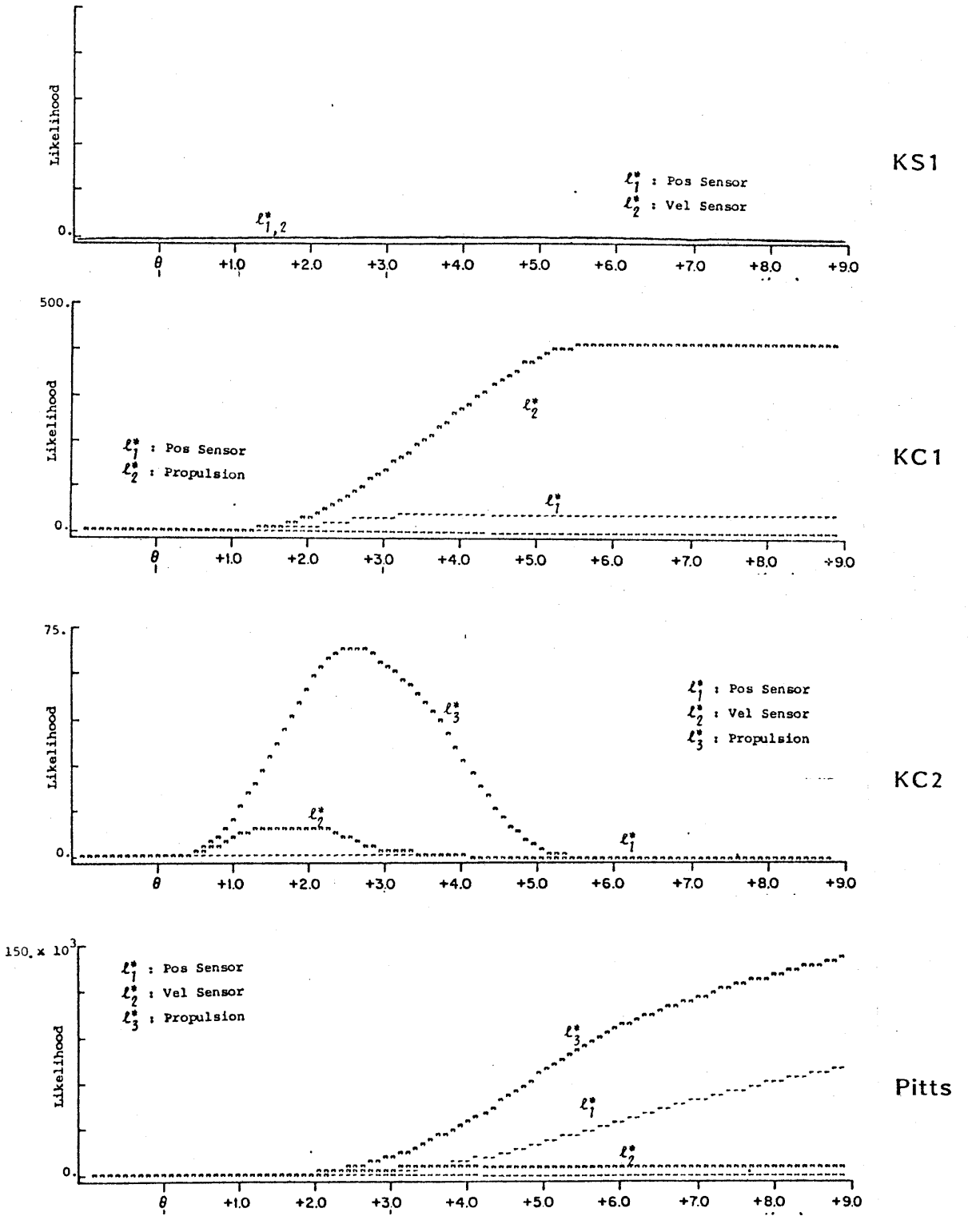

Figure 4.73

Maximum Likelihood Ratios, Stuck PCU

a vehicle at rest begins to accelerate, as a sudden jump is not observed in the output.

Scenario

The gain of the velocity sensor was decreased 10% from 1.0 to 0.9. The vehicle was commanded at time 1.0 sec to accelerate at service limits. Commanded, measured, and actual velocities are shown in Figure 4.74.

Results

The GLR algorithm using the models KS1, KC2 and Pitts' was run on the data. KC1 was not used as the velocity sensor is not modelled. The likelihood ratios for a failed velocity sensor (Figure 4.75) reach significant values by the time the vehicle has reached a velocity of 3m/s. Using Pitts' model produced the best failure location identification results, as the likelihood ratios for the other possible failure locations remain small. This is an example of the increased detection ability afforded by more detailed models.

4.6.6. PCU (Voltage Actuator) Scale Factor Change

Scenario

PCU gain was changed to be 90% of its normal value. Initially at rest, at time 1.0s the vehicle was commanded to accelerate at service limits. Commanded and actual velocities are shown in Figure 4.76.

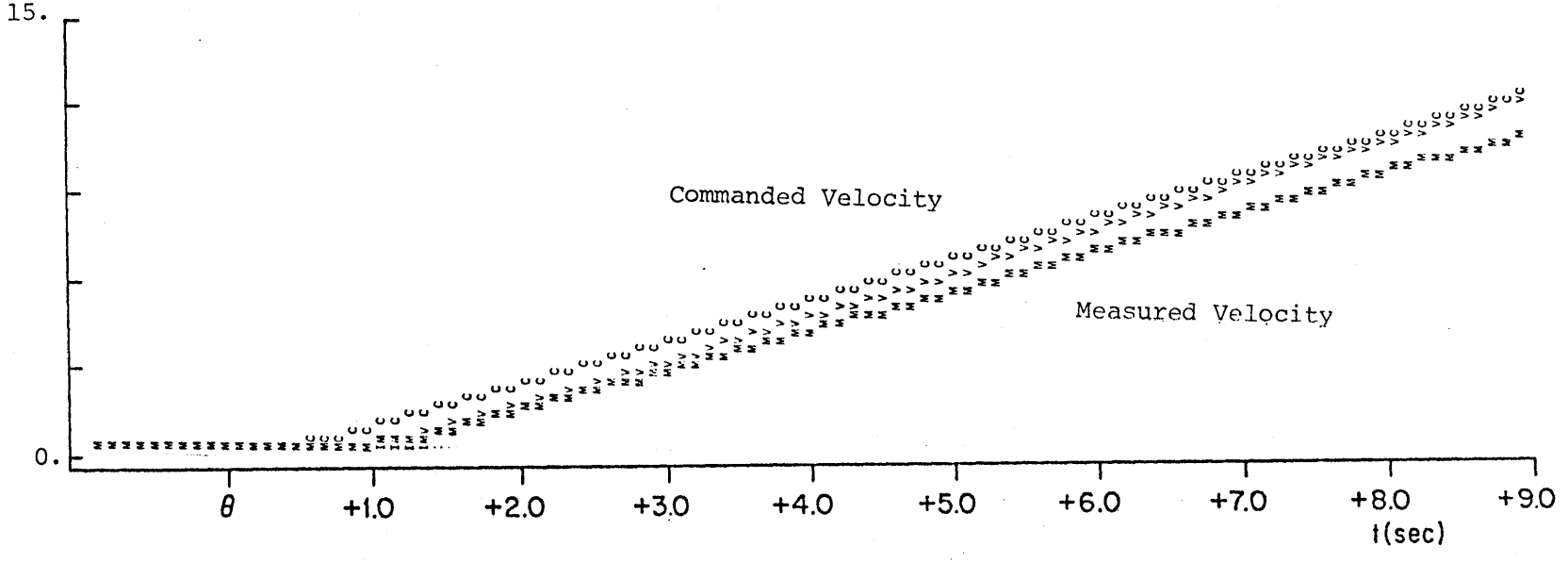

Figure 4.74

Vehicle Behavior, Velocity Sensor Scale Factor Change

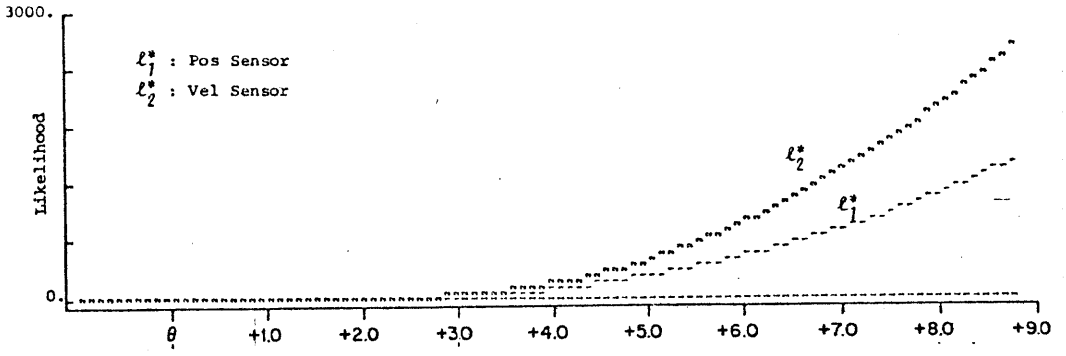

KS1

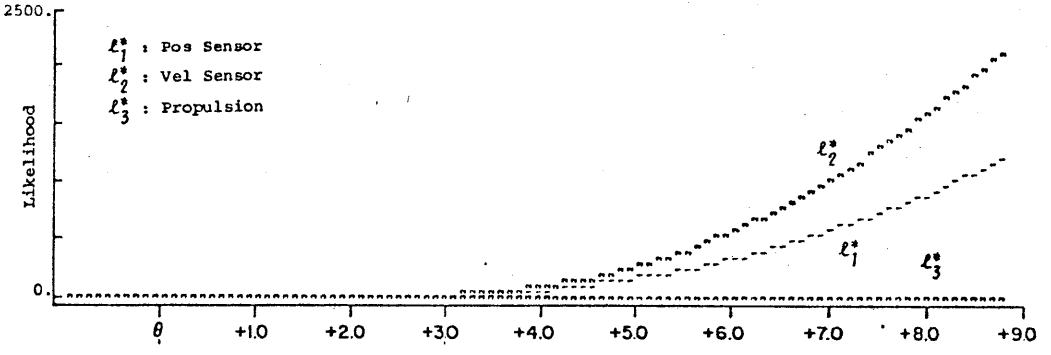

KC2

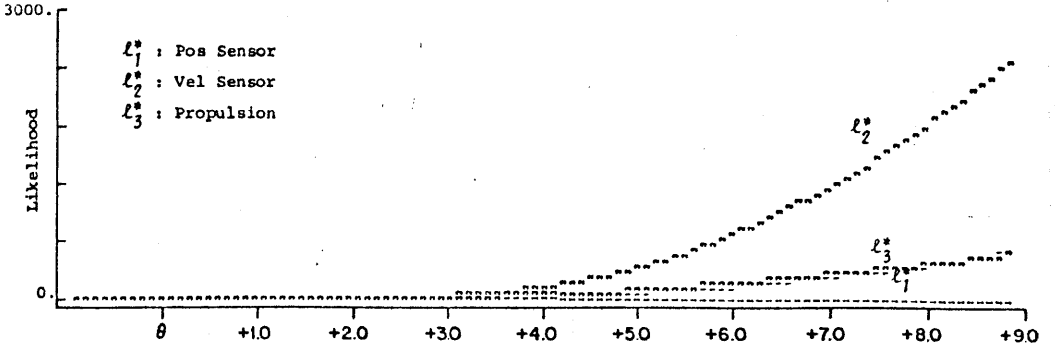

Pitts

Figure 4.75

Maximum Likelihood Ratios, Vel Sensor Scale Factor Change

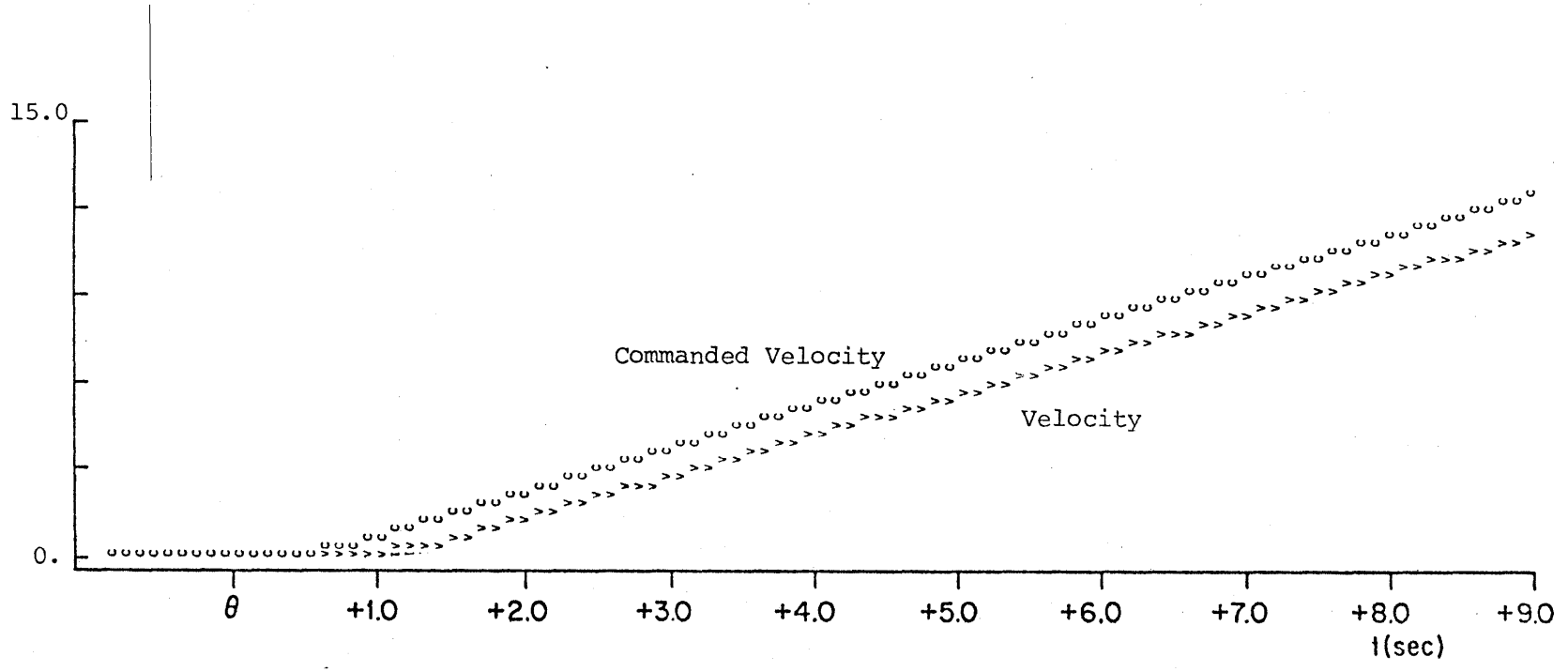

Figure 4.76

Vehicle Behavior, PCU Scale Factor Change

Results

The algorithm using KC1, the kinematic model driven by the velocity command, detected and identified the failure location (Figure 4.77). The likelihood ratio continues to grow throughout the maneuver. Using KC2, the kinematic model driven by the acceleration command, however, the algorithm produced a likelihood ratio which peaks 1.5 seconds after the maneuver is begun, and then decays.

The differences in the behavior of the two likelihood ratios using the two different vehicle models can be explained by examining the filter residuals, Figure 4.78. The signature of the failure remains continuously visible in the residuals using the velocity command driven model, as there is a continued discrepancy between commanded and actual velocity.

With the acceleration command driven model, the failure signature appears only temporarily.

This example illustrates how the same failure can produce signatures with significantly different characteristics depending on model choices. We thus see the key role system model choice plays in detection algorithm design to achieve desired performance goals.

4.7 Summary

In this chapter, the GLR method has been applied to an AGT vehicle for on-board detection of position sensor, velocity sensor, and propulsion system failures.

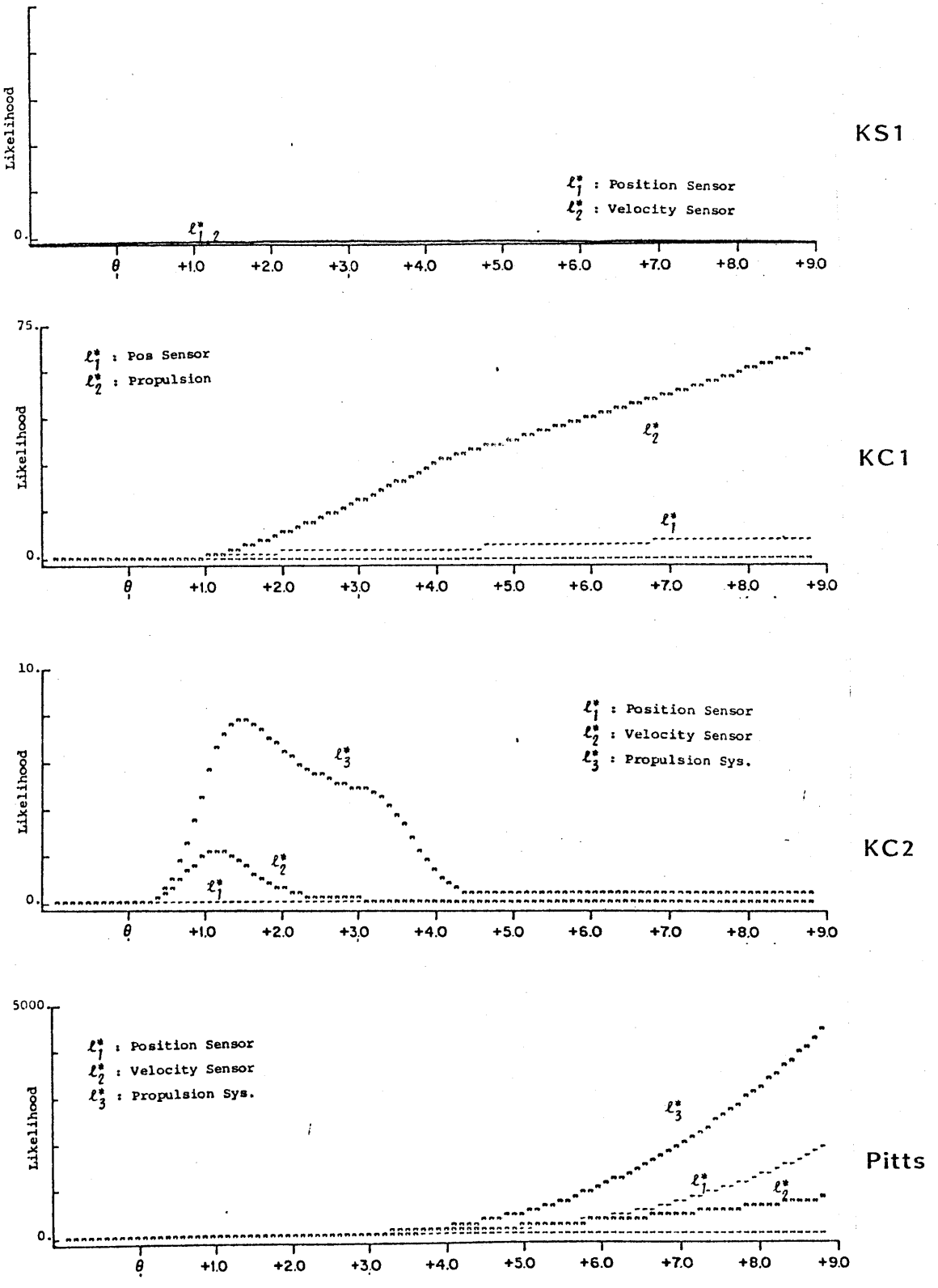

Figure 4.77

Maximum Likelihood Ratios, PCU Scale Factor Change

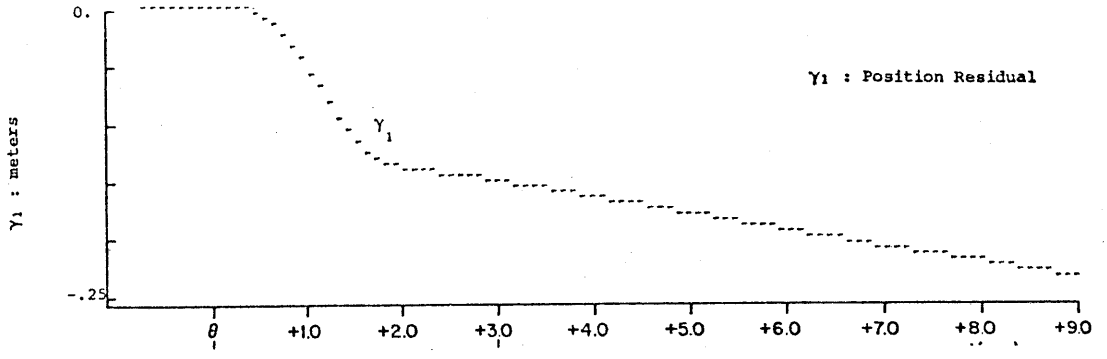

KC1

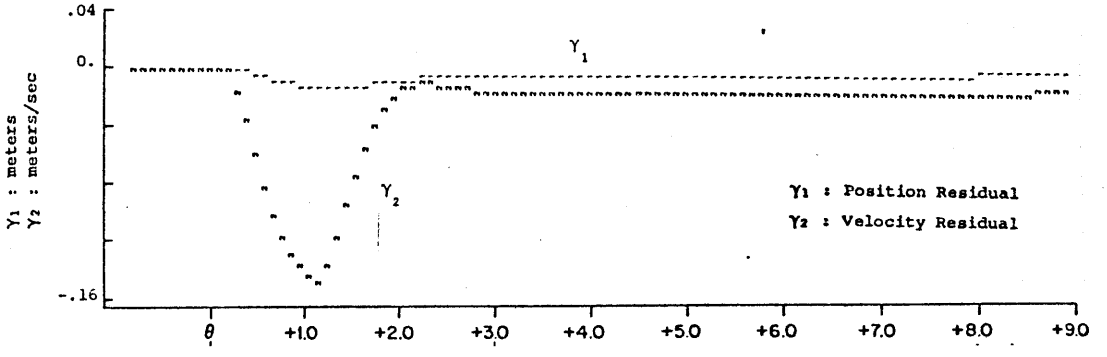

KC2

Figure 4.78

Residuals, PCU Scale Factor Change; KC1, KC2

We have seen that detection of these failures is feasible, and can be done in the presence of random plant and sensor noise.

External disturbances, such as winds and grades, pose problems for the detection system, since their effect on the vehicles' transient response is qualitatively similar to propulsion failures.

Tradeoffs between detection probability, false alarm probability, time to detect, and failure location identification have been established. We have concentrated on how the choice of a system model and how the use of physically redundant sensors affect these tradeoffs.

It has been demonstrated that as model complexity is increased, so is false alarm sensitivity to unmodelled effects and external disturbances. Simple vehicle models employing kinematic relationships have been shown to provide acceptable detection ability coupled with a decreased sensitivity to external disturbances.

Physically redundant sensor pairs have been shown to improve algorithm performance by decreasing failure identification delay.

Finally, the GLR algorithm, designed for the detection of additive bias failures (which cause sudden jumps in measurements or actuators), can be shown to detect failures involving sensor or actuator scale factor changes or stuck outputs (whose effects appear gradually).

CHAPTER V

FAILURE DETECTION IN VEHICLE-FOLLOWER SYSTEMS

5.1 Introduction

In chapter four, vehicle failure detection strategies have been examined involving single vehicles only; the methods explored would be implemented on-board the vehicle for detection of position sensor, velocity sensor, and propulsion system failures. It was assumed that the only communication the vehicle had with the outside world was the acquisition of control commands from a wayside computer.

In practice, however, proposed AGT vehicle systems will require vehicles to travel in closely packed strings, with inter-vehicle headways on the order of one-half second. Such short headways are required to permit large passenger throughput, especially in personal rapid transit (PRT) class systems where vehicle capacity may be limited to four to six persons. In short-headway systems, much of the vehicle longitudinal control functions will be performed on-board the vehicle, and will likely be based on vehicle-follower control strategies [8, 9, 10, 22, 23, 26]. Vehicle-follower control requires accurate measurement of inter-vehicle spacing and relative velocity, and will thus require communication of vehicle states from one vehicle to another (possibly via the wayside) or the use of an inter-vehicle spacing sensor on-board each vehicle; such spacing sensors may employ radar, sonor, microwave or laser technologies. The control system requires the determination of inter-vehicle spacing with a high degree of reliability; thus adequate redundancy must be designed into the system, and a method implemented for failure detection.

In this chapter, we extend the GLR methodology for failure detection to a vehicle-follower system. The GLR algorithm will be applied to detection of failures in the spacing sensor and in measurements communicated to each vehicle from its predecessor. This will be done by augmenting a model of a single vehicle with a simple kinematic model of the vehicle it is following. Using this dual-vehicle model in the GLR algorithm, the detection of failures will be tested.

First, however, we will present a brief discussion of vehicle-follower control strategies and give the details of a specific operating policy to provide the background for our experiments.

5.2 Vehicle-Follower Longitudinal Control

In a vehicle-follower longitudinal control scheme, AGT vehicles travel in closely packed strings with each vehicle following the preceeding vehicle according to a specific operating policy. A wayside controller communicates control commands to the lead vehicle, and can thus control the behavior of the string. Vehicles may merge into or diverge from the string at intersections along the guideway.

A number of operating policies for maintaining inter-vehicle spacing have been developed [26]. These include constant-separation, constant-time headway, constant K-factor and safe-approach policies. The GLR method for failure detection can be used in conjunction with any of these policies.

To illustrate how the GLR algorithm can be applied to vehicle-follower control systems, the safe-approach control method of [26] has been chosen as the operating policy to be used in the simulations.

The safe-approach method can be viewed as a composite steady-state operating policy combining constant-time headway and constant-separation policies. The unique feature of the strategey is the way in which it governs the speed of a vehicle approaching its predecessor with the intention of achieving steady-state spacing. The overtaking vehicle is slowed down as it approaches proper spacing to insure that it can stop safely should the preceeding vehicle stop on service or emergency limits at any time.

The safe-approach controller on-board each vehicle employs velocity and spacing measurements to generate the vehicle's velocity command in accordance with the safe-approach policy, as follows:

$$v_c = v_2 + \frac{s - s_{min}}{2\ (C1)v_2 + C2 + C3} \qquad (5\text{-}1)$$

with

$$s_{min} = C1\ (v_2^2 - v_1^2) + C2\ (v_2 - v_1) + C3\ v_2 + C4 \qquad (5\text{-}2)$$

where v_c is the following vehicle's velocity command, v_2 is the following vehicle's velocity, v_1 is the preceeding vehicle's velocity, s is front-to-front spacing and C1, C2, C3 and C4 are constants. Values for these constants can be found in [26]. A block diagram of this "velocity command generator" is shown in Figure 5.1. The velocity command computed by the safe-approach velocity command generator can be sent to the velocity regulator of Figure 2.3 to implement the command. In practice, a blending function can be used to blend the velocity commands during transitions for wayside control to vehicle-following mode.

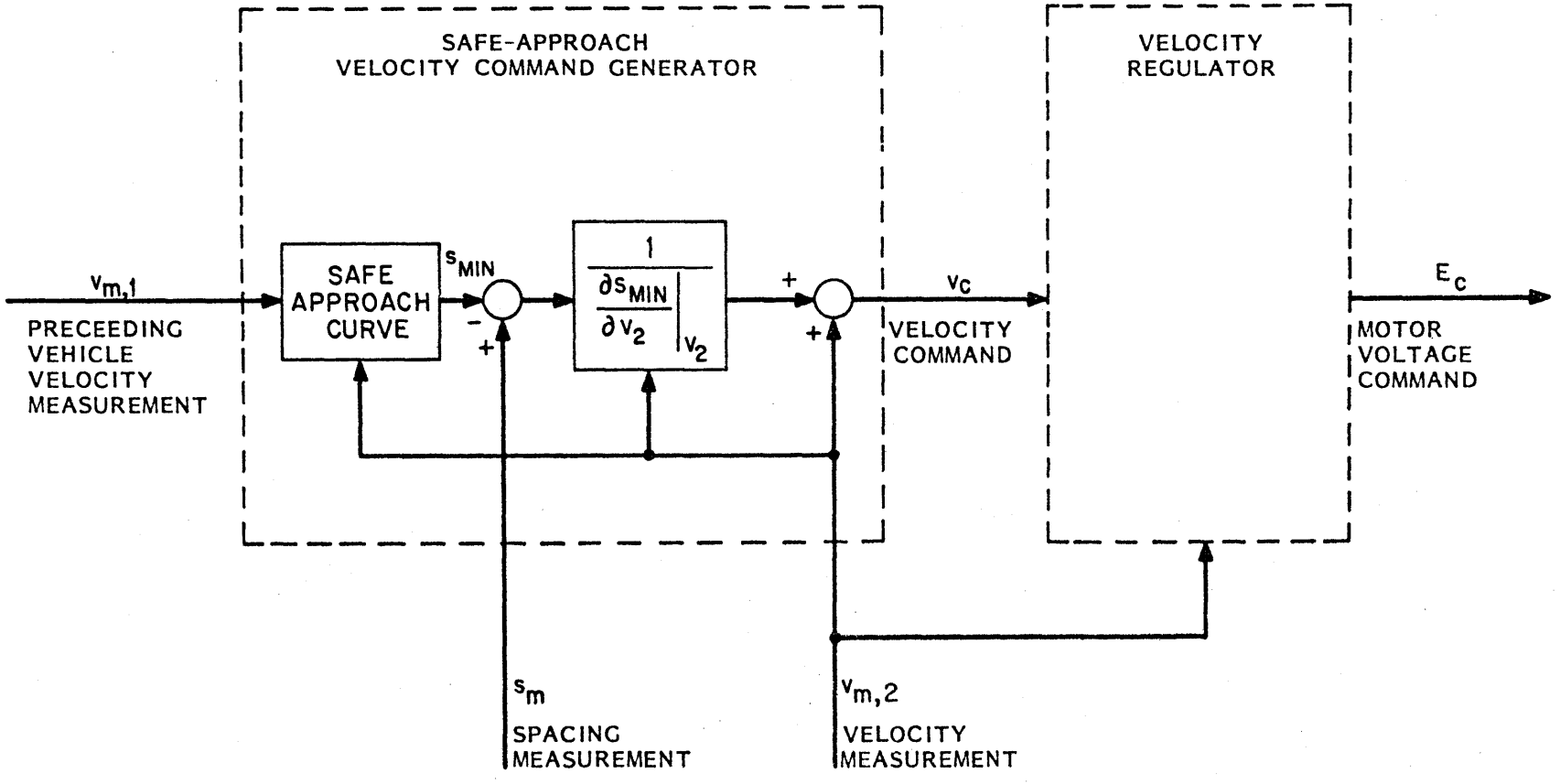

Figure 5.1

Safe-Approach Controller Velocity Command Generator

5.3 Application of the GLR Method

5.3.1 Modelling Vehicles in Vehicle-Following Mode

The single vehicle models examined in chapter four can be augmented to include a description of each vehicle's predecessor. The GLR algorithm can then be applied to this dual-vehicle model and implemented on-board each vehicle for detection of failures.

Complexity of the preceeding vehicle's model, which will be implemented in the detection algorithm on-board the following vehicle, will depend on the amount of information available to each vehicle about its predecessor.

In this study, we assume each vehicle has a spacing sensor, and in addition, receives communicated measurements of its predecessor's position and velocity. The spacing measurement is used directly in the vehicle-follower control calculations; should a failure be detected in this sensor, spacing is computed via the difference of each vehicle's position measurement. If a subsequent failure is detected in a position sensor, the estimated failure magnitude provided by the GLR algorithm could be used to permit the vehicle to continue operation, although in a degraded mode, so as not to block the guideway. This configuration of sensors and communicated measurements thus gives each vehicle $(\text{fail-operational})^2$ capability. In addition, it permits an accurate kinematic model of the preceeding vehicle to be used in the failure detection algorithm.

For illustration purposes, we will use the kinematic sensor driven model KS1 to represent the dynamics of each vehicle. This model can be

augmented with a similar model of each vehicle's predecessor, as follows:

$$\begin{matrix}\text{Veh. Model}\\ \text{Prec. Veh. Model}\end{matrix}\left\{\begin{bmatrix}\dot{x}(t)\\ \hline \dot{x}_p(t)\end{bmatrix}=\begin{bmatrix}0 & 0\\ \hline 0 & 0\end{bmatrix}\begin{bmatrix}x(t)\\ \hline x_p(t)\end{bmatrix}+\begin{bmatrix}1 & 0\\ \\ 0 & 1\end{bmatrix}\begin{bmatrix}v_m(t)\\ \hline v_{m,p}(t)\end{bmatrix}+\begin{bmatrix}n_2(t)\\ \hline n_{2,p}(t)\end{bmatrix}\right. \tag{5-3}$$

with the measurement equation:

$$\begin{bmatrix}s_m(t)\\ x_m(t)\\ \hline x_{m,p}(t)\end{bmatrix}=\begin{bmatrix}1 & -1\\ 1 & 0\\ \hline 0 & 1\end{bmatrix}\begin{bmatrix}x(t)\\ \hline x_p(t)\end{bmatrix}+\begin{bmatrix}n_3(t)\\ n_1(t)\\ \hline n_{1,p}(t)\end{bmatrix} \tag{5-4}$$

where the state variables are the vehicles' positions, the velocity measurements are used to drive the state equation, and $n_i(t)$ are sensor noise processes. We assume that the spacing measurement $s_m(t)$ is front-to-front spacing.

Discretization of the above model with a sampling interval of $\Delta t = 0.1$ seconds produces:

$$\begin{bmatrix}x(k+1)\\ x_p(k+1)\end{bmatrix}=\begin{bmatrix}1 & 0\\ 0 & 1\end{bmatrix}\begin{bmatrix}x(k)\\ x_k(k)\end{bmatrix}+\begin{bmatrix}0.1 & 0\\ 0 & 0.1\end{bmatrix}\begin{bmatrix}v_m(k)\\ v_{m,p}(k)\end{bmatrix}+\begin{bmatrix}n_2(k)\\ n_{2,p}(k)\end{bmatrix} \tag{5-5}$$

$$\begin{bmatrix}s_m(k)\\ x_m(k)\\ x_{m,p}(k)\end{bmatrix}=\begin{bmatrix}1 & -1\\ 1 & 0\\ 0 & 1\end{bmatrix}\begin{bmatrix}x(k)\\ x_k(k)\end{bmatrix}+\begin{bmatrix}n_3(k)\\ n_1(k)\\ n_{1,p}(k)\end{bmatrix} \tag{5-6}$$

The sensor noise processes are assumed to be uncorrelated, zero-mean, Gaussian, with 1σ levels given in Table 5.1.

Using the above model which uses only the kinematic relationships among the sensors, the GLR algorithm will not be sensitive to external disturbances or modelling errors, and can be expected to have low false alarm rates.

5.3.2 GLR Algorithm Design

The design of the GLR algorithm is done as before, following the steps outlined in chapter three.

Kalman-Bucy filter gain and covariance matrices are given in Table 5.2.

Failure direction vectors are chosen and indexed for the following possible failure locations:

$$\underline{f}_1 = \begin{bmatrix} 1 \\ 0 \\ 0 \end{bmatrix} \qquad (\in \text{Output-Space}) \quad \text{Spacing Sensor}$$

$$\underline{f}_2 = \begin{bmatrix} 0 \\ 0 \\ 1 \end{bmatrix} \qquad (\in \text{Output-Space}) \quad \text{Preceeding Vehicle Position Sensor}$$

$$\underline{f}_3 = \begin{bmatrix} 0 \\ 1 \\ 0 \end{bmatrix} \qquad (\in \text{Output-Space}) \quad \text{Position Sensor}$$

Table 5.1

Dual Vehicle Model Sensor Noise Characterization

Sensor Noise 1σ Levels

	$n_1(k)$ Position	$n_2(k)$ Velocity	$n_3(k)$ Spacing
Preceeding Vehicle :	0.1 m	0.1 m/s	—
Following Vehicle :	0.1 m	0.1 m/s	0.01 m

Noise Covariance Matrices For Kalman-Bucy Filter

$$R = E[\ (n_3\ n_1\ n_{1,p})^T (n_3\ n_1\ n_{1,p})\ ]$$

$$= \begin{bmatrix} 1.0e\text{-}4 & & \\ 0. & 1.0e\text{-}2 & \\ 0. & 0. & 1.0e\text{-}2 \end{bmatrix}$$

$$Q = (0.1)^2\ E[\ (n_2\ n_{2,p})^T (n_2\ n_{2,p})\ ]$$

$$= \begin{bmatrix} 1.0e\text{-}4 & \\ 0. & 1.0e\text{-}4 \end{bmatrix}$$

Table 5.2

Kalman-Bucy Filter Matrices; Dual Vehicle Model

K A L M A N F I L T E R -

CLOSED LOOP EIGENVALUES

REAL PART	IMAGINARY PART
0.267178087374890D+00	0.0
0.904875078027504D+00	0.0

CLOSED LOOP MATRIX

5.86027D-01	3.18848D-01
3.18848D-01	5.86027D-01

KBF FILTER GAIN MATRIX H

3.64588D-01	4.93854D-02	4.57395D-02
-3.64588D-01	4.57395D-02	4.93854D-02

PREDICTED ERROR COVARIANCE MATRIX

5.93854D-04	4.57395D-04
4.57395D-04	5.93854D-04

UPDATED ERROR COVARIANCE MATRIX

4.93854D-04	4.57395D-04
4.57395D-04	4.93854D-04

RESIDUAL COV MATRIX (V) -

3.72916D-04	1.36459D-04	-1.36459D-04
1.36459D-04	1.05939D-02	4.57395D-04
-1.36459D-04	4.57395D-04	1.05939D-02

RESIDUAL COV MATRIX INVERSE (V-INVERSE) -

2.70824D+03	-3.64588D+01	3.64588D+01
-3.64588D+01	9.50615D+01	-4.57395D+00
3.64588D+01	-4.57395D+00	9.50615D+01

$$\underline{f}_4 = \begin{bmatrix} 0 \\ 1 \end{bmatrix} \qquad \text{(State-Space)} \qquad \begin{matrix} \text{Preceeding Vehicle} \\ \text{Velocity Sensor} \end{matrix}$$

$$\underline{f}_5 = \begin{bmatrix} 1 \\ 0 \end{bmatrix} \qquad \text{(State-Space)} \qquad \text{Velocity Sensor}$$

The failure signatures for each of these failure locations are shown in Figure 5.2. The behavior of the failure signatures is unique for each of the possible failures.

The information measures $a_i(r)$ for each of the possible failure locations are shown in Figure 5.3. Observe that a relatively large amount of information about a spacing sensor failure is available immediately following the occurence of the failure.

5.4 Performance Results

Simulations were performed of a pair of AGT vehicles with the first under wayside control and the second following the first. Gaussian noise was not included in the simulations.

Initially, both vehicles are at a velocity of 15m/s, and at steady-state front-to-front spacing of 7.7 meters. Vehicle length is assumed to be 2.5 m; thus 5.2 meters actually separate the vehicles.

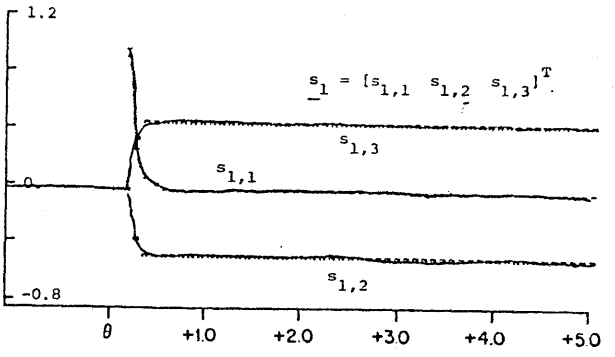

Spacing Sensor Bias

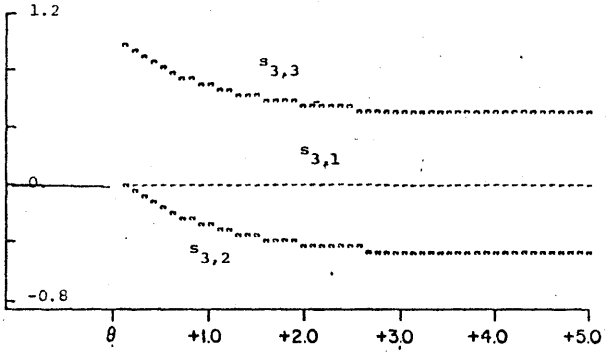

Preceeding Veh. Pos Sensor Bias

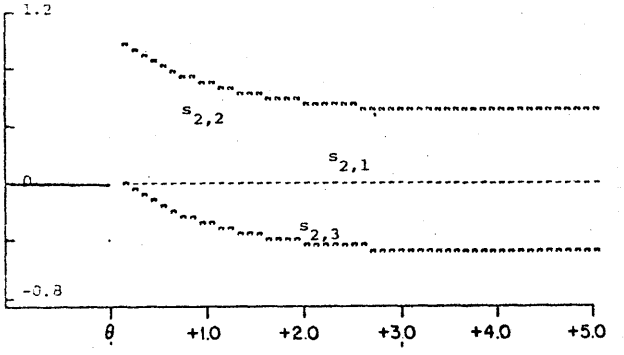

Pos Sensor Bias

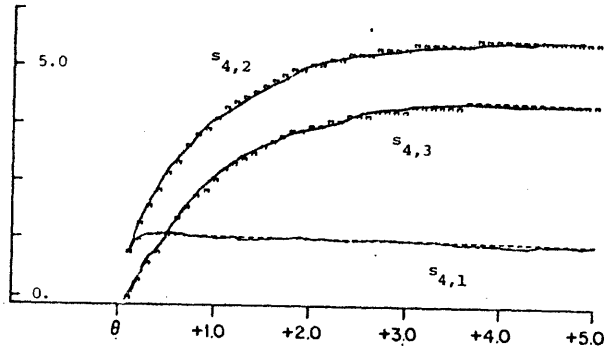

Preceeding Veh. Vel Sensor Bias

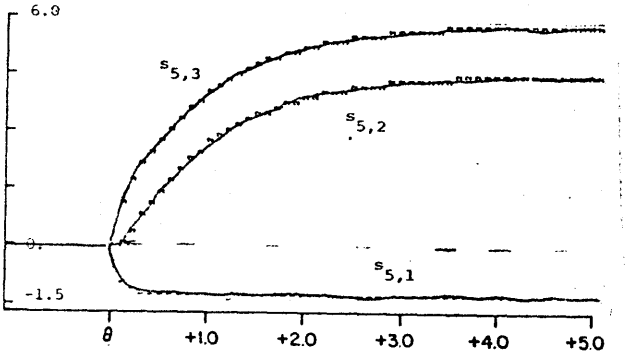

Vel Sensor Bias

Figure 5.2

Failure Signatures, Dual Vehicle Model

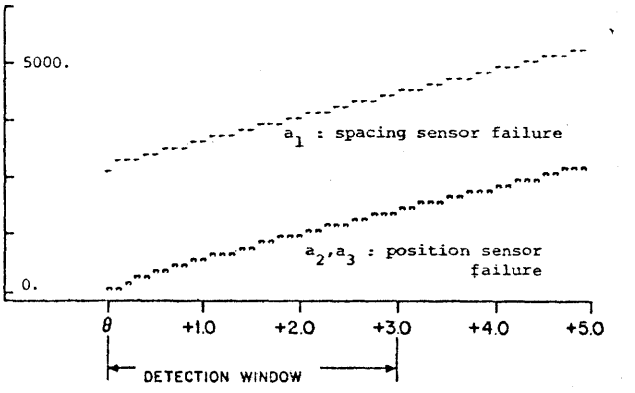

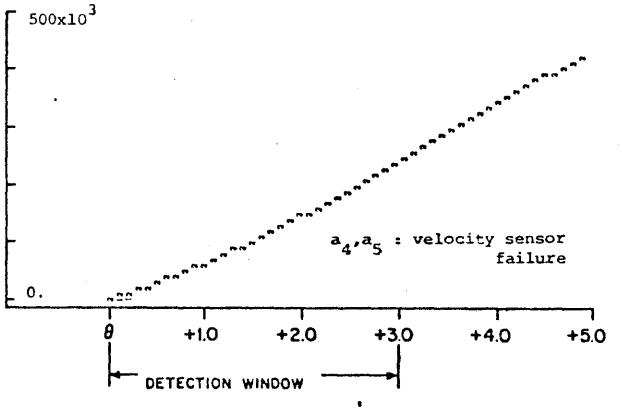

Figure 5.3
Information Measures, Dual Vehicle Model

5.4.1 Line-Speed Change Maneuver

A vehicle-following maneuver was performed to test the operation of the safe-approach controller and to examine the detection algorithm's sensitivity to a maneuver.

Scenario

The preceeding vehicle was commanded to accelerate from 15m/s to 18m/s at service limits. Behavior of the two vehicles is shown in Figure 5.4.

Results

Likelihood ratios, Figure 5.5, reach peak values of 5.0 during the period of maximum acceleration. The increase of the MLR's is due solely to the effects of sampling.

The controller performs as expected, and the maneuver will not cause false alarms.

5.4.2 Preceeding Vehicle Position Sensor Bias

Scenario

A 1.0m bias appears in the preceeding vehicle's position measurement received by the following vehicle at time θ=1.0s. The bias could be caused by a failure of the sensor or a component of the communication link. Since the measurement is not used directly in control law calculations, the failure does not affect vehicle behavior.

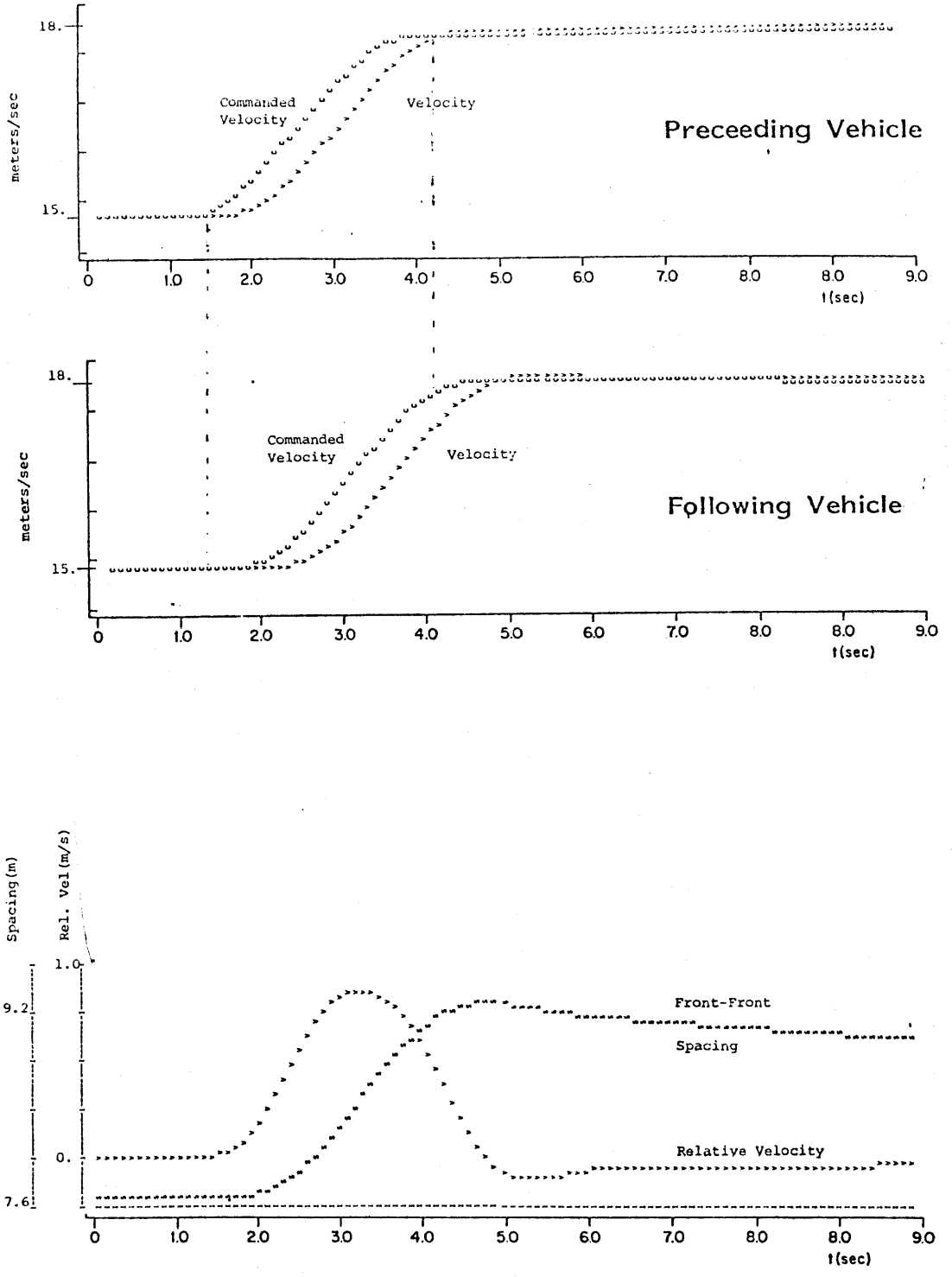

Figure 5.4

Vehicle Behaviors, Line-Speed Change Maneuver

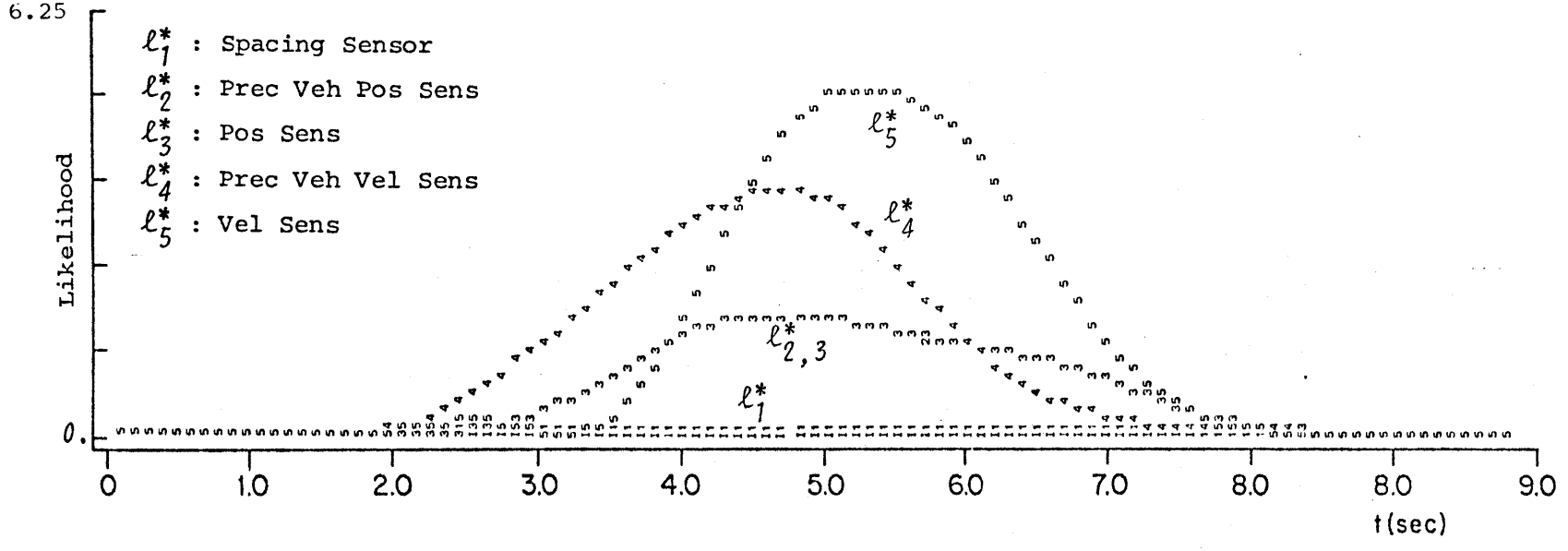

Figure 5.5

Maximum Likelihood Ratios, Line-Speed Change Maneuver

Results

The failure is detected instantly, and the location identified without delay or ambiguity by the detection algorithm on-board the following vehicle.

The likelihood ratio, ℓ_2^*, for the preceeding vehicle's position sensor (Figure 5.6) grows until the failure time leaves the 3.0 second detection window. The likelihood ratio then decays, and soon thereafter, the algorithm becomes unable to determine whether the failure is in the preceeding or the following vehicle's position measurement. In this case, the size of the detection window is critical to the identification of the failure's location; detection and identification must be accomplished before θ leaves the window.

5.4.3 Preceeding Vehicle Velocity Sensor Bias

Scenario

At time θ=1.0s a 1.0m/s bias developes in the preceeding vehicle's velocity sensor. On-board the preceeding vehicle, the velocity regulator, observing what it believes to be an overspeed conditions, slows the vehicle (as in section 4.3.2). On-board the following vehicle, the safe-approach controller, believing the preceeding vehicle to now be at a velocity of 16m/s, commands the vehicle to increase its velocity, as shown in Figure 5.7. Vehicle spacing decreases, and if corrective action is not taken, the vehicles collide 7.0 seconds following the failure.

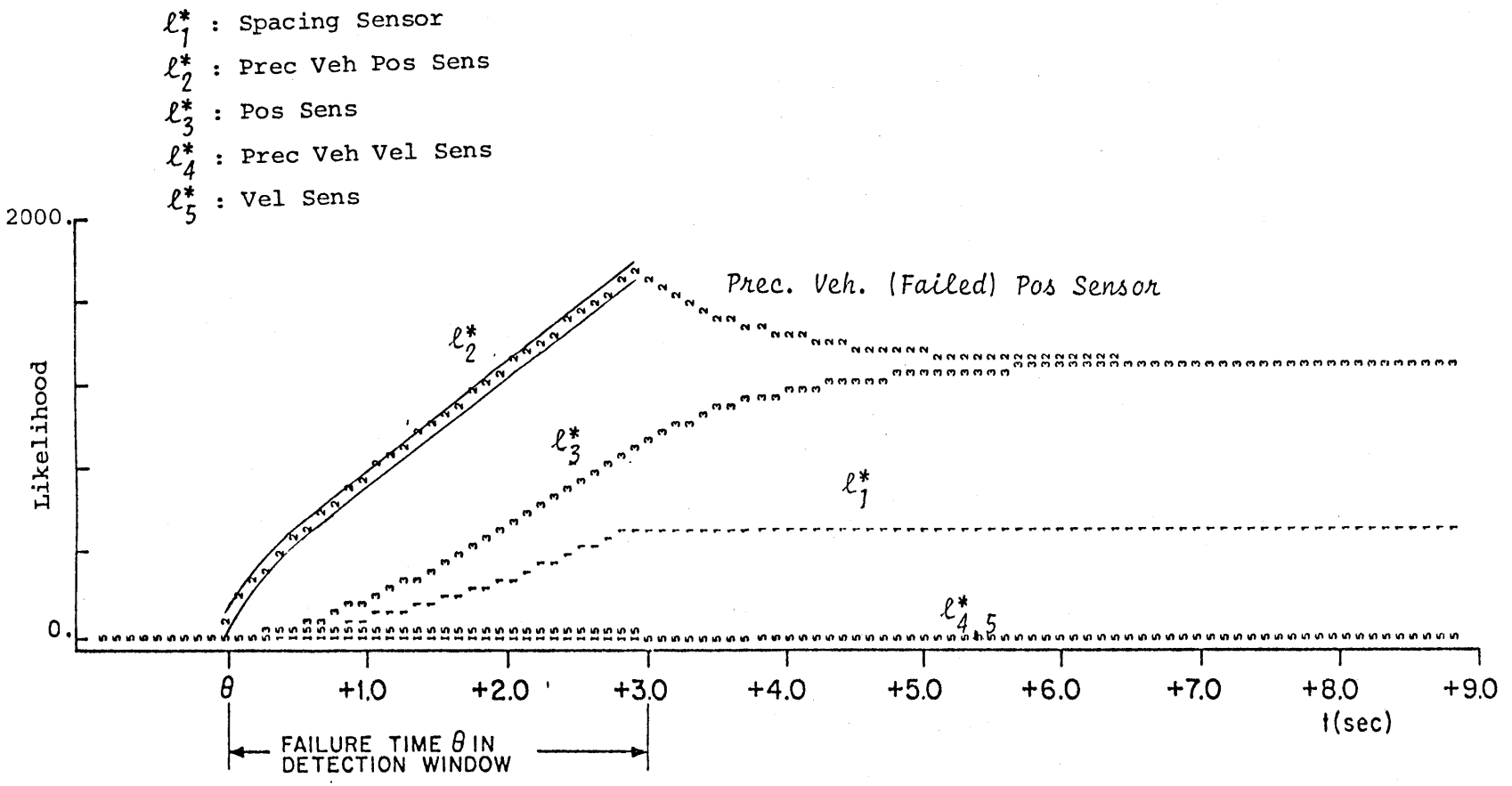

Figure 5.6

Maximum Likelihood Ratios, Preceeding Vehicle Position Sensor Bias

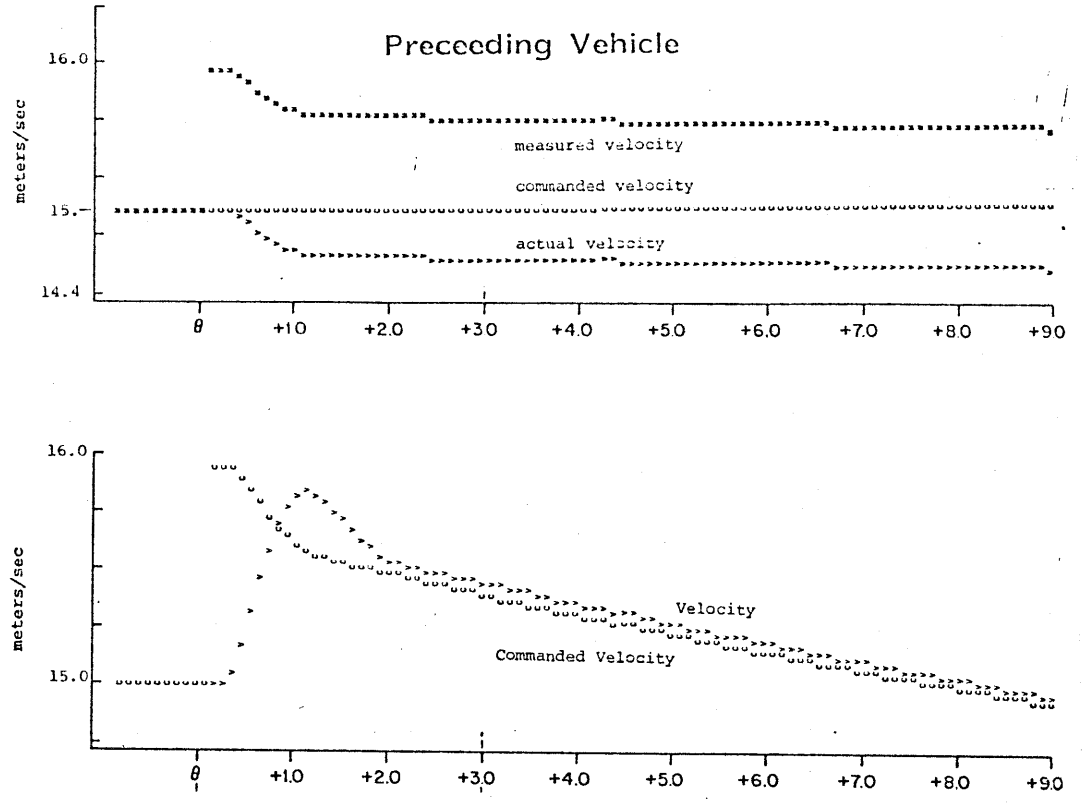

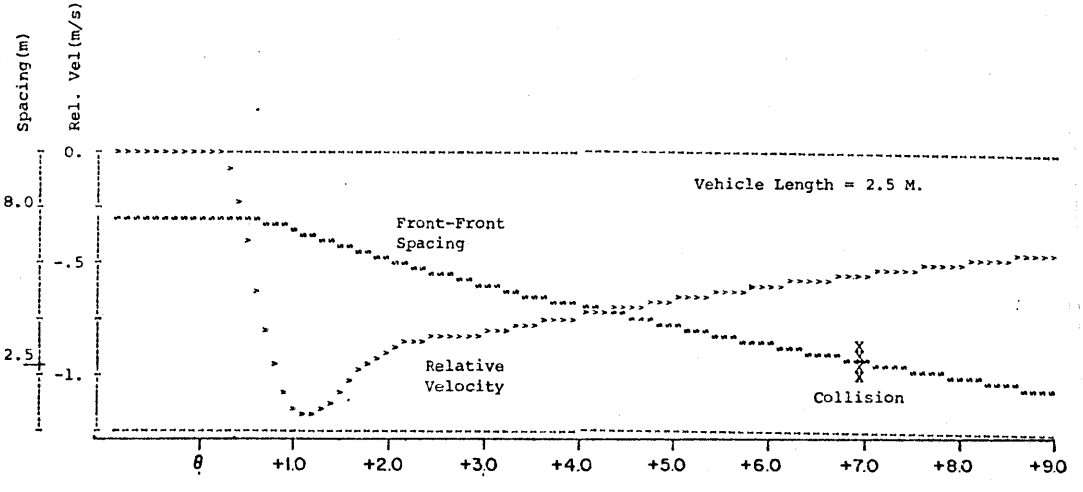

Figure 5.7

Vehicle Behaviors, Preceeding Vehicle Velocity Sensor Bias

Results

Likelihood ratios are shown in Figure 5.8. The MLR for the failed sensor, ℓ_4^*, jumps to a value of 27 at the occurrence of the failure, has reached 260 one-half second later, and is near 3000 by the time θ has left the detection window. A delay is observed, however, before the location of the failure can be confidently decided. The standard deviation of ℓ_4^*, is shown in the figure; it is not unti 1.0s following the failure that ℓ_5^* leaves the 1σ region around ℓ_4^* . If the failure decision was deferred until this point, vehicle spacing will have decreased only slightly more than a meter, from 7.7 to 6.5 meters.

Since the likelihood ratios are proportional to β^2, and their standard deviations proportional to β, there will be even less of a delay before the location of larger failures can be confidently determined.

Summary of Results

1) If undetected, the failure will cause a collision.
2) The likelihood ratio ℓ_4^* grows linearly following the failure.
3) ℓ_4^* remains large even after θ has left the detection window.
4) Although ℓ_4^* always remains larger than the other MLR's, there is a slight delay before the algorithm confidently determines whether the failed velocity sensor is on-board the following or preceeding vehicle. The length of this delay will be less for larger magnitude failures.

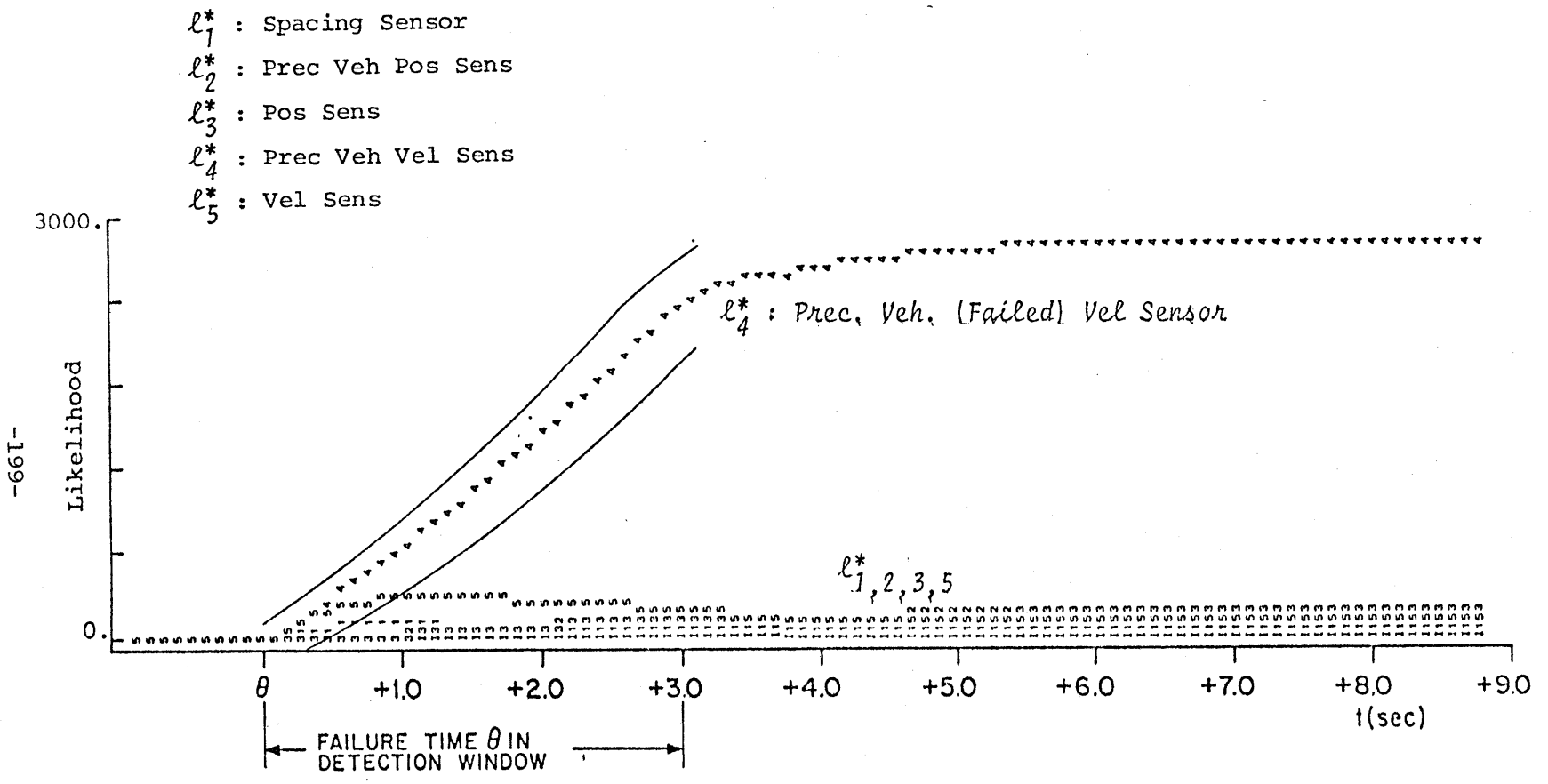

Figure 5.8

Maximum Likelihood Ratios, Preceeding Vehicle Velocity Sensor Bias

5.4.4 Spacing Sensor Bias Failure

Failures in the spacing sensor must be quickly and accurately detected, as this sensor is critical to vehicle safety.

Scenario

At time θ=1.0s, a 1 meter bias develops in the following vehicle's spacing sensor, so that measured spacing jumps from 7.7 to 8.7 meters. The safe-approach controller commands the following vehicle to increase velocity to close the observed gap (Figure 5.9). Actual spacing begins decreasing past the safe distance. Should the preceeding vehicle now execute an emergency stop, the vehicles may collide.

Results

At time θ, the spacing sensor likelihood ratio ℓ_1^* immediately jumps to a value near 3000 (Figure 5.10). However, there is an apparent ambiguity whether the location of the failure is the spacing sensor or one of the velocity sensors, as ℓ_4^* and ℓ_5^* are within one standard deviation of ℓ_1^*.

As another observation is made, the algorithm identifies the failed spacing sensor, and ℓ_4^* and ℓ_5^* decay rapidly.

The spacing sensor MLR, ℓ_1^*, continues increasing until the failure time θ leaves the detection window, at which time ℓ_1^* falls below ℓ_2^* and ℓ_3^*. This illustrates the importance of the first few residuals which are observed after the failure, for without them, the failure signature

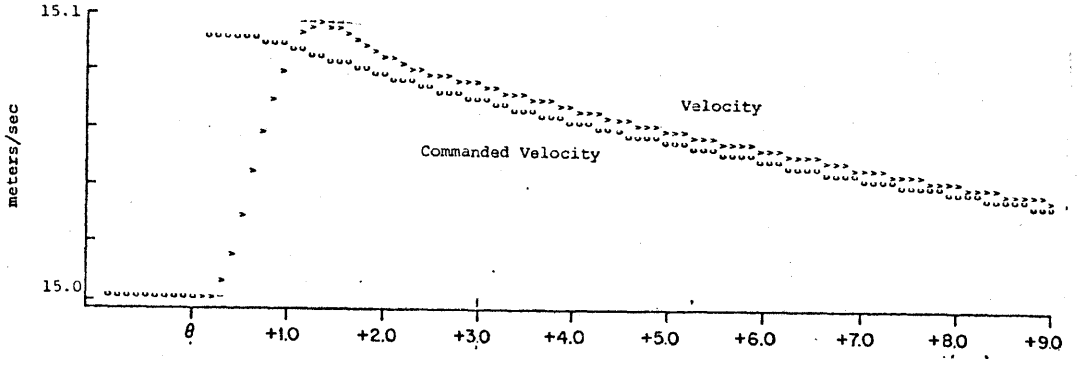

Following Vehicle

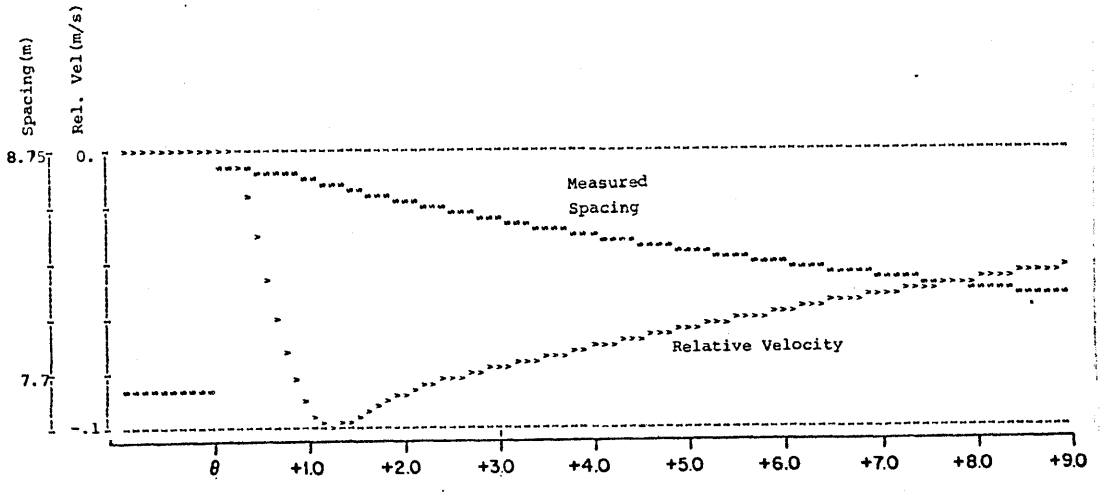

Figure 5.9

Vehicle Behavior, Spacing Sensor Bias

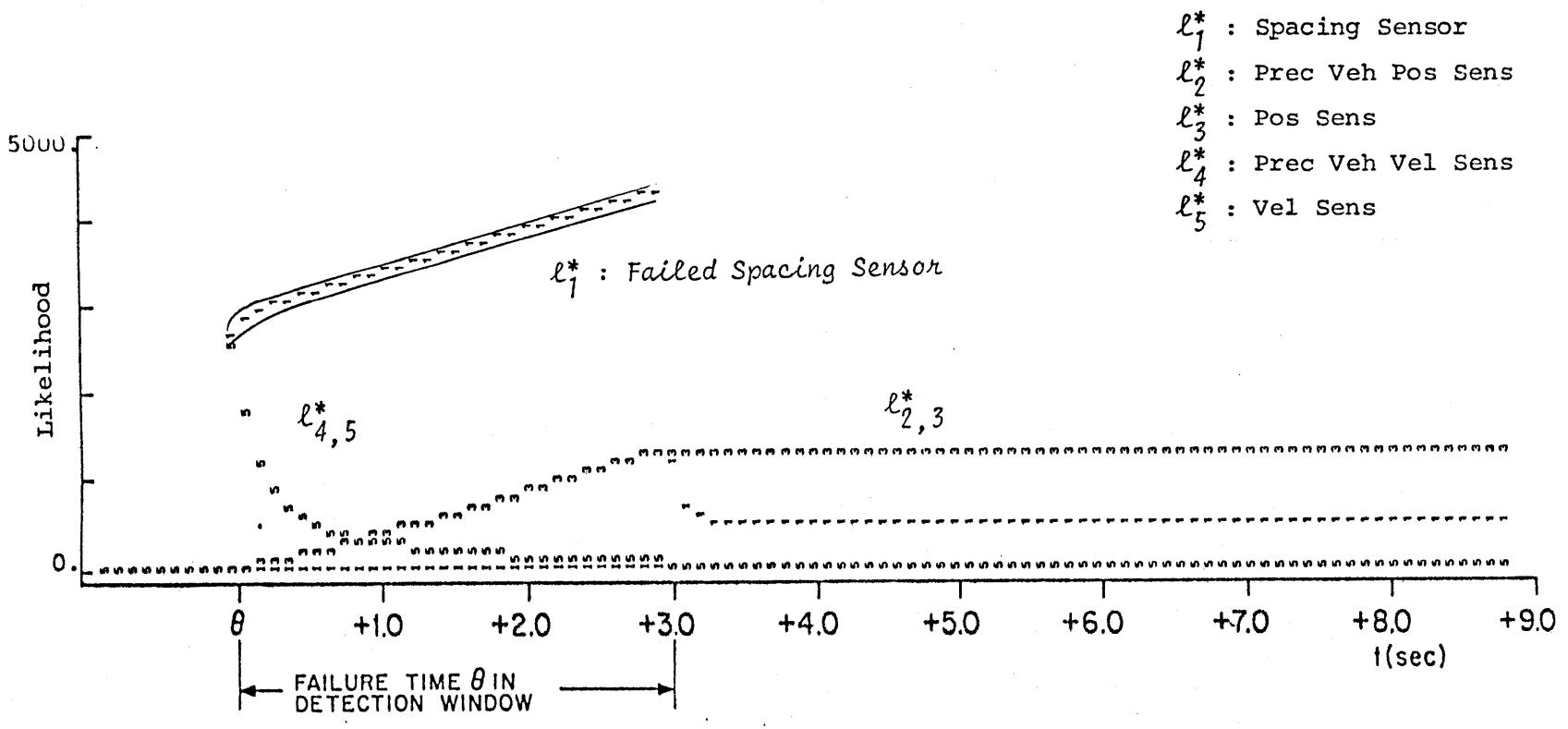

Figure 5.10

Maximum Likelihood Ratios, Spacing Sensor Bias

appears to the algorithm as a position sensor failure.

Summary of Results.

1) The spacing sensor bias causes safe spacing limits to be violated.

2) Detection of the failure is instantaneous, due to the redundancy afforded by each vehicles position measurement and the spacing sensor.

3) Correct and confident identification occurs within 0.2 sec.

4) The failure location will be incorrectly identified once the failure time leaves the detection window.

5.5 Summary and Conclusions

In this chapter, the GLR method has been applied to failure detection in a vehicle-follower AGT system. An algorithm has been designed for implementation on-board each vehicle for detection of failures in the vehicle's sensors, as well as detection of errors in state measurements received from its predecessor, as shown in Figure 5.11.

The algorithm has been shown to be able to detect and identify bias failures in the preceeding vehicle's communicated position and velocity measurements, and in the spacing sensor. These failures, if undetected, are likely to cause collisions.

The algorithm presented is applicable to any vehicle and any vehicle-following operating policy, as the vehicle model used employs only the kinematic relationships among the vehicles' sensors.

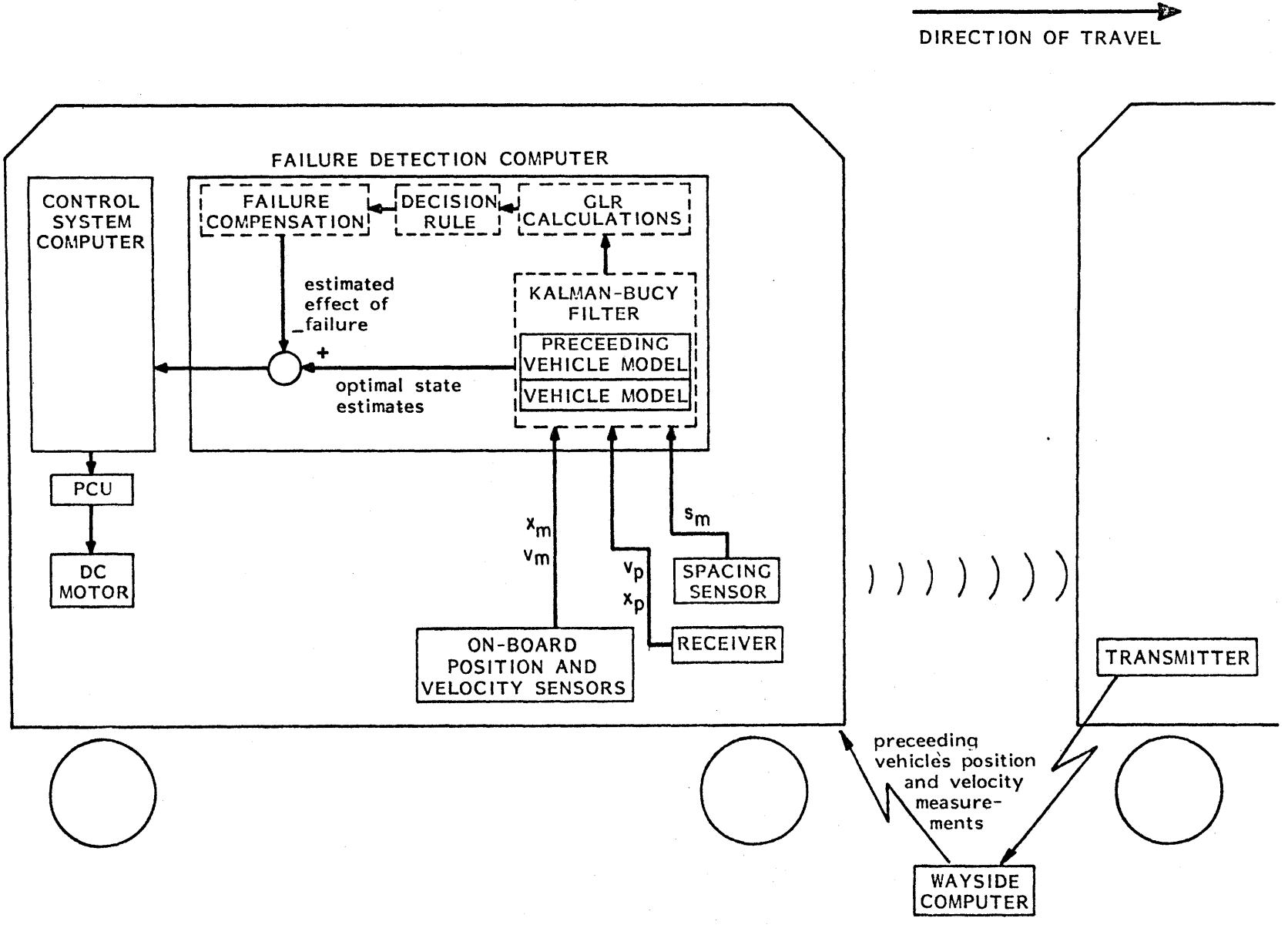

Figure 5.11 - Vehicle Follower Detection System Block Diagram

CHAPTER VI

SUMMARY AND CONCLUSIONS

6.1 Overview

The successful implementation of proposed automated guideway transit (AGT) transportation systems will depend on the development of safe and reliable longitudinal control systems. In high capacity AGT systems having headways on the order of one-half second, methods for the rapid detection of, and response to, vehicle failures are critically important to passenger safety. The success of these methods will play a part in determining achievable headways having adequate margins of safety.

Vehicle-follower control schemes, capable of providing short vehicle headways, necessary for high capacity, require accurate and reliable measurements of vehicle states (e.g. position, velocity, inter-vehicle spacing); detection of failures, especially in vehicle sensors, takes on ever increasing importance in such systems.

In this study, a methodology has been developed for the detection and identification of vehicle failures in an AGT system. This approach, based on the generalized likelihood ratio (GLR) algorithm, permits rapid detection of sensor and propulsion system failures. We have applied the method both to a single AGT vehicle operating in isolation and to a pair of vehicles operating at close headway governed by a vehicle-follower control law.

The GLR method has been previously proven successful in detecting sudden events (e.g., failures) in a variety of applications. It is an easily implemented software algorithm which processes data in real-time to detect the occurrence of sudden departures of an actual system from a simple, idealized linear model. The difference between observations of the actual system and predictions made by the model, called the residual, has a characteristic behavior when failures occur which is unique to different failures in various components of the system. By looking for these characteristic behaviors (failure signatures) in the retained past history of observations (detection "window") the algorithm detects the occurrence of failures. A set of maximally informative statistics (likelihood ratios) are generated which represent the likelihood that one of these failure signatures has been found. These likelihood ratios can be used in a decision rule with parametric thresholds to make detection decisions.

The GLR approach for failure detection in AGT vehicles has many advantages over both traditional methods for reliability enhancement (e.g. voting among redundant sets of instruments) and new methods recently proposed (the "detection filter" approach by Vander Velde at M.I.T.). This approach is unique in that in addition to rapid failure detection capability the algorithm:

1) provides optimal estimates (using modern system-theoretic techniques) of key system variables which can be fed directly to the longitudinal control system when there are no failures,

2) provides analytic redundancy for key sensors to save hardware costs, and most importantly,

3) allows for continued (possibly degraded) operation in the presence of certain failures by providing estimates of the extent (magnitude) of the failure; these estimates can be employed by the control system to compensate for the effect of the failure on the vehicle.

6.2 Research Summary and Discussion of Results

In this study, an idealized model of an AGT vehicle was developed. Possible failure modes for the vehicle's sensors and propulsion system were identified and a simple model to describe these failures developed. The GLR algorithm was designed for the detection of position sensor, velocity sensor, and propulsion system failures in the vehicle, and tested using computer simulations. Rapid detection of a variety of failure types was shown to be feasible, and could be performed in the presence of Gaussian sensor and vehicle plant noise. The effects on the detector algorithm of vehicle maneuvers and wind and grade forces were studied, as these disturbances may cause false alarms. It was shown that with systematic algorithm design tradeoffs false alarms from these external disturbances can be avoided.

After examination of detection algorithm issues for an isolated vehicle, the GLR method was applied to detection of failures in vehicles operating at close headways operating under a vehicle-follower control

system. Using simulations of a vehicle pair, it was shown that failures in the spacing sensor and errors in measurements communicated from the preceeding vehicle could rapidly be detected. Without detection of these faults, collisions of the vehicles occurred.

In both the single and dual vehicle tests, the GLR algorithm provided accurate estimates of the failure time and the magnitude of the error; these estimates would be used by the control system to compensate for the failure, thus permitting a fail-operational response.

The concentration of the study has been on the methodological algorithm approach, and not on the issues of developing specific decision rules or failure compensation schemes. Wherever possible we have emphasized the qualitative aspects of the results, to emphasize the generality of the approach and how the results could be applied to automated transit systems different than the examples studied.

Important measures to characterize failure detection algorithms in general and the GLR approach in particular were found to be

1) detection feasibility;
2) false alarm characteristics;
3) detection delay;
4) failure location identification ability.

These performance attributes when considered in the framework of the GLR algorithm were found to be closely related to:

1) choice of vehicle model used in the algorithm;

2) sensor configurations employed;

3) history of system observations retained for processing in the detection algorithm (length of detection window);

4) settings of detection thresholds and ratio of modelled plant to sensor noise intensities.

The impact of each of these factors on performance is summarized below.

Vehicle Model Used in Detection Algorithm

The vehicle model used in the GLR algorithm critically affects detection performance. We have found that complex (detailed) models which contain uncertain parameters, although providing the best detection ability with minimum detection delay under ideal conditions, are sensitive to external disturbances and unmodelled effects and may thus produce unacceptable false alarm rates.

We found that simplified models which model kinematic relationships are less sensitive to external (wind and grade) disturbances since the kinematic relationships are known with certainty and continue to accurately model the vehicle's behavior even in the presence of disturbances. Use of these models in the algorithm produces lower false alarm rates and still permits failure detection capability, although a degradation in performance was observed in some cases (e.g. difficulty identifying a stuck position sensor). Using models which describe only the kinematic relationships

between sensor outputs was found to eliminate false alarms from wind and grade altogether, and still allowed detection of sensor failures. However, propulsion system failures could not be detected since the propulsion dynamics are not modelled.

Sensor Configurations

The GLR approach does not require physically redundant sensors for failure detection, as the algorithm provides analytic redundancy by employing measurements from other, analytically related, sensors. However, the use of physically redundant sensor sets in conjunction with the algorithm will always improve failure identification. We found that although detection of certain failures may not be improved, the use of dual-redundant sensors significantly reduces the delay before the location of the failure can be unambiguously identified.

Although traditional voting algorithms require three identical sensors to permit fail-operational/fail-safe capability following two subsequent sensor failures, only dual-redundant sensors are required to permit an equal failure response capability using the GLR algorithm.

Detection Window

In the framework of the GLR algorithm, the "detection window" represents a period in time of past system observations which are retained for processing by the detection algorithm; this window is searched for the onset of a failure signature. The length and location of this window relative to "current" time plays a key role in algorithm performance.

It was found that certain failures produce signatures which grow with time; longer or delayed windows will assure eventual detection of these failures, although with possible delays. Other failures produce signatures which decay with time, longer windows will not improve detection of these failures. Tradeoffs between computational burden and detection window length also clearly exist.

Decision thresholds; Noise intensities

The sensitivity of the detection algorithm to failures and disturbances can be adjusted parametrically to optimize false alarms vs. detection probabilities. Although detailed decision rules were not developed in this study, decision rule thresholds can be selected in a systematic fashion to facilitate performance tradeoffs.

In addition, the relative detection sensitivity to failures which occur in sensors vs. vehicle dynamics (propulsion) can be parametrically adjusted via the relative intensities of the modelled plant and sensor noise used in algorithm design; the modelled noise intensities in essence set the detection algorithm's bandwidth, which affects false alarms sensitivity to background noise and detection speed.

6.3 Computational Complexity

The scope and complexity of the calculations required for the a-priori design of the GLR algorithm for a specific implementation requires the use of a general purpose computer. However, the calculations required during on-line operation of the algorithm can be minimal, as recursive expressions

can easily be found for these computations. The detection algorithm should thus be implemented in an on-board computer (e.g. a micro-processor based architecture). In addition, the modular nature of the GLR algorithm suggests parallel processing implementations.

To give the reader a feel for the simplicity of the on-line calculations, the algorithm was implemented in this study (ignoring I/O) in approximately 60 FORTRAN statements, most of which were devoted to matrix operations.

For an algorithm design having n state variables, p measurements, q possible failure locations and r data points in the detection window, each time step of algorithm operation requires:

	multiplications	additions
Kalman-Bucy Filter Update	$n^2+2nm+2n$	$n^2+2np+n+p$
Likelihood Ratio Computation	$q(p+2)r$	$q(p)r$

For the three state vehicle model and the full three second detection window used in this study, 400 multiplications and 212 additions were required at each time step.

6.4 Areas for Future Research

Additional research is needed for the development and testing of decision rules and methods for coupling the detection algorithm to the control system. An adaptive filtering scheme employing the GLR algorithm

for failure compensation is given in [32]. Testing of such approaches in the context of AGT vehicle systems is still required.

In this study, the GLR algorithm was tested on simulated data from an idealized AGT vehicle model. Analysis and testing of the approach on actual recorded data is still necessary.

The GLR algorithm for failure detection can provide significant improvements in vehicle safety and reliability. The resulting reliability enhancement, however, is limited by the reliability of the computer hardware implementing the algorithm. Although the state-of-the-art in digital hardware reliability is ever-increasing, this issue must still be addressed. Processor hardware failures may either cause failure detection capability to be lost, or may themselves produce false detection alarms needlessly hindering efficient operation of the vehicle system; processor failures (e.g. memory errors causing algorithm constants to be zeroed or biased, A/D converter faults, etc.) could appear to the GLR algorithm as vehicle sensor failures.

Although we have briefly examined possible methods for detection of processor faults within the framework of the GLR algorithm (e.g. the development of "processor failure signatures"), it appears that detection of these failures is best left to redundant, fault-tolerant computer architectures [40,41]. Additional study is clearly needed, however.

APPENDIX A

NOTATION

Chapters are divided into sections, which are numbered 1.1, 1.2, etc. Sections may be divided into subsections, numbered 1.1.1., 1.1.2., etc., and so on. Figures, tables, and equations are numbered consecutively within each chapter, prefixed by the chapter number. Equation numbers appear in parentheses ( ), and references in brackets [ ].

Vectors are denoted by lower case letters and are underlined, e.g., $\underline{x}$. Scalars are lower case but not underlined. Matrices are written as uppercase letters. These rules are occasionally broken (e.g. the constants C_0, C_1, K_M, C1, C2, C3, C4) to be consistent with other sources.

Variables with a (^), e.g., $\hat{x}$, are estimates of the variable's true value.

Notation for Mathematical Operations

x^T	transpose of the vector x
A^T	transpose of the matrix A
A^{-1}	inverse of the square matrix A
$\dot{x}(t)$	time derivative of the time-varying vector x(t)
$\max_{\theta}$	the maximum with respect to θ
$\arg\max_{\theta}$	the value of θ which produces the maximum

Abbreviations

AGT	Automated Guideway Transit
GLR	Generalized Likelihood Ratio
KC1	Kinematic Velocity Command Driven Vehicle Model
KC2	Kinematic Acceleration Command Driven Vehicle Model
KS1	Kinematic Sensor Driven Vehicle Model
LR	Likelihood Ratio
MLR	Maximum Likelihood Ratio
PCU	Power Conditioning Unit
Pitts	Refers to Vehicle and DC Motor Model by Pitts [19]

APPENDIX B

DISCRETIZATION OF CONTINUOUS-TIME SYSTEMS

Given the linear continuous-time stochastic system:

$$\dot{\underline{x}}(t) = A\underline{x}(t) + B_c\underline{u}(t) + \underline{\omega}_c(t) \tag{B-1}$$

$$\underline{z}(t) = C\underline{x}(t) + \underline{n}_c(t) \tag{B-2}$$

where the zero mean white noise processes $\underline{\omega}_c(t)$ and $\underline{n}_c(t)$ have covariance matrices $Q_c = Q_c^T \geq 0$ and $R = R^T \geq 0$ a statistically equivalent discrete-time linear stochastic system can be computed:

$$\underline{x}(k+\Delta t)\ \Phi\underline{x}(k) + B\underline{u}(k) + \underline{\omega}(k) \tag{B-3}$$

$$\underline{z}(k) = C\underline{x}(k) + \underline{n}(k) \qquad k=0,\ \Delta t,\ 2*\Delta t,.... \tag{B-4}$$

where the zero mean, uncorrelated, Gaussian processes $\underline{\omega}(k)$ and $\underline{n}(k)$ have covariance matrices $Q = Q^T \geq 0$ and $R = R^T \geq 0$, and

$$\Phi = e^{A\Delta t} \tag{B-5}$$

$$B = \left(\int_0^{\Delta t} e^{A\sigma}\, d\sigma \right) B_c \tag{B-6}$$

$$Q = \int_0^{\Delta t} e^{A\sigma}\, Q_c\, e^{A^T\sigma}\, d\sigma \tag{B-7}$$

If the continuous-time control $\underline{u}(t)$ is not held piecewise constant over the interval $[k,\ k + \Delta t)$, the system (B-3), (B-4) will contain errors

caused by the effects of sampling $\underline{u}(t)$.

The matrix exponentials can be computed on a digital computer using a Pade approximation [42].

APPENDIX C

AGT VEHICLE SIMULATOR AND GLR ALGORITHM PROGRAMS

This appendix briefly describes the computer programs used to simulate the behavior of an AGT vehicle and to test the GLR algorithm.

A FORTRAN program was written to simulate the general, linear, discrete-time system:

$$\underline{x}(k+1) = A\underline{x}(k) + B\underline{u}(k) + L\underline{w}(k) + \underline{f}_D(k) \tag{C-1}$$

$$\underline{z}(k) = C\underline{x}(k) + D\underline{u}(k) + \underline{v}(k) + \underline{f}_S(k) \tag{C-2}$$

with state vector $\underline{x}$, controls $\underline{u}$, measurements $\underline{z}$, Gaussian noise processes $\underline{w}$ and $\underline{v}$, and failure vectors $\underline{f}_D$ and $\underline{f}_S$.

This program was used to simulate the vehicle with the structure given in Figure 4.7, the dynamics of Figure 2.7, and the controller of Figure 2.3. The dual-vehicle simulations used the controller of Figure 5.1.

Plant noise, wind and grade were added via the disturbance process w(t), (Figure 2.7), with

$$-w(t) = w_n(t) + w_g(t) + w_w(t)$$

where w_n is a Gaussian noise process, w_g is the effect of grade, and w_w the effect of wind. The grade and wind disturbances are given by

$$w_g(t) = C_2 W g(t) + C_3 W \dot{g}(t) \tag{C-3}$$

$$w_w(t) = C_2 W_D v_w(t) + C_3 W_D \dot{v}_w(t) \tag{C-4}$$

where

W = Vehicle Weight

$= f_{grav} M = (9.807)M$

$g(t)$ = percent grade (e.g. .06=6% uphill grade)

$v_w(t)$ = wind velocity (headwind positive)

W_D = linearized drag

$= \rho A C_D (\bar{V}+\bar{V}_w)\,\mathrm{sgn}(\bar{V}+\bar{V}_w)$

$\bar{V}$ = nominal vehicle velocity

$\bar{V}_w$ = nominal wind velocity

$$C_2 = \left(\frac{r_w}{n}\right)^2 \frac{R}{J_T L}$$

$$C_3 = \left(\frac{r_w}{n}\right)^2 \frac{1}{J_T}$$

$$J_T = J_M + M\left(\frac{r_w}{n}\right)^2$$

Values used are given in Tables 2.1 and 2.2.

The system (C-1) and (C-2) was entered in the continuous-time form, and the equivalent discrete-time system computed, using the method given in Appendix B. Simulated data was written to disk files for storage and processing.

The GLR algorithm was implemented in a FORTRAN program which processed the simulated data from the AGT vehicle simulator.

Both programs were run on the MIT-IPS IBM 370 under VM/370 - CMS.

REFERENCES

(1) Strickland, L.R., 'Automated Guideway Transit Technology Overview', US DOT Report UMTA-VA-06-0041-78-1, Feb. 1978

(2) Anderson, J.H. and E.T. Powner, 'Optimal Digital Computer Control of Cascaded Vehicles in High-Speed Transit Systems in the Presence of Measurement Noise and Stochastic Input Disturbances', Transportation Research, Vol. 4, pp 185-198, 1970.

(3) Athans, M., W.S. Levine and A.H. Levis, 'On the Optimal and Suboptimal Position and Velocity Control of a String of High-Speed Moving Trains', Electronic Systems Laboratory Report, M.I.T., Nov. 1966.

(4) Athans, M., and A.H. Levis, 'Sampled-Data Control of High-Speed Trains', Electronic Systems Laboratory Report, M.I.T., Jan. 1968.

(5) Brown, S.J. Jr., E.J. Hinman, E.E. Mooring, and G.L. Pitts, 'Control Concepts for the Morgantown Project', Applied Physics Laboratory, John Hopkins University (APL/JHU), CP 007/TPR 022, Aug. 1971.

(6) Brown, S.J. Jr., 'Characteristics of a Linear Regulator Control Law for Vehicles in an Automatic Transit System', APL/JHU, CP 009/TPR 020, Jan. 1972.

(7) Brown, S.J. Jr., 'Point-Follower Automatic Vehicle Control; A General Analysis', APL/JHU, CP 057/TPR 025, May 1977.

(8) Caudill, R.J., and W.L. Garrard, 'Vehicle Follower Longitudinal Control for Automated Guideway Transit Vehicles', Univ. of Minn., Feb. 1977.

(9) Chiu, H.Y. G.B. Stupp, Jr., and S.J. Brown, Jr., 'Vehicle Follower Controls for Short Headway AGT Systems; Functional Analysis and Cenceptual Designs', APL/JHU, CP 051/TPR 035, Dec. 1976

(10) Chiu, H.Y., G.B. Stupp, Jr., and S.J. Brown, Jr., 'Vehicle Follower Control with Variable-Gains for Short Headway AUtomated Guideway Transit Systems' (APL/JHU), J. of Dyn. Sys, Meas., and Cntrl, pp. 183-189, Sept. 1977.

(11) Chu, K.C., 'Decentralized Control of High Speed Vehicular Strings', Transportation Science, Vol. 8, No. 4, Nov. 1974.

(12) Garrard, W.L., G.R. Hand and R. Raemer, 'Suboptimal Feedback Control of a String of Vehicles Moving in a Single Guideway', Transpn. Res., Vol. 6, pp. 197-210, 1972

(13) Garrard, W.L., and A.L. Kornhauser, 'Use of State Observers in the Optimal Feedback Control of Automated Transit Vehicles', J. of Dyn Sys, Meas, and Cntrl, Vol. 95, No. 2. June 1973.

(14) Garrard, W.L. , and A.L. Kornhauser, 'Design of Optimal Feedback Systems for Longitudinal Control of Automated Transit Vehicles', Transpn. Res., Vol. 7, pp. 125-144, 1973.

(15) Hinman, E.J., R.B. McDowell, and R.A. Makofski, 'Control Considerations for Short Headway AGV Systems', APL/JHU, CP 003/TPR 018, Oct. 1971.

(16) Hinman, E.J., 'Command and Control Studies for Personal Rapid Transit, Program Status, 1974', APL/JHU, CP 039/TPR 030, April 1975.

(17) Lang, R.P., 'Morgantown Personal Rapit Transit Control System Design Summary', (Boeing Aerospace Co.) UMTA Report UMTA-MA-06-0048-75-4 Dec. 1975.

(18) Pitts, G.L., 'Augmented Block Guidance for Short Headway Transportation Systems', APL/JHU, CP 019/TPR 023, Sept. 1972.

(19) Pitts, G.L., 'Control Allocation Investigation: Sampling Rate Selection', APL/JHU, TIR-009, UMTA-MD-06-0018-74-2, April 1974.

(20) Powner, E.J., J.H. Anderson, and G.H. Qualtrough, 'Optimal Digital Computer Control of Cascaded Vehicles in High Speed Transportation Systems', Transpn Res., Vol. 3, pp. 101-112, 1969.

(21) Pue, A.J., 'Implementation Trade-Off Study for a Short Headway AGT System', APL/JHU, FIC(2)-77-U-013, May 25, 1977.

(22) Pue, A.J., 'A Vehicle Follower Control Approach for Short Headway AGT Systems', Proc. Conference on AGT Technology Development, Cambridge Ma., UMTA-MA-06-0048-78-1, 1978.

(23) Pue, A.J., 'A State Constrained Approach to Vehicle-Follower Control for Short Headway AGT Systems', APL/JHU.

(24) Saridis, G., and Z. Rekasius, 'Design of Approximately Optimal Feedback Controllers for Systems with Bounded States', IEEE Transactions on Automatic Control, Vol. AC-12, No. 4, Aug. 1967.

(25) Schumacher, P.J. 'The Vehicle Control and Reliability Project', (United Technologies corp., Otis Elevator Co.), Proc. Conf. on AGT Technology Devel., Camb., Ma. , UMTA-MA-06-0048-78-1, 1978.

(26) Schumacker, P.J., ed., 'Volume 3 Longitudinal Control Analysis and Design (Part B-PRT Systems)', Vehicle Longitudinal Control and Reliability Project, Otis Elevator Co., (C.S. Draper Lab.), UMTA-IT-06-0148-79-8, May 1979.

(27) Yang, S.C., and W.L. Garrard, 'A Low Sensitivity Modern Approach to the Longitudinal Control of Automated Transit Vehicles', J. of Dyn. Sys., Meas., and Cntrl, Vol. 95, No. 2, June 1974.

(28) VanderVelde, W.E., 'Application of Failure Detection Theory to Reliable Longitudinal Control of Guideway Vehicles', Dept. of Aeronautics and Astronautics, M.I.T., March 1979.

(29) Beard, R.V., "Failure Accommodation in Linear Systems Through Self-Reorganization', Phd Thesis, Dept. of Aero. and Astro., M.I.T. Feb. 1971.

(30) Jones, H.L., 'Failure Detection in Linear Systems', Phd Thesis, Dept. of Aero. and Astro., M.I.T., Aug. 1973.

(31) Van Trees, H.L., Detection,Estimation, and Modulation Theory, Part I, John Wiley and Sons, Inc., New York, 1971.

(32) Willsky, A.S., and H.L. Jones, "A Generalized Likelihood Ratio Approach to State Estimation in Linear Systems Subject to Abrupt Changes', Proc. of the 1974 IEEE Conf. on Decision and Control, Pheonix, Ariz., November 1974.

(33) Willsky, A.S., and H.L. Jones, 'A Generalized Likelihood Ratio Approach to the Detection ad Estimation of Jumps in Linear Systems', IEEE Transactions on Automatic Control, Vol. AC-21, No. 1, pp. 108-112, Feb. 1976.

(34) Bueno, R., E.Y. Chow, S. Gershwin, and A.S. Willsky, "Research Status Report to NASA Langley Research Center: A Dual-Mode Generalized Likelihood Ratio Approach to Self-Reorganizing Digital Flight Control System Design', Electronic Systems Laboratory Report, M.I.T., Paper No. P-633, Nov. 1975

(35) Chow, E.Y. , A.S. Willsky, S.B. Gershwin, and P.K. Houpt, 'Dynamic Detection and Identification of Incidents on Freeways' Vol. IV: The GLR Method', Electronic Systems Laboratory Report ESL-R-767, M.I.T., Sept. 1977.

(36) Gustafson, D.E., A.S. Willsky, and J.Y. Wang, "Final Report: Cardiac Arrythmia Detection ad Classification Through Signal Analysis', The C.S. Draper Laboratory, Cambridge, MA., Rept. No. R-920, July 1975.

(37) Jazwinski, A.H., Stochastic Processes and Filtering Theory, Academic Press, New York, 1970.

(38) Chow, E.Y., 'Analytic Studies of the Generalized Likelihood Ratio Technique for Failure Detection', S.M. Thesis, Dept. of Elec. Engr. and Computer Sci., M.I.T., Feb. 1976.

(39) Bueno, R.A., 'Performance and Sensitivity Analysis of the GLR Method for Failure Detection', S.M. Thesis, Dept. of Elec. Engr. and Comp. Sci., M.I.T., Feb. 1977.

(40) Deyst, J.J., Jr., and A.L. Hpkins, Jr., 'Highly Survivable Integrated Avionics', Astronautics and Aeronautics, pp. 30-41, Sept. 1978

(41) Hopkins, A.L., Jr., T.B. Smith, III, and J.H. Lala, 'FTMP-A Highly Reliable Fault-Tolerant Multiprocessor for Aircraft', Proc. of the IEEE., Vol. 66, No. 10, Oct. 1978.

(42) Van Loan, C.F., "Computing Integrals Involving the Matrix Exponential', IEEE Transactions on Automatic Control, Vol. AC-23, No. 3, June 1978.